

# Investigation of RNA binding proteins regulated by mTOR

Thesis submitted to the University of Leicester  
for the degree of Doctor of Philosophy

Katherine Morris BSc (University of Leicester)

March 2017



# Investigation of RNA binding proteins regulated by mTOR

**Katherine Morris**, MRC Toxicology Unit, University of Leicester, Leicester, LE1 9HN

The mammalian target of rapamycin (mTOR) is a serine/threonine protein kinase which plays a key role in the transduction of cellular energy signals, in order to coordinate and regulate a wide number of processes including cell growth and proliferation via control of protein synthesis and protein degradation. For a number of human diseases where mTOR signalling is dysregulated, including cancer, the clinical relevance of mTOR inhibitors is clear. However, understanding of the mechanisms by which mTOR controls gene expression is incomplete, with implications for adverse toxicological effects of mTOR inhibitors on clinical outcomes.

mTOR has been shown to regulate 5' TOP mRNA expression, though the exact mechanism remains unclear. It has been postulated that this may involve an intermediary factor such as an RNA binding protein, which acts downstream of mTOR signalling to bind and regulate translation or stability of specific messages. This thesis aimed to address this question through the use of whole cell RNA binding protein capture using oligo-d(T) affinity isolation and subsequent proteomic analysis, and identify RNA binding proteins with differential binding activity following mTOR inhibition.

Following validation of 4 identified mTOR-dependent RNA binding proteins, characterisation of their specific functions with respect to growth and survival was conducted through depletion studies, identifying a promising candidate for further work; LARP1. Having selected LARP1 from depletion screens, overexpression co-IP experiments conducted alongside known binding partner PABP and subsequent arrays allowed for preliminary identification of mRNAs to which LARP1 binds. Finally, we showed evidence for differential binding of mRNA subsets between LARP1 and PABP, opening a new caveat for the role of the effector protein LARP1 in mTOR dependent gene expression regulation.

## **Acknowledgements**

First and foremost, I would like say a massive thank you to Professor Martin Bushell for not only giving me the opportunity to do this PhD, but also for his incredible and unwavering support, encouragement and patience over the last four years in his lab. My eternal gratitude goes also to Dr Ewan Smith for being an amazing mentor, colleague and friend throughout the life of this project. Special thanks to Dr Ania Wilczynska for all of her guidance and encouragement; to Dr David Ferland-McCollough for teaching me many of the initial methods I learnt; and to Dr Jack Godfrey, for never failing to keep me grounded. A huge thank you to the members of the Bushell Lab past and present, for the advice, laughs and support, but most of all for making it a truly wonderful place to be, even when it seemed science was determined to ruin my day.

Thank you to the proteomics group led by my secondary supervisor Professor Kelvin Cain; in particular to Mrs Rebekah Jukes-Jones and Dr Claudia Langlais for all the time and effort put into the mass spectrometry aspect of this project, and the feedback and discussions which followed. I'm grateful also to members of the Willis group for their contributions, in particular Dr Mark Stoneley for his method development input in the early stages and Dr Ruth Spriggs for help with analysis.

Finally, I would like to thank my parents - Chris and Sharon, my sisters, my partner Nik and all the friends near and far, who may not have understood exactly what I did but understood that I loved it, and supported me throughout.

## Contents

|             |   |           |
|-------------|---|-----------|
| <b>1</b>    | <b>INTRODUCTION.....</b>  | <b>18</b> |
| <b>1.1</b>  | <b>GENES TO PROTEINS: CONTROL OF GENE EXPRESSION .....</b>              | <b>18</b> |
| <b>1.2</b>  | <b>EUKARYOTIC TRANSLATION: AN OVERVIEW .....</b>                        | <b>19</b> |
| 1.2.1       | RIBOSOMES .....   | 19        |
| 1.2.2       | TRANSLATIONAL INITIATION.....   | 23        |
| 1.2.3       | TRANSLATIONAL ELONGATION.....   | 29        |
| 1.2.4       | TERMINATION OF TRANSLATION .....  | 30        |
| 1.2.5       | REGULATION OF TRANSLATIONAL CONTROL.....                                | 31        |
| <b>1.3</b>  | <b>RNA BINDING PROTEINS .....</b>                                       | <b>31</b> |
| 1.3.1       | RNA BINDING DOMAINS AND POST-TRANSCRIPTIONAL MODIFICATIONS.....         | 32        |
| 1.3.2       | RNA BINDING PROTEINS INVOLVED IN RNA PROCESSING AND SPLICING .....      | 33        |
| 1.3.3       | RNA BINDING PROTEINS, SEQUESTRATION AND SPATIAL REGULATION.....         | 34        |
| 1.3.4       | RNA BINDING PROTEINS AND TRANSLATIONAL CONTROL .....                    | 35        |
| 1.3.5       | RNA BINDING PROTEINS AND METABOLISM .....                               | 35        |
| 1.3.6       | RNA BINDING PROTEINS AND RNA DECAY .....                                | 36        |
| 1.3.7       | DISEASE STATES ARISING FROM RNA BINDING PROTEIN DYSREGULATION .....     | 37        |
| 1.3.8       | METHODOLOGIES FOR IDENTIFICATION OF CELLULAR RNA BINDING PROTEINS ..... | 37        |
| <b>1.4</b>  | <b>SIGNALLING CASCADES AND SIGNAL TRANSDUCTION .....</b>                | <b>40</b> |
| 1.4.1       | KINASES VS PHOSPHATASES .....   | 41        |
| 1.4.2       | THE MAMMALIAN TARGET OF RAPAMYCIN SIGNALLING .....                      | 41        |
| 1.4.3       | MTOR ACTIVATION AND SIGNAL TRANSDUCTION .....                           | 44        |
| 1.4.4       | MTOR REGULATION OF TRANSLATION .....                                    | 45        |
| 1.4.5       | MTOR AND METABOLISM .....   | 50        |
| 1.4.6       | MTOR AND AUTOPHAGY.....   | 50        |
| 1.4.7       | MTOR SIGNALLING AND DISEASE.....  | 51        |
| 1.4.8       | DEVELOPMENT OF KINASE INHIBITORS.....                                   | 51        |
| 1.4.9       | THERAPEUTIC RELEVANCE OF MTOR INHIBITORS.....                           | 52        |
| <b>1.5</b>  | <b>PROJECT AIMS .....</b>   | <b>53</b> |
| <b>2.</b>   | <b>MATERIALS AND METHODS .....</b>                                      | <b>56</b> |
| <b>2.1.</b> | <b>BUFFERS AND SOLUTIONS .....</b>                                      | <b>56</b> |
| <b>2.2.</b> | <b>CELL CULTURE TECHNIQUES.....</b>                                     | <b>57</b> |
| 2.2.1.      | GENERAL CELL CULTURE .....  | 57        |
| 2.2.2.      | SIRNA TRANSFECTIONS.....  | 57        |
| 2.2.3.      | GROWTH CURVES AND CELL COUNTING .....                                   | 58        |
| 2.2.4.      | FACS ANALYSIS .....   | 58        |
| 2.2.5.      | MICROSCOPY TO ASSESS CELL MORPHOLOGY .....                              | 59        |
| <b>2.3.</b> | <b>RNA TECHNIQUES .....</b>   | <b>59</b> |
| 2.3.1.      | RNA EXTRACTION .....  | 59        |
| 2.3.2.      | RT-QPCR WITH SYBRGREEN .....  | 60        |

|             |  |           |
|-------------|--|-----------|
| 2.3.3.      | SUCROSE GRADIENT POLYSOME PROFILING .....                  | 61        |
| <b>2.4.</b> | <b>PROTEIN TECHNIQUES .....</b>                            | <b>63</b> |
| 2.4.1.      | SONICATION AND NORMALISATION OF PROTEIN BY BRADFORD .....  | 63        |
| 2.4.3.      | WESTERN BLOTTING .....                                     | 65        |
| 2.4.4.      | WHOLE CELL RNA BINDING PROTEIN INTERACTOME CAPTURE .....   | 67        |
| 2.4.5.      | MASS SPECTROMETRY .....                                    | 69        |
| 2.4.6.      | MASS SPECTROMETRY ANALYSIS .....                           | 70        |
| 2.4.7.      | FLAG-TAGGED PCMV-LARP1 /PABPC1 CO-IMMUNOPRECIPITATION..... | 71        |
| <b>2.5.</b> | <b>METABOLOMICS .....</b>                                  | <b>72</b> |
| 2.5.1.      | SEAHORSE MITOCHONDRIAL STRESS TEST.....                    | 73        |
| 2.5.2.      | SEAHORSE GLYCOLYTIC STRESS TEST .....                      | 74        |
| 2.5.3.      | CRYSTAL VIOLET NORMALISATION .....                         | 74        |

### **3. IDENTIFICATION OF RNA BINDING PROTEINS CHANGING THEIR RNA BINDING ACTIVITY FOLLOWING MTOR INACTIVATION .....**

|             |  |           |
|-------------|--|-----------|
| <b>3.1.</b> | <b>INTRODUCTION .....</b>  | <b>77</b> |
| 3.1.1.      | PREVIOUS WORK IDENTIFYING RNA BINDING PROTEINS.....  | 77        |
| <b>3.1.</b> | <b>RESULTS .....</b>   | <b>78</b> |
| 3.1.1.      | OPTIMISATION OF MTOR INHIBITION SHOWED 60 MINUTE TREATMENT WITH 200 NM TORIN1 TO BE SUFFICIENT FOR INHIBITION OF BOTH MTORC1 AND MTORC2 .....  | 78        |
| 3.1.2.      | WHOLE CELL RNA BINDING PROTEIN CAPTURE OPTIMISATION CONFIRMED SPECIFICITY OF PROTOCOL AND ENRICHMENT OF KNOWN RNA BINDING PROTEINS .....   | 80        |
| 3.1.3.      | INTEGRATION OF 200 NM TORIN1 TREATMENTS BEFORE RNA BINDING PROTEIN CAPTURE INDICATED SUCCESSFUL INHIBITION OF MTOR SIGNALLING AND ENRICHMENT OF RNA BINDING PROTEINS .....   | 82        |
| 3.1.4.      | MASS SPECTROMETRY OF OLIGO(DT) <sub>25</sub> PULLDOWN AND ANALYSIS IDENTIFIED 214 RNA BINDING PROTEINS WHICH APPEARED ACROSS ALL REPLICATES .....  | 84        |
| 3.1.5.      | STATISTICAL ANALYSIS USING THE BIOCONDUCTOR PACKAGE LIMMA IDENTIFIED A SUBSET OF 31 PROTEINS EITHER SIGNIFICANTLY INCREASING OR DECREASING BINDING TO RNA BY 1.3 FOLD FOLLOWING MTOR INHIBITION, RELATIVE TO CONTROL ..... | 87        |
| 3.1.6.      | SELECTION AND SUCCESSFUL VALIDATION OF FOUR SPECIFIC RBPS CHANGING THEIR BINDING ACTIVITY FOLLOWING TORIN1 TREATMENT .....   | 90        |
| <b>3.2.</b> | <b>DISCUSSION .....</b>  | <b>93</b> |

### **4. INVESTIGATING THE ROLES OF MTOR-REGULATED RNA BINDING PROTEINS IN CELL SURVIVAL AND PROLIFERATION .....**

|             |  |            |
|-------------|--|------------|
| <b>4.1.</b> | <b>INTRODUCTION .....</b>  | <b>104</b> |
| <b>4.2.</b> | <b>RESULTS .....</b>   | <b>105</b> |
| 4.2.1.      | SERBP1 DEPLETION LEADS TO A MODEST SLOW IN PROLIFERATION OVER A 96 HOUR PERIOD OF GROWTH 105                                   |            |
| 4.2.2.      | SERBP1 DEPLETION BY SIRNA DOES NOT LEAD TO ANY OBVIOUS MORPHOLOGICAL CHANGES IN HELA CELLS AT 72 HOURS POST TRANSFECTION ..... | 106        |

|  |            |
|--|------------|
| 4.2.3. DIFFERENCE IN CELL NUMBER FOLLOWING SERBP1 DEPLETION BY siRNA FOR 72 HOURS IS NOT DUE TO INDUCTION OF APOPTOSIS, NOR CHANGES IN CELL CYCLE DISTRIBUTION, AS DETERMINED BY FACS ANALYSIS         | 109        |
| 4.2.4. PWP2 DEPLETION BY siRNA CAUSED DRAMATIC DECREASE IN THE PROLIFERATION RATE OF HELA CELLS, WITH NO CONCLUSIVE INDUCTION OF AUTOPHAGY   | 112        |
| 4.2.5. DEPLETION OF PWP2 BY siRNA DOES NOT LEAD TO ANY EXTREME MORPHOLOGICAL CHANGES IN HELA CELLS 72 HOURS POST-TRANSFECTION.   | 112        |
| 4.2.6. DIFFERENCE IN CELL NUMBER 72 HOURS FOLLOWING KNOCKDOWN OF PWP2 WAS NOT EXPLAINED BY INDUCTION OF APOPTOSIS IN HELA CELLS, NOR BY LARGE CHANGES IN CELL CYCLE DISTRIBUTION                       | 115        |
| 4.2.7. DEPLETION OF TRIM25 BY siRNA LED TO A DECREASE IN VIABLE CELL NUMBER OF A THIRD BY 96 HOURS POST-TRANSFECTION   | 118        |
| 4.2.8. THERE WERE NO OBVIOUS MORPHOLOGICAL CHANGES IN HELA CELLS 72 HOURS FOLLOWING DEPLETION OF TRIM25  | 118        |
| 4.2.9. DIFFERENCE IN CELL NUMBER 72 HOURS FOLLOWING KNOCKDOWN OF TRIM25 WAS NOT EXPLAINED BY INDUCTION OF APOPTOSIS IN HELA CELLS, OR BY LARGE CHANGES IN CELL CYCLE DISTRIBUTION                      | 121        |
| 4.2.10. LARP1 DEPLETION IN HELA CELLS LEADS TO A SIGNIFICANT AND LARGE DIFFERENCE IN VIABLE CELL NUMBER ONWARDS FROM 24 HOURS POST-TRANSFECTION  | 124        |
| 4.2.11. LARP1 DEPLETION LEADS TO DRAMATIC MORPHOLOGICAL CHANGES 72 HOURS POST-TRANSFECTION, POSSIBLY DUE TO INDUCTION OF APOPTOSIS, AS INDICATED BY PAPR CLEAVAGE                                      | 127        |
| 4.2.12. DEPLETION OF LARP1 BY siRNA FOR 72 HOURS LEADS TO APOPTOSIS OF HELA CELLS, POSSIBLY DUE TO A DEFECT IN MITOSIS AS INDICATED BY CELL CYCLE DISTRIBUTION   | 127        |
| 4.2.13. INVESTIGATION OF EFFECTS OF LARP1 DEPLETION IN A VARIETY OF CELL LINES INDICATES P53 STATUS MAY DETERMINE OUTCOME OF CELL FATE   | 131        |
| 4.2.14. DEPLETION OF LARP1 IN A549 CELL LINE LEADS TO A REDUCED GROWTH RATE, AS WELL AS AN INCREASE OF TOTAL P53 LEVELS  | 135        |
| 4.2.15. A549 CELLS SHOWED A SMALL INCREASE IN APOPTOTIC POPULATIONS 72 HOURS FOLLOWING TRANSFECTION WITH siRNA AGAINST LARP1, AS WELL AS A SMALL INCREASE IN THE PROPORTION OF CELLS IN G1 AND S PHASE | 138        |
| 4.2.16. SIMULTANEOUS KNOCKDOWN OF P53 AND LARP1 IN A549 CELLS DOES NOT APPEAR TO INITIATE GREATER LEVELS OF APOPTOSIS, AS DETERMINED BY PARP CLEAVAGE  | 141        |
| <b>4.3. DISCUSSION</b>   | <b>143</b> |

**5. IDENTIFICATION OF MRNAS BOUND BY LARP1 AND ITS BINDING PARTNER PABP, AND INVESTIGATION OF THEIR RELATIONSHIP IN POST-TRANSCRIPTIONAL REGULATION..... 150**

|  |            |
|--|------------|
| <b>5.1. INTRODUCTION</b>   | <b>150</b> |
| <b>5.2. RESULTS</b>  | <b>151</b> |
| 5.2.1. LARP1 AND PABP INTERACT IN HELA CELLS, AS SHOWN THROUGH FLAG CO-IMMUNOPRECIPITATION EXPERIMENTS | 151        |
| 5.2.2. DEPLETION OF PABP USING siRNA IN HELA CELLS LEADS TO APOPTOSIS AND SLOWED PROLIFERATION         | 153        |
| 5.2.3. DEPLETION OF PABP USING siRNA IN A549 CELLS ALSO LEADS TO APOPTOSIS AND SLOWED PROLIFERATION    | 154        |

|  |                |
|--|----------------|
| 5.2.4. ENDOGENOUS CO-IMMUNOPRECIPITATION OF LARP1 AND PABP IN THE PRESENCE AND ABSENCE OF TORIN1, AND SUBSEQUENT ARRAYS ALLOWED IDENTIFICATION OF MRNA BOUND TO EACH .....   | 157            |
| 5.2.5. TOTAL MRNA LEVELS OF SEVERAL TARGETS DETERMINED BY QPCR FOLLOWING DEPLETION OF LARP1 OR PABP IN THE PRESENCE AND ABSENCE OF TORIN1 TREATMENT.....   | 164            |
| 5.2.6. WESTERN BLOTS OF CO-IP EXPERIMENTS FOLLOWING OVEREXPRESSION OF LARP1 AND PABP IN BOTH HELA AND A549 CELLS SHOWS COMPARABLE INTERACTION BETWEEN CELL LINES.....  | 169            |
| 5.2.7. COMPARATIVE QPCR OF MRNA BOUND BY LARP1 OR PABP IN BOTH HELA AND A549 SHOWS DIFFERENTIAL BINDING BETWEEN PROTEINS, AS WELL AS EFFECTS OF TORIN1 ON BINDING OF CERTAIN MESSAGES<br>170   |                |
| 5.2.8. POLYSOME PROFILING OF TORIN1 TREATED A549 CELLS SHOWS SHIFT OFF POLYSOMES TO SUB-POLYSOMAL FRACTIONS .....  | 180            |
| 5.2.9. SEAHORSE INVESTIGATION OF LARP1 DEPLETED A549 SHOWED SOME DIFFERENCES IN MITOCHONDRIAL RESPIRATORY RESERVE CAPACITY FOLLOWING LARP1 DEPLETION.....  | 180            |
| 5.2.10. SEAHORSE INVESTIGATION OF GLYCOLYTIC CAPACITY OF LARP1 DEPLETED A549 SUGGESTS DIFFERENTIAL RELIANCE ON GLYCOLYSIS FOR ATP PRODUCTION .....   | 187            |
| 5.2.11. LACTATE DEHYDROGENASE A AND MALATE DEHYDROGENASE 2 PROTEIN LEVELS WERE UNCHANGED FOLLOWING PROLONGED LARP1 DEPLETION, DESPITE APPEARING AS POTENTIAL TARGETS OF LARP1 BINDING IN CO-IP/GENE EXPRESSION ARRAY EXPERIMENTS ..... | 189            |
| <b>5.3. DISCUSSION .....</b>   | <b>189</b>     |
| <br><b>6. FINAL DISCUSSION .....</b>   | <br><b>195</b> |
| <br><b>SUPPLEMENTAL FIGURES.....</b>   | <br><b>204</b> |
| <br><b>BIBLIOGRAPHY .....</b>  | <br><b>209</b> |

## **Table of Figures**

|   |     |
|---|-----|
| Figure 1.1 Schematic outlining key processes in ribosome biogenesis.....  | 21  |
| Figure 1.2 Overview of translation initiation.....  | 28  |
| Figure 1.3 Workflow for whole cell RBP interactome capture in conjunction with mTOR inhibition.....   | 39  |
| Figure 1.4 Overview of roles of mTORC1 and mTORC2.....  | 43  |
| Figure 1.5 Overview of mTOR signalling pathway.....   | 47  |
| Figure 3.1 mTOR signalling is inhibited following 1 hour treatment with 200 nm Torin1.....  | 79  |
| Figure 3.2 Whole cell RNA Binding Protein capture by oligo(dT) affinity isolation....   | 81  |
| Figure 3.3 Successful use of whole cell RBP capture in conjunction with mTOR inhibition following treatment with 200 nM Torin1.....                               | 83  |
| Figure 3.4 PCA showing variance between replicates and treatments within this study.....  | 86  |
| Figure 3.5 Volcano plot of 214 RNA Binding Proteins identified as present in three replicates in this study.....  | 88  |
| Figure 3.6 Comparisons of HeLa interactomes between this study and previous study show strong reproducibility.....  | 89  |
| Figure 3.7 Table of RNA Binding Proteins whose fold change of 1.3 or greater following Torin1 treatment exhibits a p-value < 0.05.....                            | 91  |
| Figure 3.8 Bar chart of RBP fold changes following 200 nM Torin1 treatment, as selected from cut-off exclusion within Volcano plot.....                           | 92  |
| Figure 3.9 Validation by western blot of RBP fold changes identified by mass spectrometry, following 200 nM Torin1 treatment.....                                 | 94  |
| Figure 3.10 Summary of key information available in literature on each of the 4 RNA Binding Proteins validated as changing binding following mTOR inhibition..... | 95  |
| Figure 4.1 Growth curves following SERBP1 knockdown showed modest slow in cellular growth rate relative to scrambled siRNA control.....                           | 107 |
| Figure 4.2 Cell morphology and PARP cleavage following 72 hours siRNA knockdown of SERBP1.....  | 108 |
| Figure 4.3 FACS analysis following 72 hours knockdown of SERBP1, shows depletion does not lead to an increased rate of apoptosis in HeLa cells.....               | 110 |
| Figure 4.4 Cell cycle distribution following 72 hours SERBP1 knockdown shows depletion does not lead to changes in cell cycle distribution in HeLa cells.....     | 111 |
| Figure 4.5 Growth curves following PWP2 knockdown showed dramatic slow in cellular growth rate relative to scrambled siRNA control.....                           | 113 |
| Figure 4.6 Cell morphology and PARP cleavage following 72 hours siRNA knockdown of PWP2.....  | 114 |
| Figure 4.7 FACS analysis following 72 hours knockdown of PWP2 shows depletion does not lead to an increased rate of apoptosis in HeLa cells.....                  | 116 |

|  |     |
|--|-----|
| Figure 4.8 Cell cycle distribution following 72 hours PWP2 knockdown shows depletion does not lead to changes in cell cycle distribution in HeLa cells.....                          | 117 |
| Figure 4.9 Growth curves following TRIM25 knockdown showed modest slow in cellular growth rate relative to scrambled siRNA control.....  | 119 |
| Figure 4.10 Cell morphology and PARP cleavage following 72 hours knockdown of TRIM25 shows knockdown is efficient but does not elicit notable visual changes in cell morphology..... | 120 |
| Figure 4.11 FACS analysis following 72 hours knockdown of TRIM25 shows depletion does not lead to an increased rate of apoptosis in HeLa cells.....                                  | 122 |
| Figure 4.12 Cell cycle distribution following 72 hours TRIM25 knockdown shows depletion does not lead to changes in cell cycle distribution in HeLa cells.....                       | 123 |
| Figure 4.13 Growth curves following LARP1 knockdown showed dramatic slow in cellular growth rate relative to scrambled siRNA control.....  | 125 |
| Figure 4.14 Cell morphology and PARP cleavage following 72 hours siRNA knockdown of LARP1 shows knockdown is efficient and provokes notable visual changes in cell morphology.....   | 126 |
| Figure 4.15 FACS analysis following 72 hours knockdown of LARP1 shows depletion leads to a dramatically increased rate of apoptosis in HeLa cells.....                               | 129 |
| Figure 4.16 Cell cycle distribution following 72 hours LARP1 knockdown shows depletion leads to a depletion of cells in G1 phase in HeLa cells.....                                  | 130 |
| Figure 4.17 PARP cleavage and p53 signalling in 4 different cell lines following 72 hours LARP1 depletion by siRNA.....  | 132 |
| Figure 4.18 Growth curves in A549 cell line following LARP1 knockdown showed slow in cellular growth rate relative to scrambled siRNA control.....                                   | 136 |
| Figure 4.19 Cell morphology and PARP cleavage following 72 hour LARP1 knockdown in A549 cells provokes notable visual changes in cell morphology.....                                | 137 |
| Figure 4.20 FACS analysis following 72 hours knockdown of LARP1 shows depletion leads to a modestly increased rate of apoptosis in A549 cells.....                                   | 139 |
| Figure 4.21 Cell cycle distribution following 72 hours LARP1 knockdown shows a depletion of cells in G1 phase in A549 cells.....   | 140 |
| Figure 4.22 PARP cleavage following 72 hour depletion of LARP1 and p53 in A549 cell line.....  | 142 |
| Figure 5.1 Co-immunoprecipitation experiment in HeLa cells over expressing Flag-tagged GFP, PARP and PABP shows interaction in an RNA-independent manner....                         | 152 |
| Figure 5.2 Growth curves following PABP knockdown in HeLa cells showed slow in cellular proliferation rate relative to scrambled siRNA control.....                                  | 155 |
| Figure 5.3 Cell morphology following 72 hours siRNA knockdown of PABPC1 knockdown instigates notable visual changes in HeLa cell morphology.....                                     | 156 |
| Figure 5.4 Growth curves following PABP knockdown in A549 cells showed slow in cellular proliferation rate relative to scrambled siRNA control.....                                  | 158 |

|   |     |
|---|-----|
| Figure 5.5 Endogenous LARP1 immunoprecipitation experiments with gene expression arrays to identify mRNAs showing enriched binding.....   | 160 |
| Figure 5.6 Differences between messages constitutively versus induced enrichment following Torin1 treatment in endogenous IPs of LARP1 and PABP.....                                    | 161 |
| Figure 5.7 Overlap and differentials between LARP1 and PABP bound mRNA from endogenous IP and gene expression arrays, in the presence and absence of Torin1 treatment.....              | 162 |
| Figure 5.8 Categories of a selection of mRNA identified from endogenous IP experiments as binding LARP1 and/or PABP, and any differences following Torin1 treatment of HeLa cells.....  | 163 |
| Figure 5.9 Samples generated for qPCR analysis of total mRNA abundance in A549 cells, following depletion of LARP1 or PABPC1 in the presence and absence of Torin1 treatment.....       | 165 |
| Figure 5.10 RT-qPCR analysis of total mRNA abundance of a selection of genes in A549 cells, following depletion of LARP1 or PABPC1 in the presence and absence of Torin1 treatment..... | 167 |
| Figure 5.11 Co-immunoprecipitation experiment in the presence of an RNase inhibitor in cells over expressing Flag-tagged GFP, LARP and PABP shows RNA-dependent interaction.....        | 171 |
| Figure 5.12 RT-qPCR validations of LARP1 and PABP bound mRNA targets following purification using FLAG-tagged overexpressed proteins in HeLa and A549 cells.....                        | 173 |
| Figure 5.13 Polysome profile for Torin1 treated A549 cells .....  | 181 |
| Figure 5.14 OCR and ECAR in A549 cells during a mitochondrial stress test conducted 48 hours post transfection with LARP1 siRNA.....  | 183 |
| Figure 5.15 Functionality of glycolytic pathway in A549 cells depleted of LARP1 investigated using Seahorse analyser.....   | 188 |
| Figure 5.16 Investigation of LDHA and MDH2 protein levels, two gene targets of LARP1 RBP activity.....  | 190 |

## Table of Tables

|   |    |
|---|----|
| TABLE 1.1 SUMMARY OF EUKARYOTIC INITIATION FACTORS INVOLVED IN THE PROCESS OF TRANSLATION INITIATION .....                              | 24 |
| TABLE 2.1 LIST OF QPCR PRIMERS USED IN THIS STUDY .....   | 61 |
| TABLE 2.2 COMPOSITION OF SDS-PAGE RUNNING GELS USED FOR WESTERN BLOTTING (RECIPE FOR RESOLVING BUFFER CAN BE FOUND IN SECTION 2.1)..... | 65 |
| TABLE 2.3 LIST OF PRIMARY ANTIBODIES AND SUPPLIERS USED IN WESTERN BLOTTING IN THIS STUDY .....   | 66 |
| TABLE 2.4 RECIPES FOR UNBUFFERED MEDIA REQUIRED FOR SEAHORSE EXPERIMENTS .....  | 74 |

## Abbreviations

|            |  |
|------------|--|
| 2-DG       | 2-Deoxyglucose   |
| 4E-BP      | eIF4E-binding protein  |
| aa-tRNA    | Aminoacyl-tRNA   |
| ADH1       | Alcohol dehydrogenase (yeast)                                    |
| AMD1       | Adenosylmethionine decarboxylase 1                               |
| AMP        | Adenosine monophosphate  |
| AMPK       | Adenosine monophosphate-activated kinase                         |
| APS        | Ammonium persulphate   |
| ARE        | Adenylate and uridylate rich elements                            |
| ATP        | Adenosine triphosphate   |
| BCL-2      | B-Cell CLL/Lymphoma 2  |
| BCL7C      | B-Cell CLL/Lymphoma 7C   |
| CCR4/CNOT1 | C-C motif chemokine receptor 4/CCR4-NOT1 transcription complex 1 |
| CHX        | Cycloheximide  |
| CNOT7/GAF1 | CCR4/NOT transcription complex subunit 7                         |
| co-IP      | Co-immunoprecipitation   |
| CYBA       | Cytochrome B-245 Alpha Chain                                     |
| DBA        | Diamond Blackfan Anaemia   |
| DEPTOR     | DEP domain containing mTOR-interacting protein                   |
| DMEM       | Dulbecco's Modified Eagles Medium                                |
| DMSO       | Dimethyl sulphoxide  |
| DNA        | Deoxyribonucleic acid  |
| dNTP       | Deoxynucleotide  |
| DTT        | Dithiothreitol   |
| ECAR       | Extracellular acidification rate                                 |
| ECL        | Electrochemical luminescence                                     |

|                   |  |
|-------------------|--|
| EDTA              | Ethylenediaminetetraacetic acid                      |
| eEF-              | Eukaryotic elongation factor -                       |
| eEF2K             | Eukaryotic elongation factor 2-kinase                |
| eIF-              | Eukaryotic initiation factor -                       |
| ETC               | Electron transport chain                             |
| FACS              | Fluorescence-activated cell sorting                  |
| FBS/FCS           | Fetal bovine serum (foetal calf serum)               |
| FCCP              | Carbonyl cyanide-4-(trifluoromethoxy)phenylhydrazone |
| FDR               | False discovery rate                                 |
| FKBP12            | Intracellular 12 kDa FK506-binding protein           |
| FLAG              | Peptide corresponding to sequence: DYKDDDDK          |
| FOS               | Proto-oncogene c-Fos                                 |
| GDF15             | Growth and differentiation factor 15                 |
| GDP               | Guanidine diphosphate                                |
| GO                | Gene Ontology  |
| GTP               | Guanidine triphosphate                               |
| GUK1              | Guanylate kinase 1                                   |
| HDMS <sup>E</sup> | High definition mass spectrometry                    |
| HIST1H4H          | Histone H4   |
| HIST2H2AC         | Histone H2A type 2C                                  |
| HMOX1             | Heme oxygenase 1                                     |
| HNRPQ             | Heterogeneous nuclear ribonuclear protein Q          |
| HSP6              | Hermansky-Pudlak syndrome 6                          |
| HuR               | Hu antigen R   |
| IC <sub>50</sub>  | Half maximal inhibitory concentration                |
| IDS               | Iduronate 2-Sulfatase                                |
| IgG               | Immunoglobulin G                                     |

|                       |  |
|-----------------------|--|
| IMS                   | Ion mobility spectrometry                                |
| IP                    | Immunoprecipitation                                      |
| IRES                  | Internal ribosome entry site                             |
| kDa                   | Kilodalton   |
| LAM                   | La Motif   |
| LARP1                 | La related protein 1                                     |
| LC3                   | Light Chain 3  |
| LDHA                  | Lactate dehydrogenase                                    |
| Leu                   | Leucine  |
| lncRNA                | Long non-coding RNA                                      |
| logFC                 | Logged fold change                                       |
| MALAT1                | Metastasis associated lung adenocarcinoma 1              |
| MAPK                  | Mitogen activated protein kinase                         |
| MDH                   | Malate dehydrogenase                                     |
| Mdm2                  | Mouse double-minute 2                                    |
| Met-tRNA <sub>i</sub> | Methionine-associated initiator tRNA                     |
| mLST8                 | Mammalian lethal with SEC13 protein 8                    |
| MMP                   | Matrix metalloproteinase                                 |
| mRNA                  | Messenger RNA  |
| mRNP                  | Messenger ribonucleoprotein                              |
| MS                    | Mass spectrometry  |
| mSIN1                 | Mammalian stress-activated kinase interacting protein 1  |
| mTOR                  | Mechanistic (or mammalian) target of rapamycin           |
| mTORC1                | Mechanistic (or mammalian) target of rapamycin complex 1 |
| mTORC2                | Mechanistic (or mammalian) target of rapamycin complex 2 |
| MYC                   | v-Myc Avian Myelocytomatosis Viral Oncogene Homolog      |
| ncRNA                 | Non-coding RNA   |

|                  |   |
|------------------|---|
| OCR              | Oxygen consumption rate   |
| ORF              | Open reading frame  |
| p21              | Cyclin-dependent kinase inhibitor 1                                   |
| p53              | Tumour protein p53  |
| PABP/ PABPC1     | Poly(A) binding protein / Poly(A) binding protein cytoplasmic isoform |
| PAGE             | Polyacrylamide Gel Electrophoresis                                    |
| PAR-CL           | Photoactivatable ribonucleoside cross-linking                         |
| PARP             | Poly ADP ribose polymerase  |
| PAZ              | Piwi/Argonaute/Zwille domain  |
| P-bodies         | Processing bodies   |
| PBS              | Phosphate buffered saline   |
| PCA              | principal component analysis  |
| PDCD4            | Programmed Cell Death 4   |
| PDK1             | Phosphoinositide-dependent kinase 1                                   |
| PI               | Propidium Iodide  |
| PI3K             | Phosphoinositide 3-kinase   |
| PIC              | Pre-initiation complex  |
| PIP <sub>3</sub> | Phosphatidylinositol (3,4,5)-triphosphate                             |
| PKB/Akt          | Protein Kinase B  |
| PKC- $\alpha$    | Protein Kinase C alpha  |
| PLGS             | ProteinLynx Global Server   |
| poly(A)          | poly-adenosine  |
| poly(U)          | poly-uracil   |
| PRAS40           | Proline-rich Akt substrate of 40 kDa                                  |
| PROTOR           | Protein observed with RICTOR  |
| PSF              | PTB-associated splicing factor  |
| PTBP1            | Polypyrimidine tract-binding protein 1                                |

|        |   |
|--------|---|
| PTEN   | Phosphatase and tensin homolog                            |
| PWP2   | Periodic Tryptophan protein 2 homolog                     |
| qPCR   | Quick polymerase chain reaction                           |
| RAPTOR | Regulatory associated protein of mTOR                     |
| RBD    | RNA binding domain  |
| RBP    | RNA binding protein                                       |
| RGG    | Arginine-Glycine-Glycine                                  |
| RHOV   | Ras homolog family member V                               |
| RICTOR | Rapamycin-insensitive component of mTOR                   |
| RISC   | RNA induced silencing complex                             |
| RNA    | Ribonucleic acid  |
| RP     | Ribosomal protein   |
| RPLx   | Ribosomal protein x of large subunit                      |
| RPSx   | Ribosomal protein x of small subunit                      |
| RRM    | RNA recognition motif                                     |
| rRNA   | Ribosomal RNA   |
| RT     | Reverse Transcription                                     |
| RTKs   | Receptor tyrosine kinases                                 |
| S6K    | Ribosomal protein 6 of small subunit kinase               |
| SAMM50 | Sorting and assembly machinery component 50               |
| SDS    | Sodium dodecyl sulfate                                    |
| Ser    | Serine  |
| SERBP1 | Plasminogen activator inhibitor binding protein 1         |
| SGK1   | Serum/glucocorticoid regulated kinase 1                   |
| SILAC  | Stable isotope labelling with amino acids in cell culture |
| siRNA  | Small interfering RNA                                     |
| snoRNA | Small nucleolar RNA                                       |

|              |  |
|--------------|--|
| SREBP1       | Sterol regulatory element binding protein 1          |
| SVA          | Surrogate variable analysis                          |
| TBST         | Tris-buffered saline with Tween                      |
| TEMED        | Tetramethylethylenediamine                           |
| Thr          | Threonine  |
| TIA-1        | T-cell intracellular antigen-1                       |
| TIAR         | TIA-1 related protein                                |
| TNF $\alpha$ | Tumour necrosis factor alpha                         |
| TOP          | Terminal oligopyrimidine tract                       |
| TRIM25       | Tripartite motif containing protein 25               |
| tRNA         | Transfer RNA   |
| TSC          | Tuberous sclerosis protein                           |
| TTP          | Tristetraprolin                                      |
| ULK1         | Unc-51 Like Autophagy Activating Kinase 1            |
| USP10        | Ubiquitin binding protein 10                         |
| UTR          | Untranslated region                                  |
| UV           | Ultraviolet  |
| WD40         | 40 amino acid length Tryptophan-Aspartic acid repeat |

## **1 Introduction**

This thesis aims to address the mechanisms of post-transcriptional regulation of gene expression by RNA binding proteins (RBPs) downstream of the mTOR signalling pathway. With this in mind, I will begin this chapter with an introduction to gene expression and protein synthesis, before describing how these processes can be influenced by cis-acting factors such as RNA binding proteins (RBPs). Finally, in the last part of this chapter I will outline how the mTOR pathway influences such post-transcriptional regulation, what is known about subsets of mRNAs (such as 5' TOP mRNAs) on which it exerts said influence, and how emerging technologies and mTOR targeting compounds may be used to investigate outstanding gaps in our knowledge.

### **1.1 Genes to proteins: control of gene expression**

The synthesis of proteins is fundamental to all living cells. Gene expression involves the decoding of DNA to RNA to protein, in what is termed the central dogma of molecular biology. The first key step in this process is the transcription of specific segments of genetic information from the DNA template by DNA polymerases, to generate an intermediary RNA molecule. Genes encoding a specific protein amino acid sequence are termed messenger RNA (mRNA); these molecules require further processing following transcription, outlined later in this section. However several genes simply encode an RNA product, such as ribosomal RNA (rRNA), transfer RNA (tRNA) or small nucleolar RNA (snoRNA), where each of these holds a specific function without needing to be translated into protein.

In the cases where transcription has generated a nascent pre-mRNA molecule, it is then processed, involving a series of post-transcriptional modifications including splicing of exons, the attachment of a m<sup>7</sup>G(5')pp(5')N cap structure (where N represents any nucleotide) to the 5' end of the mRNA, and also addition of a poly(A) tail to the 3' end by poly(A) polymerases. Once maturation of the mRNA is complete, it is transported to the cytoplasm from the nucleus where it was synthesised; here the recruitment of ribosomes and other factors allow it to be translated into protein during the process of translation.

A single gene may transcribe multiple copies of RNA, which in turn may be translated

many times over to synthesise identical protein molecules, thereby bringing about amplification of a response leading to an accumulation of functional proteins. Cells are able to control the process of protein synthesis according to diverse stimuli or environmental conditions, for example, through exerting control over the production of mRNA globally, or specific translational control over the sequence, life cycle or localisation of mRNA. Protein synthesis can also be regulated by external stimuli action on other proteins, a concept first formulated over 50 years ago, upon discussion of enzymatic adaptation in response to the altered abundance of a specific metabolite (Jacob & Monod 1961).

## **1.2 Eukaryotic Translation: an overview**

The decoding of the mRNA transcript into an ordered sequence of covalently bonded amino acids in a predetermined sequence is a complex and energy consuming process involving coordination of multiple key factors and complexes (reviewed by (Jackson et al. 2010; Gebauer & Hentze 2004)). Translation can be broken down into three key stages; initiation, elongation and termination, Briefly, translational initiation culminates in the recruitment of the ribosome thereby forming the 80S initiation complex at the AUG start codon, before the ribosome is able to 'read' the mRNA triplet codon in 5' to 3' direction during the phase of elongation of the polypeptide chain, ultimately reaching a termination codon which stimulated release of the polypeptide chain and the dissociation of ribosomal machinery from the mRNA.

### **1.2.1 Ribosomes**

Ribosomes are large complexes formed of 4 ribosomal RNAs (rRNAs) and around 80 ribosomal proteins (RPs) in two separate subunits known as the 40S (or small) and 60S (large) subunits in eukaryotes, designated as such according to their sedimentation under centrifugation on the Svedberg (S) scale. Each 80S ribosome is formed of one of each of these subunits in a functional complex. The 40S subunit enables the interaction between the triplet codons of the mRNA and the tRNA anticodons, whilst the large subunit contains the peptidyl-transferase region responsible for catalysing peptide bonds between amino acids in the elongating de novo protein molecule (reviewed in (Steitz 2008)). Ribosomes have been shown to contain three tRNA binding sites

(El'skaya et al. 1997) termed the amino-acyl site (A site) the peptidyl site (P site) and the exit site (E site).

Ribosomes are synthesised in the nucleolus before being exported to the cytosol, where they exist free or as a membrane-bound component of rough endoplasmic reticulum organelles. Their role in translation is essential; scanning for the initiation codon of an mRNA to commence translation, catalysing the formation of peptide bonds in nascent polypeptide during translation elongation and also hydrolysis of the final peptidyl-tRNA bond during termination (Tamura 2011). The link between the mRNA codon and the corresponding amino acid to be incorporated into the nascent polypeptide chain is provided by tRNA. Amino acids conjugated to tRNAs, known as aminoacyl-tRNAs (aa-tRNAs) are delivered in a complex to the A site (as outlined later in this chapter) as part of the ternary complex. For the 61 distinct sense codons possible on the mRNA there exist only 20 amino acids; thus synonymous codon usage across aa-tRNAs is key to the process of decoding.

Emerging evidence showing heterogeneity in ribosomes, as a result of various factors including differences in the proteins associating with ribosomal subunits under certain conditions, has led to the concept that these “specialised” ribosomes could confer specialised control over the process of translation (Xue & Barna 2012). Possible regulation of translation at the level of the ribosome is discussed further in section 1.2.5.

#### **1.2.1.1 Ribosome Biogenesis in eukaryotes**

Ribosome biogenesis is a considerably energy expensive process, which requires highly temporal and spatial coordination of factors for processing, assembly and export of each of the two ribosomal subunits. The various components of nascent ribosomes, both structural and catalytic, are transcribed by three RNA polymerases known as RNA polymerase I, II and III (Mayer & Grummt 2006). RNA polymerase I transcribes a 47S precursor rRNA in the nucleolus, which is then enzymatically processed to produce 4 mature rRNA species: 28S, 18S and 5.8S (Tschochner & Hurt 2003). The fourth rRNA component of the ribosome, 5S rRNA, is synthesised by RNA polymerase III in the

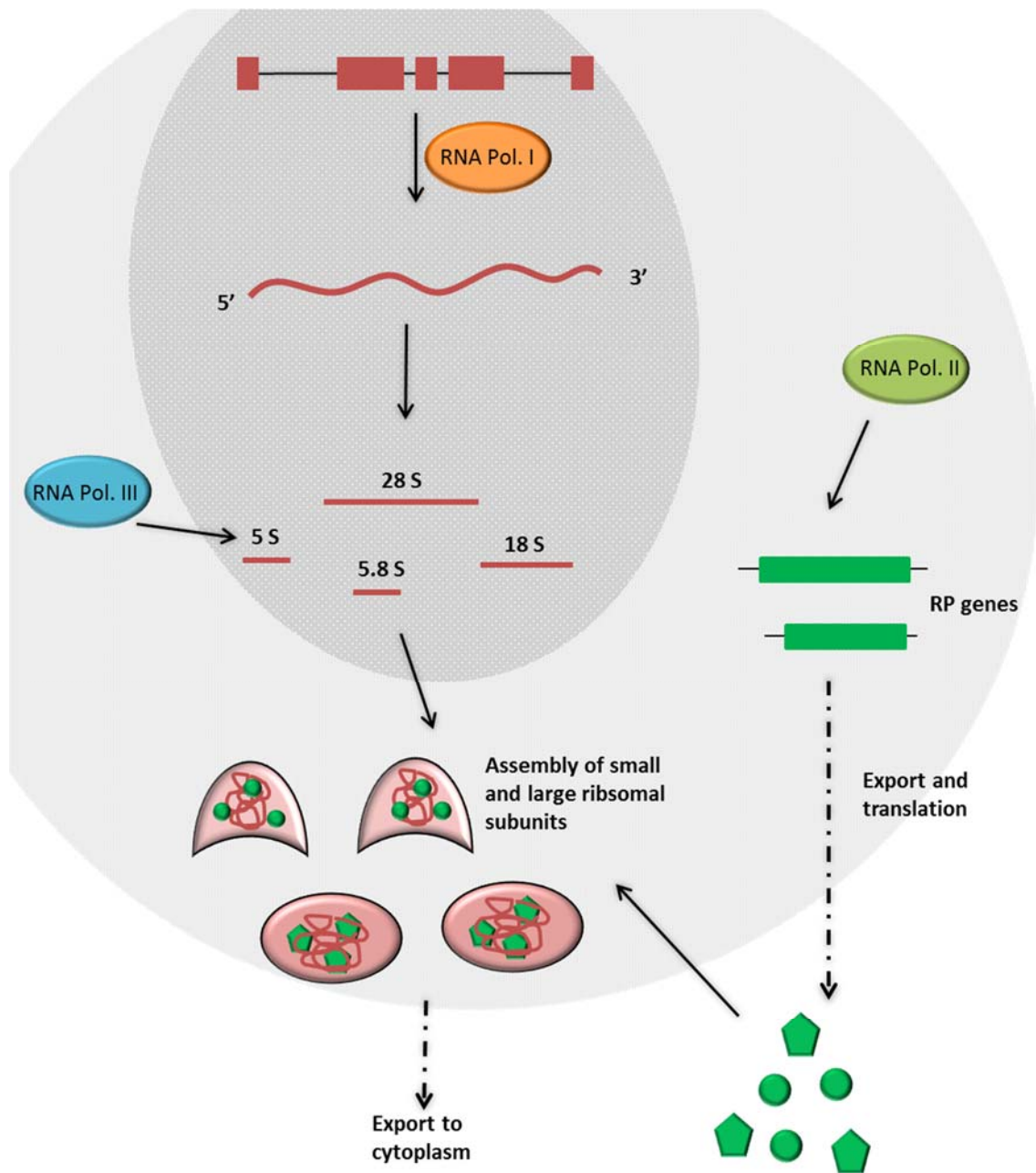


Figure 1.1 Schematic outlining key processes in ribosome biogenesis, including transcription of ribosomal RNA and ribosomal protein (RP) genes by RNA polymerases, cleavage and assembly of subunits (adapted from Jastrzebski et al. 2004)

nucleus before undergoing a series of processing steps in the cytosol, and being reimported into the nucleus before assembly can occur alongside the other three rRNA molecules (Ciganda & Williams). RNA polymerase II is responsible for the transcription of the mRNA encoding RPs, which are subsequently translated in the cytoplasm prior to re-import into the nucleus to be involved in assembly of the 40S and 60S ribosomal subunits. Once in the nucleus, the 5S, 28S and 5.8S rRNAs associate with 47 ribosomal proteins to form the large 60S subunit, whilst the 18S rRNA associates with 33 ribosomal subunits to form the 40S subunit.

Defects in ribosome biogenesis, such as those which arise due to mutations, lead to ribosomal stress and disruption of translation. Diseases arising from such defects are referred to as ribosomopathies; this includes the condition Diamond-Blackfan anaemia, a condition affecting production of erythrocytes as well as increasing the risk of certain cancers. Diamond-Blackfan anaemia has been associated with deletions or mutations in several ribosomal proteins of the small subunit, including rpS19, which has been shown to cause around a quarter of cases (Devlin et al. 2010).

#### **1.2.1.2 Ribosomal stress**

The energy demands of ribosomal biogenesis are very high, owing to the need to synthesise so many individual components prior to assembly (Granneman & Tollervey 2007). This means that any infidelities or stresses affecting this process lead to an arrest in rRNA transcription, as well as an immediate impact on global translation due to the reduction of functional ribosomes (Grummt 2013; Tafforeau et al. 2013). Furthermore a growing body of evidence indicates alterations in one or several of the steps in ribosomal biogenesis can result in oncogenesis (Golomb et al. 2014). Impaired biogenesis of either the large or small ribosomal subunit has been shown to initiate a ribosomal stress response through the upregulation of RPL11, which in turn stabilises p53 and allows for its accumulation (Fumagalli et al. 2009). This accumulation of p53 can lead to cell cycle arrest, or in cases where p53 is mutated, uncontrolled cell growth and proliferation.

### **1.2.2 Translational initiation**

The first stage of the translation of mRNA into protein, referred to as translational initiation, is a rate-limiting step, at which the most regulatory control is exerted (Sonenberg & Hinnebusch 2009; Jackson et al. 2010). Two crucial events in the initiation of cap-dependent translation are the association between the 48S pre-initiation complex with the 5' capped mRNA, and the binding of the initiator tRNA to the start codon (usually an AUG). An alternate form of translation initiation, deemed cap-independent, relies on an internal ribosome entry segment (IRES) within the 5' UTR. The complex RNA structure of the IRES allows association of the ribosome and the initiation of translation, without the requirement of scanning from the 5' end of the mRNA. In either case, the entire process is facilitated and governed by a selection of initiation factors (and in the case of cap-independent translation, *trans*-acting factors), whose availability and activation status is controlled by many signalling pathways within the cell. Here the focus will be on discussing cap-dependent translation initiation and related factors. A summary of the key eukaryotic initiation factors involved in translation initiation can be found in Table 1.1.

#### **1.2.2.1 Formation of the ternary complex**

The first step in initiation of protein synthesis is the formation of a ternary complex, comprising a GTP-bound heterotrimeric eukaryotic initiation factor 2 (eIF2), and a methionine bound initiator tRNA (Met-tRNA<sub>i</sub>). The initiating methionyl tRNA is distinct from the other 20 amino acids, and is required to be delivered to the start codon by the eIF2 complex. GDP-bound eIF2 is not able to form a complex with Met-tRNA<sub>i</sub> and must recycle it to GTP, a process catalysed by the guanine exchange factor eIF2B, before participation in further initiation cycles.

Once formed, the ternary complex associates with the 40S ribosomal subunit, the initiation factors eIF1 and eIF1A and finally a large, multi-subunit scaffolding protein, eIF3 to form the 43S pre-initiation complex. Factors eIF1 and eIF1A synergistically promote the binding of the 40S subunit at the correct AUG start codon (Pestova & Hellen 2001; Passmore et al. 2007), with eIF1A also having been shown to stabilise the binding of the ternary complex and the 40S subunit without mRNA binding (Chaudhuri et al. 1999).

| Name           | Function  |   |
|----------------|---|---|
| eIF2           | Formation of eIF2-GTP/Met-tRNA <sub>i</sub> ternary complex, mediating ribosomal recruitment of 40S subunit. GTP/GDP exchange on eIF2 mediated by eIF2B |   |
| eIF3           | Multi-subunit; binds eIF1, eIF5 and eIF4G. Enhances attachment of 43S pre-initiation complex to mRNA for start codon scanning                           |   |
| eIF1           | Promotes scanning in correct context, assembly of 43S pre-initiation complex. Activity enhanced by eIF1A  |   |
| eIF4F complex  | eIF4E   | Binds to m <sup>7</sup> GpppG 5' cap structure of mRNA, is inhibited by 4E-BPs and released following mTOR activation   |
|                | eIF4A   | ATP-dependent RNA helicase, responsible for unwinding secondary RNA structure ahead of the 43S pre-initiation complex   |
|                | eIF4G   | Scaffold protein bringing together eIF4E, eIF4A, eIF3, PABP, and mRNA. Has been shown to enhance eIF4A helicase activity, and circularise mRNA through PABP association |
| eIF4B (+eIF4H) | RBP enhancing eIF4A helicase activity   |   |
| eIF5           | GTPase activating protein, stimulates hydrolysis of eIF2-GTP upon start codon recognition   |   |
| eIF5B          | GTPase, activity mediates joining of 60S ribosomal subunit to mRNA associated 40S subunit   |   |

**Table 1.1 Summary of eukaryotic initiation factors involved in the process of translation initiation (adapted from Jackson et al., 2010)**

### **1.2.2.2 The eIF4F complex**

Eukaryotic initiation factors also play a crucial role in initiation through facilitating the recruitment of the 40S ribosomal subunit at the cap structure of the mRNA, allowing subsequent unwinding of mRNA to remove inhibitory secondary structure and thereby scanning to position at the AUG start codon. Several initiation factors have been identified to interact directly with the mRNA, their presence crucial for the progression of translation.

The interaction between the 43S pre-initiation complex and the 5' cap of the mRNA is facilitated by a heterotrimeric complex of initiation factors, known as the eIF4F complex. The eIF4F complex is comprised of eIF4G, eIF4E and eIF4A; a scaffolding protein, cap-binding protein and ATP-dependent RNA helicase respectively. In addition, the initiation factor eIF4B can contribute through enhancement of the helicase activity of eIF4A, allowing for the unwinding of any RNA secondary structures ahead of the ribosome during scanning.

### **1.2.2.3 eIF4E and its regulation by 4E-BPs**

Firstly, the 5' m7G cap is recognised by the cap-binding protein, eukaryotic initiation factor 4E (eIF4E) within the eIF4F complex. Indeed, it has been shown that the affinity of binding increases when eIF4E is greater when bound to the scaffolding protein eukaryotic initiation factor 4G (eIF4G) (Haghighat & Sonenberg 1997).

There exists in eIF4E a key point of translational regulation; its binding to the 5' m7G cap of mRNA brings it into proximity with eIF4G as part of the eIF4F complex. Its ability to interact with eIF4G is governed by a family of proteins known as the eIF4E binding proteins (4E-BPs). When hypo-phosphorylated, the 4E-BPs compete with eIF4G for binding to eIF4E, since they share a common binding site. The binding of eIF4E to its regulatory 4E-BPs thereby interfere with assembly of the eIF4F complex at the 5' cap of mRNA, preventing translation initiation (Sonenberg 1993). However phosphorylation of the 4E-BPs relieves eIF4E of their binding, and allows translation to occur through the recruitment of eIF4G. This phosphorylation is carried out downstream of active mTOR signalling, in response to mitogenic cues, outlined in greater detail in section 1.4.4.

#### **1.2.2.4 eIF4G**

Initiation factor eIF4G acts as a scaffolding protein, in particular ensuring the coordination of eIF4E and eIF4A in the cap-binding complex of eIF4F. Crucially, interactions between eIF4G and eIF3 result in recruitment of the 43S pre-initiation complex to the mRNA. Many regulatory mechanisms exist to affect translation through targeting eIF4G to thereby disrupt the formation of the eIF4F complex and ribosome recruitment. These include the cleavage of eIF4G following cellular stress, its sequestration in stress granules during heat shock, and also its phosphorylation (Morley et al. 1998; Kimball et al. 2003; Raught et al. 2000).

Furthermore, eIF4G is also able to interact with poly(A) binding protein (PABP), an evolutionarily conserved RNA binding protein with a specific affinity for the 3' poly(A) tail of mature mRNA. It is able to interact with the poly(A) tail and eIF4G concurrently, resulting in circularisation of mRNA (Kessler & Sachs 1998; Imataka et al. 1998; Gebauer & Hentze 2004). This closed-loop conformation has been postulated to provide both a platform for the influence of 3' UTR regulatory sequences on translation (Gebauer & Hentze 2004), as well as a potential mechanism for the recycling of ribosomes to promote re-initiation ((Jackson et al. 2010), supplementary information available online). Circularised mRNA in this way has already been shown to promote 40S subunit recruitment, enhancing translation initiation (Tarun & Sachs 1996; Tarun et al. 1997; Wells et al. 1998).

#### **1.2.2.5 eIF4A**

Through its function as an ATP-dependent DEAD box helicase, eIF4A stimulates translation initiation as part of the eIF4F complex, by acting to unwind any secondary structures in the 5' UTR of the mRNA that may otherwise stall ribosomes scanning for the start codon. Similarly to eIF4E, eIF4A is able to carry out its function alone; however its activity is far greater in association with the other components of the eIF4F complex, as well as another initiation factor, eIF4B (Sonenberg & Hinnebusch 2009; Korneeva et al. 2005).

Inhibition of eIF4A can occur through binding by a protein known as programmed cell death 4 (PDCD4). PDCD4 binds to eIF4A via its MA3 domain; this interaction prevents

the association of eIF4A with eIF4G, which possesses the very same domain in its C-terminus (Dorrello et al. 2006; Suzuki et al. 2008). This inhibitory effect is alleviated through phosphorylation of PDCD4 by S6 kinases downstream of active mTOR signalling at Ser<sup>67</sup>, allowing for formation of eIF4F complex and the initiation of translation (Yang et al. 2003; Dorrello et al. 2006).

#### **1.2.2.6 eIF3**

Eukaryotic initiation factor 3 (eIF3) is a large, multi-subunit initiation factor which acts as a scaffolding protein, recruiting and stabilising the interaction between the 40S subunit and the ternary complex (reviewed by (Hinnebusch 2006)). It is comprised of 13 different subunits in humans, giving the eIF3 complex itself a molecular mass of around 800 kDa. Once bound as part of the pre-initiation complex, eIF3 increases the sedimentation rate of the 40S ribosomal subunit on the Svedberg scale to 43S.

Many putative phosphorylation sites have been identified across the eIF3 subunits, though detangling the functions of the individual subunits' phosphorylations has proved challenging (Fonseca et al. 2014). However interactions between eIF3 and S6K1, a substrate of mTOR (discussed late in section 1.4.4), have been shown in the absence of amino acids or presence of rapamycin, through various co-IP experiments and m<sup>7</sup>GTP pulldown assays (Holz et al. 2005). Altogether these in vitro studies suggest a connection between eIF3, S6Ks and mTORC1 in the control of translation, though the exact physiological impact has not been elucidated as yet.

#### **1.2.2.7 Formation of the 80S initiation complex**

Following attachment of the 43S pre-initiation complex, scanning of the mRNA in a 5' to 3' direction occurs; this involves the unwinding of secondary structures ahead of the complex which would otherwise blocking its movement along the mRNA, however the exact mechanism through which this movement occurs remains unknown (reviewed in (Jackson et al. 2010)). The recognition of the correct initiation codon, in the correct context, during scanning is primarily due to eIF1. The proposed mechanism for this, also reviewed in Jackson et al. (2010), eIF1 initiates a conformational change in the 43S

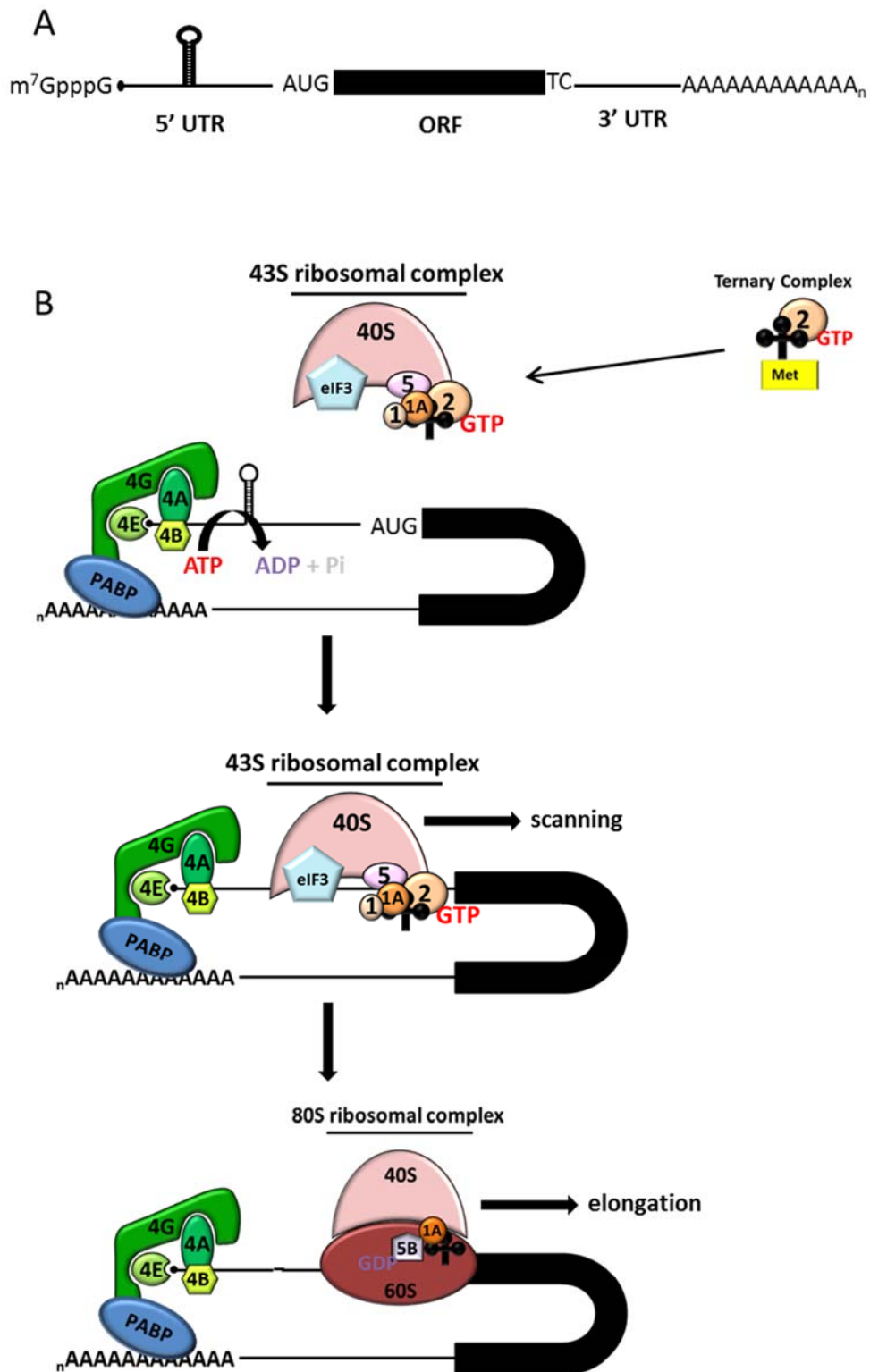


**Figure 1.2** (A) Schematic showing structure of processed mRNA, including m<sup>7</sup>GpppG cap, 5' untranslated region (UTR) containing secondary structure, AUG start codon, open reading frame (ORF), termination codon (here annotated as TC), 3' UTR and poly(A) tail. (B) Process of translation initiation (based on Gebauer and Hentze, 2004), showing key eukaryotic initiation factors, accessory factors (e.g. PABP) and complexes.

complex which strengthens the interaction between the 40S ribosome and the mRNA at the initiation codon. Once start codon recognition has successfully occurred, the 40S ribosomal subunit in conjunction with the other components of the 43S pre-initiation complex, are poised for the assembly of the full, 80S ribosome.

Formation of the 80S ribosome is the final step in translation initiation, occurring through joining of the 60S ribosomal subunit to the mRNA-bound 48S initiation complex. This occurs through hydrolysis of GTP on eIF2, as catalysed by two other initiation factors; eukaryotic initiation factor 5 (eIF5) and 5B (eIF5B) (Pestova et al. 2000). Following GTP hydrolysis on both eIF2 and eIF5B, the 60S subunit is able to join the 48S initiation complex primed on the AUG codon, and release initiation factors eIF1, eIF1A, eIF2 and eIF3. This leaves a complete 80S ribosome present on the start codon of the mRNA, ready for the next phase of translation: elongation.

### **1.2.3 Translational elongation**

After formation of the 80S initiation complex at the start codon, the ribosome translocates along the mRNA from the 5' to the 3' end, decoding the triplet codons through codon-anticodon recognition interactions between the incoming aminoacyl-tRNA molecule and the A-site codon of the mRNA. In this way, amino acids are each covalently linked one at a time to the amino acid before by the peptidyl transferase activity of the ribosome, thereby lengthening the polypeptide chain according to the sequence of the mRNA. Multiple ribosomes can be present and actively translating along a single mRNA at any one time; a cluster of several ribosomes in the process of translation, connected by a single mRNA strand, is termed a polysome.

Three eukaryotic elongation factors are involved in the elongation cycle step of translation in eukaryotes; namely eEF1A, eEF1B and eEF2. Based on their mRNA codon compatibility, aa-tRNAs are recruited to the aminoacyl site (A site) of actively elongating ribosomes by GTP-bound eEF1A. eEF1B functions as a guanine exchange factor for eEF1A, exchanging GDP for GTP to allow repetition of recruitment of tRNAs to the ribosome. The ribosome then translocates along the mRNA, so the tRNA that was in the A site sits in the peptidyl site (P site), allowing recruitment of a new aa-tRNA to the A site and formation of a peptide bond between the amino acids. Translocation

of the ribosome is promoted in a GTP-dependent manner by eukaryotic elongation factor 2 (eEF2); following translocation of the peptidyl-tRNA the adjacent deacylated tRNA transfers to the exit site (E site) and leaves the ribosome, whilst the growing polypeptide chain is extended out during synthesis through a cleft in the 60S subunit. This is a cyclical process; repeated exchange of GDP for GTP in both the process of tRNA recruitment as well as in ribosomal translocation allows for rapid repetition of these processes. As a result, the energy consumption cost during the process of translation elongation is substantial.

As a means of inhibiting this step of translation, eEF2 can be phosphorylated by the eEF2-kinase (Redpath & Proud 1993). Increasing the rate of translation through elongation phase is achieved through treatment of cells with insulin or growth-stimulating serum, which results in the dephosphorylation of eEF2 (Redpath et al. 1996). Over-expression of eEF2 is abundant in both gastric and colorectal cancers, occurring in over 90% of cases (Nakamura et al. 2009).

#### **1.2.4 Termination of translation**

Termination of translation occurs upon the arrival of the translational machinery at a termination codon; UGA, UAA or UAG, signalling the polypeptide chain is completely synthesised. These termination codons do not correspond to a specific aa-tRNA, instead their presence in the A site of the ribosome recruits two release factors; eukaryotic release factor 1 (eRF1) and eukaryotic release factor 3 (eRF3). These bind GTP forming a complex able to bind the A site, allowing the terminal aminoacyl-tRNA bond to be cleaved through GTP enabled hydrolysis, releasing the nascent polypeptide and ribosomal subunits (Jackson et al. 2012; Mugnier & Tuite 1999).

Following translation termination, it is possible for translation to re-initiate, particularly if the 40S ribosomal subunit has remained bound to the mRNA and reaches an appropriate start codon downstream (reviewed in Kozak 1992), or where mRNA have been circularised through the interaction between PABP and eIF4G, usually in cases where the 5' open reading frame (ORF) is relatively short (Jackson et al. 2012).

### **1.2.5 Regulation of translational control**

Cells' ability to differentiate between global translational control versus that of transcript-specific control is crucial for the modulation of cellular responses to various stimuli. Binding of a vast array of proteins to mRNA is one way in which the life cycle and translation of these genes can be controlled in response to such stimuli; some examples of these RNA binding proteins will be outlined in the next section of this chapter. As another example of how global and transcript-specific control of gene expression are not mutually exclusive, a subset of mRNAs termed 5' TOP mRNAs is detailed further in sections 1.4.4.1 and 1.4.4.2. In the case of these mRNAs, a global downregulation of translation in response to various conditions non-conducive to cellular growth (for example nutrient deprivation or starvation) is simultaneously coupled with increased translation of 5' TOP mRNAs.

Possible contributors to "specialised" ribosomes' modulation of gene expression (in addition to those discussed briefly in section 1.2.1) could include post-translational modifications of ribosomal subunits, or modification to less conserved rRNA sequences. The former could be of particular interest with respect to RPS6 phosphorylation by mTOR. RPS6 is located at the interface of the 40S and 60S ribosomal subunits, nearby to the binding site of the mRNA-tRNA interaction (Nygård & Nika 1982). As yet, though these phosphorylations on RPS6 are well-characterised, their precise effect has not been determined; mutational studies changing target residues to alanines did not appear to affect translation though cell growth did appear affected (Ruvinsky et al. 2005).

### **1.3 RNA binding proteins**

As described above, various stages of translation are mediated by proteins with the ability to bind mRNA, referred to as having an RNA binding protein function. Examples of RNA binding proteins (RBPs) discussed so far include PABP and eIF4G, the binding of which directly influences translation. In the following section, the roles, domains and mechanisms of action of several RBPs will be discussed in more depth, to set the scene on their role in the regulation of gene expression.

RNA binding proteins (RBPs) facilitate multiple aspects of RNA life cycle, including transport, splicing, degradation and sequestration. Furthermore, they present key players in the post-transcriptional regulation of gene expression, and therefore it is crucial that our understanding of their contributions to RNA regulation networks continues to develop. Consequently, the translation of bound messages is inevitably affected; the impact RBPs have on the expression of messages in this way means their altered activity can ultimately change the repertoire of expressed messages in a cell, allowing for modulation of reactions to stimuli such as nutrients, growth factors, toxins or drug treatment.

In the upcoming sections, I aim to discuss some existing knowledge on RNA binding proteins, providing examples where possible of several well characterised RBPs and their functions in relation to the RNA life cycle. I will also discuss some of the methodologies used for identification and investigation of this family of proteins thus far, and the insights such techniques have yielded.

### **1.3.1 RNA binding Domains and post-transcriptional modifications**

The majority of the RNA binding proteins identified over the last few decades possess classical architecture and well characterised RNA binding domains (RBDs). Initial predictions regarding the scope of RBPs within the proteome used these already identified RBDs, and indicated the existence of hundreds of RBPs (Anantharaman et al. 2002). However development of novel techniques to identify and validate RBP interactomes in various eukaryotic cell systems has led to this number expanding greatly to over 1,200, when merging data collected across human cell lines (Beckmann et al. 2015; Castello et al. 2012; Baltz et al. 2012). This increase can be largely attributed to the identification of novel RBPs which do not possess canonical RBDs, nor indeed any known associated function with respect to RNA processing and regulation.

Some of the classical, better characterised RNA-binding domains include the RNA recognition motif (RRM), DEAD or DEAH box, Zinc finger domain, the heterogeneous nuclear ribonucleoprotein K-homology domain (types I and II), Pumilio or FBF (often referred to as PUF domain), double stranded RNA binding domain, and the Piwi/Argonaute/Zwille (PAZ) domain, to name a few (Lunde et al. 2007; Glisovic et al.

2008; Castello et al. 2012). Several novel RBDs have been reported or proposed, including the tryptophan-aspartic acid 40 (WD40) repeat domain, the SAF-A/B, Acinus and PIAS (SAP) domain, and the highly disordered region formed by RRG (arginine-glycine-glycine) boxes (Castello et al. 2012; Glisovic et al. 2008); several proteins containing these domains were identified as possessing RNA binding functionality in HeLa cells by Castello et al. (2012).

RNA binding proteins can contain one or more RBD in order to provide specificity in RNA binding; PABP for example contains four RNA recognition motifs in its sequence, the multiple repeats of this one domain is believed to provide greater specificity of binding of larger target mRNA (Maris et al. 2005). RNA binding proteins often contain secondary functional domains or auxiliary domains, in addition to canonical binding domains. Such auxiliary domains can provide stabilisation through manipulation or even contact of RNA themselves in order to augment primary interactions or to provide sites for protein-protein interactions with other mRNP complex members (Biamonti & Riva 1994).

### **1.3.2 RNA binding proteins involved in RNA processing and splicing**

Removal of introns from pre-mRNA is a complex process involving many factors and the formation of spliceosome complexes, leading to cleavage at exon-intron junctions and subsequent ligation of exons within the mRNA. This gives rise to a mature mRNA, or in some cases, multiple possible mature mRNA sequences, allowing several protein isoforms from a single original gene transcript. One RNA binding protein essential for mRNA splicing is PTB-associated splicing factor (PSF), a 100 kDa nuclear protein which forms part of a key splicing complex with polypyrimidine tract-binding protein (PTBP1), required in early stages of spliceosome formation (Patton et al. 1993). PSF contains two RRM domains as well as three RGG repeats, all shown to be domains which are capable of providing RNA binding functionality, though it is the second RRM which has been shown to confer the RNA binding activity in the intact protein (Yarosh et al. 2015). In addition its amino terminus is remarkably rich in proline and glutamine residues, a property common to other RBPs and transcription factors (Patton et al. 1993). It exhibits a preferential affinity for polypyrimidine tracts, particularly poly(U), similar to its complex partner PTBP1 (Patton et al. 1991; Patton et al. 1993).

### **1.3.3 RNA binding proteins, sequestration and spatial regulation**

Messenger ribonucleoprotein (mRNP) complexes form where mRNAs become bound by proteins, in several instances forming granules allowing for the storage, localised translational control or decay of these messages. Two such types of mRNP granules in somatic cells include stress granules and cytoplasmic processing bodies (P-bodies), both dynamic complexes whose assembly is dependent on the cellular pool of non-translating mRNAs (Teixeira et al. 2005). However components of these two granules differ; in P-bodies initiation factors are generally excluded (though eIF4E and a related transported protein eIF4E-T can be present, (Andrei et al. 2005)) whereas in stress granules often eIF4E, the eIF4F complex, eIF2 and 3, PABP and the small ribosomal subunit can often be seen, following stalled translation initiation (Buchan & Parker 2009). In this section, some examples of other RBPs involved in the formation of each of these mRNPs will be discussed briefly.

T-Cell restricted intracellular antigen-1 (TIA-1) and TIA-1-related protein (TIAR) are two closely related translational repressors involved in the localisation of nascent mRNA transcripts in stress granules, following translational arrest due to cellular stresses (Kedersha et al. 1999; Damgaard & Lykke-Andersen 2011). Both TIA1 and TIAR possess 3 RRM s which allow for their mRNA binding, with the second RRM being primarily responsible for their preferential association with poly(U) stretched within the mRNA sequence whilst the other two RRM s' roles appear to be enhancing the affinity of this interaction (Dember et al. 1996). Their carboxy-terminus harbours glutamine and asparagine rich regions, which then allow for self-aggregations that ultimately result in stress granule formation. Evidence from a study by Nover et al. (1989) suggested that specific mRNA transcripts can be found in stress granules, with 'housekeeping' transcripts appearing to be sequestered, whilst other enzymes and protein chaperones involved in repair and stress responses were excluded from stress granule formation. It is possible that the transcript-specific modulation of response may be due to recruitment of specific RBPs. This has become an increasingly intriguing concept recently as one group showed that after amino acid starvation, TIA-1 and TIAR have been shown to bind the 5' end of TOP mRNAs downstream of mTOR signalling, thereby

arresting translation initiation and shifting these messages from polysomes to stress granules (Damgaard & Lykke-Andersen 2011).

#### **1.3.4 RNA binding proteins and translational control**

A prime example of RNA binding proteins involved in translational control exists in PABP. PABP contains four RRM domains for RNA binding as well as a proline-rich region at its carboxyl terminus, which is responsible for its protein-protein interactions. As outlined previously in section 1.2.4, PABP binds to the poly(A) tail at the 3' end of mature mRNA, often as it simultaneously binds the eIF4G within the eIF4F complex at its 5' end, thereby circularising the mRNA. This circularisation is believed to provide a platform for ribosome recycling and re-initiation, hence augmenting its translation. Interactions between PABP and eIF4G also help to prevent eIF4E dissociation and improve the unwinding abilities of eIF4A (Haghighat & Sonenberg 1997; Bi & Goss 2000), all of which contribute to optimising translation initiation. PABP is also able to regulate its own translation, through association with an oligoadenylate tract in the 5' UTR of its own transcripts (Deo et al. 1999), in a poly(A) tail independent mechanism of translational control.

Conversely, PABP binding has also been shown to assist in the decreased translation of messenger RNA, both through association with the RNA induced silencing complex (RISC) to enhance miRNA mediated repression of mRNA translation, as well as through recruitment of the CNOT7/GAF1 deadenylase to promote deadenylation and subsequent degradation of messages (Jinek et al. 2010). Furthermore, PABP can interact with one of the eukaryotic translation termination factors, eRF3, which appears to both prevent multimerisation of PABP as well as augmenting termination (Hoshino et al. 1999; Cosson et al. 2002).

#### **1.3.5 RNA binding proteins and metabolism**

Among the more surprising members of the expanding RBP repertoire were several metabolic enzymes with no previously documented RNA binding functionality identified in Huh-7 cells, over half of which were classed as oxidoreductases and transferases (Beckmann et al. 2015). Many of these enzymes fell under the remit of GO terms including glycolysis/gluconeogenesis, citrate cycle, pyruvate or glutathione

metabolism and oxidative phosphorylation: all key components of carbon metabolism central to cellular energy metabolism. In this study it was postulated that these enzyme-RBPs may have a secondary function in translational regulation, or on the other hand, could in fact be regulated themselves by RNA binding, for example in the context of providing an allosteric competitor for their usual substrates, or as scaffolds to enable localisation within a cell (Beckmann et al. 2015). This recent development in RNA biology could provide an entirely separate facet to the function of RNA binding proteins in modulating cellular responses, either alongside or outside of gene expression.

### **1.3.6 RNA binding proteins and RNA decay**

RNA binding proteins can offer roles in both stabilisation and decay of mRNA transcripts; an example of each will be discussed briefly in this section in Hu antigen R (HuR, also known as ELAVL1) and tristetraprolin (TTP) respectively.

HuR is the only ubiquitously expressed member of the Hu/elav family of RBPs which also includes the neuronally expressed HuB, HuC and HuD (Hinman & Lou 2008). HuR binding has many functions with respect to the mRNAs to which it binds, including stabilisation (discussed here), translational repression and translational upregulation. Its RNA binding is mediated via three RRM; target mRNAs usually possess uridine or AU-rich elements in their 3' UTR, though mRNAs possessing the same properties in the 5' UTR have also been shown to be bound by HuR (Meng et al. 2005). A large number of mRNAs have been shown to be targets of HuR stabilisation, including several involved in cancer such as p21, eIF4E, Mdm2, Bcl-2 and MMP9 (Srikantan & Gorospe 2012). The method by which HuR stabilises these transcripts remains unrevealed, though it is possible that its binding simply protects the mRNA from decay via allosteric inhibition of other RBPs which would otherwise mediate RNA degradation.

Tristetraprolin (TTP) was named for the three repeats of four prolines in its sequence, and is a member of a family of proteins referred to as the TIS11 family of RNA binding proteins (Lai et al., 1990). TTP binds adenylate and uridylylate rich element (ARE) sequences present in the 3' UTR of mRNAs, via two zinc finger domains, thereby targeting these mRNA for degradation (Lai et al. 2000). This degradation has been

shown to primarily be a result of TTP recruitment of the deadenylase complex CCR4/CNOT1, leading to deadenylation of the ARE-containing mRNA, ultimately leading to its rapid decay. It can be found localised in both P-bodies and stress granules, making it less clear whether the degradation of ARE-containing mRNAs is strictly governed by TTP binding; however the dynamic nature of these complexes as discussed earlier implies exchange of TTP-bound mRNA is likely dependent on stimulus (Sanduja et al. 2011).

### **1.3.7 Disease states arising from RNA binding protein dysregulation**

Aberrant RBP activity or expression has also been implicated as a causative factor of various disease states, including cancer, metabolic and neurological pathologies (Darnell 2010; Norris & Calarco 2012; Srikantan & Gorospe 2012). Many such conditions specifically arise from defects in tightly controlled events such as pre-mRNA splicing or translation initiation where the imbalance in specific proteins' abundance or activation status can lead to severe consequences, though the established connection between ribosomal stress and p53 activation also provides a potential contribution to several ribosomopathies.

Examples include Diamond-Blackfan Anaemia (DBA), a ribosomopathy discussed earlier in section 1.2.1.2 resulting from mutations in several ribosomal proteins including RPL5, RPL11, RPS17 and most frequently RPS19. Another class of disorders highly related to mutations in RBPs are those of a neurological nature; according to one study by Castello et al. (2013) 59 RBPs were linked to hereditary neurological conditions, including leukoencephalopathy with vanishing white matter.

### **1.3.8 Methodologies for identification of cellular RNA binding proteins**

Numerous approaches have been employed with the aim of better characterising RNA binding protein-RNA interactions, RNA binding domains and functions. Initial computational predictions through the use of *in silico* algorithms were used to identify RNA binding proteins based on the homology of known RNA binding domains (Anantharaman et al. 2002); however this has since been shown to have identified only a very limited part of the RBP network. Two early experimental approaches adopted included the hybridisation of purified *Saccharomyces cerevisiae* proteome with

fluorophore labelled mRNAs in a large screen; between these two groups over 200 RNA binding proteins were identified (Tsvetanova et al. 2010; Scherrer et al. 2010). Alternative methodologies include the use of stable isotope labelling by amino acids in culture (SILAC) and subsequent mass spectrometry to identify RNA binding proteins bound *in vitro* to immobilised RNA probes (Butter et al. 2009). This process captured more abundant RBPs already characterised, but also failed to exclude indirect protein-protein interaction or non-physiological binding of RBPs to RNA.

Recent studies have provided a deeper insight into the extent of RNA binding protein networks previously undiscovered, including the development of a technique enabling the live capture and isolation of RBPs in contact with stretches of poly(A) RNA, such as the 3' poly(A) tail, in eukaryotic cells (Castello, Horos, et al. 2013). This technique utilised ultraviolet light at a wavelength of 254 nm to covalently crosslink proteins in direct contact with RNA, thereby capturing real time physiological interactions between RBPs and their targets. This wavelength of UV crosslinks nucleotides only with amino acids which they are in direct contact with; it does not allow for protein-protein crosslinking.

Following lysis and purification of polyadenylated RNA using oligo(dT) beads, and wash buffers sufficiently stringent as to eliminate any proteins associated in a non-covalent manner, mRNA-RBP complexes solely were thereby purified. Digestion of the RNA in these complexes using a cocktail of RNases leaves behind the interactome of RNA binding proteins, which can be identified using label-free mass spectrometry techniques. A similar technique was used by other groups, as well as in parallel by Castello, Horos, et al. (2013) in development of the whole cell RBP interactome capture mentioned earlier. This involved the pre-incorporation of RNA with photoactivatable-ribonucleoside crosslinking (PAR-CL) using UV at 365 nm, and subsequent SILAC mass spectrometry (Baltz et al. 2012; Castello, Horos, et al. 2013). Both techniques yielded identified RBP datasets of similar sizes with large overlap as well as unique RBPs to each study; this was not greatly surprising though considering the differing chemistries between techniques, as well as the consideration that one

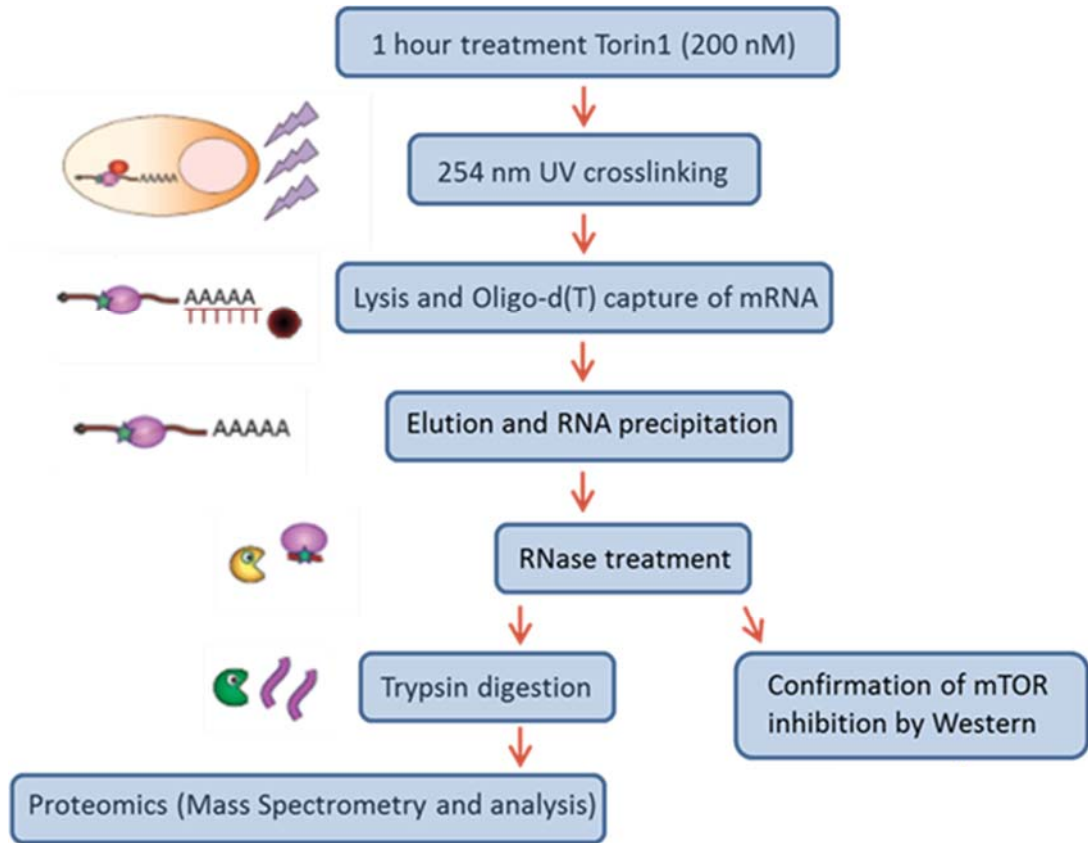


Figure 1.3 Workflow for whole cell RBP interactome capture in conjunction with mTOR inhibition, as used in this study. (Adapted from Castello et al., 2013)

study was performed in HEK293 cells and another in HeLa cells. Ultimately however, the use of conventional UV crosslinking at 254 nm was as powerful and yet more straightforward than PAR-CL.

This methodology has been applied to various cell types to date in order to expand the known repertoire of RBPs. As mentioned previously, HEK293 and HeLa cells, both human cell lines, provided the start point for this field of investigations in RNA biology. It has also since been applied to mouse embryonic stem cells (Kwon et al. 2013), *Saccharomyces cerevisiae*, and human Huh-7 cells (Beckmann et al. 2015), to name a few. Merging the data acquired from each of these systems has helped to identify more conserved RBPs, as well as those across a variety of human cell lines.

#### **1.4 Signalling cascades and signal transduction**

Cells are able to respond to external stimuli such as mitogens or nutrients through the activation of intracellular signalling pathways, sometimes (but not exclusively) through an intermediary receptor protein on the cell surface. Proteins perform many basic yet indispensable roles in intra- or extracellular signal communication; transduction of this signal to effector proteins such as translational machinery, metabolic enzymes, or transcription factors (among many others) relies on a successive relay of signalling proteins. Furthermore, proteins are also often responsible for molecular transport through pumps and channels within membranes, enzymatic reactions, metabolism and cellular structure.

Signal transduction within a cell is often achieved through the joining of multiple proteins in order to form a functional complex, or through regulation of catalytic activity of enzymes and conformation of proteins via post-translational modifications. Such modifications usually include the covalent addition or removal of a small molecule to specific amino acid side chains within the polypeptide chain, such as an acetyl- or methyl- group, or most frequently a phosphate group. Such a modification is termed “phosphorylation”, and imposes a novel negative charge upon the protein. Generally these modifications cause an alteration in activity or association, thereby providing an element of control on the receiving protein.

During a phosphorylation reaction, the terminal phosphate is enzymatically cleaved from an ATP molecule, before being transferred and covalently linked to the hydroxyl group on a serine, threonine or tyrosine residue on the target protein. The added negative charge provides a point of attraction and potential interaction with positively charged amino acid side chains of other proteins, allowing for binding of ligands and altering a protein's overall activity. Proteins responsible for attaching phosphate groups to other proteins as a means of changing their catalytic activity, interacting partners or conformation so as to ultimately initiate a signalling cascade are termed kinases. De-phosphorylation, or the removal of phosphate modifications on a protein, is carried out by proteins termed phosphatases. This is equally as important in cellular signalling; it provides a rapid means to terminate or regulate the duration and intensity of a signal. Together, the interplay between kinase and phosphatase activity within a cell drive the regulated switching on and off of different proteins' activities, as well as the enabling or terminating of interactions between different proteins within complexes and pathways.

#### **1.4.1 Kinases vs phosphatases**

Kinases are one of the largest eukaryotic gene families, and are further sub-classified according to the target amino acid residues to which they attach the phosphate group (Manning et al. 2002). They therefore fall into one of three categories; the largest is serine/threonine kinases, followed by tyrosine kinases and then the smallest group, tyrosine-kinase like kinases. For some proteins, a single phosphorylation allows for complete transfer to an active state, with specific downstream substrates. However, the requirement for integration of signals from multiple signalling pathways, as a result of various stimuli or specific criteria being met, is managed in some proteins through a complex series of phosphorylations and other modifications at multiple sites by various upstream effectors. Such proteins can require a specific "barcode" of site modifications, possibly in a specific sequence, so that they can meet their full activated state potential.

#### **1.4.2 The mammalian target of rapamycin signalling**

The mammalian or mechanistic target of rapamycin (mTOR) is a serine/threonine kinase which exists in two key complexes; mTOR complex 1 and mTOR complex 2

(mTORC1 and mTORC2 respectively). Though these two complexes are comprised certain shared protein components, they also contain unique proteins which contribute to their individual roles and distinct substrates. Shared components include mammalian lethal with SEC13 protein 8 (mLST8) and dishevelled, Egl-10, pleckstrin-domain-containing mTOR interacting protein (DEPTOR), which are common to both complexes. mTORC1 also contains the following unique proteins: regulatory associated protein of mTOR (RAPTOR), the substrate competitor proline-rich Akt substrate of 40 kDa (PRAS40), whilst mTORC2 alone harbours the rapamycin-insensitive component of TOR (RICTOR), protein observed with RICTOR (PROTOR) and mammalian stress-activated kinase interacting protein 1 (mSIN1).

Of the two complexes, mTORC1 is the better characterised due to its increased sensitivity to the bacterial macrolide rapamycin, whereas mTORC2 activity is only affected by rapamycin following chronic treatment at higher doses (Sarbasov et al. 2006). This rapamycin sensitivity is governed by the formation of a complex between rapamycin and the intracellular 12 kDa FK506-binding protein (FKBP12), which then binds and inhibits mTOR predominantly when part of mTORC1 rather than mTORC2 (Laplante & Sabatini 2012a). The mechanism for this inhibition is not fully understood at the biochemical level, however it could be as a result of steric hindrance of the interaction between RAPTOR and mTOR (Chen et al. 1995; Kim et al. 2002), negative impact on structural integrity or kinase specificity (Laplante & Sabatini 2012a).

mTOR functions as a master regulator of cellular growth and proliferation, which it achieves through the integration of diverse intracellular and extracellular energy cues, phosphorylation of substrates and ultimately the control of anabolic and catabolic processes such as mRNA translation, lipid synthesis and autophagy (reviewed in Fonseca et al. 2014; Laplante & Sabatini 2009; Alers et al. 2012). The difference in composition between the two complexes determines the substrate specificity and downstream functions; mTORC1 mainly regulates translation, synthesis of various RNAs including ribosomal RNA and transfer RNA (both of which are crucial constituents

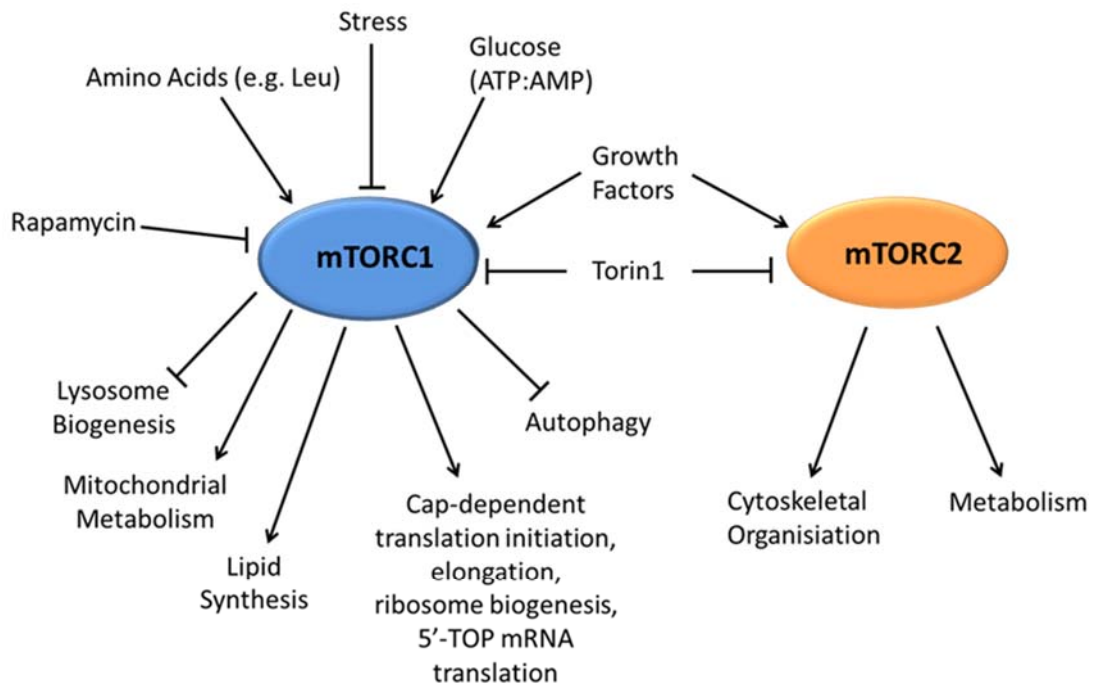


Figure 1.4 Overview of roles of mTORC1 and mTOR2, including positive and negative stimuli specific to each of the complexes.

of translational machinery as discussed earlier), as well as lipid biogenesis, ribosomal protein and initiation factor synthesis and autophagy (protein recycling). Conversely, mTORC2 regulates aspects of cell survival and cytoskeletal arrangement (Sarbasov et al. 2004).

As a kinase, the key mechanism by which mTORC1 and mTORC2 exert their control over the downstream processes discussed here is through phosphorylations of target residues on effector proteins. In the next section, I aim to outline some key aspects of the mTOR signal transduction network, as well as how it relates to the input of growth signals and the output of cellular growth and proliferation, amongst other functions.

### **1.4.3 mTOR activation and signal transduction**

A wide range of stimuli have been shown to contribute to mTORC1 and mTORC2 activation. Most notably, growth factors, nutrient and amino acid availability, high ATP: AMP ratios, oxygen availability, inflammatory cytokines (e.g. tumour necrosis factor  $\alpha$ , or TNF $\alpha$ ) and hormones have all been shown to influence this signalling pathway. Inhibitory stimuli also play a part in this signalling pathway; hypoxia, cell stress and conditions non-conducive to growth (e.g. nutrient deprivation, amino acid starvation) all acts to inhibit mTOR signalling. Often, the balance of mTOR signalling is struck from integration of multiple inputs altogether in order to modulate cellular growth.

Growth factors and hormones (e.g. insulin) stimulate mTOR pathway signalling via binding and activating receptor tyrosine kinases (RTKs) at the cell membrane, promoting auto-phosphorylation and activation of phosphoinositide 3-kinase (PI3K). This results in production of phosphatidylinositol (3,4,5)-triphosphate (PIP<sub>3</sub>), which activates Akt/Protein Kinase B (PKB) signalling. Akt is also directly activated by mTORC2 through phosphorylation at Ser<sup>473</sup>, along with two other kinases of the same family; SGK1 and PKC- $\alpha$ , the latter of which is involved in mTORC2 mediated cytoskeletal rearrangement (Sarbasov et al. 2004; Sarbasov et al. 2005). mTORC2 is responsive to growth factors in order to achieve this Akt activation, but the knowledge of this relationship is poorly understood (Laplane & Sabatini 2012b).

Akt acts in two ways to drive mTORC1 phosphorylation; firstly through inhibition of PRAS40 interaction with mTORC1 and secondly through the inactivation by phosphorylation of the tuberous sclerosis complex (TSC, comprised TSC1 and 2). TSC1/2 acts as a GTPase activating protein (GAP) for a GTPase known as Rheb. Under active mTOR signalling, the inactivity of TSC1/2 allows Rheb to strongly stimulate mTORC1 kinase activity upon association with the complex. In an inactive mTOR network, the conversion of Rheb to its inactive form following interaction with TSC1/2 prevents this from occurring (Laplante & Sabatini 2013). mTORC2 can also be activated through stimulation by growth factors, however little is known about this aspect of mTOR signalling. TSC1/2 can also be phosphorylated and inhibited by activated adenosine monophosphate-activated protein kinase (AMPK), in response to glucose or a high ATP:AMP ratio in cells (Laplante & Sabatini 2012b).

Amino acids (and their availability) are fundamental to the activation of mTORC1, acting entirely independently of TSC1/2 (Smith et al. 2005). The sensory mechanism through which cells are able to detect amino acids has been partially described recently (Sancak et al., 2010), shown to involve the Rag GTPases; and four Rag proteins, RagA to RagD. In the presence of amino acids, the mTORC1 complex translocates to the lysosomal membrane, where it is able to dock through association between the RAPTOR subunit and the multi-subunit complex referred to as Ragulator, itself associated with Rag proteins (Sancak et al. 2010). However, much regarding mTOR signal transduction downstream of amino acid sensing remains to be elucidated.

#### **1.4.4 mTOR regulation of translation**

mTORC1 possesses two key, well-characterised targets responsible for transduction of growth signals in the cell. The first of these, which were among the first mTOR targets discovered, are the 4E-BPs (Hara et al. 1997). As mentioned earlier in section 1.2.2.4, these translational repressors are responsible for binding eIF4E and thereby preventing its association with the 7-methylguanosine cap structure localised at the 5' terminus of mRNAs, consequently halting translation initiation. Four key phosphorylations of 4E-BPs must occur to result in the release of eIF4E and before translation initiation can commence, in the following specific sequence; Thr<sup>46</sup>, Thr<sup>37</sup>, Thr<sup>70</sup> and finally Ser<sup>65</sup> (Gingras et al. 2001; Herbert et al. 2002). These residues are

conserved in all three 4E-BP family members (Tee & Proud 2002). These phosphorylations occur downstream of active mTORC1, following stimulation with various growth stimuli including growth factors, hormones such as insulin and amino acid availability. Interestingly however, despite rapamycin preferentially inhibiting mTORC1 activity, treatment with this inhibitor is not sufficient to prevent phosphorylation of most of these residues (Gingras et al. 2001), only strongly inhibiting that of serine 65.

Due to their prime position in the control of cellular proliferation and growth downstream of mTORC1, 4E-BPs present a key point of oncogenic transformation, making them and mTOR activity upstream highly clinically relevant. A cohort of mRNAs possessing long, structured 5' UTRs have recently been termed "eIF4E-sensitive" mRNAs, and include those encoding several pro-oncogenic, pro-survival proteins. Among these are c-Myc, cyclins, MMPs and angiogenesis related proteins (Nandagopal & Roux 2015). Their "sensitivity" stems from their requirement for eIF4A helicase activity, unwinding secondary structures that may form in the UTR, and as a consequence, their increased sensitivity to eIF4E levels (Nandagopal & Roux 2015).

The second integral and highly studied targets of mTORC1 in the context of translation are the ribosomal S6 kinases (S6Ks or RPS6Ks). This family of kinases are so named as their main target of phosphorylation is the ribosomal protein S6 (S6 or RPS6), a constituent of the small ribosomal subunit. Two genes have been discovered encoding for RPS6Ks; *rps6kb1* and *rps6kb*, each of which encodes two protein isoforms, as a result of alternative splicing and use of differential start codons. These isoforms are the P70 and P85 isoforms of S6K1 in addition to the P54 and P60 isoforms of S6K2 (Coffer & Woodgett 1994; Lee-Fruman et al. 1999); the longer isoforms in each case possess a nuclear localisation signal, however P70S6K is predominantly cytoplasmic. As a working example in this text I will describe the function of this isoform in particular, referring to it as either S6K or RPS6K, since the regulation of the four isoforms' activity is fairly conserved (Jastrzebski et al. 2007).

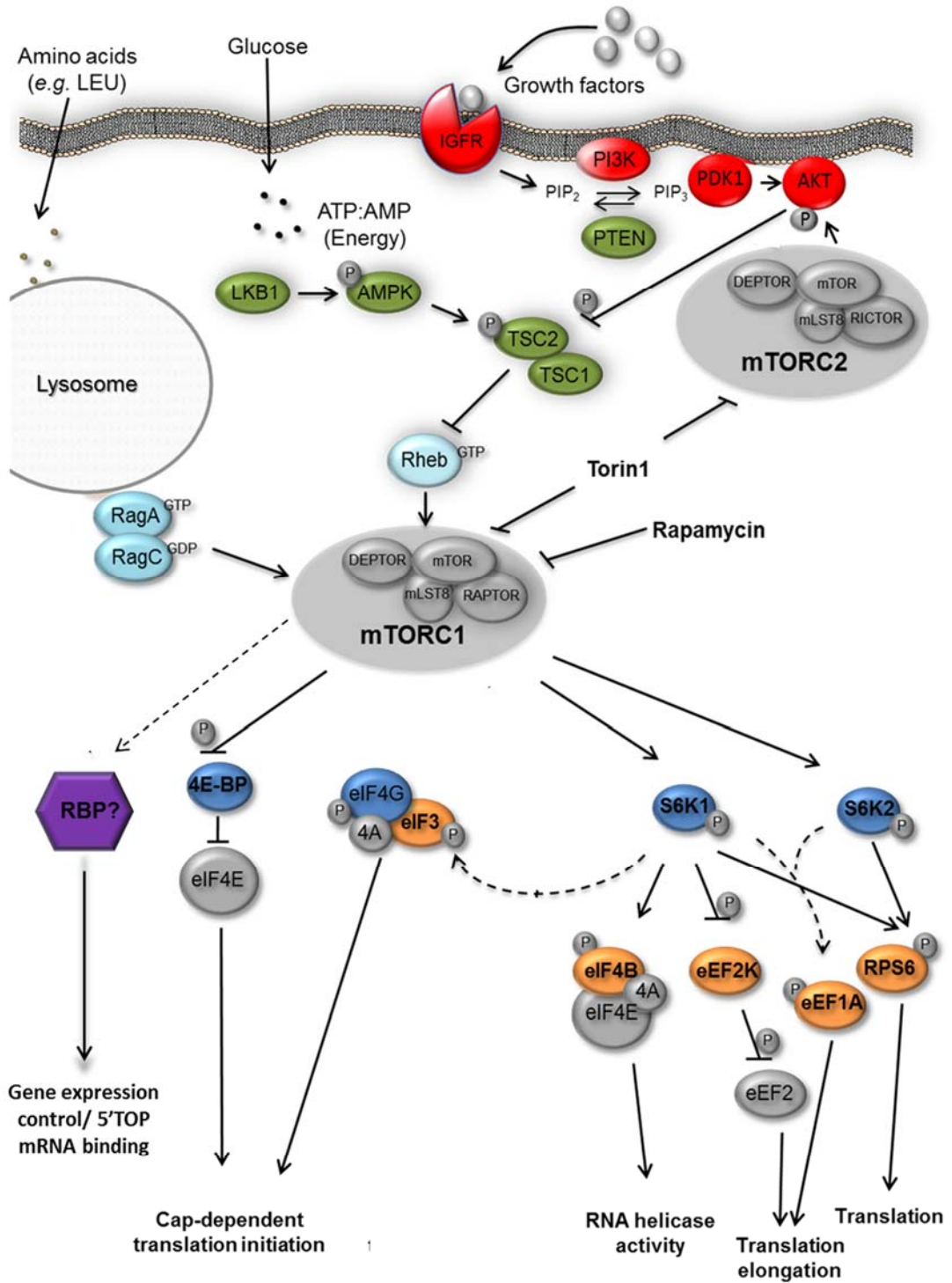


Figure 1.5 Overview of the mTOR signalling pathway (adapted from Fonseca et al., 2014), and key stimuli initiating mTOR activation and phosphorylation of downstream substrates, including S6K and 4E-BP. This study aims to investigate potential RBP targets of mTOR that function as intermediary factors to regulate 5' TOP mRNA expression.

S6K1, like 4E-BPs, is phosphorylated at multiple residues in a hierarchical way; firstly by an unidentified proline directed kinase (or kinases) at Ser<sup>411/418</sup>, Thr<sup>421</sup> and Ser<sup>424</sup> before phosphorylation of Ser<sup>371</sup>, Thr<sup>389</sup> by mTORC1 and finally Thr<sup>229</sup> (Mukhopadhyay et al. 1992). As well as phosphorylation of RPS6, S6Ks are responsible for the phosphorylation of several other proteins involved in translation at varying stages of the process; including eIF3, eIF4B, PDCD4, many of which were discussed to some extent earlier in this chapter, and elongation factors eEF1A/B and eEF2K, which will be discussed later in this section.

S6Ks phosphorylate several serine residues at the C-terminal end of RPS6, including Ser<sup>235/236</sup>, Ser<sup>240/244</sup> and Ser<sup>247</sup> (Krieg et al. 1988) downstream of active mTORC1 signalling; however to this date the exact function of these phosphorylations remains undetermined. S6Ks have been linked to modulation of a specific subset of mRNAs downstream of mTOR referred to as 5' TOP mRNAs, discussed in greater detail in sections 1.4.4.1 and 1.4.4.2.

Another mechanism through which mTORC1 has a direct impact on translation through S6K1 is the phosphorylation of eEF2K, which impact directly on the translocation activity of eEF2 and therefore the rate of translational elongation. Active mTORC1, for example as a result of growth factors, reduces eEF2 phosphorylation by phosphorylating eEF2K; this has been proposed to promote ribosomal interaction and enhance translation, though this model is yet to be confirmed (Wang et al. 2001).

#### **1.4.4.1 5' Terminal Oligopyrimidine mRNAs**

The 5' TOP motif has been identified in several messages encoding components of translational machinery, including all ribosomal proteins, several elongation factors including eEF2, some factors involved in ribosome biogenesis and also PABP (Fonseca et al. 2015; Meyuhas 2000). It is believed that the presence of this string of C and U residues within a subset of mRNAs encoding key translational apparatus may provide a translational regulation mechanism for cells to better regulate growth. Defining features of the 5' TOP motif include the presence of a cytosine (C) residue after the 5' m<sup>7</sup>G cap structure, followed by an uninterrupted stretch of 4 to 14 pyrimidines, usually comprised of an almost equal proportion of cytosine to uracil residues (Meyuhas

2000). Other common features of 5' TOP mRNAs include GC rich sequences succeeding the TOP motif, and frequently a short UTR.

Early experiments looking at RNAs encoding ribosomal subunits found that these messages were highly sensitive to nutrient deprivation; in growing cells, these messages are loaded with ribosomes and translated at maximal efficiency, whereas under starved or mTOR inhibited conditions they were shown to dissociate from polysomes rapidly, to non-translating populations under these conditions (Jefferies et al. 1997; Geyer et al. 1982; reviewed in Hornstein et al. 2001). Follow up experiments from this led to the revelation of the key TOP motif common the 5' UTRs of these messages (Yamashita et al. 2008).

#### **1.4.4.2 Regulation of 5' TOP message translation by mTOR**

Two studies first connected the regulation of TOP mRNA expression with mTOR signalling pathway, demonstrating how treatment of cells with rapamycin decreased their expression (Jefferies et al. 1994; Terada et al. 1994). Later, Meyuhas and colleagues connected other known mTOR stimuli including amino acid availability and insulin treatment with the stimulation of TOP mRNA expression (Meyuhas 2000). Recent large transcriptome scale ribosome profiling studies have confirmed the sensitivity of TOP mRNA translation to mTOR inhibitors, though no further detail on the exact mechanism came to light alongside (Hsieh et al. 2012; Thoreen et al. 2012). Specifically, their studies showed that depletion of 4E-BPs conferred resistance of TOP regulation to the effects of mTORC1 inhibition; however other groups have recently shown evidence that it may not be quite so exclusively down to 4E-BP activity (Miloslavski et al. 2014).

In addition to the stimulation of ribosomal protein translation directly via 4E-BP and S6K regulation stimulating 5' TOP mRNA translation, the activation of S6K by mTORC1 leads to increased activity of RNA polymerases I and III. As a consequence, cells are able to increase synthesis of ribosomal RNA (rRNA) and transfer RNA (tRNA), both of which are essential contributors to the process of de novo protein synthesis, and thereby cell growth (reviewed in Laplante & Sabatini 2013).

#### **1.4.5 mTOR and metabolism**

As well as its role in control of cellular growth through regulation of de novo protein synthesis, mTOR has recently been shown to have a key role in the biosynthesis of lipids, an integral part of cell membranes, cell signalling molecules and as a source of energy (reviewed in Laplante & Sabatini 2009). Insulin is one of the key stimuli for activating mTOR, initiating its activation through upstream PI3K and Akt. This leads to increased uptake of glucose, which can be converted to fatty acids for storage as lipids. In addition to this conversion strategy, it also leads to the increased transcription of genes involved in the de novo synthesis of lipids via the sterol regulatory element binding protein 1 (SREBP1) transcription factor (Laplante & Sabatini 2009).

#### **1.4.6 mTOR and autophagy**

In addition to the anabolic role of mTOR in the synthesis of new proteins, it also influences catabolic processes such as autophagy. Autophagy is the controlled degradation of excess or damaged cellular proteins and organelles in order to recycle their components, generally initiated under conditions of nutrient deprivation but also during cellular processes such as differentiation, development and multiple disease states including cancer (reviewed in Mowers et al. 2016). The key signalling kinase in mammals integrating autophagy with mTOR signalling is a serine/threonine kinase, ULK1; in cases of mTOR activation an inhibitory phosphorylation on ULK1 leads to suppression of autophagy downstream, whereas inactive mTOR is unable to phosphorylate ULK and therefore allows it to form a complex with phosphorylated Atg13 and the scaffold protein FIP200 (Akers et al. 2012).

This complex then translocates to the membrane of a pre-autophagosome, thereby initiating the biogenesis of the autophagosome alongside a second multi-subunit complex referred to as Class III complex (Akers et al. 2012). The full autophagosome is then formed through recruitment of other complexes, including LC3-B, which is formed from a cleaved, lipidated protein Light Chain 3 (LC3), and attached to the membrane of the autophagosome (Kabeya et al. 2000; Wu et al. 2006). Once formed, the autophagosome sequesters cytoplasmic contents, including proteins for recycling, and fuses with a lysosome to encourage degradation. Therefore, mTOR is upstream of degradation processes allowing for the internal supply of amino acids, glucose and

other nutrients, in conditions where these are sensed to be low in order to prolong cell survival and direct these constituents into the most vital of biosynthetic and metabolic pathways.

#### **1.4.7 mTOR signalling and disease**

mTOR signalling can become dysregulated in a variety of human diseases, including type 2 diabetes, cancer and neurodegeneration (Laplante & Sabatini 2012a); its influence in such a variety of ailments attributed to its central role in cellular homeostasis and growth control. Dysregulation of this pathway can occur at points both upstream and downstream of mTORC1 and mTORC2; mutations in PTEN are highly frequent in cancers, and form part of the phosphoinositide cycle, opposing PI3K. Increased signalling by PI3K has been shown to drive mTORC1-independent mechanisms of cell survival and proliferation such as Akt and mitogen-activated protein kinase (MAPK) (O'Reilly et al. 2006; Carracedo et al. 2008). Therefore in addition to these mutations often hyper-stimulating growth and proliferation to oncogenic proportions, they are often highly difficult to target with inhibitors due to the activation of feedback loops that allow cells to overcome the inhibition.

Downstream of mTORC1, mutations in eIF4E results in an uncontrolled activation of cap-dependent translation, and subsequently cell growth, cell cycle progression and proliferation (Dowling et al. 2010). In particular, it is believed that eIF4E may exacerbate this through the specific upregulation of particular transcripts, including those encoding pro-oncogenic proteins such as MMP9, Bcl-2, c-Myc and cell cycle proteins (Laplante & Sabatini 2012a). Similarly, with the ultimate consequence of S6K activation being an increase in cell growth, this second target of mTOR has potential roles in oncogenic progression, for example through driving lipid biosynthetic processes for anabolism of cell membranes, and inhibiting autophagy to drive accumulation of damaged or mutated proteins, thereby driving tumour progression (reviewed in Laplante & Sabatini 2012a).

#### **1.4.8 Development of kinase inhibitors**

Considering the range of diseases associated with the deregulation of mTOR signalling, the clinical relevance of mTOR inhibitors is evident. Rapamycin, a compound

synthesised by the bacterium *Streptomyces hygroscopicus*, was the first discovered direct inhibitor of mTORC1 activity. It has been indispensable in its use to delineate the roles of this specific complex in mTOR signalling as a whole, due to the afore-described differential sensitivity of each complex to its activity.

Rapamycin was originally used to inhibit the mammalian immune response, then later as its ability to inhibit cellular proliferation was discovered, interest shifted to use as an anti-cancer therapeutic. It does invoke several substantial side effects, including increased susceptibility to infection, mucositis and dermatological disorders, adverse effects on fertility, adverse gastrointestinal reactions and impairment of several metabolic functions. In cases where these side effects are outweighed by the potential success of treatment, such as in cancer and transplant patients, many of these side effects are considered against potential benefits and rapamycin is therefore used as a treatment. However in terms of use as preventative treatment, these side effects are not considered acceptable.

Several analogs of rapamycin (termed “rapalogs”) have been developed, including everolimus and temsirolimus, with mildly improved pharmacokinetics. Their use has been extended within a similar remit to rapamycin, but generally the results of such compounds have been disappointing. More recently, focus has shifted to development of a different class of mTOR inhibitors, namely those which inhibit both complexes and also dual PI3K/mTOR inhibitors such as PI-103. An example of the former is Torin1, an ATP-competitive mTORC1 and mTORC2 inhibitor developed by Thoreen et al. (2009), the compound used in this study. Torin1 has been shown to suppress both mTORC1 and 2 activity without impacting PI3K in an off-target manner, having a strong impact on cell growth, cap-dependent translation and autophagy (Feldman et al. 2009; Thoreen et al. 2009). It has also been shown to have a comparable effect to rapamycin on the phosphorylation of mTOR substrates S6Ks, RPS6 and an even greater effect on phosphorylation of 4E-BP1 (Thoreen et al. 2009).

#### **1.4.9 Therapeutic relevance of mTOR inhibitors**

Development of therapeutics to inhibit mRNA translation, specifically initiation, has been emerging as a more selective means to target aberrant translation.

Unsurprisingly, global inhibition of protein synthesis through indiscriminately targeting the elongation step of translation, targets healthy cells in addition to cancerous tissue, leading to a wealth of toxic side effects (Malina et al. 2012). Development of compounds which act via targets such as eIF4E, the 4E-BPs or indeed the mTOR pathway and substrates, by ultimately controlling 4E recruitment into the eIF4F initiation complex, is currently being considered as an approach to bypass these issues.

Rapamycin analogs (or rapalogs), such as temsirolimus and everolimus, have been approved for use in treatment of certain cancers; however the side effects from such treatments can be severe. Furthermore, resistance has been shown to occur in many cancers through feedback and activation of the PI3K signalling pathway, and subsequent elevation of cellular MYC levels (M. Yu et al. 2011). Consequently, the clinical relevance of development of inhibitors such as ATP-competitive kinase inhibitor Torin1 has been far more promising, as mentioned previously; it targets both mTOR signalling complexes. In addition, its inhibition of this signalling pathway is notably more efficient at preventing activation of eIF4E and inhibiting translation initiation, with fewer off-target effects as determined by kinase screening (Thoreen et al. 2009; Feldman et al. 2009). In addition to reduced side effects, the heightened specificity of compounds such as Torin1 has the potential to further the understanding of mTOR signalling and its targets, and their roles in disease.

### **1.5 Project aims**

This introduction has outlined the process through which gene expression leads to the synthesis of nascent proteins, and how this process is regulated both directly, via the mTOR pathway, as well as through trans-acting factors in RBPs. Following the recent development of the whole cell RBP interactome capture methodology by Castello, Horos, et al. (2013), and its application across various cell lines and species, the appreciation of how extensively RBP networks modulate post-transcriptional control continues to grow rapidly. Unidentified effector molecules downstream of mTOR signalling are likely to be responsible for the continuing mystery of precisely how these kinases control the translation of subsets of genes including 5' TOP mRNAs.

The work in this thesis focuses on elucidating whether these effector molecules downstream of mTOR are in fact RNA binding proteins, and their relevance to translation and translational control. In Chapter 3, through adaptation of the interactome capture technique, applied in conjunction with Torin1 treatment, we aim to identify and validate RBPs showing differential binding following inhibition of the mTOR pathway. Following validation of mTOR dependent RNA binding proteins, depletion studies outlined in Chapter 4 proceed with characterisation of these proteins' cellular functions, before finally in Chapter 5 where work begins to determine which mRNAs these RBPs bind and possible impacts this binding may have on cellular functions such as metabolism.

**Chapter 2 –**  
**Materials and**  
**Methods**

## 2. Materials and Methods

### 2.1. Buffers and Solutions

Unless otherwise specified, all chemicals used in solutions were purchased from Sigma Aldrich or Thermo Fisher Scientific.

#### **Resolving buffer (to make 1L)**

|                 |        |
|-----------------|--------|
| 1.5M Tris pH8.8 | 181.6g |
| 0.25% TEMED     | 2.5ml  |
| 1% SDS          | 10g    |

#### **Stacking buffer (to make 1L)**

|                  |       |
|------------------|-------|
| 0.25M Tris pH6.8 | 30.2g |
| 0.12% TEMED      | 1.2ml |
| 0.2% SDS         | 2g    |

#### **10X SDS PAGE running buffer (to make 1L)**

|            |        |
|------------|--------|
| Tris pH8.3 | 30.25g |
| Glycine    | 144g   |
| SDS        | 10g    |

#### **10X Transfer buffer (to make 1L)**

|         |      |
|---------|------|
| Tris    | 30g  |
| Glycine | 144g |

#### **TBST (to make 10L)**

|             |              |
|-------------|--------------|
| 1M Tris pH8 | 100ml (10mM) |
| Tween 20    | 10ml         |
| NaCl        | 90g (150mM)  |

## **Western sample buffer (5X)**

62.5 mM Tris HCl pH 7.5

7% (w/v) SDS

20% (w/v) sucrose

0.01% (w/v) Bromophenol Blue

(+5% BME on day of use)

## **2.2. Cell culture techniques**

### **2.2.1. General cell culture**

HeLa, A549, U2OS, and HEK293 cell lines were all cultured in Dulbecco's Modified Eagles Medium (DMEM, GIBCO Cat #41966) supplemented with 10% Foetal Bovine Serum (FBS) and 1% L-Glutamine. H1299 stably-transfected doxycycline-inducible cell lines were generously gifted by Patricia Muller, and cultured in DMEM supplemented with 10% tetracycline-free FBS and 1% L-Glutamine. Induction of p53 vectors' gene expression was achieved through the addition of 1 $\mu$ g/ml doxycycline to culture media prior to other treatments. MCF10A cells were cultured in DMEM/F12 (GIBCO) supplemented with 5% horse serum, 1% L-Glutamine, 500 ng/ml hydrocortisone, 10 ng/ml cholera toxin and 20 ng/ml human recombinant EGF (Peprotech, USA).

All cell lines were passaged routinely every 3 to 5 days, and cultured in humidified conditions at 37°C with 5% CO<sub>2</sub>.

### **2.2.2. siRNA transfections**

Silencer RNA (siRNA) transfections were performed using Dharmafect 1, 2 or 4 (Dharmacon Cat # T-2001-03, T-2002-03 and T-2004-03 respectively) and OptiMEM + GlutaMAX (GIBCO Cat # 11058) at various seeding densities, dependent on cell type. Negative control siRNA used in all cases was ON-TARGETplus non-targeting siRNA #3 (Thermo Scientific, D-001810-30). siRNA against LARP1, SERBP1, PWP2, TRIM25 and PABPC1 were all silencer select siRNAs (Ambion, applied bio, Cat # s23665, s25142,

s11609, s15206, and s25665 respectively) used at 5 nM in all cases. An siRNA targeting p53 was custom ordered from Eurofins, Luxembourg; used at a final concentration of 20 nM (sequence: (+)5'-GACUCCAGUGGUAUUCUAC(dTdT)-3', (-)5'-GUAGAUUACCACUGGAGUC(dTdT)-3'). All cell lines were reverse transfected with the exception of doxycycline-inducible H1299 cell lines, which were forward transfected 24 hours after plating and/or induction of expression vectors as described.

### **2.2.3. Growth curves and cell counting**

HeLa cells were seeded at 40,000 cells per well in a 6 well plate in 5 ml media, reverse transfected in triplicate. At indicated times post-transfection cells were harvested, removing and keeping media from each well, followed by washing each well in 2 ml cold PBS, adding each wash to the harvested media. Cells were trypsinised using 0.5 ml 1x Trypsin EDTA per well and incubating at 37°C for 5 minutes. Equal volumes of media were added per well, pipetted up and down thrice to detach and resuspend all cells, and the full 1 ml added to the respective falcon tube of culture media and PBS wash. This was conducted in order to ensure all cells were harvested and counted, including those which had detached from the plate. Cells were spun down at 1500 x g for 4 minutes, and media aspirated. Cell pellet from each falcon tube was thoroughly resuspended in 1 ml of fresh media, from which 100 µl was taken and added to 10 ml CASY ton (Roche, Cat # 05 651 808 001) and cell number counted using the CASY® Model TT cell counter and analyser (Roche Innovatis). The remaining cells for each condition were pooled and resuspended in 900 µl PBS. Where used for FACS, this was split further: 500 µl was taken for protein analysis by SDS-PAGE (see 2.3.2) and the remaining 400 µl used for FACS and split equally between analyses (see 2.1.5). Otherwise, the entire remaining 900 µl was used for protein analysis by SDS-PAGE.

### **2.2.4. FACS analysis**

For analysis of apoptosis, cells were diluted 1 in 5 in 1x Annexin Buffer (10 mM HEPES/NaOH pH 7.4, 5 mM KCl, 1 mM MgCl<sub>2</sub>, 1.8 mM CaCl<sub>2</sub>, 150 mM NaCl) in 5 ml FACS tubes (Polystyrene Round-Bottom tube with cell strainer cap, Falcon Cat # 352235) on ice. 1µl/ml of Annexin V-FITC dye (Bender Med Systems, UK), diluted 1 in 5, was added to each tube and incubated for 15 minutes in the dark, at room temperature. 1 µl DRAQ7 dye (Abcam, Cat # ab109202) was subsequently added,

tubes were placed on ice and fluorescence measured using BD FACS Canto II (BD Biosciences, San Jose, USA).

Cell-cycle analysis was carried out through first fixing the cells in ice-cold 70% ethanol: 30% PBS, added dropwise while vortexing vigorously, and incubated overnight at 4°C. Following this, cells were washed in chilled PBS and stained with 10ug/ml propidium iodide (PI) in PBS, with 0.1 mg/ml RNase A for 2 hours at 4°C. Cells were left at 37°C for 30 mins prior to FACS analysis, where incorporation of PI was measured using the 488 nm laser on the BD FACSCanto II. For each condition 10,000 cells were measured.

### **2.2.5. Microscopy to assess cell morphology**

10x magnification Phase Contrast images of siRNA transfected cells were captured using the Zeiss Axiovert 200 M Microscope (Carl Zeiss, UK) at 48 and 72 hours post-transfection. A minimum of three images per condition were captured (one per well); the position of the well captured was chosen manually, at random, and a representative image selected from these for figures.

## **2.3. RNA techniques**

### **2.3.1. RNA extraction**

RNA extraction and purification was conducted using Trizol reagent (Invitrogen Cat # 15596 -018) as per manufacturers' instructions. In brief, 1 ml of Trizol was added to each cell pellet and incubated at room temperature for 5 minutes, before 200µl of chloroform was added. Tubes were shaken vigorously for 1 minute before being incubated for a further two minutes at room temperature. Samples were subsequently centrifuged at 11,200 r.p.m. for 20 minutes at 4°C. The aqueous layer was transferred to fresh, labelled Eppendorf tube and 2 µl glycogen and 750 µl isopropanol were added before vortexing and leaving to incubate at room temperature for 10 minutes. Tubes were then centrifuged at 11,200 r.p.m. for 15 minutes, and supernatant removed carefully without disturbing the pellet. 1 ml 75% ethanol was added; tubes were vortexed and centrifuged at 7,500 x g for 5 minutes at 4°C. Supernatants were discarded and pellet left to air dry briefly before resuspension in 100 µl nuclease free H<sub>2</sub>O.

100  $\mu$ l of 1:1 acid phenol-chloroform was added to each tube, before vortexing and centrifuging at 11,200 r.p.m. for 15 minutes at 4°C. Aqueous phases were transferred to fresh pre-labelled Eppendorf tubes, and 2  $\mu$ l glycogen 0.1x volume Sodium Acetate (pH 5.2) and 2.5 volumes of absolute ethanol was added before the tubes were inverted and placed in -80°C freezer overnight to aid precipitation. Following this, samples were centrifuged at 11,200 r.p.m for 15 minutes at 4°C to pellet RNA before being re-suspended in a suitable volume of ddH<sub>2</sub>O. RNA concentration was quantified using a NanoDrop 2000 UV-Vis Spectrophotometer (LabTech) as per manufacturer's instructions.

### 2.3.2. RT-qPCR with SybrGreen

Reverse transcription (RT) reactions were achieved using 200 ng of total RNA, or in the case of co-IP experiments, equal volumes of elution or pulldown samples along with equal concentrations of RNA across input conditions. Following necessary dilutions of RNA, RT reactions were achieved using a SuperScript III reverse transcriptase kit (Life Technologies, Cat # 18080044), a prepared mix of dNTPs (Life Technologies, Cat # 10216018, 10218014, 10217016, 10219012) and random primers (Invitrogen, Cat # 48190-011) to generate cDNA template. RNase inhibitor RNasin Plus was added (Promega, Cat # N2611) to minimise RNA degradation during the RT reaction.

A 1x reaction mix is outlined below:

|                                       |             |
|---------------------------------------|-------------|
| RNA (+H <sub>2</sub> O where diluted) | 5 $\mu$ l   |
| Nuclease free H <sub>2</sub> O        | 6 $\mu$ l   |
| Random primers (250 ng)               | 0.5 $\mu$ l |
| dNTPs (10 mM)                         | 0.5 $\mu$ l |
| 5x First Strand Buffer                | 4 $\mu$ l   |
| RNasin Plus RNase inhibitor           | 1 $\mu$ l   |
| DTT                                   | 1 $\mu$ l   |
| SuperScript® III                      | 1 $\mu$ l   |

5 µl cDNA generated from the RT reaction provided the template for qPCR, using gene specific primers for which a list of sequences can be found in Table 2. Primers were used at a final concentration of 250 nM in qPCR, in a final volume of 20 µl per well in a MicroAmp® Fast 96 well Reaction Plate (Life Tech, Cat # 4346907) with 10 µl SYBR™ Green Master Mix (Life Tech, Applied Bio, Cat # 4385612).

| Gene             | Forward Primer (5'-3')     | Reverse Primer (5'-3')    |
|------------------|----------------------------|---------------------------|
| <b>ACHY</b>      | CCCTCAACATGCTTCTGGACGA     | AACTTGCTCTTGGTGACGG       |
| <b>BCL7C</b>     | TCGGAAGGTTCCCTGCAAAA       | GCTCCTCCTTGGTCAGCATT      |
| <b>CYBA</b>      | TTTGGTGCCTACTCCATTGTGG     | AGGACGGCCCCGAACATAGTA     |
| <b>EEF2</b>      | CGTGCCATCACTCAACCATAA      | CTCCGGACTCTGGAAATAAATATTG |
| <b>EIF4A1</b>    | Gifted by Dr A. Wilczynska |                           |
| <b>FOS</b>       | TTGCCTAACCGCCACGATGA       | AGAAGTCCTGCGCGTTGACA      |
| <b>GDF15</b>     | GATACTCACGCCAGAAGTGCG      | TCACGTCCCACGACCTTGA       |
| <b>GUK</b>       | GGCGTCTCTGAGGAAATCA        | CCCAGGATGTTCCAACCACA      |
| <b>HIST1H4H</b>  | CCAAACGCAAGACCGTGACA       | TGCAGCAAGCAGGAGCCTTA      |
| <b>HIST2H2AC</b> | GGCTCGGGACAACAAGAAGA       | AGAACGGCCTGGATGTTAGG      |
| <b>HMOX1</b>     | TTCAAGCAGCTCTACCGCTC       | GGGGCAGAATCTTGCACTTT      |
| <b>IDS</b>       | CCAACTCGACCACAGATGCT       | GCCAGTGAGGAAAGAAACGC      |
| <b>LDHA</b>      | Gifted by Dr E. Smith      |                           |
| <b>MALAT1</b>    | GCTCTGTGGTGTGGGATTGA       | GTGGCAAAATGGCGGACTTT      |
| <b>MDH2</b>      | TCGGCCCAGAACAATGCTAA       | TTTCACAGCGGCTTTGGTCT      |
| <b>MYC</b>       | TACAACACCCGAGCAAGGAC       | GAGGCTGCTGGTTTTCCACT      |
| <b>SAMM50</b>    | ACTGTCAAGTGGGAAGGCGT       | GATGACCATGGCGTGCGAAA      |

**Table 2 - List of qPCR primers used in this study**

Unless otherwise stated, the fold-change in expression between control and conditions was calculated using the  $\Delta$ CT method of normalisation. Statistical significance of fold change values for qPCR was calculated using the paired, two tailed student's t-test, expressed as a p-value.

### **2.3.3. Sucrose Gradient Polysome Profiling**

#### **2.3.3.1. Preparation of Gradients**

Stocks of sucrose solutions were prepared to varying concentrations (w/v): 10%, 20%, 30%, 40% and 50% through the addition of 5ml 10X Gradient Buffer (1.5M NaCl, 150mM MgCl<sub>2</sub>, 150mM Tris-HCl pH 7.5, 1 mg/ml cycloheximide, 10 mg/ml heparin, 0.2 µm filtered) to 5, 10, 15, 20 or 25g sucrose respectively, made up to a final volume of 50 ml with RNase free water.

Clean Sorvall 12ml Polyallomer tubes (Cat # 03699) were used for the preparation of gradients; 2.1 ml of 50% sucrose was added first before covering with Parafilm® (Sigma, Cat # BR701605) and placing tubes in -80°C freezer for approximately 30 minutes. Once frozen, a layer of 2.1ml 40% sucrose was placed on top before replacing the tubes at -80°C. This layering process was repeated in decreasing concentrations of sucrose for each level, keeping the tops of tubes covered. Once established, gradients were stored at -20°C until the day prior to use; at this stage the required number were placed overnight at 4°C to equilibrate.

### **2.3.3.2. Harvesting cells**

Cells were plated in 10 cm dishes to achieve 70-80% confluence after 24 hours. Media of plated cells was spiked with cycloheximide to a final concentration 100 µg/ml, and incubated at 37°C for a further 3 minutes before being placed on ice. Cells were scraped in media, collected in pre-chilled 50 ml falcon tubes and then plates were scraped again in an additional 5 ml ice cold PBS-CHX per dish, added to corresponding falcon tubes and centrifuged at 1400 r.p.m. for 5 minutes at 4°C. Supernatant was removed; pellets resuspended in 1 ml ice cold PBS-CHX and transferred to pre-labelled pre-chilled 1.5 ml Eppendorf tubes, before centrifugation at 13,000 r.p.m. for 1 minute at 4°C. Once again supernatant was removed and pellets resuspended in 400 µl of 1X lysis buffer by very gentle pipetting. Following centrifugation at 13,000 r.p.m. for another minute the supernatant was transferred to a fresh pre-labelled Eppendorf; 100 µl was taken for protein normalisation and SDS-PAGE, the other 300 µl was kept on ice until ready to load on the gradient.

### **2.3.3.3. Gradient Running**

Once supernatant was loaded on gradient, weights of tubes were balanced to each other to <0.01g difference or better using 1X lysis buffer. Gradients were placed in pre-cooled buckets, attached to a pre-cooled ultra-centrifuge rotor and centrifuged at 38,000 r.p.m. for 2 hours at 4°C (acceleration 9, deceleration 6) (Thermo Scientific). Following fractionation, gradient were loaded onto a gradient density fractionation system (Presearch, UK), and a solution of blue 65% sucrose was pumped into the bottom of the gradient at a rate of 1 ml/min (KD Scientific), resulting in displacement of lysate sample through a UA-6 UV/Vis detector measuring the absorbance at 254 nm

wavelength. Fractions were collected in pre-labelled 14 ml Polypropylene Round-Bottom tubes (Falcon, Cat # 352059) containing 3 ml 7.7M guanidine hydrochloride at minute intervals, using Foxy Jr fraction collector (Teledyne Isco).

#### **2.3.3.4. RNA precipitation following Polysome profiling**

Once fractions were collected, 4 ml absolute ethanol was added to each tube, vortexed thoroughly and samples stored overnight at -20°C. After precipitation, samples were centrifuged at 4,000 r.p.m. for 45 minutes at 4°C, the supernatants aspirated; pellets resuspended in 400 µl nuclease free H<sub>2</sub>O and vortexed. Samples were left to equilibrate for 2 minutes before transfer to fresh, pre-labelled Eppendorf tubes. Next, 40 µl 3M sodium acetate (pH 5.2) and 1 ml absolute ethanol were added, before storage at -20°C overnight. Following precipitation samples were centrifuged at 13,000 r.p.m. for 30 minutes at 4°C, supernatant aspirated and pellet washed in 800 µl ice cold 75% ethanol. This step was followed by a 10 minute centrifuge at 13,000 r.p.m. at 4°C, all supernatant and residual ethanol aspirated and pellet air dried for 2 minutes in Eppendorf tubes, before resuspension in 22 µl nuclease free H<sub>2</sub>O.

Half this volume was taken from each fraction and pooled according to the traces from gradient running into “sub-polysomal” and “polysomal” fractions. To these an equal volume of filtered 5M lithium chloride was added before the samples were precipitated overnight at 4°C. Samples were then centrifuged at 13,000 r.p.m. for 30 minutes at 4°C, supernatant aspirated and pellet washed in 75% ethanol. Samples were vortexed and left at room temperature for 2 minutes before centrifugation once again at 13,000 r.p.m. for 10 minutes at 4°C.

### **2.4. Protein techniques**

#### **2.4.1. Sonication and Normalisation of protein by Bradford**

Cell pellets were lysed in RIPA buffer (20 mM Tris HCl pH 7.5, 150 mM NaCl, 15 mM MgCl<sub>2</sub>, 0.5% NP40, 1 mM EDTA, made up with H<sub>2</sub>O and filtered through a 0.2 µm filter. On day of use, 1 cOmplete EDTA free protease inhibitor cocktail tablet, 1:1000 1 M NaF and 1:1000 1 M β-glycerophosphate were added) and pulse sonicated for 5 minutes in an ice slurry water bath. Lysates were then left on ice for 30 minutes, before being centrifuged for 15 minutes at 13,000 r.p.m in a 4°C centrifuge for clarification.

Supernatants were then taken and quantified by Bradford reagent (BIO-RAD, as per manufacturer's instructions). Unless otherwise stated, protein samples were normalised to the sample with the weakest absorbance using the same lysis buffer as were harvested in, and 30 µl normalised lysate loaded per well of SDS-PAGE gels.

#### **2.4.2. SDS-Polyacrylamide Gel Electrophoresis (SDS-PAGE) and Transfer**

Normalised protein lysates were separated by SDS-PAGE using the Bio-Rad Protean II mini-gel system; resolving gel compositions are available in Table 3 and in all cases were cast to 1.5 mm thickness. Once set, wells were cast above SDS-PAGE running gel using stacking gel (3.6 ml H<sub>2</sub>O, 5 ml 2X Stacking Buffer, 1.34 ml Acrylamide (30%, PROTOGEL Cat # A2-0072), 100 µl APS and 6 µl TEMED), using casting combs as per manufacturer's instructions.

Following SDS-PAGE proteins were transferred by wet transfer in the Bio-Rad Protean II mini-gel system, set up according to manufacturer's instructions. One volume 10X Transfer buffer (see section 2.1) was added to two volumes methanol, diluted to 1X with H<sub>2</sub>O and chilled before use. With the exception of 8% gels, transfer was over a 1 hour 30 minute period at a 0.25 A current. 8% gels were transferred at 65 V for 2 hours 30 minutes.

| Components            | 8% Gel | 10% Gel | 12% Gel | 15% Gel |
|-----------------------|--------|---------|---------|---------|
| Water (ml)            | 4.6    | 4.0     | 3.3     | 2.3     |
| Resolving Buffer (ml) | 2.5    | 2.5     | 2.5     | 2.5     |
| Acrylamide (30%) (ml) | 2.7    | 3.3     | 4.0     | 5       |
| 10% APS ( $\mu$ l)    | 100    | 100     | 100     | 100     |
| TEMED ( $\mu$ l)      | 6      | 6       | 6       | 6       |

**Table 3 - Composition of SDS-PAGE running gels used for western blotting (recipe for Resolving buffer can be found in section 2.1).**

### 2.4.3. Western Blotting

Membranes were blocked to minimise background signal using 5% Milk in TBS-Tween before incubation overnight at 4°C in primary antibody. A list of antibodies, suppliers and respective dilutions can be found in Table 4. Where stated, primary antibodies were detected through incubation with ECL™ anti-Rabbit IgG Horseradish Peroxidase (HRP) conjugated secondary (GE Healthcare, NA934V), and developed using Clarity Electrochemical luminescence; in all other cases IR-dye-labelled secondary antibodies (LI-COR) were used and detected through scanning on a LI-COR laser based image detector, prior to analysis using Image Studio software (v.2.1). In both cases, secondary antibodies were diluted 1:10,000 in 5% Milk-TBS-Tween incubating for 1 hour at room temperature.

| Target                    | Supplier            | Catalogue number | Species raised in |
|---------------------------|---------------------|------------------|-------------------|
| <b>α-tubulin</b>          | Abnova              | H00007277-M01    | Mouse             |
| <b>Bcl-2</b>              | Santa Cruz          | 2870             | Rabbit            |
| <b>β-tubulin</b>          | Santa Cruz          | Sc-9104          | Rabbit            |
| <b>Histone H3</b>         | Abcam               | Ab1791           | Rabbit            |
| <b>HNRPQ</b>              | Abcam               | Ab10687          | Mouse             |
| <b>LARP1</b>              | Abcam               | Ab86359          | Rabbit            |
| <b>LC3B</b>               | Cell Signalling     | #2775            | Rabbit            |
| <b>LDHA</b>               | Cell Signalling     | #3582            | Rabbit            |
| <b>MDH</b>                | Abcam               | Ab181873         | Rabbit            |
| <b>P(Thr389)-P70S6K</b>   | Cell Signalling     | #9234            | Rabbit            |
| <b>P(Ser15)-p53</b>       | Cell Signalling     | #9284            | Rabbit            |
| <b>P(Ser240/244)-RPS6</b> | Cell Signalling     | #2215            | Rabbit            |
| <b>P(Ser473)-AKT</b>      | Cell Signalling     | #4060            | Rabbit            |
| <b>PABPC1</b>             | Simon Morley (gift) | -                | Rabbit            |
| <b>PARP</b>               | Cell Signalling     | #9542            | Rabbit            |
| <b>PSF</b>                | Santa Cruz          | Sc-101137        | Mouse             |
| <b>PTBP1</b>              | Willis Lab (gift)   | -                | Rabbit            |
| <b>PWP2</b>               | Atlas Antibodies    | HPA024573        | Rabbit            |
| <b>SERBP1</b>             | Bethyl Laboratories | A303-938A        | Rabbit            |
| <b>Total 4E-BP1</b>       | Cell Signalling     | #9644            | Rabbit            |
| <b>Total p21</b>          | Santa Cruz          | sc-397           | Rabbit            |
| <b>Total p53</b>          | Santa Cruz          | sc-126           | Rabbit            |
| <b>Total P70S6K</b>       | Cell Signalling     | #2708            | Rabbit            |
| <b>Total RPS6</b>         | Cell Signalling     | #2217            | Rabbit            |
| <b>TRIM25</b>             | Abcam               | ab167154         | Rabbit            |
| <b>USP10</b>              | Cell Signalling     | #5553            | Rabbit            |

**Table 4 - List of primary antibodies and suppliers used in western blotting in this study**

**2.4.4. Whole Cell RNA Binding Protein Interactome Capture**

15 cm plates were seeded with  $1.75 \times 10^6$  HeLa cells (equal number of plates per condition) in a total volume of 16 ml DMEM media (supplemented as described in section 2.2.1). 24 hours after seeding, media was further supplemented with an additional 2% FBS and 1% L-Glutamine per plate and returned to incubator. 30 minutes later cells were treated with a final concentration of 200 nM Torin1 (Tocris Biosciences) or equal volume of dimethyl sulphoxide (DMSO) control, before returning to the incubator for 1 hour.

Plates were aspirated and washed twice with 8ml ice-cold PBS, then aspirated dry. Plates were placed two at a time, lids removed, in a UV cross-linker on ice and exposed to  $150 \text{ mJ/cm}^2$  UVC (254 nm). 2 ml Lysis Buffer (20 mM Tris pH 7.4, 500 mM LiCl, 0.5% LiDS, 1 mM EDTA all filtered, plus 5 mM DTT and 1 x cComplete protease inhibitor cocktail tablet added fresh on day of use) was used per plate, scraped thoroughly with a cell scraper and pooled according to condition into 50 ml falcon tubes. Lysates were then passed through a 21G needle 10 times each, and left to equilibrate with end over end rotation at room temperature for 10 minutes. Meanwhile 500  $\mu\text{l}$  magnetic oligo(dT)<sub>25</sub> beads (NEB, Cat # S1419S) were aliquoted per 2 ml Eppendorf tube, washed in 750  $\mu\text{l}$  lysis buffer and left to equilibrate with end over end rotation at room temperature for 5 minutes. Lysates in falcon tubes were briefly spun down following equilibration, and 1.9 ml added to each 2 ml tube containing equilibrated beads. Lysates were incubated for 1 hour and 15 minutes with end over end rotation.

Using a magnetic rack, beads were separated from supernatant, which was discarded. Beads were then subjected to a series of wash steps in two different wash buffers, each with end over end rotation for the duration of the wash; wash buffer 1 (20 mM Tris pH 7.4, 500 mM LiCl, 0.1% LiDS, 1 mM EDTA, plus 5 mM DTT added fresh on day of use) for two 10 minute washes, and wash buffer 2 (20 mM Tris pH 7.4, 200 mM LiCl, 1 mM EDTA) for two 5 minute washes. Between each wash tubes were very briefly spun down, beads were separated using magnetic racks and supernatant discarded.

Following the last supernatant removal tubes were spun down a second time briefly, returned to magnetic racks and the final drops of wash buffer two removed.

Beads were then resuspended gently in 0.5 ml LS buffer (Tris pH 7.4, 200 mM LiCl, 1 mM EDTA) and incubated for 5 minutes standing at room temperature before removal of buffer using a magnetic rack. Beads were briefly centrifuged and replaced on magnetic rack to remove residual LS buffer. Beads were then resuspended in 60  $\mu$ l elution buffer (20 mM Tris pH 7.4, 1 mM EDTA) per tube using a cut off tip, and incubated at 92°C for 4 minutes shaking at 450 r.p.m. Tube were then immediately placed on the magnetic rack and supernatants removed and pooled into a fresh pre-labelled 2 ml tube.

A second round of elution was conducted by pooling remaining beads into one or two tubes through 25  $\mu$ l per original tube elution buffer transfer, using a cut off tip to minimise loss or shearing damage to beads. The elution step was repeated and supernatant removed and pooled with the first elution. RNA concentration was then measured using a NanoDrop 2000 UV-Vis Spectrophotometer (LabTech).

RNA was then precipitated through addition of 40  $\mu$ g glycogen (Roche, Cat # 10901393001), 10% volume Sodium acetate pH 5.2, vortexed and 3x volume of 100% ethanol, before precipitation overnight at -80°C. RNA was then pelleted through a 1 hour centrifugation at 13,000 r.p.m. at 4°C. Pellet was washed in 70% ethanol, air dried and resuspended in 60  $\mu$ l elution buffer with added 1 mM MgCl<sub>2</sub>. Following this, 5  $\mu$ l Benzonase (Sigma 250 U/ $\mu$ l) and 4  $\mu$ l 30,000 U RNase I (Ambion) were added to each tube and incubated for 2 hours at 37°C to digest RNA. Inputs were also digested for the purposes of western blots; 90  $\mu$ l was taken from the input set aside pre-pulldown, and to it 2 volumes of elution buffer (+ 1 mM MgCl<sub>2</sub>) was added, before addition of RNase I and /Benzonase as for pulldown samples.

Digested Inputs and pulldown samples were then checked for mTOR inhibition through SDS-PAGE western blotting for mTOR signalling pathway substrates, and where the experiment was to be used for mass spectrometry, 70  $\mu$ l of oligo(dT)<sub>25</sub> pulldown samples were heated at 95°C for 5 minutes before being loaded and run on Novex 4-12% Bolt gels, approximately 2.5 cm into the gel. Samples were loaded with spacer

lanes between ladder and samples and between each sample in order to minimise contamination. This protocol also applied to the gels run for comparison of non-crosslinked and crosslinked untreated control experiments, as does the method for Colloidal Coomassie staining (section 2.4.5).

#### **2.4.5. Mass Spectrometry**

Once samples were approximately 2.5 cm into the gel, the run was stopped, gel removed and placed in a sterile 15 cm cell culture plate. Gels were then stained in ProtoBlue™ Safe Colloidal Coomassie Blue G-250 stain (National Diagnostics) 7 parts: 3 parts 100% ethanol for several hours at room temperature on a benchtop rocker. Gels were de-stained overnight by pouring off stain and replacing with ultra-pure water, and storing overnight at 4°C in a parafilm sealed 15 cm plate.

Gels were then prepared for mass spectrometry analysis by Rebekah Jukes-Jones according to the following protocol: total lanes were cut into equal numbers of slices and gel sections transferred to the wells of a 96-well PCR plate. Sections were then alternately washed in 80 µl of 50 mM ammonium bicarbonate and 80 µl 100% acetonitrile a minimum of three times to remove residual stain. Samples were reduced with 10 mM dithiothreitol (20 minutes at 56°C) and alkylated with 100 mM iodoacetamide (20 minutes, in the dark), before subsequent washes with 50 mM ammonium bicarbonate / 100% acetonitrile.

Gel slices were resuspended with 15 µl trypsin digestion buffer (11.11 µg per ml in 25 mM ammonium bicarbonate; Sequencing Grade Modified Trypsin, Promega Corporation, USA). The plate was sealed and incubated at 30°C overnight, following which 80 µl extraction buffer (0.2% trifluoroacetic acid) was added to each well and the plate incubated at room temperature for one hour to extract protein. Samples were then transferred to Eppendorf tubes and dried for 1 hour with a Savant DNA Speed Vac (Thermo Scientific, USA). Dried peptide samples were resuspended with 5% formic acid / acetonitrile (9:1), vortexed and transferred to glass vials. Samples were spiked with two internal standards, yeast ADH1 (accession P00330) and bovine serum albumin (P02769) to a final concentration of 20 fmol per µl (MassPREP standards, Waters Corporation, UK).

#### 2.4.6. Mass Spectrometry Analysis

Peptide mixtures were analysed by nanoflow liquid chromatography coupled to a Synapt G2S mass spectrometer (NanoAcquity UPLC system and Synapt G2S mass spectrometer, Waters Corporation, UK), using a 25 cm by 75  $\mu\text{m}$  I.D., 1.7  $\mu\text{m}$  BEH130 C18 column. Sample injections of 2  $\mu\text{l}$  were separated using a reversed phase 90 minute, 3-40% acetonitrile solvent gradient, at 0.3  $\mu\text{l}$  per minute. Mass spectrometry analysis was performed in a data-independent manner, using ion mobility HDMS<sup>E</sup>, with IMS wave velocity in the helium cell set to 650 m/s. The mass spectrometer was programmed to step between 4 eV (low energy) and 20-50 eV (elevated collision energy) in the gas cell, using a scan time of 1 second and a mass range of 50 to 2,000  $m/z$ .

Protein identifications and absolute quantification information were extracted from raw data files using ProteinLynx Global Server (PLGS version 3, Waters Corporation, UK) in combination with ISOQuant (Kuharev and Tenzer, Germany, open source under <http://www.immunologie.uni-mainz.de/isoquant/>). Data processing was performed with the low energy threshold and high energy threshold set to 135 and 30 respectively. The human UniProt database, including reverse sequences (UniProtKB/SwissProt, release 2014\_05, 11.06.2014, 20265 entries) was used in PLGS, with peptide mass tolerance and fragment mass tolerance set to automatic, with an allowed maximum of one missed cleavage. Ion matching requirements were set to one or more fragments per peptide, three plus fragments per protein and one or more peptides per protein, with a False Discovery Rate (FDR) of 1%. Processed, database searched PLGS data files were loaded into ISOQuant for quantitative analysis using an FDR of 0.1%, only returning an absolute fmol amount of protein if three reliable peptide hits were available for quantification (i.e. "TOP3" method). This software used first past matches, thereby ignoring any peptides generated by in-source fragmentation or modified peptides.

Spiked in tryptic digests of yeast ADH1 internal standard was used to calculate absolute amounts of identified proteins. Software did not identify splicing isoforms of proteins independently of one another, instead identifying them as a single protein

based on peptides. Data from TOP3 ISOQuant analysis was exported as a spreadsheet in Microsoft Excel and analysed as discussed in Chapter 3.

#### **2.4.7. Flag-tagged pCMV-LARP1 /PABPC1 CO-immunoprecipitation**

15 cm plates were seeded with  $1.5 \times 10^6$  HeLa cells and incubated for 24 hours, after which the plates were transfected with 16.8  $\mu\text{g}$  Flag-tagged pCMV-GFP control, pCMV-LARP1 or pCMV-PABP, diluted in a total volume of 2.1 ml with OptiMEM+GlutaMAX (GIBCO Cat # 11058). This vector mix was added 1:1 to a mix of Lipofectamine 2000 transfection reagent (Invitrogen Cat # 52887) diluted 1 in 10 in OptiMEM. Plates were then returned to the incubator for a further 24 hours before beginning the harvest and co-immunoprecipitation (co-IP).

Plates were washed twice in 10 ml PBS, before scraping and resuspension in 2 ml of co-IP buffer per plate (20 mM Tris HCl pH 7.5, 200 mM NaCl, 15 mM  $\text{MgCl}_2$ , 0.5% NP40, 1 mM EDTA, filtered through a 0.2  $\mu\text{m}$  filter, plus 1:1000  $\beta$ -mercaptoethanol and cOmplete protease inhibitor cocktail tablet (Roche, Cat # 11873580001) added fresh on day of use). Depending on condition, either RiboLock RNase inhibitor (Thermo Fisher Cat # EO0381) was added, 1  $\mu\text{l}$  per ml buffer (“minus RNase”) or an RNase cocktail of RNase A, RNase 1 and Benzonase were added in a mix of ratios 1:1:1, 10  $\mu\text{l}$  per 2 ml tube just before the IP incubation (“plus RNase”).

Plates were incubated on ice for 5 minutes before lysates were scraped and pooled into 50 ml falcon tubes, passed through a 21 G needle five times and equilibrated with end over end rotation for 10 minutes. In this time, 60  $\mu\text{l}$  AntiFLAG® M2 Magnetic Beads (Sigma, Cat # M8823) per IP was aliquoted and beads washed twice with 1 ml CO-IP buffer. Once equilibration was finished, lysates were spun down for 15 minutes at 4°C at 13,000 r.p.m. and supernatants collected into fresh falcon tubes.

Protein concentration of each condition was determined by Bradford (BIO-RAD Protein Assay Dye Reagent Cat # 500-0006) measuring absorbance at 595 nm, and lysates normalised through dilution using co-IP buffer. Samples were then normalised for protein over the conditions relative to the lowest concentration, through dilution with IP buffer. 500  $\mu\text{l}$  of lysate was aliquoted into a labelled Eppendorf for western blotting, to which sample buffer was added 1:4.

AntiFLAG® beads were spun down and resuspended in original volume of lysis buffer; 60 µl of beads was then aliquoted into Eppendorfs for IPs. 2 ml of normalised protein was then incubated with end over end rotation for 1 and a half hours at 4°C (if “plus RNases” condition, at this point 10 µl RNase cocktail added; if “minus RNase”, 12 µl yeast tRNA was spiked-in to each tube; Sigma Aldrich Cat # 15401-029). Following the incubation period, supernatant was discarded and beads washed 4 times over using 1 ml IP lysis buffer, pooling common condition samples after the first wash each time. Following the final aspiration of the washes, beads were resuspended or eluted dependent on condition.

In the plus RNase condition, beads were resuspended in a final volume of 150 µl IP lysis buffer using a cut-off pipette tip. To this, 40 µl of sample buffer was added and 30 µl per lane of westerns. In the “minus RNase” condition, an additional elution step was undertaken to elute the FLAG-tagged overexpressed proteins from the beads. This set of steps first involved the 1:25 dilution of 46.8 µg of 3x FLAG peptide, to form a FLAG elution buffer, after which a series of three elution cycles could be performed. For each cycle, beads were resuspended in 60 µl of FLAG elution buffer, and incubated for 10 minutes at 4°C whilst shaking at 350 r.p.m. At the end of this 10 minute period samples were placed on a magnetic rack, elution removed and pooled into a freshly labelled Eppendorf (along with previous elutions). Once all three cycles were completed, the elution was split for RNA analysis (80%) and western blotting (20%). Finally, the beads were resuspended in 150 µl IP lysis buffer, to which 30 µl sample buffer was added, for use in western blotting.

## **2.5. Metabolomics**

A549 cells were seeded and reverse transfected in a 6 well plate as described in section 2.2.3 and allowed to grow under normal conditions for 24 hours. Following this, cells were harvested using trypsinisation and pooled according to transfection condition. Cells were then spun and counted using a haemocytometer, and re-seeded in a Seahorse culture plate at the following densities: control siRNA transfected at 50,000 per ml, and LARP1 siRNA transfected at 65,000 per ml (plating 500 µl per well). The Seahorse culture plate was then spun very briefly to minimise cells adhering elsewhere than the bottom of the well, and cultured for a further 24 hours prior to

Seahorse BioAnalyser investigations. Two external wells and two central wells were left cell-free, to act as a background control for the measurements of the Seahorse Flux analyser.

Regardless of experiment, XF sensor cartridge plates were calibrated through immersion of probes in a flux plate containing 1 ml of XF Calibrant per well (Seahorse Bioscience, cat # 100840-000), and incubated in a CO<sub>2</sub> free incubator at 37°C overnight prior to runs.

### **2.5.1. Seahorse Mitochondrial Stress Test**

On the day of experiment, cells were checked to ensure a monolayer had formed at the bottom of the wells, and the Seahorse Bioanalyser was switched on to allow it to reach 37°C . Cells were washed 3 times in unbuffered media, aspirating bar the last 100 µl each time to avoid disturbing the monolayer. Following the final wash, cells were left in a total volume of 675 µl media and left to equilibrate for no longer than one hour in a CO<sub>2</sub> free incubator whilst drug treatments were prepared and probe plate calibrated. Unbuffered media for both Seahorse test types was made up as outlined in Table 5, pH 7.2-7.4 with NaOH and filtered prior to use.

Drug treatments were made up in pre-labelled bijoux tubes in 5 ml media to 10x the required dose. Oligomycin was made to a dose of 5 µM, carbonyl cyanide-4-(trifluoromethoxy)phenylhydrazone (FCCP) to a final dose of 4 µM and Rotenone to 10 µM. These were then pipetted into wells A, B, C or D (one per injection well) of the calibration plate at the following volumes: well A or D, 75 µl; well B, 83 µl; and well C, 90 µl. Once prepped, the calibration plate was loaded and a half hour calibration programme initiated.

| <b>Ingredient</b>      | <b>Mitochondrial test media</b> | <b>Glycolysis test media</b> |
|------------------------|---------------------------------|------------------------------|
| H <sub>2</sub> O       | 980 ml                          | 980 ml                       |
| Powdered DMEM          | 1 bottle/L                      | 1 bottle/L                   |
| <b>D-Glucose</b>       | 11 mM                           | -                            |
| Glutamax               | 1 mM                            | 1 mM                         |
| 100 mM Sodium Pyruvate | 1 mM                            | 1 mM                         |
| NaCl                   | 1.85 g/L                        | 1.85 g/L                     |
| Phenol Red             | 'pinch'                         | 'pinch'                      |

**Table 5 Recipes for unbuffered media required for Seahorse experiments**

### **2.5.2. Seahorse Glycolytic Stress Test**

The Glycolytic stress test, or glycolytic function test, shares many of the same set-up steps as the mitochondrial stress test (for example, set up of machine, wash steps, drug loading in calibration plate and subsequent calibration). However it requires an unbuffered glucose-free media, the recipe for which can be found in Table 5, and requires the preparation of a different set of drug treatments. These drug treatments are still prepared in 5 ml unbuffered filtered media, to concentrations 10x required dose and are as follows: glucose at 500 mM, Oligomycin as previously, and 2-deoxyglucose (2-DG) at 500 mM also.

### **2.5.3. Crystal Violet Normalisation**

Normalisation for Seahorse XF24 readings was achieved through crystal violet staining of DNA. Following Seahorse BioAnalyser experimental runs finishing, plates were aspirated and wells washed once in PBS, and fixed for 20 minutes in a solution of 3% paraformaldehyde, 2% sucrose in PBS. Fixing solution was aspirated and wells were washed once in water. Cells were stained in 0.1% Crystal Violet, 10% ethanol solution for 15 minutes, before washing several times in water to remove excess stain. Stain was extracted using 200 µl of 10% acetic acid per well for 20 minutes, gently shaking.

200 µl of stain was then extracted from each well, diluted 1:5 in water and vortexed. From this dilution, 200 µl placed in wells of a 96 well plate and absorbance measured at 590 nm using a PowerWave XS2 plate reader (Bio-Tek instruments). Seahorse

readings were then normalised according to the absorbance measured in each well in the Seahorse analysis macro provided by Seahorse Bioscience.

## **Chapter 3**

### **3. Identification of RNA Binding Proteins changing their RNA binding activity following mTOR inactivation**

#### **3.1. Introduction**

##### **3.1.1. Previous work identifying RNA Binding Proteins**

As discussed previously, mTOR is a key signalling pathway involved in many processes, including cell growth and proliferation in response to stimuli such as nutrient availability, growth factors and insulin signalling. It plays a central role in the control of translation through directly influencing cap-dependent translation, and has also been shown to regulate the expression of a highly abundant subset of genes known as 5' TOP mRNAs. These genes encode for all ribosomal proteins, as well as other factors involved in translation, therefore their expression is pivotal to assembly of new ribosomes and the further progress of de novo protein synthesis. However, the exact mechanism of how mTOR controls the expression of these genes has not been elucidated. Recent work has suggested the involvement of an intermediary factor downstream of mTOR or possibly S6K, such as an RNA binding protein, which could bind and thereby regulate mRNA expression or stability in response to mTOR signalling.

Many approaches have been undertaken with the purpose of expanding our understanding of RNA binding protein networks and the messages they bind, including predictive computational models (Anantharaman et al. 2002), genome wide arrays using RNA probes (Scherrer et al. 2010; Tsvetanova et al. 2010) and variations on protein-RNA crosslinking techniques (Hafner et al. 2010; König et al. 2010). One such method, developed by (Castello, Horos, et al. 2013) allows for the capture of physiological *in vivo* RNA-protein interactions in living cells, through the application of UV crosslinking at 254 nm to covalently link amino acids to nucleotide bases of RNA in direct contact. Single proteins in complex with poly(A)<sup>+</sup> RNA can then be captured using oligo(dT)<sub>25</sub> magnetic beads, stringently washed to remove contaminant proteins, eluted and identified using label-free mass spectrometry. Developed in HeLa cells, interactome capture has been used in other cell types and organisms, including HEK293 cells, mouse embryonic stem cells, *Caenorhabditis elegans*, *Saccharomyces*

*cerevisiae* and most recently, *Drosophila melanogaster* (Baltz et al. 2012; Kwon et al. 2013; Beckmann et al. 2015; Matia-González et al. 2015; Sysoev et al. 2016).

Use of this methodology to investigate the dynamic responses to stimuli such as drug treatment was initially proposed but as yet, no studies have been published using this methodology. The use of such a technology for comparison of untreated and treated sample sets could provide insight into the role which changes in RBP interactomes exert in post-transcriptional control of messages, affecting gene expression in order to regulate cellular responses to such stimuli. This would potentially include better understanding of downstream pathways influenced by drug treatment, as well as implications of toxicological and off-target effect on clinical outcomes.

In this chapter, I aim to use whole cell RNA Binding Protein capture to identify RNA binding proteins from whole cell extracts which change their binding activity specifically upon mTOR inactivation in HeLa cells.

### **3.1. Results**

#### **3.1.1. Optimisation of mTOR inhibition showed 60 minute treatment with 200 nM Torin1 to be sufficient for inhibition of both mTORC1 and mTORC2**

In order to optimise the mTOR inhibition and maximise the difference between our untreated and treated conditions in the oligo(dT)<sub>25</sub> capture of RBPs, we initially examined what duration of treatment with our chosen ATP-competitive inhibitor, Torin1, was sufficient to achieve the inhibition of both mTORC1 and mTORC2 signalling. In the literature, Torin1 was shown to effectively inhibit both mTOR complexes at a final concentration of 200 nM, including effects on translation and autophagy. At this concentration it was also shown Torin1 could be used to inhibit mTOR signalling without off target impact on PI3K activity, therefore this was the concentration chosen for this study (Thoreen et al. 2009). In order to stimulate mTOR signalling and ultimately translation in both groups, media in which cells were cultured was supplemented with an additional 2% FBS and 1% L-Glutamine 30 minutes before treatment with Torin1 or an equal volume of DMSO, our vehicle control. Fig 3.1 shows the phosphorylation and therefore activation status of multiple downstream components of both the mTORC1 and mTORC2 signalling cascade, at various time points following inhibition with 200 nM Torin1.

**A**

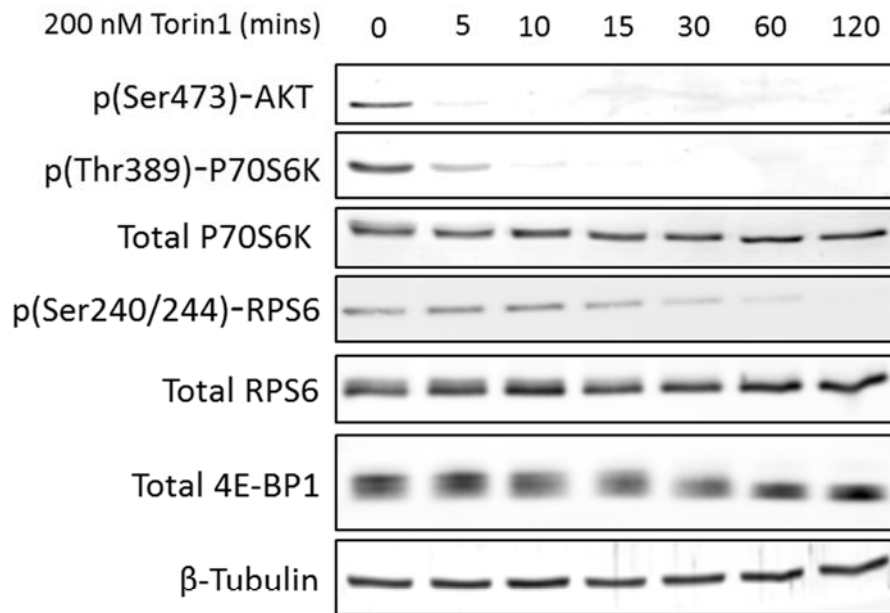


**Figure 3.1 mTOR signalling is inhibited following 1 hour treatment with 200 nm Torin1.** HeLa cells were supplemented with FBS and L-Glutamine for 30 mins as described in materials and methods. Cells were then treated with vehicle control (DMSO) or 200 nM Torin1 for indicated times, before being harvested, lysed and subjected to western blotting. (A) Western blots to show phosphorylation status of several downstream targets of mTORC1 and mTORC2 signalling, following treatment with 200 nm Torin1 for indicated durations of time.  $\beta$ -tubulin was used as a loading control.

As early as 5 minutes following treatment the mTORC2 substrate Akt was dephosphorylated, and only 10 minutes following treatment the levels of P70S6K phosphorylated at Threonine 389 were ablated, with no effect on total levels of the protein. RPS6, a key downstream target of mTORC1 in the context of translational control and growth signalling, was dephosphorylated at the target Serine sites of position 240 and 244 later, with dephosphorylation occurring at 60 minutes following Torin1 treatment. There was no change in total levels of RPS6. Another key target of mTOR signalling, 4E-BP1, showed a clear band shift after 60 minutes of Torin1 treatment; at early time points a triplet band can be seen indicating 4E-BP1 exists in multiple states according to three separate phosphorylations (Mukhopadhyay et al. 1992), each causing a small size shift. As the time increments of treatment increase, the number of visible bands decreases to two and then one identifiable band, indicating mTOR inhibition has successfully resulted in dephosphorylation of 4E-BP1. Therefore, after 60 minutes of treatment, phosphorylated Akt, P70S6K, RPS6 and 4E-BP1 were ablated. From this it was decided that 200 nM Torin1 treatment for 60 minutes was sufficient for inhibition of both mTORC1 and mTORC2 signalling, and thus would be the duration of treatment for use in this study.

### **3.1.2. Whole cell RNA binding protein capture optimisation confirmed specificity of protocol and enrichment of known RNA binding proteins**

As outlined in the first chapter, the method of interactome capture was developed (Castello, Horos, et al. 2013) as a means to capture and identify RNA Binding Proteins in vivo, thereby providing a method for studying the repertoire and roles of RBPs in control of mRNA expression. The scale of experiment to be used in this study was notably smaller in comparison, primarily with the purpose of tailoring the protocol to a different objective; this study was concerned less with depth and more with the differentials in repertoire between conditions. As such the protocol was subjected to a selection of modifications before use, which had been made primarily to allow for increased speed in sample processing, minimising the number of freeze-thaw cycles to which lysates were subjected and overall ease of use. Speed was crucial in steps such as washing before UV crosslinking, lysis and scraping, in order to minimise RNA degradation. In order to ensure these changes did not affect the specificity of the

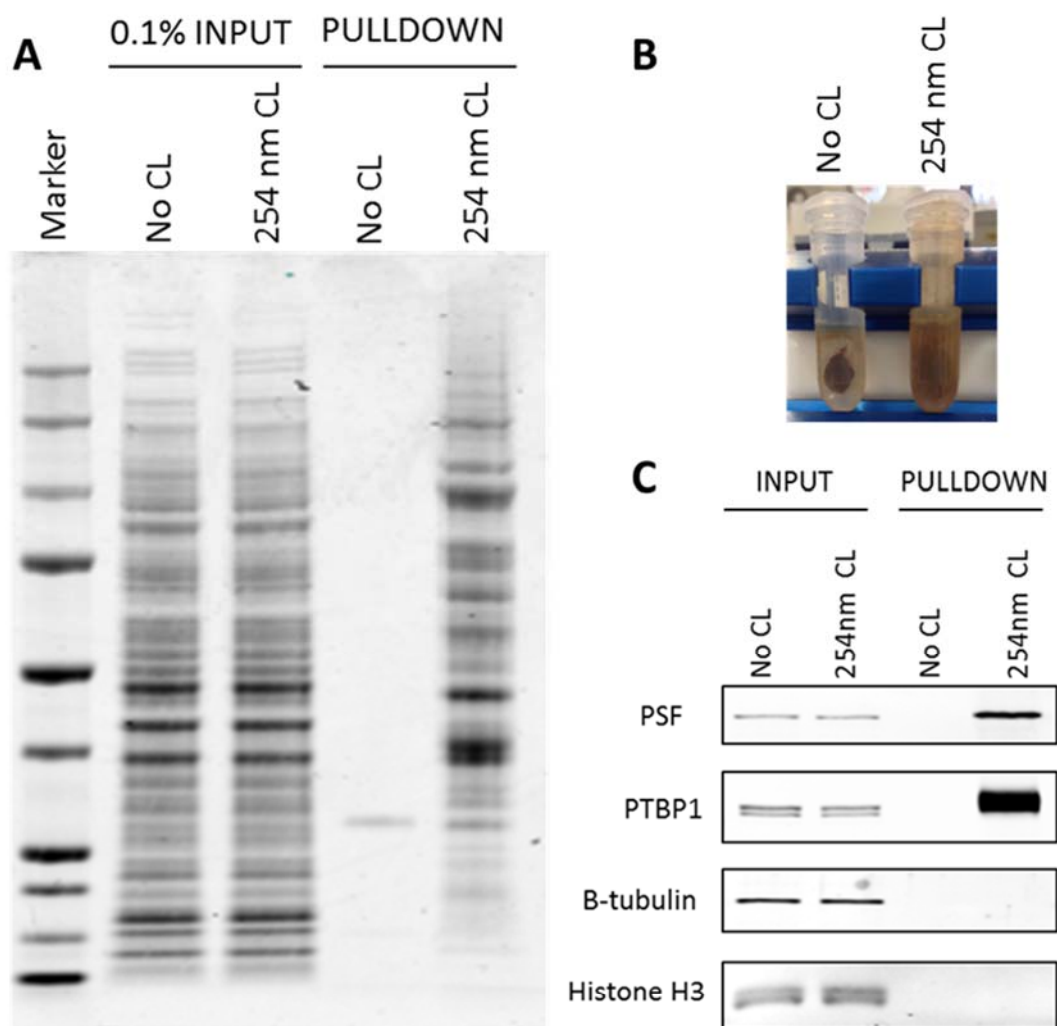


**Figure 3.2 Whole cell RNA Binding Protein capture by oligo(dT) affinity isolation adapted from Castello et al (2013) showed specificity of the protocol.** 24 hours after plating, HeLa cells were washed twice with PBS and plates placed on ice. Cells were then either subjected to 150 mJ/cm<sup>2</sup> 254 nm UV (+CL) or no UV (No CL) before lysis. (A) Eluted proteins following interactome capture and their corresponding inputs, detected by SDS-PAGE and colloidal coomassie staining; showing the selectivity of the protocol in the cleanliness of the non crosslinked (noCL) control lane. Visible band common to all lanes indicates RNases used in sample digestion. (B) As described by Castello et al (2013), a bead halo can be seen when placed on a magnetic rack in the 254 nm crosslinked (+CL) sample, absent in the noCL sample. (C) Eluates were analysed by SDS-PAGE and western blotting against known RBPs PSF and PTBP1, and proteins with no known RNA binding capacity, histone H3 and B-tubulin.

protocol, several optimisations suggested in the original protocols paper (Castello, Horos, et al. 2013) were performed. The efficiency of the UV 254 nm crosslinking of RBPs to RNA was checked, along with western blotting to check enrichment for known RBPs, as well as controls that should not be binding. Following conventional UV crosslinking at 254 nm, poly(A) RNAs were pulled down by oligo(dT)<sub>25</sub> affinity isolation, and compared to a non-irradiated group. Fig 3.2B shows the bead “halo” surrounding the beads in the crosslinked sample as described by Castello et al., when placed on the magnetic rack. Eluates of both the crosslinked and non-crosslinked samples were run on a NUPAGE 4to 12% Bolt gel; proteins were detected by Colloidal Coomassie staining and scanning using a LICOR scanner (Fig3.2A), as well as by SDS-PAGE and western blotting against known RBPs (PSF, PTBP1) and proteins that should not be enriched (histone H3, B-tubulin) (Fig 3.2C). This shows the method is effective in selecting and enriching only for RNA Binding proteins, and that in the absence of crosslinking there are no proteins pulled down non-specifically with the oligo(dT)<sub>25</sub> beads.

### **3.1.3. Integration of 200 nM Torin1 treatments before RNA Binding Protein capture indicated successful inhibition of mTOR signalling and enrichment of RNA binding proteins**

Though the technique of whole cell RBP interactome capture is being applied to an ever expanding variety of cell systems, including human cell lines, yeast and nematodes, as yet integration of this technique with inhibitory treatment has to the best of knowledge not been published. In this study, the aim is to investigate the differential binding of RBPs following inhibition of the mTOR signalling pathway, in order to identify any RBPs whose binding activity is mTOR dependent. As such, we needed to elicit as extensive as possible a differential between our conditions where mTOR signalling was stimulated versus the condition of Torin1 inhibition. As such we decided to stimulate mTOR signalling in all cells through media supplementation with FBS and L-glutamine above basal availability, prior to inhibition in one condition with 200 nM Torin1 treatment.

In order to verify the success of mTOR stimulation and inhibition across the two conditions, comparison of the inputs of untreated and treated samples by western

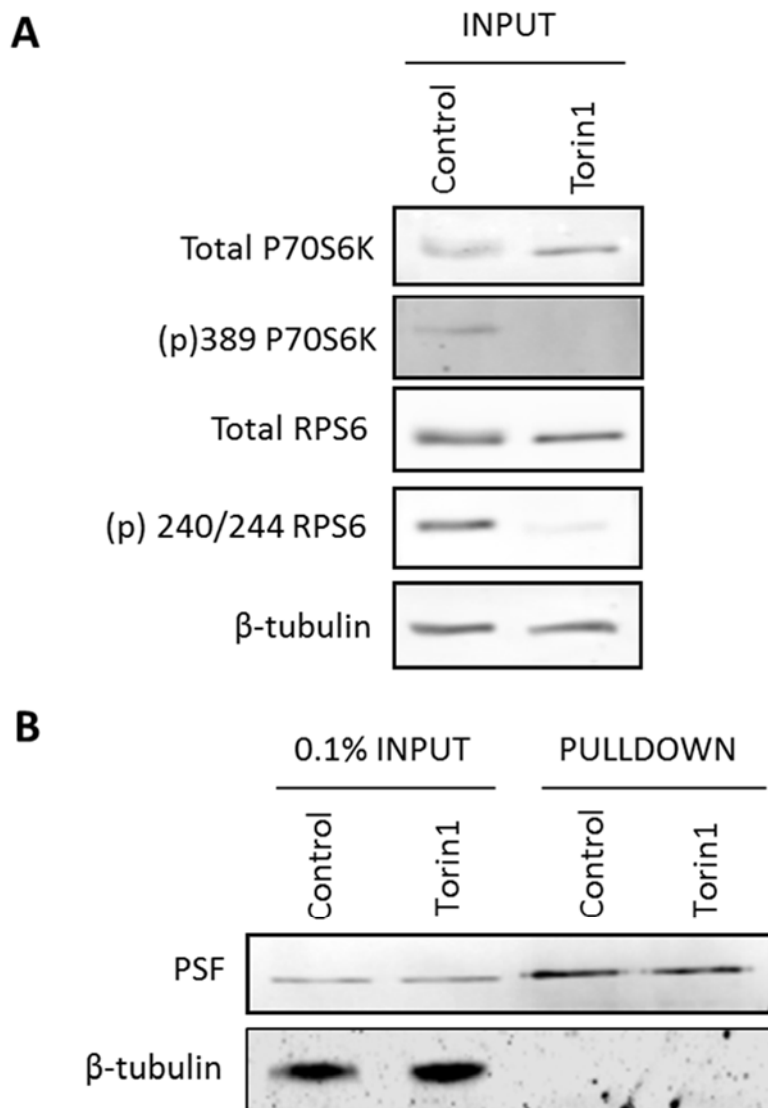


**Figure 3.3 Successful use of whole cell RBP capture in conjunction with mTOR inhibition following treatment with 200 nM Torin1.** Following pre-treatment with FBS and L-Glutamine for 30 mins, HeLa cells were treated with 200 nM Torin1 or vehicle control (DMSO) for 60 minutes. Cells were then subjected to 254 nm UV cross-linking and whole cell RBP interactome capture was performed. (A) Representative input checks for mTOR signalling inhibition by SDS-PAGE and western blotting against total and phosphorylated levels of downstream substrates P70S6K and RPS6. (B) Representative westerns performed on inputs and following oligo(dT)<sub>25</sub> pulldown verify enrichment of one known RBPs, PSF, and one negative control,  $\beta$ -tubulin.

blotting was performed. This allowed qualitative validation that mTOR targets are dephosphorylated relative to control treatments, prior to identification RNA binding proteins via mass spectrometry. Representative blots from one such repeat are shown in Figure 3.3A; blotting against phosphorylated forms of P70S6K and RPS6 shows dephosphorylation in Torin1 treated samples relative to controls, without an overall change in total levels of the proteins, indicating successful inhibition of mTOR signalling in cells used for RBP capture. Furthermore, western blots against known RNA binding protein PSF and negative control  $\beta$ -tubulin verify specific enrichment of RBPs following crosslinking and oligo(dT)<sub>25</sub> pulldown, thus confirming successful crosslinking of protein bound to RNA (Figure 3.3B).

#### **3.1.4. Mass spectrometry of oligo(dT)<sub>25</sub> pulldown and analysis identified 214 RNA binding proteins which appeared across all replicates**

To identify the repertoire of RBPs bound to the RNA from each condition, equal volumes of the eluates from the oligo(dT)<sub>25</sub> pulldown were run approximately 2.5 cm into a NUPAGE 4-12% Bolt gel for analysis by label-free mass spectrometry. Gels were then cut to an equal number of slices per condition and processed by Rebekah Jukes-Jones, according to methods described in methods section 2.4.5/2.4.6.

Raw data were processed in ProteinLynx Global Server (PLGS), then run through ISOQuant software package (Jörg Kuharev and Stefan Tenzer, University of Mainz, Germany, open source under: "<http://www.immunologie.uni-mainz.de/isoquant/>") against a combined target-decoy database of human proteins (UniProtKB/SwissProt, release 2014\_05, 11.06.14, 20265 entries, including reverse sequences), for absolute protein quantification. The search was set according to the parameters described in methods section 2.4.6. Spiked ADH1 yeast tryptic digests were used as an internal means of normalisation; it is also important to note this database did not identify individual isoforms of one protein.

Proteins were identified using the ISOQuant "TOP3" software package and exported as a list for each biological replicate, after processing according to the parameters outlined. The "TOP3" software utilises the top three most abundant unique peptides in order to generate a semi-quantitative value for the femtomolar amounts of each

protein detected (Kuharev et al. 2015). Following consolidation of results for each biological repeat, and removal of contaminants such as keratins or non-human spike-ins, the resulting list was reviewed manually and any detected proteins with observed femtomole counts (fmol) in fewer than 3 of the initial 5 biological repeats, in both treated and untreated groups, were removed. Previous groups have noted the confounding influence which absent observations or low fmol counts exerts on statistical analysis of large MS datasets (Fei et al. 2011; Blakeley et al. 2010), as well as from standard experimental variability caused by reagent batches, handling or conditions on different days (Leek et al. 2010). Subsequently, batch effects were identified through conducting a preliminary principle component analysis (PCA) on the dataset (data not shown), the distribution of which ultimately led to the decision to remove two of the biological repeats as outliers due to large variability, and continue the analysis of mass spectrometry data with an  $n=3$ .

The R script used for analysis in this study is available in the supplemental materials. Briefly, a data matrix was generated from the consolidated  $n=3$  ISOQuant TOP3 spreadsheet, involving the exclusion of any proteins with missing observations in the first instance, reducing the total number of proteins in the interactome considered in this study down to 214. Label-free mass spectrometry is a large source of variation affecting the reproducibility of results; in order to determine the greatest differential between the repeat experiments was due to treatment with Torin1 and not inter-experimental from alternative sources, a principal component analysis (PCA) was performed (Figure 3.4A). In brief, a PCA is constructed through transformation of primary variables in a data set to a reduced scale or dimension, and identifying the principal components which explain how the data varies. The largest variances are assumed the most important and plotted in the appropriate number of dimensions, relative to the largest or “principal” component. Here, in Figure 3.4A, the variance considered most important is labelled PC1 (on the x axis), which explains 83.1% of variance in results. The second most important component, PC2, is plotted on the y axis and is calculated to explain only 6.7% of the variance. From the distribution of the points across the PCA plot in Figure 3.4A, it can be seen that the variance of PC1 can be explained by the difference between experiment E versus experiments B and C,

**A**

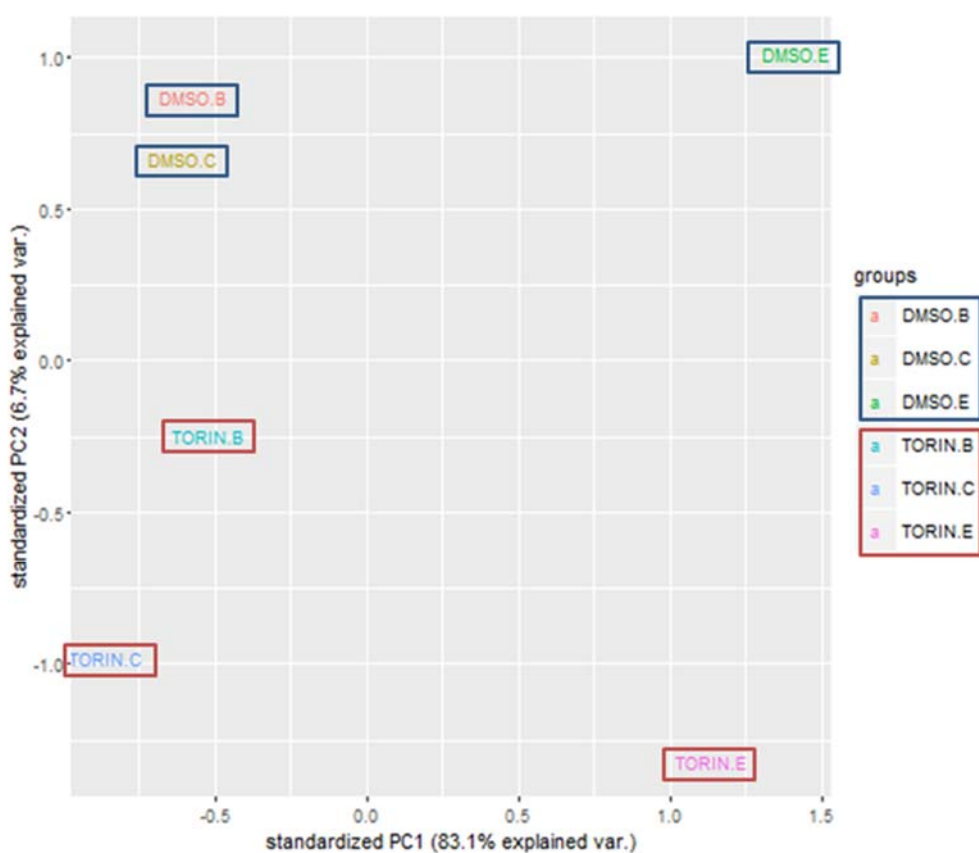


**Figure 3.4 PCA showing variance between replicates and treatments within this study.** Following MS, ISOQuant analysis and removal of contaminants, a list of 214 identified proteins was analysed for batch effects through subsection to Principle Component Analysis (A) PCA performed on experiment vs treatment showing sample distribution across replicates (annotated B, C and E).

despite the spread across PC2 appearing to cluster according to treatment, indicating a greater source of variation was inter-experimental than treatment. Thus, these three biological repeats were processed using the SVA package (Leek et al. 2012), which confirmed inter-experimental conditions across the biological replicates to be a source of variability and adjusted for this batch effect accordingly (see R script, Supplemental Figure S1).

**3.1.5. Statistical analysis using the Bioconductor package *limma* identified a subset of 31 proteins either significantly increasing or decreasing binding to RNA by 1.3 fold following mTOR inhibition, relative to control**

Once adjusted using the sva package, a paired t-test was performed on the data using the openly available limma Bioconductor package in R (Ritchie et al. 2015). Of the 214 proteins carried forward for statistical analysis, 31 passed a significance cut-off p-value < 0.05; concurrently falling into either the “increased binding” category, where the fold change in the detected fmol protein following mTOR inhibition was greater than 1.3, or the “decreased binding” category, where the fold change following mTOR inhibition is less than 0.75 following treatment. The distribution of the 214 proteins’ fold changes relative to their significance value (both on a log scale) is shown in the volcano plot in Figure 3.5. Those designated as having increased binding are highlighted in green, and those proteins designated as decreased binding in red.

The interactome repertoire of HeLa cells as reported by Castello et al. (2012) was compared with our list generated, which was also performed in HeLa cells (Figure 3.6). Compared against the 860 proteins comprising the HeLa interactome detected by Castello et al. ((2012); supplemental material available online), 92.5% of the 214 proteins in this study had been identified previously. As noted before, the amount of starting material in each study varied considerably; the study by Castello et al. used a vast amount more than was used here, and therefore it is likely that this accounts for a notable proportion of the difference in size of repertoire identified by each group.

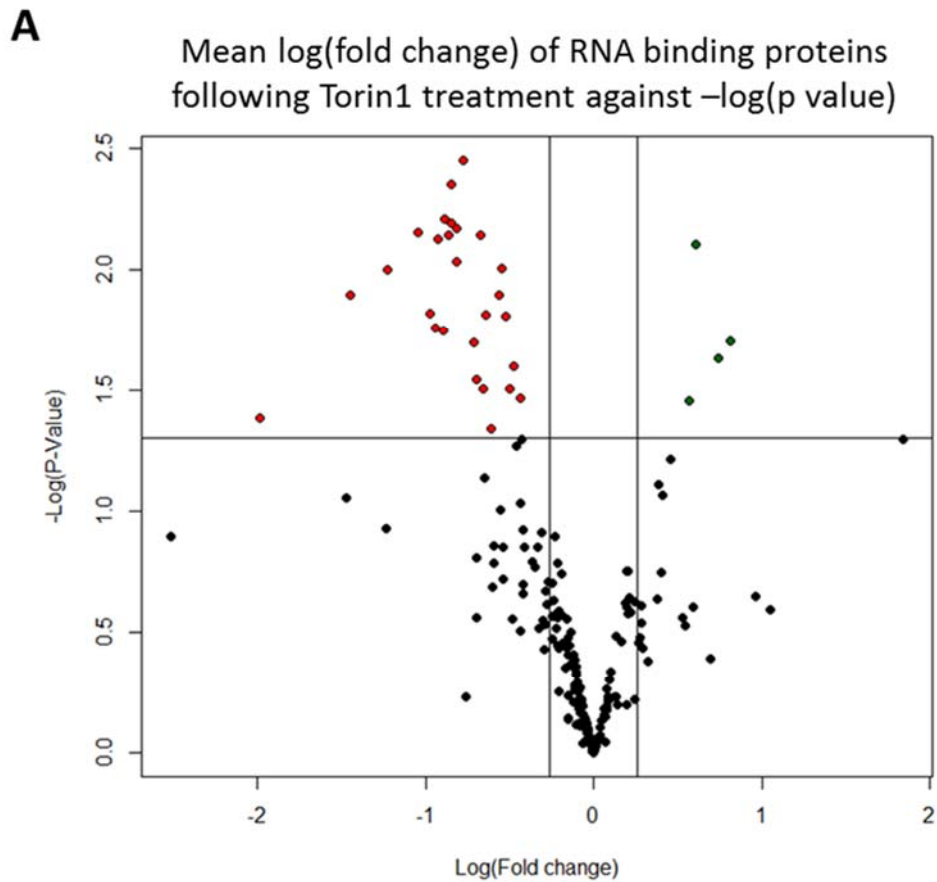


**Figure 3.5** Volcano plot of 214 RNA Binding Proteins identified as present in three replicates in this study. Highlighted points are those proteins whose binding increased (green) or decreased (red) following 60 minute treatment with 200 nM Torin1. Following a paired t-test performed using limma, only proteins whose fold changes were greater than 1.3 and exhibited a p-value < 0.05 (horizontal line on plot) were designated as changing binding following mTOR inhibition.

**A**

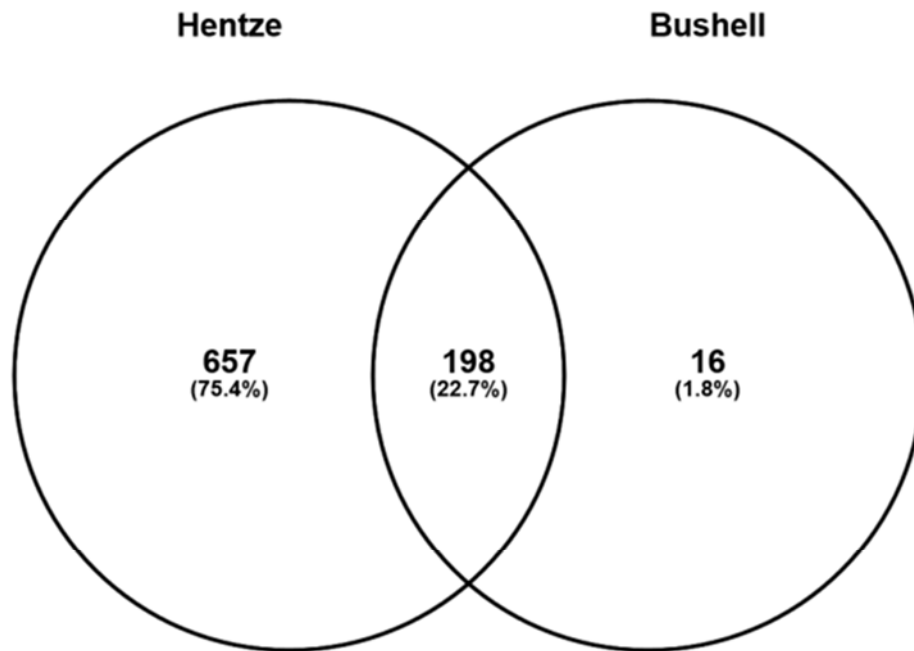


**Figure 3.6 Comparisons of HeLa interactomes between this study and previous study show strong reproducibility.** (A) Overlap between final 214 proteins following filtering (see section 3.2.3) identified in this study, and the HeLa interactome as identified by Castello et al. (2012).

### **3.1.6. Selection and successful validation of four specific RBPs changing their binding activity following Torin1 treatment**

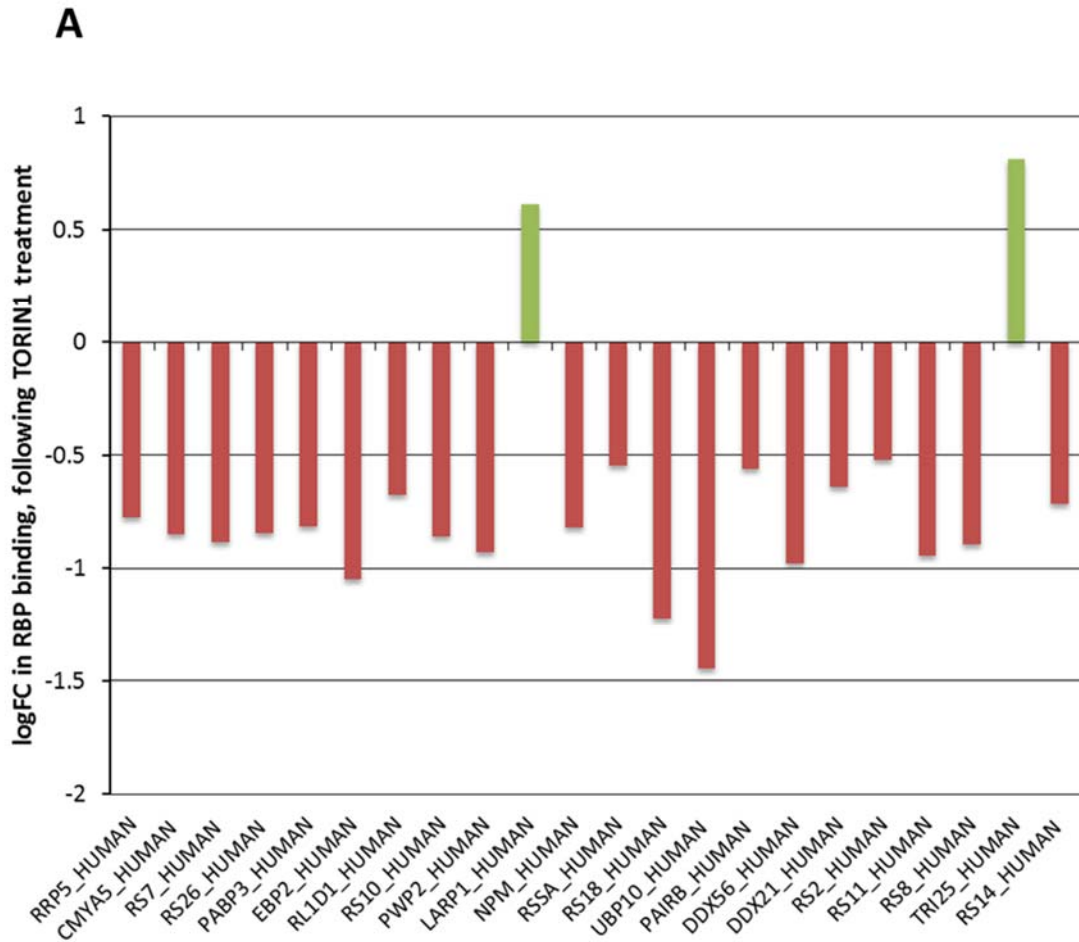
Of the 31 proteins highlighted in our volcano plot, 22 possessed an adjusted p-value (also termed q-value) equal to or lower than 0.2 following multiple correction testing by the Benjamini-Hochberg method, applied using limma (Hochberg & Benjamini 1990). These 22 proteins are shown above the red line, indicating the arbitrarily selected cut-off q-value, in the table in Figure 3.7. This cut-off value was assigned to limit the number of proteins selected for further validation in the first instance, as it indicated a 20% False Discovery Rate following multiple correction; statistically this can be interpreted to one in every five proteins validated being a potential false positive.

Figure 3.8 displays the logged fold changes of each of the 22 proteins which passed the aforementioned designated cut-off q value < 0.2. The analysis identified two RBPs increased their binding following Torin1 treatment; these were Tripartite Motif containing protein 25 (TRIM25) and La-related protein 1 (LARP1), shown in green. Both have been identified previously as RNA Binding Proteins (Kwon et al. 2013; Castello et al. 2012). Of the RBPs identified as having significantly decreased binding following Torin1 treatment, when analysed using DAVID functional analysis (Huang et al. 2009a; Huang et al. 2009b), 10 were identified as associated with the GO annotation for comprising the cellular component of “small ribosomal subunit” and therefore would perhaps be expected to decrease poly(A)+ binding in a situation where translation is inhibited. These included ribosomal proteins RPS7, RPS26, RPS10, RPSA, RPS18, RPS2, RPS11, RPS8 and RPS14, which are all members of the small ribosomal subunit, as well as the structural protein nucleophosmin (Wilson & Doudna Cate 2012). Others, including DEAD Box Helicase 56 and DEAD Box Helicase 21 (DDX56 and DDX21), were identified from both their GO annotations and the literature as helicases involved in the processing of ribosomal RNA and ribosome assembly. Aside from proteins identified as helicases or structural components of the 40S ribosomal subunit, Serpine mRNA Binding Protein 1 (SERBP1, annotated in mass spectrometry lists as PAIRB) consistently showed the largest fmol counts of the 22 proteins, and according to ISOQuant analysis possessed among the greatest identified percentage sequence coverage (data not shown). Thus, SERBP1 was selected as a candidate for validation

**A**

| "RBP"       | logFC    | AveExpr    | t        | P.Value   | "adj.P.Val" | B        |
|-------------|----------|------------|----------|-----------|-------------|----------|
| RRP5_HUMAN  | -0.77218 | 5.25474711 | -6.07311 | 0.003528  | 0.162865378 | -1.51373 |
| CMYA5_HUMAN | -0.85026 | 6.609187   | -5.70813 | 0.0044389 | 0.162865378 | -1.65226 |
| RS7_HUMAN   | -0.88374 | 4.18605583 | -5.21886 | 0.0061585 | 0.162865378 | -1.86255 |
| RS26_HUMAN  | -0.84318 | 6.03297285 | -5.16576 | 0.0063905 | 0.162865378 | -1.88723 |
| PABP3_HUMAN | -0.81427 | 5.30311007 | -5.08689 | 0.0067552 | 0.162865378 | -1.92461 |
| EBP2_HUMAN  | -1.04789 | 3.63678698 | -5.03344 | 0.0070167 | 0.162865378 | -1.95044 |
| RL1D1_HUMAN | -0.67644 | 5.59212124 | -5.01049 | 0.0071327 | 0.162865378 | -1.96165 |
| RS10_HUMAN  | -0.86    | 5.64473303 | -5.00445 | 0.0071637 | 0.162865378 | -1.96462 |
| PWP2_HUMAN  | -0.92622 | 4.89070514 | -4.95031 | 0.0074484 | 0.162865378 | -1.99143 |
| LARP1_HUMAN | 0.610328 | 7.21259666 | 4.875438 | 0.007865  | 0.162865378 | -2.02921 |
| NPM_HUMAN   | -0.81734 | 6.50693514 | -4.65934 | 0.0092363 | 0.162865378 | -2.14304 |
| RSSA_HUMAN  | -0.54463 | 5.77439781 | -4.58493 | 0.0097745 | 0.162865378 | -2.18394 |
| RS18_HUMAN  | -1.22268 | 4.73543864 | -4.56911 | 0.0098937 | 0.162865378 | -2.19275 |
| UBP10_HUMAN | -1.44425 | 4.66098454 | -4.26294 | 0.0125885 | 0.179879036 | -2.37157 |
| PAIRB_HUMAN | -0.56122 | 7.96076494 | -4.26099 | 0.0126083 | 0.179879036 | -2.37276 |
| DDX56_HUMAN | -0.97675 | 3.68962259 | -4.03555 | 0.0151754 | 0.183748634 | -2.51509 |
| DDX21_HUMAN | -0.64031 | 7.00061162 | -4.0278  | 0.0152743 | 0.183748634 | -2.52015 |
| RS2_HUMAN   | -0.52172 | 8.84075887 | -4.01375 | 0.0154555 | 0.183748634 | -2.52935 |
| RS11_HUMAN  | -0.94102 | 5.83003954 | -3.88156 | 0.0172932 | 0.191350571 | -2.61776 |
| RS8_HUMAN   | -0.89392 | 4.92566953 | -3.84265 | 0.0178832 | 0.191350571 | -2.64443 |
| TRI25_HUMAN | 0.81043  | 4.63464152 | 3.729555 | 0.0197397 | 0.195234243 | -2.72362 |
| RS14_HUMAN  | -0.71546 | 6.31500756 | -3.71072 | 0.0200708 | 0.195234243 | -2.73706 |
| PTCD1_HUMAN | 0.742849 | 5.24674627 | 3.544881 | 0.02329   | 0.216698567 | -2.85846 |
| RS3_HUMAN   | -0.47708 | 8.00545727 | -3.46041 | 0.0251642 | 0.224380745 | -2.92246 |
| RS3A_HUMAN  | -0.69516 | 4.46193117 | -3.32381 | 0.028587  | 0.244704698 | -3.0291  |
| EF2_HUMAN   | -0.49502 | 4.73151888 | -3.23781 | 0.0310242 | 0.246373082 | -3.09825 |
| GAR1_HUMAN  | -0.65384 | 4.21719484 | -3.23579 | 0.0310845 | 0.246373082 | -3.0999  |
| SND1_HUMAN  | -0.43813 | 7.62405974 | -3.14165 | 0.0340444 | 0.258831084 | -3.17743 |
| FMR1_HUMAN  | 0.568426 | 4.51336822 | 3.111104 | 0.0350752 | 0.258831084 | -3.20299 |
| PTBP2_HUMAN | -1.98572 | 5.73592023 | -2.95521 | 0.0409399 | 0.292037712 | -3.33652 |
| FBRL_HUMAN  | -0.61116 | 5.11252897 | -2.85067 | 0.0455145 | 0.314196704 | -3.42892 |

**Figure 3.7 Table of RNA Binding Proteins whose fold change of 1.3 or greater following Torin1 treatment exhibits a p-value < 0.05. The red dashed line shows the additional chosen cut-off of adjusted p-value <0.2 to short-list RBPs for investigation.**



**Figure 3.8** Bar chart of RBP fold changes following 200 nM Torin1 treatment, as selected from cut-off exclusion within Volcano plot. Following a paired t-test using limma, including multiple correction testing using the Benjamini-Hochberg method, only the log(fold changes) of RBPs exhibiting an adjusted p-value < 0.2 (see Figure 3.6) were plotted above.

from the subset of RBPs decreasing binding following mTOR inhibition. Also selected for validation were Periodic Tryptophan Protein 2 (PWP2) and Ubiquitin Specific Peptidase 10 (USP10, annotated in mass spectrometry lists as UBP10); though these two proteins possessed relatively low fmol counts in each experiment, they were among the largest fold change decreases seen which were non-40S ribosomal subunit proteins.

Separate repeats of whole cell interactome capture in the presence of Torin1 treatment were conducted to generate independent pulldown eluates for SDS-PAGE and western blotting validation of identified RBPs (Figure 3.9). Changes in binding following Torin1 treatment of LARP1, TRIM25, PWP2 and SERBP1, as identified by mass spectrometry were all validated through western blot. The low fmol counts attributed to USP10 were likely explained by low abundance in HeLa cells overall; this hit proved difficult to detect by western, and so was excluded from future study. Also shown are two known RNA binding proteins (HNRPQ and PSF) whose binding did not change following Torin1 treatment in our study, as determined by mass spectrometry. These two proteins were selected on merit of their reproducible fmol counts, to validate the group which exhibited no fold change in binding between control and Torin1 treated conditions.

### **3.2. Discussion**

This chapter addressed the initial aim of this study; applying whole cell RBP capture techniques in combination with Torin1 treatment and subsequent mass spectrometry, we have identified several RBPs differentially binding following mTOR inhibition. Following their successful validation through western blotting as RBPs whose binding activity is affected by mTOR inhibition, the four proteins SERBP1, PWP2, TRIM25 and LARP1 were selected for further characterization. All four had been identified as RBPs in the HeLa interactome previously (Castello et al. 2012), though not all have a well characterised RNA Binding Domain (RBD). A summary table outlining some details on each of the four proteins, including speculation of RBDs, is shown in Figure 3.10. Evidence suggests the existence of an unidentified intermediary factor downstream of mTOR responsible for its ability to regulate the expression of 5' TOP mRNAs. It is

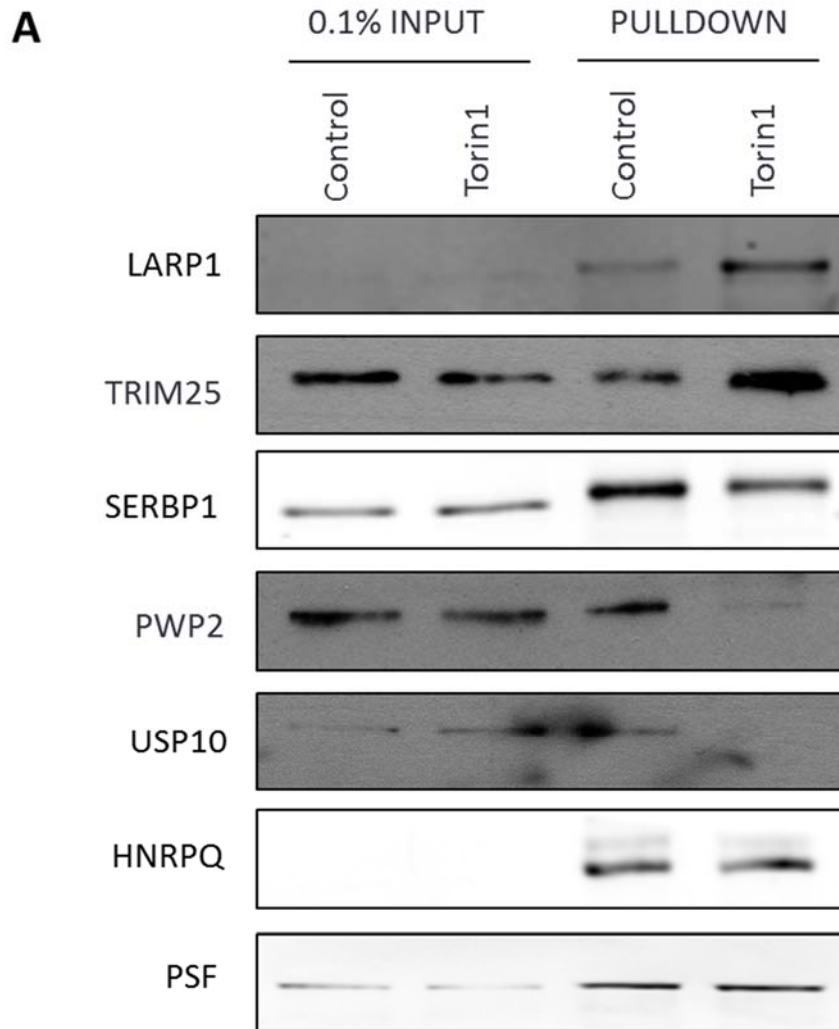


**Figure 3.9 Validation by western blot of RBP fold changes identified by mass spectrometry, following 200 nM Torin1 treatment.** Separate repeats of whole cell oligo(dT)<sub>25</sub> pulldowns were performed as for mass spectrometry, including pre-treatment for 30 minutes with FBS and L-Glutamine, followed by 60 minute treatment with 200 nM Torin1 or vehicle control (DMSO). (A) Representative western blots against several RNA Binding Proteins identified as increasing (LARP1, TRIM25) or decreasing (SERBP1, PWP2, USP10) binding, as well as two non-changers (HNRPQ and PSF), showing the validation of several identified mTOR-dependent RNA Binding Proteins.

| Protein | Size (kDa) | Function  | RNA Binding upon mTOR inhibition | RNA binding domains (known/proposed)   | Established links to mTOR   |
|---------|------------|---|----------------------------------|--|---|
| SERBP1  | 38-55 kDa  | Potential role in mRNA stability, shown to bind 3'-UTR of PAI mRNA (Heaton et al. 2001).  | <b>DECREASED</b>                 | RGG Box* (Costa et al. 2014)   | Unknown – Shown recently in complex with small ribosomal subunits and eIF3 subunits (Kristensen et al., 2012) |
| PWP2    | 102 kDa    | Involved in pre-ribosomal RNA processing and ribosomal biogenesis in yeast, highly conserved (Dasil and Bustelo, 2004).<br>Speculated role in autophagy in Zebrafish model (Boglev et al., 2013). | <b>DECREASED</b>                 | WD40 repeats* (Lau et al., 2009)   | Unknown – Connections with ribosomal stress, autophagy (both controlled by mTOR)                              |
| TRIM25  | 72 kDa     | E3 ubiquitin ligase, stabilises p53 and mdm2 (Zhang et al., 2015).  | <b>INCREASED</b>                 | Binds RNA through coil-coil domain (Kwon et al., 2013)                         | Unknown   |
| LARP1   | 123 kDa    | RNA stability, cap binding, TOP regulation, PABP binding (Mura et al., 2014; Blagden et al., 2009; Aoki et al., 2013; Fonseca et al., 2015 and others).   | <b>INCREASED</b>                 | La Motif (Nykamp et al. 2009), RRM-like*<br>DM15 region (Fonseca et al., 2015) | YES<br>(Fonseca et al., 2015; Tcherkezian et al., 2015)   |

**Figure 3.10 Summary of key information available in literature on each of the 4 RNA Binding Proteins validated as changing binding following mTOR inhibition. RNA binding domains without experimental evidence are indicated with an \*.**

believed this factor could be an mTOR dependent RNA binding protein; the validation of these four RBPs changing their binding activity following mTOR inhibition further supports this concept.

SERBP1, first named as PAI-RBP1, was originally identified as an RNA binding protein which bound the 3'-UTR of the type I Plasminogen Activator Inhibitor (PAI) mRNA, thereby regulating its stability (Heaton et al. 2001). RNA binding of SERBP1 is believed to be facilitated via three highly evolutionarily conserved RGG (arginine-glycine-glycine) boxes in succession, each separated by up to four other residues (Kiledjian & Dreyfuss 1992; Thandapani et al. 2013). As well as its role as an RBD, the RGG box has been shown to be a substrate recognition motif for protein arginine methyltransferases in other RNA binding proteins such as nucleolin (Lischwe et al. 1985), altering the protein-protein interaction profile of many proteins possessing an RGG box, and more specifically influencing localisation of SERBP1 within a cell (Lee et al. 2012).

Under normal conditions, SERBP1 has been shown to associate with other RNA binding proteins associated with stress granules, such as TIA-1, in an RNA-dependent manner (Lee et al. 2014). Then, under conditions of cellular stress such as arsenite treatment, SERBP1 localises to stress granules and P-bodies; these cytoplasmic granules harbour messenger-ribonucleoprotein particles (mRNPs) for storage, processing and even degradation (Lee et al. 2014; Decker & Parker 2012). In HEK293T cells, overexpression of SERBP1 under serum starved conditions led to reduced proliferation and G1 arrest; however under normal serum conditions this response shifted to apoptosis (Costa et al. 2014). Concurrent with this, it was found through expression arrays that overexpression of SERBP1 led to repression of several genes involved in mRNA metabolism, cell cycle and proliferation, apoptosis and transcription; though no direct connection between the phenomena has been shown, this repression is supportive of the role for SERBP1 in stress granules, where translation initiation of RNA within is stalled (Costa et al. 2014; Lee et al. 2014). Over-expression of SERBP1 has been linked to multiple cancers, including lung cancer, ovarian cancer and metastatic pancreatic cancer (Koensgen et al. 2007; Morrissey et al. 2008), where it has been associated with poor prognosis. Conversely, its increased expression has been shown to correlate with

more favourable prognosis in human breast cancer (Serce et al. 2012), thus the potential for use of SERBP1 levels as an indication of prognosis or survival remains unclear.

PWP2 is a protein 932 amino acids in length, whose sequence is highly conserved through eukaryotes from yeast to mammals. In its structure it possesses multiple WD40 repeat domains, a highly conserved repetitive region which provides a protein-protein interface; as well as a coiled-coil domain at its C-terminus (Dosil & Bustelo 2004). As well as being detected in our study, PWP2 was shown to be an RNA binding protein by two independent groups following proteomic screens (Castello et al. 2012; Baltz et al. 2012), though no work available to date has confirmed its binding domain specifically. However, recent evidence has emerged suggesting the highly conserved WD40 domain usually attributed to protein-protein interactions may provide an RNA binding capacity to proteins (Lau et al. 2009). Furthermore, the highly conserved coiled coil domain at its C-terminus has been suggested in other proteins to provide a site for RNA binding (discussed further in this section).

Identified as a key component of the 90S pre-ribosomal particle in yeast, its depletion leads to defective 18S rRNA biogenesis, ultimately affecting the synthesis of the 40S ribosomal subunit (Dragon et al. 2002; Dosil & Bustelo 2004). Simultaneously, PWP2 depletion is accompanied by defective separation following mitosis, though it is unclear whether it is a direct effect on cell cycle progression components or an indirect consequence of disrupted ribosome biogenesis (Dosil & Bustelo 2004). Ribosome biogenesis is a highly metabolically demanding process and dependent on energy status, cellular growth and proliferation, and thus is tightly controlled by mTOR signalling, specifically via S6 kinase mediated phosphorylation of RPS6 (Chauvin et al. 2014, discussed further in chapter 1). One study provided a connection to PWP2 and other associated factors involved in ribosome biogenesis downstream of RPS6 phosphorylation specifically (Chauvin et al. 2014). It was shown through use of arrays that livers of *rpS6*<sup>-/-</sup> mice displayed 25 to 55% reduction in mRNA levels of ribosome biogenesis factors. Interestingly, among the listed factors exhibiting this mRNA decrease, PWP2, GAR1, RRP12 and DDX18 appeared in our raw ISOQuant mass spectrometry results as proteins decreasing binding following mTOR inhibition, though

only PWP2 and GAR1 appeared in sufficient repeats to be considered for analysis. This suggests further influence of mTOR signalling over PWP2 abundance and activity in ribosome biogenesis, beyond the well-established control of mTOR over translation of TOP mRNAs, including ribosomal proteins.

In a vertebrate model, Boglev et al. (2013) confirmed a conserved role for PWP2 from yeast to zebrafish; here too it was shown to play a role in rRNA processing and assembly of the small ribosomal subunit, using a whole organism model possessing a truncated mutant of PWP2. Defective ribosome biogenesis arising from the deficit in 18S rRNA in the mutant zebrafish severely affects the cell growth in more rapidly proliferative tissues such as the intestinal epithelia, stimulating an increase of autophagy to prolong survival and briefly extend lifespan (Boglev et al. 2013). As outlined in the first chapter, autophagy is initiated by cells as a means to recycle cellular structures under conditions of nutrient stress sensed mainly by mTORC1, though a potential role for the AMPK signalling pathway has been suggested recently (Alers et al. 2012). The group indicated the induction of autophagy was mTOR and p53 independent, suggesting that it may instead be initiated such alternate signalling pathways.

TRIM25 is a member of the Tripartite Motif Containing Protein (TRIM) family of proteins which possesses an N-terminal RING finger domain, 2 B-box domains and has been shown to function as an E3 ubiquitin ligase through its highly conserved coiled coil domain (Zhu et al. 2016; Hatakeyama 2011). Over-expression of TRIM25 has been observed in a variety of cancers, including ovarian, breast, lung and gastric tissues (Urano et al. 2002; Qin et al. 2015; Zhu et al. 2016). In all cases, increased expression of TRIM25 was correlated with poor prognosis.

TRIM25 knockdown in both A427 lung cancer cell lines and also cells from gastric tumours resulted in a decrease in migration and invasion (Qin et al. 2015; Zhu et al. 2016). In A427 specifically however, Qin et al. (2015) commented on a reduced proliferation rate or even cell death following TRIM25 knockdown, which corroborated with the findings of multiple other studies (Ueyama et al. 2010; Zhang et al. 2015), whereas Zhu et al. (2016) specifically described no effect on proliferative capability.

TRIM25 has been shown in complex with p53 and its regulator protein Mdm2, and its over expression in vitro has been shown to increase the abundance of both, through prevention of their polyubiquitination and subsequent degradation by the 26S proteasome (Zhang et al. 2015). p53 is responsible for the transcription of a plethora of genes involved in cell cycle arrest, apoptotic initiation and also its own negative regulator Mdm2. Zhang et al. also showed reduction of TRIM25 to be responsible for an increase in the histone acetyl transferase p300, which acts to acetylate p53 and thereby increase its transcriptional activity, showing a dual function of TRIM25 with respect to the regulation of p53 levels and those of its target genes. This provides an interesting caveat of TRIM25 influence on the expression of cell cycle and survival genes as an E3 ligase; however it does not explain its function as an RBP.

TRIM25 was first identified as having an RNA binding function in mouse embryonic stem cells, by Kwon et al. (2013). Like PWP2, TRIM25 has no classical RBD; however through creation of a series of deletion mutants of the protein, it was shown that its RNA binding was dependent on the central region of the protein, which included the coiled coil domain (Kwon et al. 2013). Increasing numbers of proteins are being identified as having RNA binding capability despite harbouring no classical RBD or mRNA binding-related Gene Ontology terms, suggesting an expanding field for the annotation of novel and putative RNA binding protein motifs. A new methodology to identify RBDs of the proteins captured using the whole cell RBP technique specifically has recently been developed (Castello, Horos, et al. 2016), and has begun to provide an insight into the unknown RBDs of some of the novel RNA binding proteins discovered, though the depth appears to be lower than in the original study. Within the dataset however, (Castello, Fischer, et al. 2016) have identified possible peptides corresponding to non-canonical RBDs for SERBP1, PWP2 and LARP1, though as yet no peptides have been provided for TRIM25.

LARP1 is a member of the LARP (La-Related Protein) family of proteins, first identified in *Drosophila* (Blagden et al. 2009) as an RNA-independent interactor of the Poly-A Binding Protein (PABP). It is so named due to the 90 amino acid La Motif (LAM) shared across all members, which is similar to that of the genuine La protein. Each member of the LARP family has a different arrangement of domains attributed to its function;

those of importance for this study include an RNA recognition motif-like domain, and a C-terminal DM15 region unique to LARP1 within the family of proteins. Its RNA binding capacity is mostly attributed to this DM15 region, which has been shown to bind the 5'-UTR of several TOP mRNAs including RPS6 (Tcherkezian et al. 2014; Lahr et al. 2015; Fonseca et al. 2015), though RNA binding to the 3'-hydroxyl of the poly(A) tail of mRNA (Aoki et al. 2013), or through the LAM as shown in *C. elegans* (Nykamp et al. 2008). Increased expression of LARP1 has shown strong correlation with prognosis and clinical outcome in multiple cancers, including ovarian, cervical, breast, lung, liver and prostate (Burrows et al. 2010; Mura et al. 2015; Xie et al. 2013; Kato et al. 2015). In these cancers the increased expression of LARP1 leads to increased cell migration, invasion and tumorigenesis, as shown through siRNA studies performed by Burrows et al. (2010).

LARP1 has become an increasingly intriguing candidate as an RBP responsible for post-transcriptional control of mRNA downstream of the mTOR pathway, due to its emerging role in the apparently transcript-specific regulation of 5'-TOP mRNAs. The exact mechanism of regulation of TOP mRNAs by LARP1 is highly debated, with several groups showing conflicting results regarding whether LARP1 binding is a positive regulator (Aoki et al. 2013; Mura et al. 2015; Tcherkezian et al. 2014), or negative regulator (Fonseca et al. 2015; Merret et al. 2013) of these transcripts, or indeed whether it is a bimodal regulation where selected mRNA are stabilised and others destabilised dependent on function (Hopkins et al. 2015; Mura et al. 2015; Lahr et al. 2015). Therefore much of the role played by LARP1, and the RNAs to which it binds, remains to be elucidated in the context of post-transcriptional regulation of RNA downstream of mTOR signalling. Outstanding questions regarding LARP1 control of cellular functions, and the repertoire of RNAs to which it binds, make it an exciting addition to our investigations.

Reducing the scale of this experiment from that utilised by other groups simplified use of the protocol, eliminated the need for freeze-thaw cycles, and reduced the overall time required to acquire samples for mass spectrometry. In such a high throughput "screen"-style directed question, scaling up to include more starting material would likely have provided greater depth and coverage, though increasing overall processing

time leading up to mass spectrometry. In this instance it was considered rapid processing time would be more important due to the potentially transient nature of mTOR inhibition following aspiration of media, prior to cross linking. However, should greater depth be required to identify a greater repertoire of RBP changing their binding activity following Torin1 treatment in future, increasing the scale of the experiment is a promising way to achieve this.

As mentioned in section 3.2.3, a PCA of the original 5 repeats showed how conducting mass spectrometry following an immunoprecipitation-type methodology can introduce significant variation; such batch effects can be expected in analysis of such large datasets compiled over time (Leek et al. 2010). Batch effects have been shown to have sufficient impact such that the mean measurement between batches no longer reflects the correlation, or indeed reverses the correlation, between groups. This consequently decreases the power of the experiment and can mask the biological effect (Leek et al. 2010). Normalisation can remove non-biological variability but it is not always able to adjust for batch effects (Leek et al. 2010; Fei et al. 2011). Principal component analysis and subsequent construction of model matrices incorporating experimental processing as a factor for surrogate variable analysis suggested all batch effects could be captured and adjusted for in 3 of the 5 replicates compiled for this study. Hence these three repeats alone were carried forward for statistical analyses. The importance of adjusting for batch effect in analysis of large, high-throughput datasets, both in genomics and proteomics, is becoming more widely accepted.

The data analysis methodology of such a study to investigate a dynamic interactome could be developed further. As the use of proteomics expands, statistical analyses should evolve too; high-throughput methodologies such as next generation sequencing and ribosomal profiling have given rise to openly available packages and increasingly standardised approaches for analysis specifically for handling such complex data-sets. Alternative packages that might be applied to such an analysis include 'DESeq', a freely available package on R originally designed to address analysis of large RNA sequencing datasets since used for proteomics analysis (Anders & Huber 2010; Kuharev et al. 2015), or the 'R for Proteomics' package (Gatto & Christoforou 2014). Use of these

analysis packages requires in more in depth knowledge of the R environment than the approach used here, though can be considered for future use.

Following identification and validation of the four mTOR-dependent RBPs described here, this study moves to further characterise their function in the context of mTOR-specific regulation of gene expression. In the first instance, this will involve the use of siRNAs targeted to the mRNA of each of the 4 proteins, to characterise their cellular role with respect to processes including growth, cell cycle regulation and cell survival, before advancing to identify the specific mRNAs to which they are bound and their roles in the post-transcriptional regulation of said messages.

## **Chapter 4**

## **4. Investigating the roles of mTOR-regulated RNA Binding Proteins in cell survival and proliferation**

### **4.1. Introduction**

mTOR signalling is integral to cellular growth, stimulated by growth factors and nutrient abundance, such as amino acids and other energy signals including ATP. Activation of mTOR signalling is required for the stimulation of protein synthesis and other anabolic events, allowing cells to reach the size required to progress through M phase and proliferate. In particular mTOR is responsible for stimulating protein synthesis through phosphorylation of its two key targets, ribosomal S6 kinase (S6K) and eukaryotic initiation factor 4E binding protein 1 (4E-BP1), discussed previously (section 1.4.4). S6K is subsequently responsible for the phosphorylation of ribosomal protein S6 (RPS6), a component of the 40S ribosomal subunit. Furthermore, mTOR has been previously linked to the regulation of 5' TOP mRNAs, potentially through modulation of an intermediary binding protein that may influence translation or stability of this subset of messages. However the exact mechanism for the control over 5' TOP messages has yet to be established.

Using whole cell RNA Binding Protein capture techniques and subsequent mass spectrometry, we have identified and validated four RNA binding proteins (RBPs) whose binding changed following mTOR inhibition with Torin1. The RBPs validated were SERBP1 and PWP2, whose binding decreased, and TRIM25 and LARP1, whose binding increased following Torin1 treatment. Though validation of the changes in RNA binding capacity of these four proteins following mTOR inhibition has been shown, questions regarding how they potentially contribute to mTOR modulation of expression of mRNA, and the response brought about by mTOR signalling, remain unanswered.

All four of these validated proteins have been previously identified as RBPs through the original HeLa whole cell interactome capture and proteomics screen conducted by Castello et al. (2012). Further work by other groups has begun to characterise roles for each protein in eukaryotic cells; TRIM25 for example has been shown to have

differential expression in mouse embryonic stem cells (Kwon et al. 2013), PWP2 has a potentially well conserved function in pre-rRNA processing in yeast and possibly mammalian cells (Dasil & Bustelo 2004) and SERBP1 has been shown to interact with the eukaryotic ribosome and other factors (Anger et al. 2013). In addition, the final validated protein identified as changing binding following mTOR inhibition, LARP1, has been discussed in the context of mTOR signalling and 5' TOP regulation in the literature recently (Tcherkezian et al. 2014; Fonseca et al. 2015); and others, discussed in greater detail later in this chapter).

Here we aimed to conduct a screen using silencer RNA (siRNA) to further characterise their individual roles in cell growth and proliferation. Through depletion of each of the 4 proteins using RNAi, we can better understand their roles in processes downstream of mTOR including cell proliferation, cell cycle regulation and survival. It is well known that mTOR signalling plays a prominent role in control of cellular growth; its activity has been connected to 5' TOP mRNA translational control, which encode all the ribosomal proteins and other factors involved in translation. Investigation into the effects of depletion of each of these four validated proteins has on both growth and cell cycle is therefore a logical step to identify specific candidates for follow up here.

## **4.2. Results**

### **4.2.1. SERBP1 depletion leads to a modest slow in proliferation over a 96 hour period of growth**

With the aim of better defining the role of SERBP1 in the context of cell growth signalling, HeLa cells were reverse transfected with siRNA against the mRNA of SERBP1 and grown under usual culture conditions. The number of cells in each well at various time points could be compared back to a scrambled siRNA control seeded at the same density, and reverse transfected at the same time zero. In this way, it would be possible to investigate effects of depletion of SERBP1 on growth rate, cell viability, morphology and cell cycle progression through the use of FACS and microscopy.

The effect of SERBP1 depletion by siRNA on HeLa cell growth is shown at various time points post-transfection in Figure 4.1A. A steady reduction in proliferation with respect to control can be seen for the SERBP1 depleted HeLa cells, as indicated by lower cell

numbers from as early as 48 hours post-transfection. After 96h post-siRNA transfection the mean total cell number was 68% of that for the control transfected cells; loss of SERBP1 had reduced cellular proliferation by around a third as determined by viable cell number.

Fig 4.1B shows a representative set of western blots for one of the three growth curve experiments performed. As well as probing for SERBP1 protein levels across the time points, a blot for PARP and its 85 kDa cleavage product was conducted to indicate the extent of apoptotic activation. It shows no notable detected PARP cleavage product, indicating the difference in cell number between SERBP1 and control conditions in this instance is not necessarily due to a notable increase in apoptotic populations of cells, but possibly a result of cell cycle stalling or arrest.

#### **4.2.2. SERBP1 depletion by siRNA does not lead to any obvious morphological changes in HeLa cells at 72 hours post transfection**

Following on from growth curve experiments, where a moderate decrease in cell number was described for SERBP1 depleted HeLa cells, this study progressed to investigate its effect other key cellular processes, as well as cell morphology. The 72 hour time point post-transfection with siRNA against SERBP1 was selected for further investigations, as here the protein was clearly depleted in each of the repeats. Phase contrast microscopy was used to capture images of wells representing each condition (Figure 4.2A), showing no exaggerated difference in cell morphology, cytoskeletal arrangement, nuclear fragmentation, blebbing or obvious changes in cell size between control and SERBP1 depleted cells. Figure 4.2B is a representative western showing the extent of SERBP1 knockdown achieved, and the absence of PARP cleavage at this time point. To confirm apoptosis was not the reason for the difference in cell number as illustrated by the growth curve in Figure 4.1A, FACS analysis of cells at the 72 hour time point was conducted.

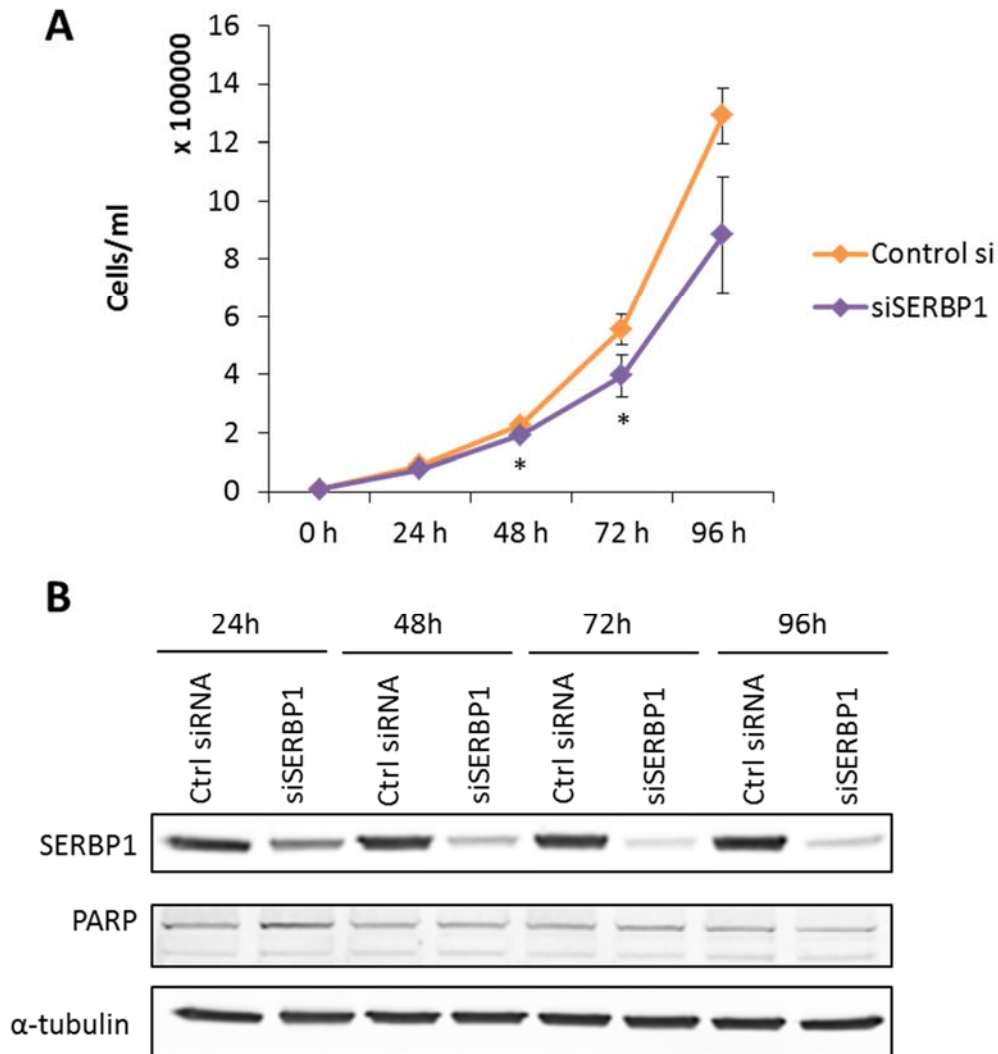


**Figure 4.1 Growth curves following SERBP1 knockdown showed modest slow in cellular growth rate relative to scrambled siRNA control.** HeLa cells were seeded at 40,000 cells per well of a 6 well plate and reverse transfected using siRNA targeting SERBP1, or a scrambled siRNA control (siCtrl). (A) Cells were left to grow for indicated durations post-transfection and harvested at indicated time points (as described in materials and methods). Viable cell number counted using a Model TT CASY Counter (in triplicate, n=3). Cell count was compared between conditions by paired t-test: \* = p value < 0.05, \*\* = p value < 0.01, \*\*\* = p value < 0.005. (B) Cells were spun to a pellet, lysed, normalised by Bradford assay and subjected to western blotting (representative shown) with indicated antibodies. Here  $\alpha$ -tubulin was used as a loading control.

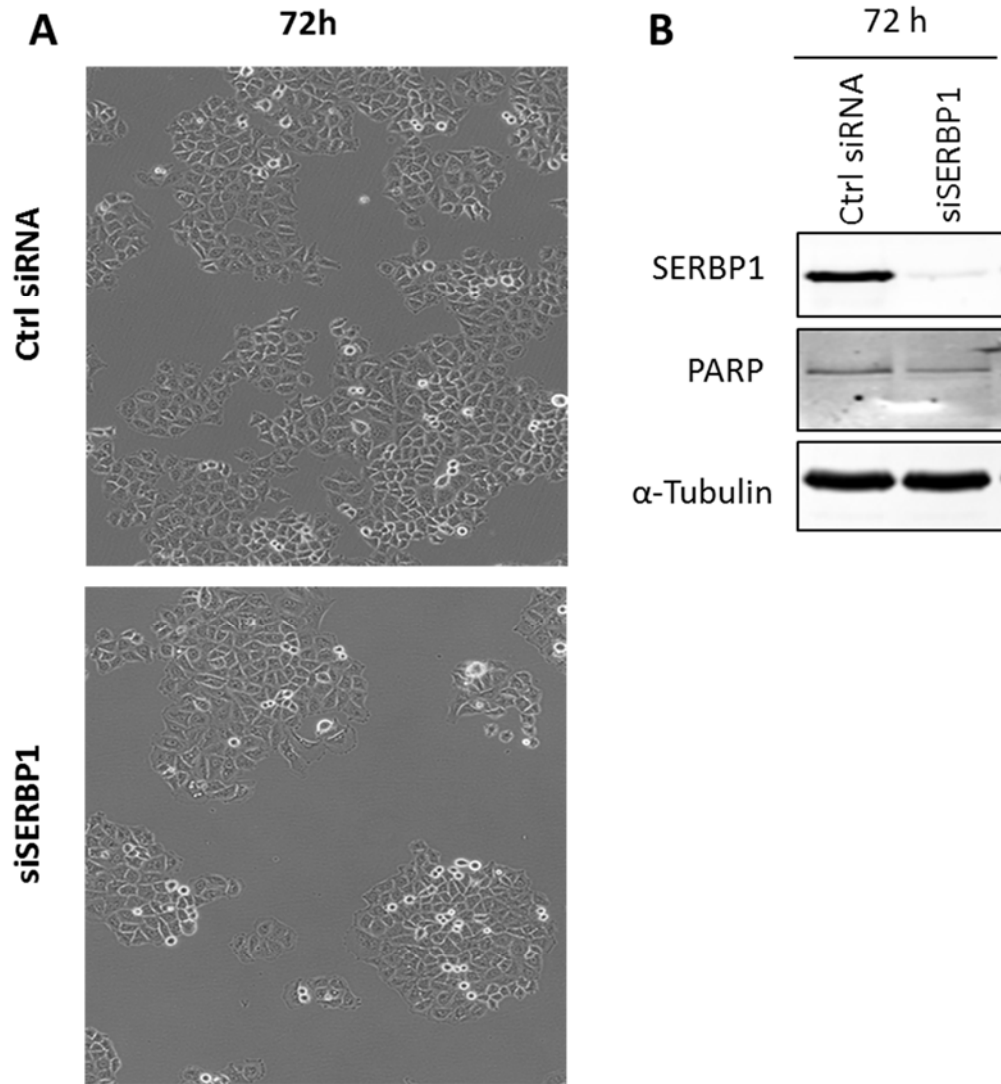


**Figure 4.2 Cell morphology and PARP cleavage following 72 hours siRNA knockdown of SERBP1, knockdown is efficient but does not elicit notable visual changes in cell morphology.** HeLa cells were seeded at 40,000 cells per well of a 6 well plate and reverse transfected with siRNA against SERBP1, or a scrambled siRNA control (siCtrl). Cells were then incubated in a humidified incubator at 37°C for 72 hours. (A) Representative images taken using 10x magnification of a phase contrast microscope showing cell morphology and density 72 hours post-transfection illustrates the slower growth rate following SERBP1 knockdown, without changes in phenotype. (B) Once harvested (as described in materials and methods), a proportion of cells were lysed and subjected to western blotting to confirm efficient knockdown of SERBP1. Apoptotic activation was determined through probing for PARP cleavage. Here  $\alpha$ -tubulin was used as a loading control.

#### **4.2.3. Difference in cell number following SERBP1 depletion by siRNA for 72 hours is not due to induction of apoptosis, nor changes in cell cycle distribution, as determined by FACS analysis**

FACS analysis following staining using Annexin-FITC or DRAQ7 fluorophores revealed that SERBP1 knockdown by siRNA did not initiate apoptosis in HeLa cells. Representative dot plots in Figure 4.3A show the populations within quadrants Q1, Q2, Q3 and Q4, which represent early apoptotic stage cells (Annexin-FITC positive only, green), late stage apoptotic cells (Annexin-FITC and DRAQ7 positive, orange), viable or unstained cells (blue), and finally necrotic cells (purple) respectively. Though a small shift in the populations can be seen from viable to early apoptotic, this represents only a mean increase of 0.83% according to the mean of three repeats. Bar charts illustrating this data (Figure 4.3B) show the proportions of the percentage of cells within each population (quadrants 1 to 3), which showed no change between conditions to have a p value termed statistically significant following a paired t-test.

An alternative possibility to consider which could have explained the difference in cell number after 96 hours was an effect on cell cycle progression or distribution. This hypothesis was investigated using FACS analysis of fixed, propidium iodide (PI) stained cells to analyse cells' DNA content. Representative dot plots of gating selection for this FACS analysis (Figure 4.4A) was extended to include cells with possible doubled DNA content or cells exhibiting aneuploidy ( $>4n$ ), such as those where mitosis has not occurred efficiently, as well as normal diploid ( $2n$ ) cells. These can be seen in the dot plots as those points above the main cluster but within the gate drawn. Those below, representing apoptotic cells and debris, were excluded at a later stage of the analysis. The percentage of cells in each stage of the cell cycle 72 hours following transfection with siRNA ( $n=3$ , Figure 4.4B) showed no change in the distribution profile, nor in tetraploid or aneuploid populations. Therefore the difference in number of cells relative to control siRNA transfected is not due to any defect in cell cycle progression. Recent literature has identified SERBP1 as being associated with ribosomal proteins and elongation factors (Anger et al. 2013); therefore it is potentially plausible that its depletion may affect protein synthesis, possibly in a negative capacity. This concept is discussed further later in this chapter.

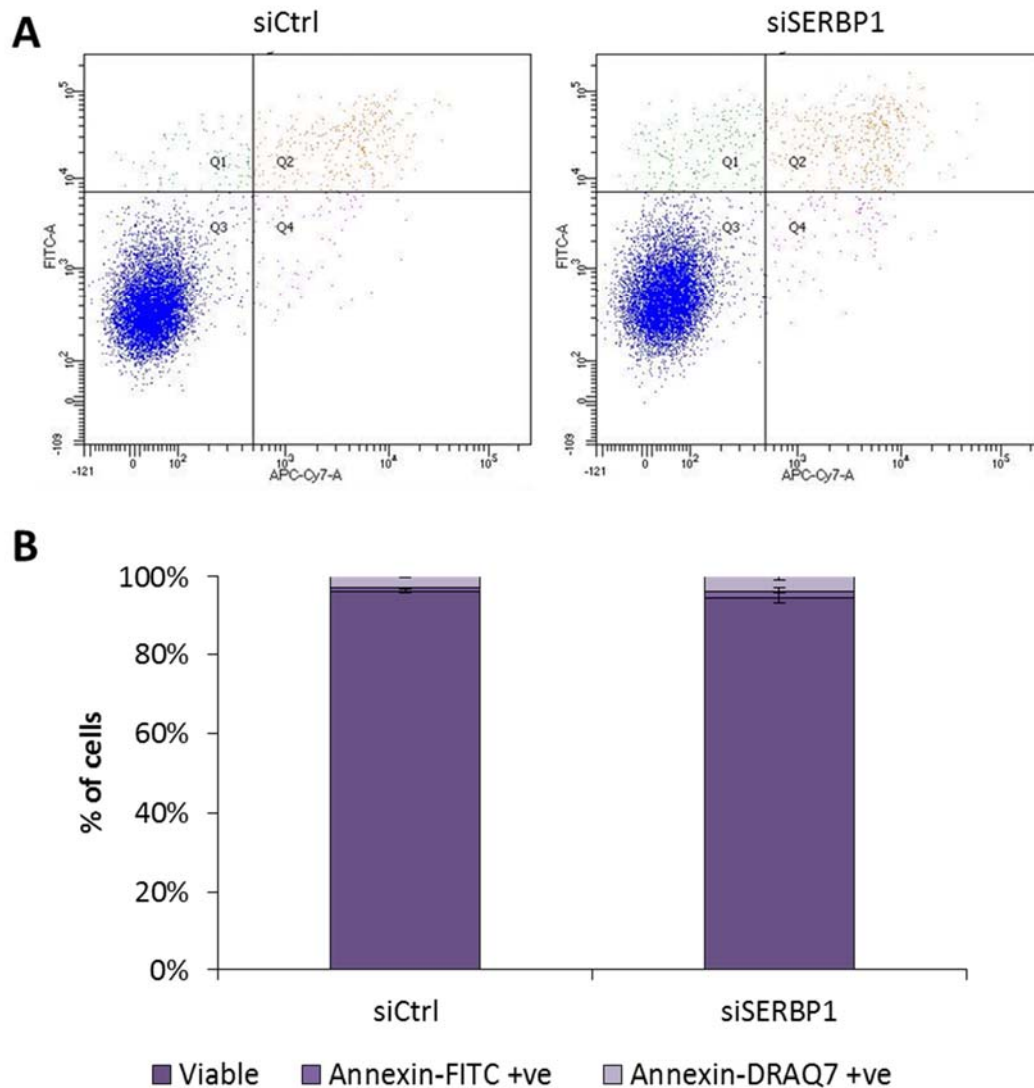


**Figure 4.3 FACS analysis following 72 hours knockdown of SERBP1, shows depletion does not lead to an increased rate of apoptosis in HeLa cells.** (Efficiency of knockdown can be seen in representative western Fig 4.2.) Following 72 hours of SERBP1 depletion using siRNA, cells were harvested and stained for FACS analysis using Annexin-FITC and DRAQ7 fluorophores. (A) Representative dot plot showing distribution of HeLa cells in quadrants Q1, Q2, Q3 and Q4, representing Annexin-FITC positive only, Annexin-FITC and DRAQ7 positive, unstained viable and DRAQ7 only stained populations respectively. (B) Bar chart showing the mean distribution between quadrant populations across repeats (n=3). A paired t-test was performed between conditions showed none to have a p value of significance (p value < 0.05).

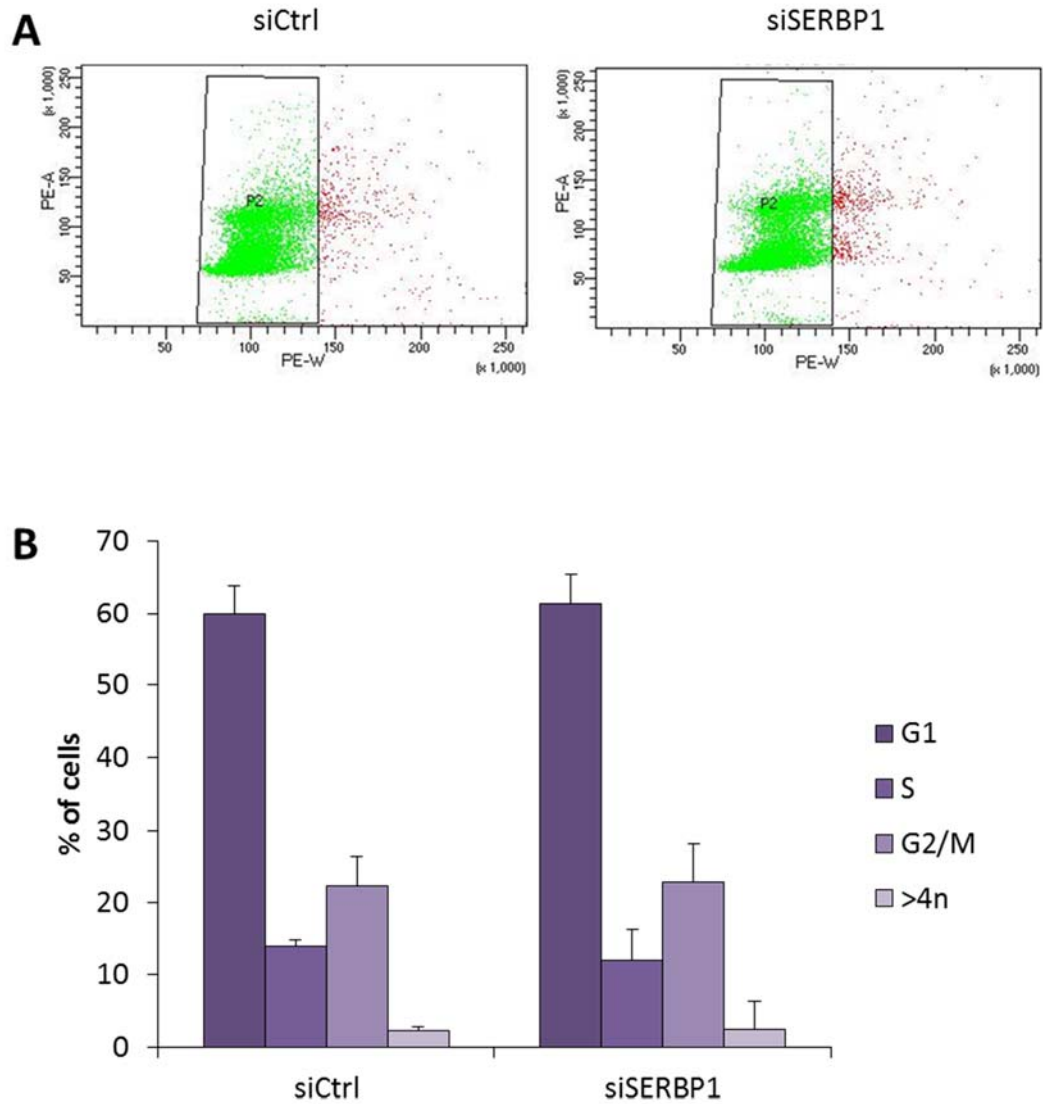


**Figure 4.4 Cell cycle distribution following 72 hours SERBP1 knockdown shows depletion does not lead to changes in cell cycle distribution in HeLa cells.** (Efficiency of knockdown can be seen in representative western Fig 4.2.) Following 72 hours of SERBP1 depletion using siRNA, cells were harvested, ethanol fixed and stained using Propidium Iodide for cell cycle FACS analysis. (A) Representative dot plot showing distribution of HeLa cells by cellular area versus stained DNA content. (B) Bar chart showing the cell cycle distribution between scrambled control siRNA transfected cells and SERBP1 siRNA transfected across repeats (n=3). A paired t-test was performed between conditions showed none to have a p value of significance (p value < 0.05).

#### **4.2.4. PWP2 depletion by siRNA caused dramatic decrease in the proliferation rate of HeLa cells, with no conclusive induction of autophagy**

In our study, alongside SERBP1, PWP2 was shown to have decreased RNA binding following Torin1 treatment. As mentioned in the previous chapter, connections have been suggested between PWP2 and autophagy in zebrafish (Boglev et al. 2013). Though autophagy is a process usually under the control of mTOR signalling the relationship between PWP2 and autophagy in these organisms was proposed to be mTOR independent. Therefore as well as investigations into the effect of PWP2 on cell growth rate (Figure 4.5A), it was decided that levels of LC3B, a marker of autophagy, would also be investigated in subsequent western blots.

PWP2 depletion by siRNA led to a slow in cellular proliferation, in fact to a greater extent than SERBP1 (Figure 4.5A), with the number of viable cells 96 hours following transfection with siRNA against PWP2 being 73% lower than in control conditions. Representative blots in Figure 4.5B show the efficiency of the PWP2 knockdown to be convincing, with no detectable protein by western from as early as 24 hours post-transfection. However, this showed LC3B was not induced above control levels at any time point, and indeed at 72 hours and onward levels were noticeably lower than control transfected cells. This could be as a result of cells in the control transfected wells reaching a level of confluency or nutrient deprivation which activated autophagy as a means to moderate growth, as media was not changed during the time course in order to ensure collection of all cells.

#### **4.2.5. Depletion of PWP2 by siRNA does not lead to any extreme morphological changes in HeLa cells 72 hours post-transfection.**

PWP2 depletion led to a dramatic decrease in cell proliferation rate (as determined by growth curve experiments), and despite evidence in the literature describing initiation of autophagy signalling in the absence of PWP2 cell lines (Boglev et al. 2013), we were unable to detect any increase in the autophagy marker LC3B above control conditions. Therefore the decrease in viable cell number following PWP2 depletion in HeLa cells remains unexplained; next we moved to investigate morphological changes instigated by PWP2 depletion.

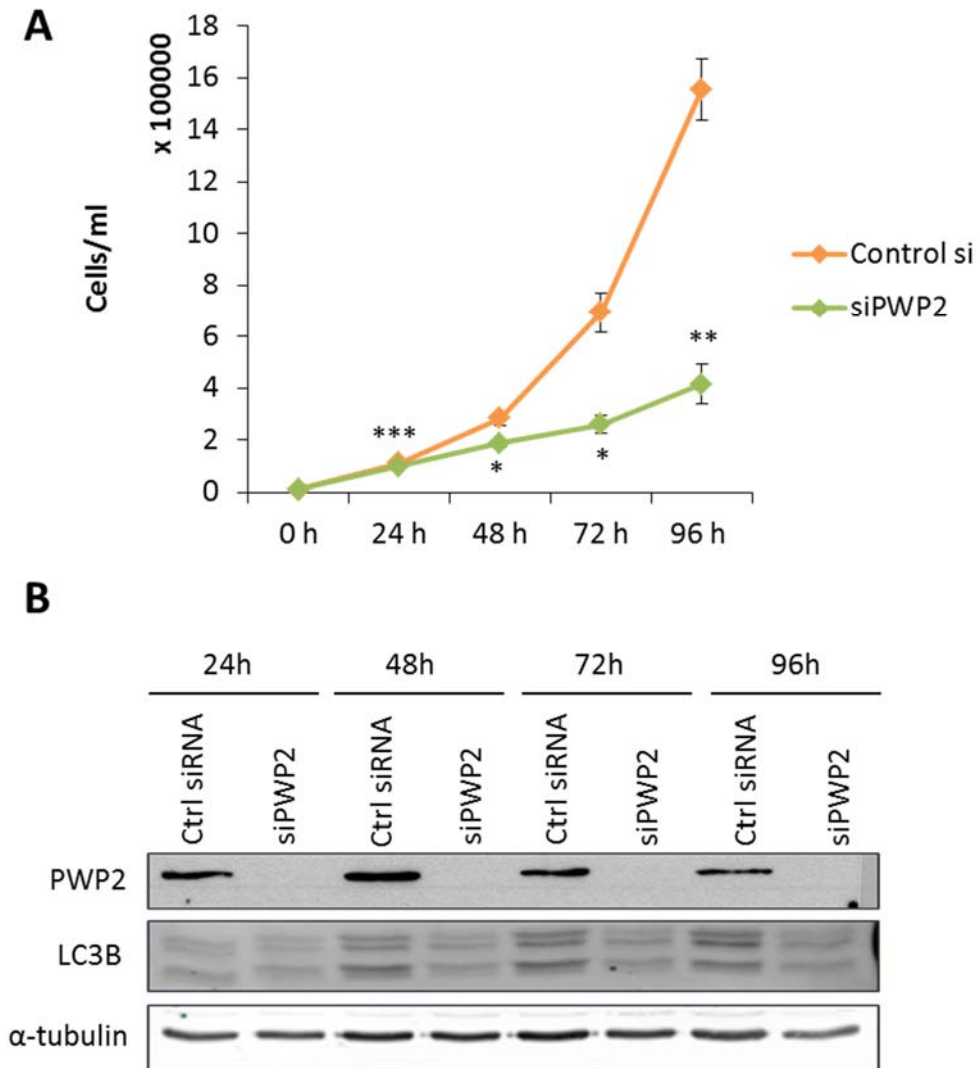


**Figure 4.5 Growth curves following PWP2 knockdown showed dramatic slow in cellular growth rate relative to scrambled siRNA control.** HeLa cells were seeded at 40,000 cells per well of a 6 well plate and reverse transfected using siRNA targeting PWP2, or a scrambled siRNA control (siCtrl). (A) Cells were left to grow for indicated durations post-transfection and harvested at indicated time points (as described in materials and methods). Viable cell number counted using a Model TT CASY Counter (in triplicate, n=3). Cell count was compared between conditions by paired t-test: \* = p value < 0.05, \*\* = p value < 0.01, \*\*\* = p value < 0.005. (B) Cells were spun to a pellet, lysed, normalised by Bradford assay and subjected to western blotting (representative shown) with indicated antibodies. Investigation of activation of autophagy was determined by probing for LC3B cleavage, to determine whether the lower cell number was due to autophagy. Here  $\alpha$ -tubulin was used as a loading control.

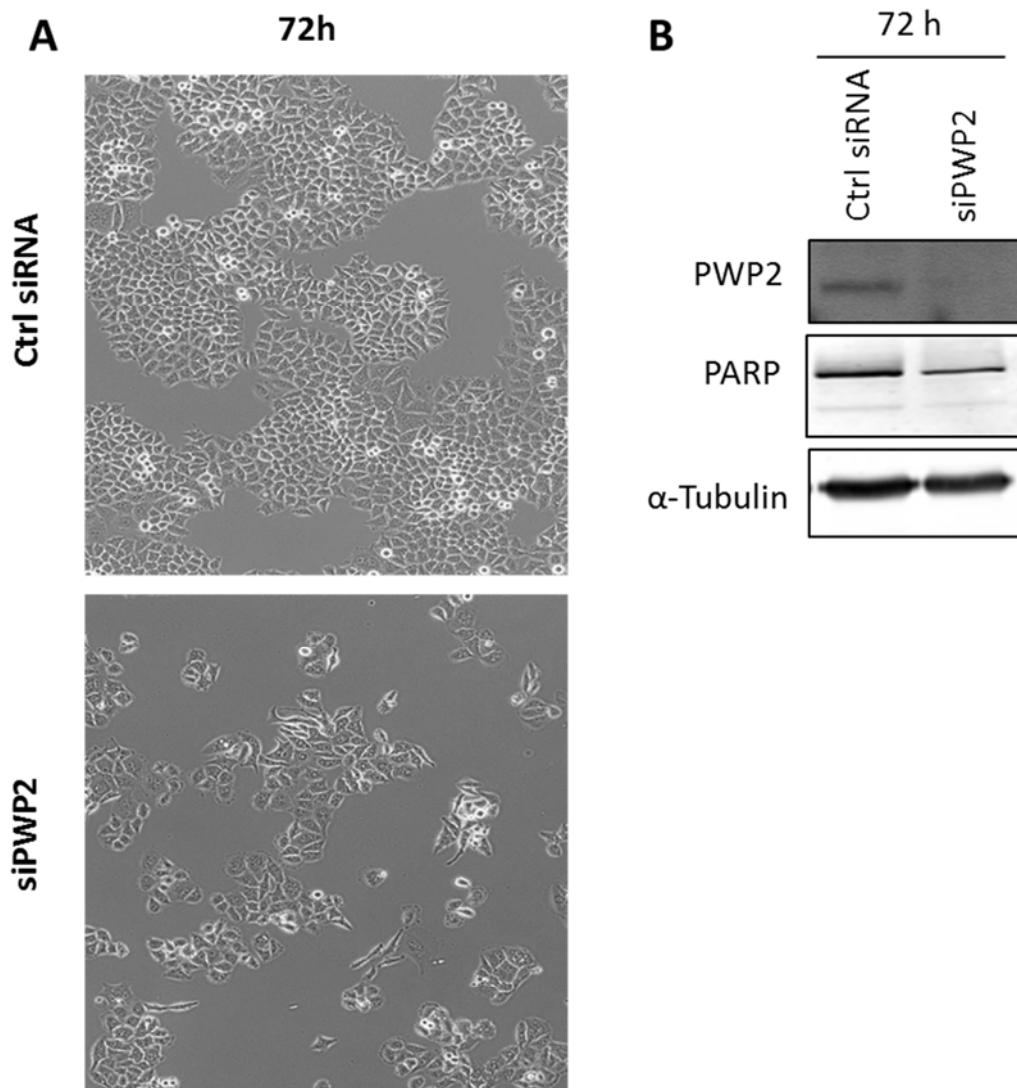


**Figure 4.6 Cell morphology and PARP cleavage following 72 hours siRNA knockdown of PWP2, knockdown is efficient with subtle visual changes in cell morphology.** HeLa cells were seeded at 40,000 cells per well of a 6 well plate and reverse transfected with siRNA against PWP2, or a scrambled siRNA control (siCtrl). Cells were then incubated in a humidified incubator at 37°C for 72 hours. (A) Representative images taken using 10x magnification on a phase contrast microscope showing cell morphology and density 72 hours post-transfection illustrates the considerably slower growth rate following PWP2 knockdown. Changes in phenotype were not dramatic, cells were slightly more grainy in appearance. (B) Once harvested (as described in materials and methods), a proportion of cells were lysed and subjected to western blotting to confirm efficient knockdown of PWP2. Apoptotic activation was determined through probing for PARP cleavage. Here  $\alpha$ -tubulin was used as a loading control.

The difference in HeLa cell number, as previously seen in growth curve experiments, was apparent at 72 hours post-transfection, though cells showed no extreme differences in cell shape or size (Figure 4.6A). However, it was noted from visual observation of wells prior to harvesting that cells appeared slightly more granular in appearance than control transfected cells. Representative blots (Figure 4.6B) showed strong depletion of PWP2 levels at the 72 hour time point post-transfection, though there was an absence of a detectable PARP cleavage product, indicating that apoptosis may not explain the difference in cell number indicated in the growth curve experiments.

#### **4.2.6. Difference in cell number 72 hours following knockdown of PWP2 was not explained by induction of apoptosis in HeLa cells, nor by large changes in cell cycle distribution**

FACS analysis using Annexin-FITC and DRAQ7 staining 72 hours following transfection with siRNA against PWP2 (representative dot plots, Figure 4.7A) showed a negligible difference between the percentage of viable cells and that of the apoptotic population. When this is quantified across n=3 in Figure 4.7B; the mean percentage of cells in the viable population decreases by only 5% following PWP2 knockdown, yet a paired t-test showed this change to have a statistically significant p value. The change in viable cell number between conditions at 72 hours post-transfection, represented as a decrease of 73% in the growth curve experiment (Fig4.5A), is therefore not explained by an increase in cell apoptosis.

As mentioned in the previous chapter, PWP2 has been linked to ribosomal RNA processing, specifically with assembly of the 90S pre-ribosomal particle in yeast, and its depletion thereby affects ribosome biogenesis (Dosil & Bustelo 2004). It has also been noted that growth rate of yeast slows considerably following depletion of Pwp2/Utp1 (Bernstein & Baserga 2004; Bernstein et al. 2007). It is plausible therefore, that its depletion in a mammalian cell line would also lead to a disruption in ribosome biogenesis, therefore slowing protein synthesis and stalling cell cycle progression and growth through eventual arrest late in G1 phase, before initiation of the start of cell cycle. Cell cycle distribution, determined by FACS of fixed cells following PI staining of

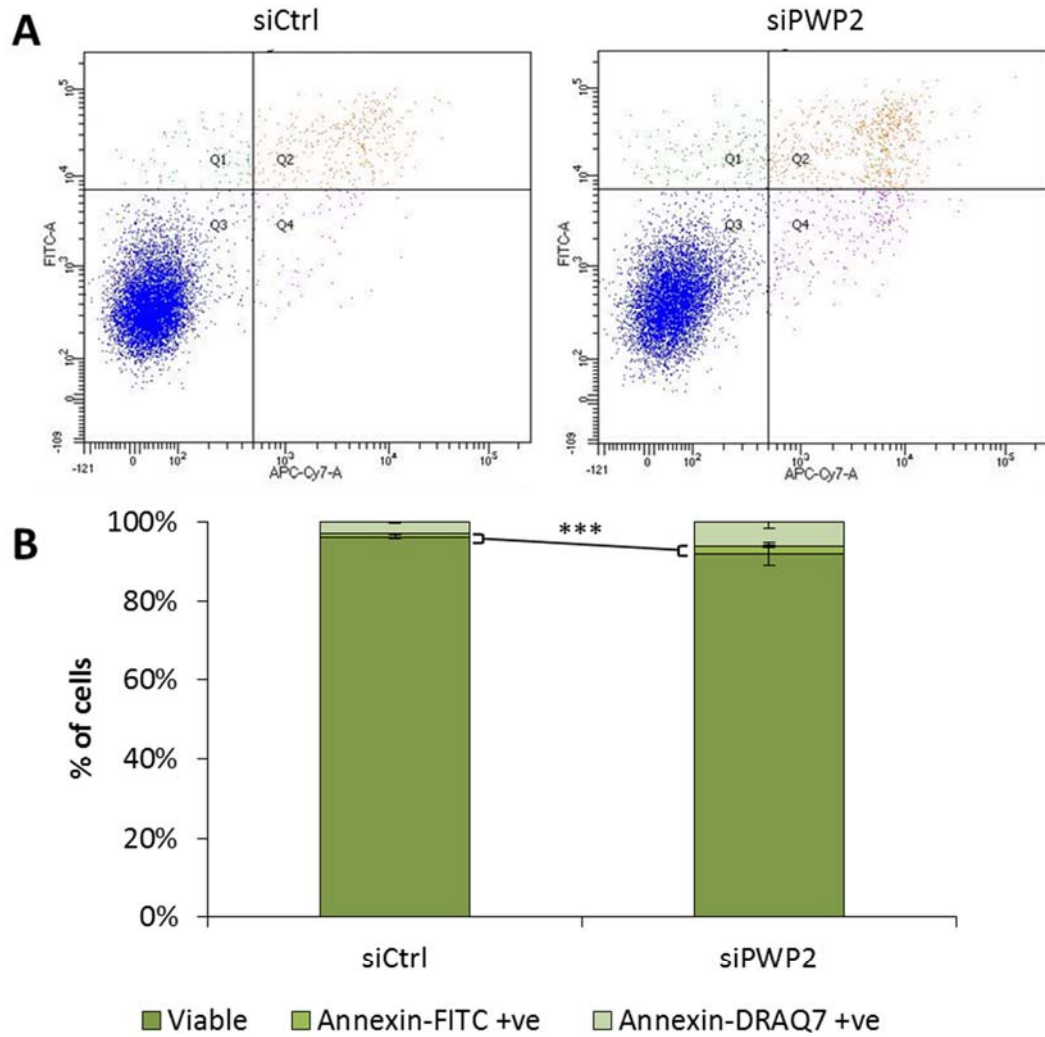


**Figure 4.7 FACS analysis following 72 hours knockdown of PWP2 shows depletion does not lead to an increased rate of apoptosis in HeLa cells.** (Efficiency of knockdown can be seen in representative western Fig 4.6) Following 72 hours of PWP2 depletion using siRNA, cells were harvested and stained for FACS analysis using Annexin-FITC and DRAQ7 fluorophores. (A) Representative dot plot showing distribution of HeLa cells in quadrants Q1, Q2, Q3 and Q4, representing Annexin-FITC positive, both Annexin-FITC and DRAQ7 positive, unstained viable and DRAQ7 only stained populations respectively. (B) Bar chart showing the mean distribution between populations across repeats (n=3). A paired t-test was performed between conditions and significance was assigned as follows: \* = p value < 0.05, \*\* = p value < 0.01, \*\*\* = p value < 0.005.

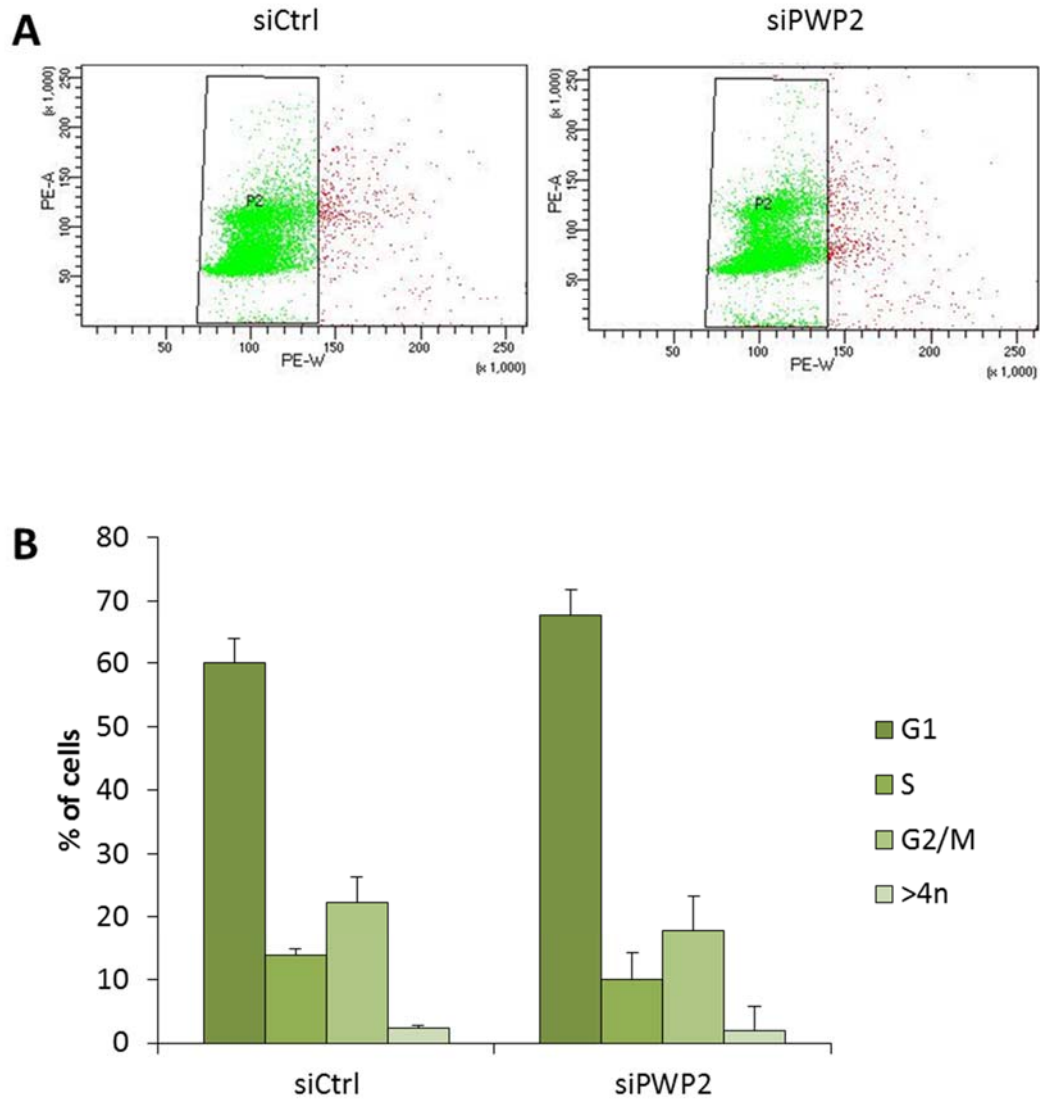


**Figure 4.8 Cell cycle distribution following 72 hours PWP2 knockdown shows depletion does not lead to changes in cell cycle distribution in HeLa cells.** (Efficiency of knockdown can be seen in representative western Fig 4.6) Following 72 hours of PWP2 depletion using siRNA, cells were harvested, ethanol fixed and stained using Propidium Iodide for cell cycle FACS analysis. (A) Representative dot plot showing distribution of HeLa cells by cellular area versus stained DNA content. (B) Bar chart showing the cell cycle distribution between scrambled control siRNA transfected cells and PWP2 siRNA transfected across repeats (n=3). A paired t-test was performed between conditions showed none to have a p value of significance (p value < 0.05).

DNA content, did not show any significant changes following 72 hours of PWP2 depletion; the G1 population increased by 7.8%, and to an even lesser extent G2/M by 5.4% (n=3, Figure 4.8B).

#### **4.2.7. Depletion of TRIM25 by siRNA led to a decrease in viable cell number of a third by 96 hours post-transfection**

As outlined in the previous chapter, TRIM25 is an E3 ubiquitin ligase first identified as having an RNA binding capacity in mouse embryonic stem cells (Kwon et al. 2013), despite having no classical or known RBD. Furthermore, it has been shown that overexpression of TRIM25 leads to the increase in abundance of p53 and Mdm2, increasing the transcription of cell cycle and survival genes (Zhang et al. 2015), hinting at a role of TRIM25 in the influence of these processes.

TRIM25 was identified in our mass spectrometry dataset as an RNA binding protein whose binding increased following treatment with the mTOR inhibitor Torin1. Depletion of TRIM25 by siRNA targeting of its mRNA had a modest effect on proliferation rate of HeLa cells (Figure 4.9A), with numbers of cells remaining comparable relative to a control siRNA transfected group until around 48 hours post-transfection. By 96 hours post-transfection, the number of viable cells in the TRIM25 depleted condition represented around 63% of that of the control group. From representative westerns (Figure 4.9B) it is clear the knockdown of TRIM25 is not particularly robust at the earlier time points of 24 and 48 hours; this may explain why at these two points the number of viable cells is as similar as is seen in Fig 4.9A; however at 72 hours post-transfection onwards levels of TRIM25 are conclusively lower. At these time points, there is no detectable PARP cleavage product, indicating the difference in viable cell number between conditions is unlikely to be due to activation of apoptotic pathways.

#### **4.2.8. There were no obvious morphological changes in HeLa cells 72 hours following depletion of TRIM25**

Previous literature has shown a role for TRIM25 in the p53/Mdm2 axis and thereby influence of p53 controlled genes including those within cell cycle and survival

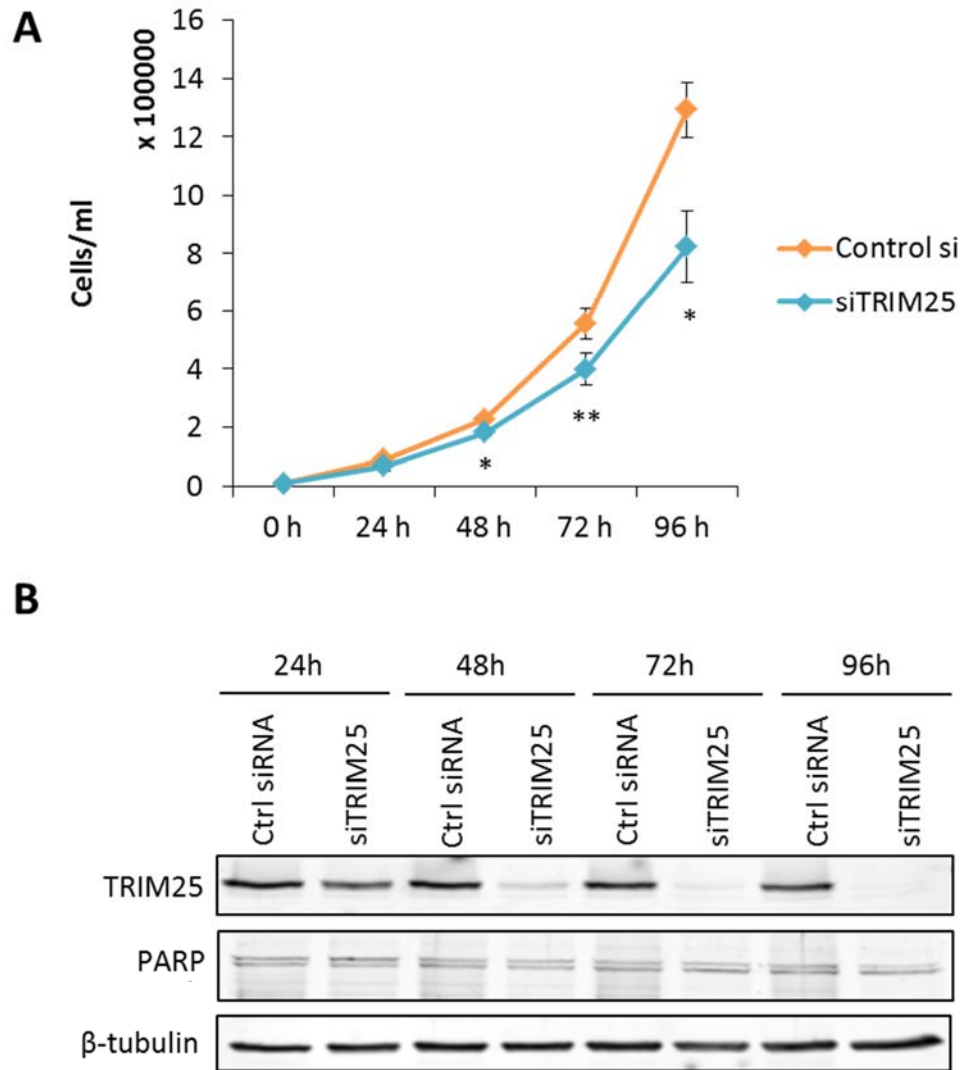


**Figure 4.9 Growth curves following TRIM25 knockdown showed modest slow in cellular growth rate relative to scrambled siRNA control.** HeLa cells were seeded at 40,000 cells per well of a 6 well plate and reverse transfected using siRNA targeting TRIM25, or a scrambled siRNA control (siCtrl). (A) Cells were left to grow for indicated durations post-transfection, and harvested at indicated time points (as described in materials and methods). Viable cell number was counted using a Model TT CASY Counter (in triplicate, n=3). Cell count was compared between conditions by paired t-test: \* = p value < 0.05, \*\* = p value < 0.01, \*\*\* = p value < 0.005. (B) Cells were spun to a pellet, lysed, normalised by Bradford assay and subjected to western blotting (representative shown) with indicated antibodies. Here  $\beta$ -tubulin was used as a loading control.

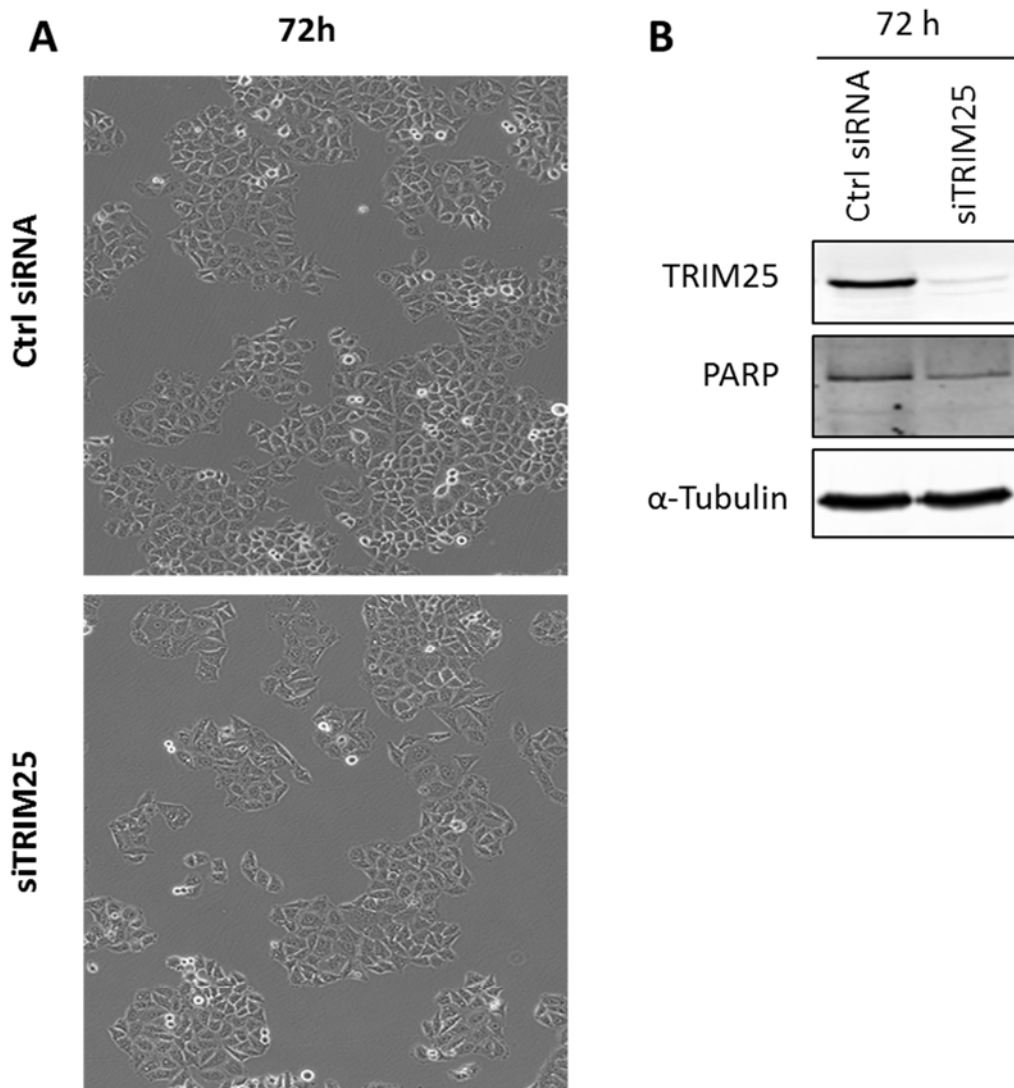


**Figure 4.10 Cell morphology and PARP cleavage following 72 hours knockdown of TRIM25 shows knockdown is efficient but does not elicit notable visual changes in cell morphology.** HeLa cells were seeded at 40,000 cells per well of a 6 well plate and reverse transfected with siRNA against TRIM25, or a scrambled siRNA control (siCtrl). Cells were then incubated in a humidified incubator at 37°C for 72 hours. (A) Representative images taken using 10x magnification of a phase contrast microscope showing cell morphology and density 72 hours post-transfection illustrates the modest slow in growth rate following knockdown of TRIM25, without changes in phenotype. (B) Once harvested (as described in materials and methods), a proportion of cells were lysed and subjected to western blotting to confirm efficient knockdown of TRIM25. Apoptotic activation was determined through probing for PARP cleavage. Here  $\alpha$ -tubulin was used as a loading control.

processes. We showed through siRNA depletion of TRIM25 in a growth curve experiment that a loss of TRIM25 caused a decrease in cell proliferation of approximately a third after 96 hours of incubation. It therefore followed to investigate the impact of TRIM25 depletion on the morphology, cell survival and cell cycle distribution of HeLa cells to determine whether these provided any clues as to how TRIM25 was causing this decrease in cell number.

As this time point was the earliest showing efficient knockdown, 72 hours of incubation post-transfection was used for further investigations. Figure 4.10A shows representative phase contrast microscopy images of control transfected and TRIM25 siRNA transfected cells; comparisons between these images show a lower cell density in the TRIM25 depleted wells relative to control. However no changes in morphology can be determined, and cells appear to be extending for contact as would be expected at that confluency. Representative western blots for this time point (Figure 4.10B) show the robust efficiency of TRIM25 knockdown; as with previous growth curve experiments there was no detectable PARP cleavage product, again suggesting the difference in cell number between conditions was unlikely to be due to apoptosis.

#### **4.2.9. Difference in cell number 72 hours following knockdown of TRIM25 was not explained by induction of apoptosis in HeLa cells, or by large changes in cell cycle distribution**

To confirm the effect of TRIM25 depletion on decreased cell proliferation was not due to apoptosis or cell cycle distribution, FACS analysis of HeLa cells 72 hours post-transfection with siRNA against TRIM25 was conducted. First, FACS analysis of live TRIM25 depleted cells using Annexin-FITC and DRAQ7 fluorophore staining (representative dot plots, Figure 4.11A) showed no shift in scatter which would indicate an increase in apoptotic cell population. Quantified over three repeats (Figure 4.11B), the percentage of cells per quadrant shows no change of statistical significance following a paired t-test. Similarly to SERBP1 knockdown therefore, there is no way of conclusively ruling the lower cell number following TRIM25 depletion to be due to an increase in apoptosis of HeLa cells.

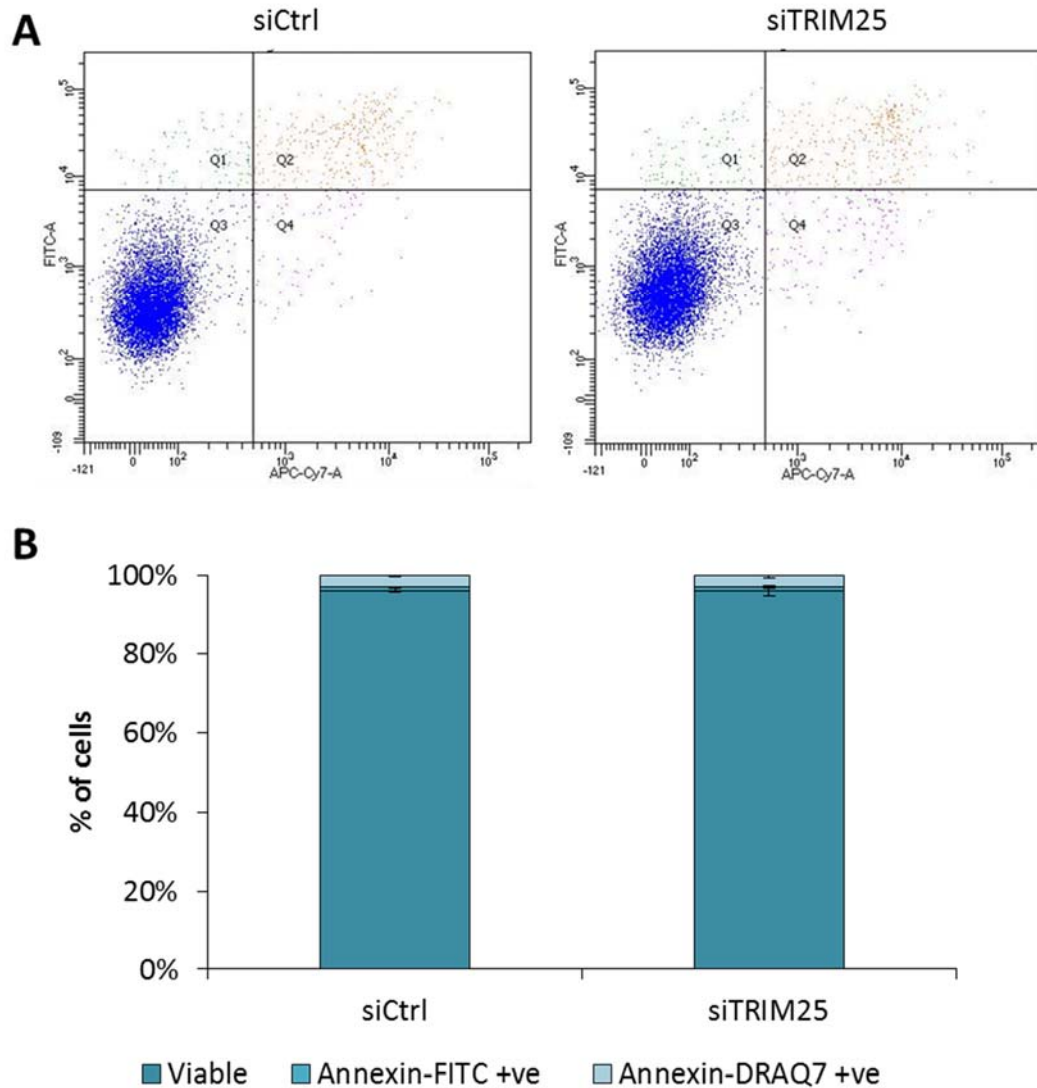


**Figure 4.11 FACS analysis following 72 hours knockdown of TRIM25 shows depletion does not lead to an increased rate of apoptosis in HeLa cells.** (Efficiency of knockdown can be seen in representative western Fig 4.10) Following 72 hours of TRIM25 depletion using siRNA, cells were harvested and stained for FACS analysis using Annexin-FITC and DRAQ7 fluorophores. (A) Representative dot plot showing distribution of HeLa cells in quadrants Q1, Q2, Q3 and Q4, representing Annexin-FITC positive, both Annexin-FITC and DRAQ7 positive, unstained viable and DRAQ7 only stained populations respectively. (B) Bar chart showing the distribution between populations across repeats (n=3). A paired t-test was performed between conditions showed none to have a p value of significance (p value < 0.05).

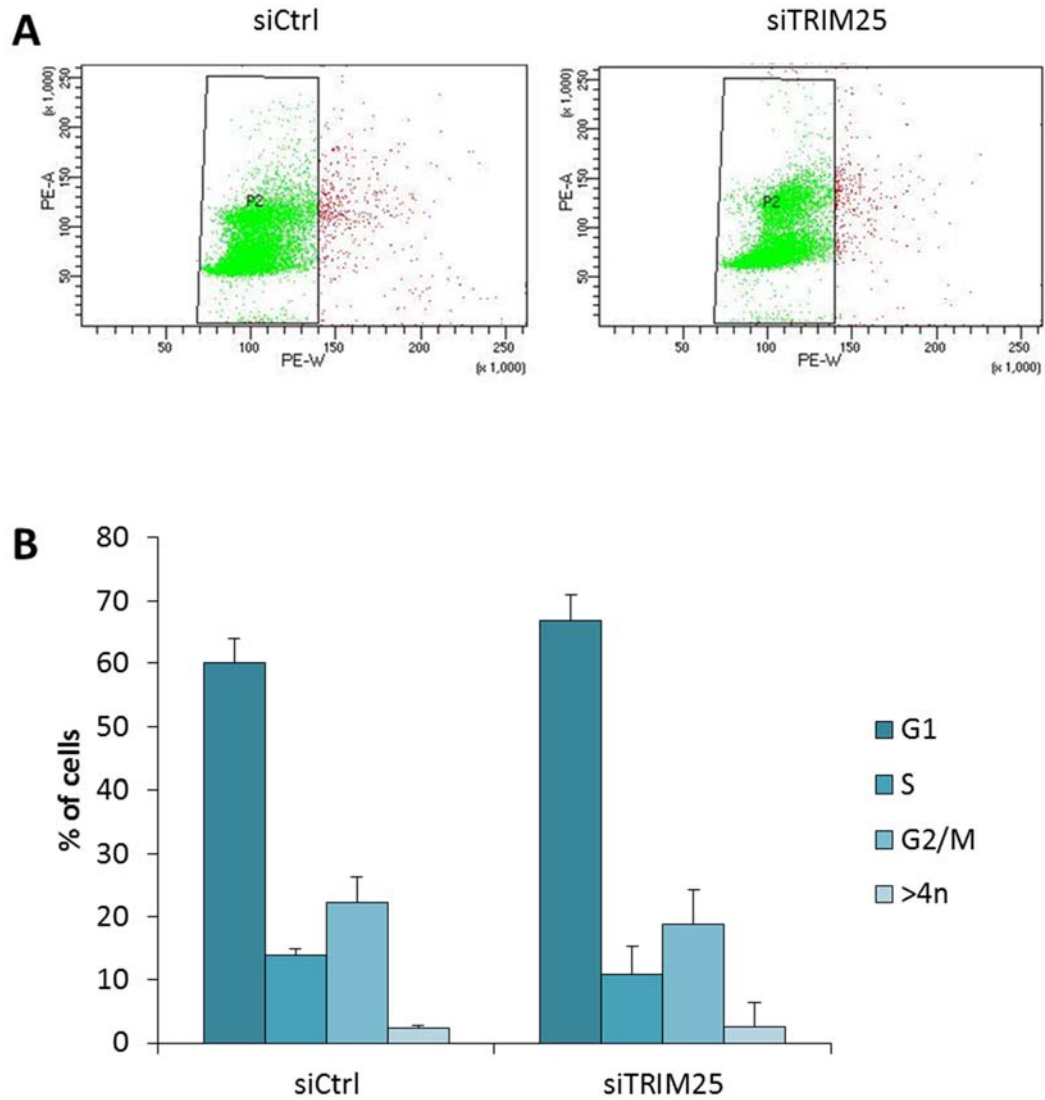


**Figure 4.12 Cell cycle distribution following 72 hours TRIM25 knockdown shows depletion does not lead to changes in cell cycle distribution in HeLa cells.** (Efficiency of knockdown can be seen in representative western Fig 4.10) Following 72 hours of TRIM25 depletion using siRNA, cells were harvested, ethanol fixed and stained using Propidium Iodide for cell cycle FACS analysis. (A) Representative dot plot showing distribution of HeLa cells by cellular area versus DNA content. (B) Bar chart showing the cell cycle distribution between scrambled control siRNA transfected cells and TRIM25 siRNA transfected across repeats (n=3). A paired t-test was performed between conditions showed none to have a p value of significance (p value < 0.05).

Propidium iodide staining of DNA content and subsequent FACS analysis of TRIM25 depleted HeLa cells was conducted in order to characterise any potential changes in cell cycle distribution. Representative dot plots (Figure 4.12A) and data combined from three repeats (Figure 4.12B) showed minimal change in the distribution of cells between cell cycle stages; a small increase of 6.7% in G1 phase relative to control transfected cells, and a small decrease of 3.5% in G2/M phase, but neither was statistically significant according to a paired two tailed t-test.

#### **4.2.10. LARP1 depletion in HeLa cells leads to a significant and large difference in viable cell number onwards from 24 hours post-transfection**

The final of the four RBPs validated was LARP1, which we confirmed does increase binding following Torin1 treatment in HeLa cells (Figure 3.9). LARP1 has already been linked to mTOR signalling and RNA binding by previous groups (Castello et al. 2012; Fonseca et al. 2015; Hopkins et al. 2015). Investigations to date have shown roles for LARP1 in post-transcriptional regulation of 5' TOP mRNAs, though controversy remains as to whether this regulation is positive or negative on translation (Blagden et al. 2009; Fonseca et al. 2015). As 5' TOP mRNAs more often than not encode ribosomal proteins and other factors involved in translation, such as elongation factors and poly(A) binding protein (PABP), the action of LARP1 binding to this subset of messages could be expected to have a profound impact on translation and therefore cell growth.

In this study, use of siRNA to knockdown levels of LARP1 in HeLa cells had a dramatic effect on cellular proliferation; across three repeats (each in triplicate) by 96 hours the mean number of cells in LARP1 siRNA transfected conditions was just under 17% of the mean number counted in control siRNA transfected groups (Figure 4.13A). Cell numbers did not increase greatly beyond 24 hours post depletion and this correlates with the decrease of LARP1 levels (Figure 4.13B). Knockdown efficiency of LARP1 is greater still 48 hours post depletion, and is accompanied by detection of the 89 kDa PARP cleavage product indicating activation of apoptosis around this time point.

Furthermore, LARP1 depletion has very recently been shown to result in the decreased abundance of mRNA encoding pro-survival genes, including the anti-apoptotic protein Bcl-2 (Hopkins et al. 2015). In the same study, it was shown that LARP1 was

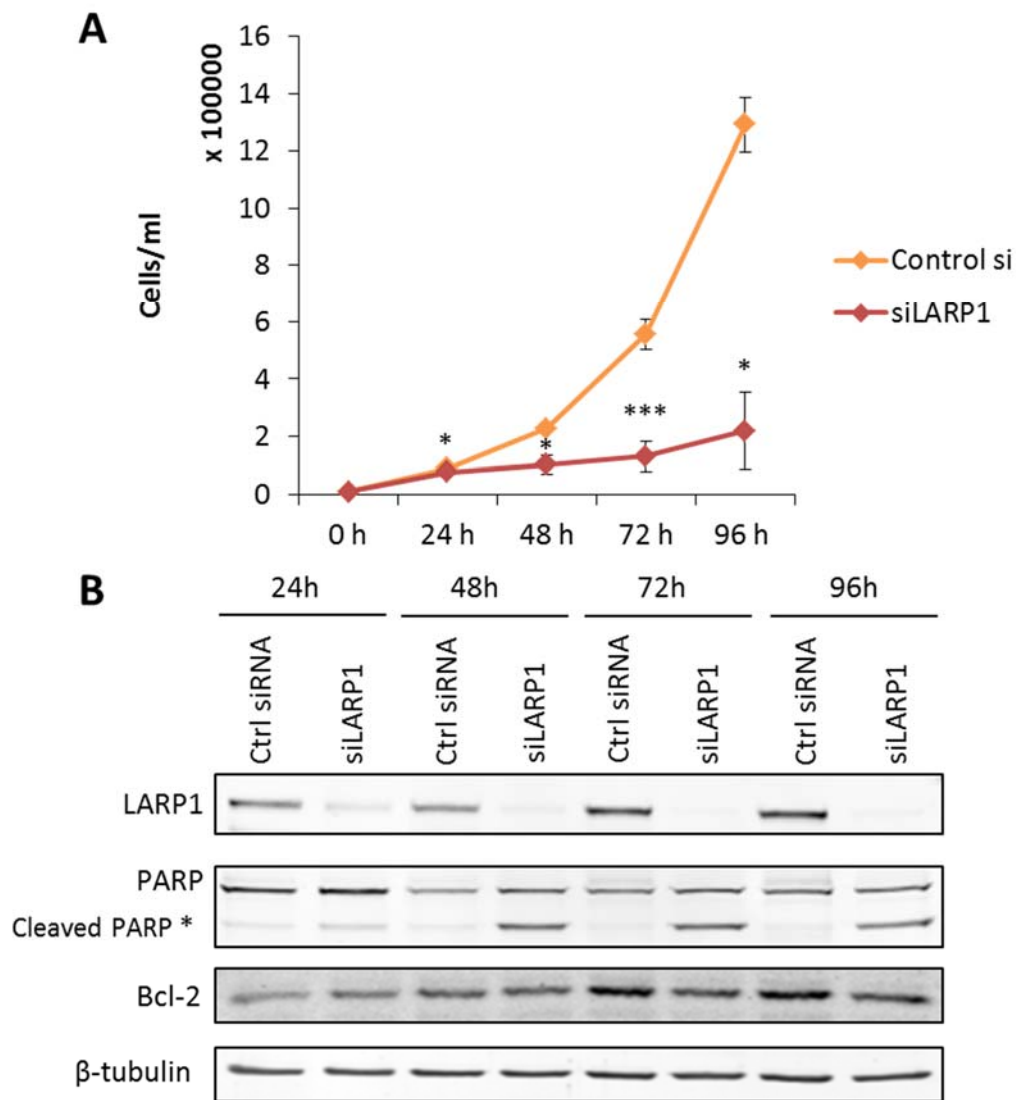


**Figure 4.13 Growth curves following LARP1 knockdown showed dramatic slow in cellular growth rate relative to scrambled siRNA control.** HeLa cells were seeded at 40,000 cells per well of a 6 well plate and reverse transfected using siRNA targeting LARP1, or a scrambled siRNA control (siCtrl). (A) Cells were left to grow for indicated durations post-transfection and harvested at indicated time points (as described in materials and methods). Viable cell number counted in triplicate using a Model TT CASY Counter (n=3). Cell count was compared between conditions by paired t-test: \* = p value < 0.05, \*\* = p value < 0.01, \*\*\* = p value < 0.005. (B) Cells were spun to a pellet, lysed, normalised by Bradford assay and subjected to western blotting (representative shown) with indicated antibodies. Here  $\beta$ -tubulin was used as a loading control.

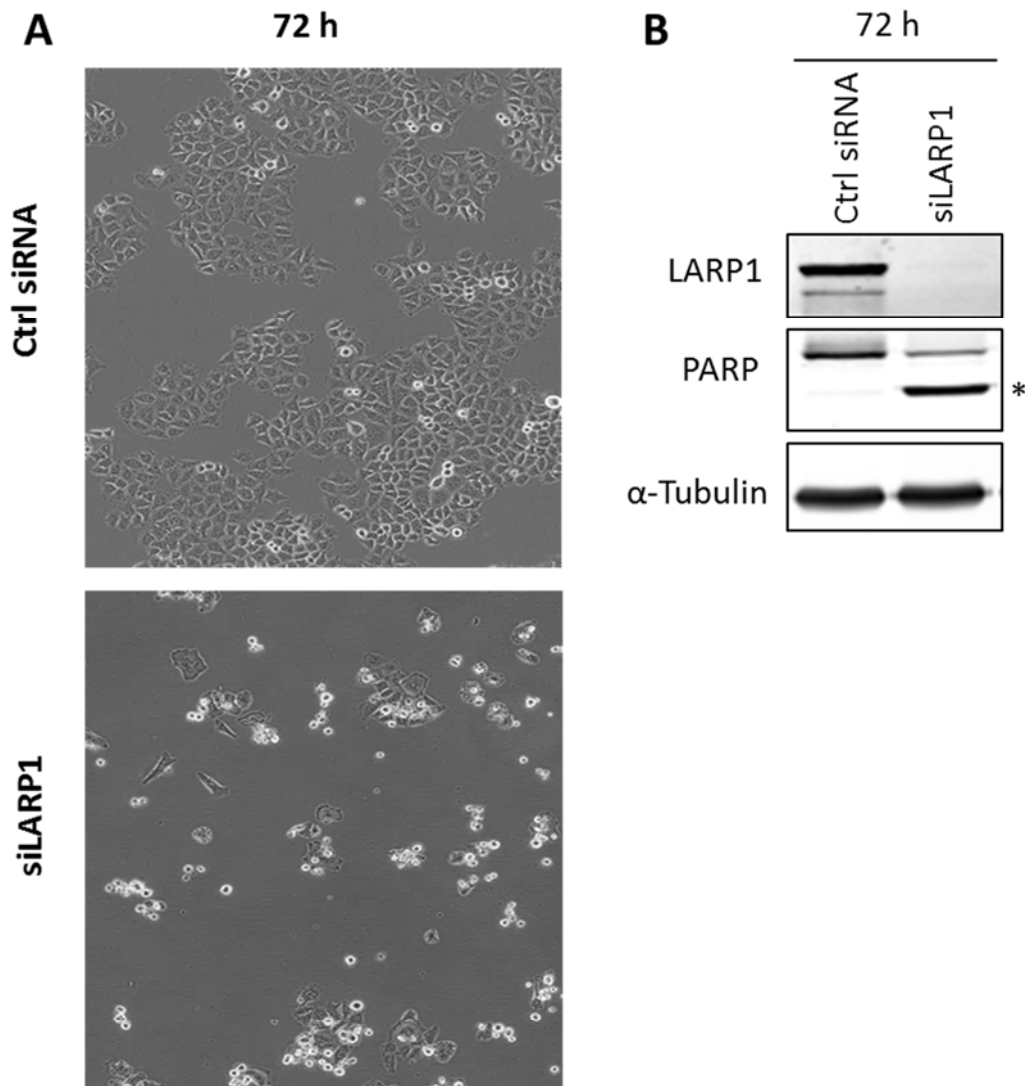


**Figure 4.14 Cell morphology and PARP cleavage following 72 hours siRNA knockdown of LARP1 shows knockdown is efficient and provokes notable visual changes in cell morphology.** HeLa cells were seeded at 40,000 cells per well of a 6 well plate and reverse transfected with siRNA against LARP1, or a scrambled siRNA control (siCtrl). Cells were then incubated in a humidified incubator at 37°C for 72 hours. (A) Representative images taken using 10x magnification of a phase contrast microscope showing cell morphology and density 72 hours post-transfection illustrates the apparent difference in cell number between conditions, as well as a dramatic change in phenotype with many cells rounded, detached or clustered. (B) Once harvested (as described in materials and methods) a proportion of cells were lysed and subjected to western blotting to confirm efficient knockdown of LARP1. Probing for PARP and its cleavage products (denoted by an \*) showed strong activation of apoptosis at this time point. Here α-tubulin was used as a loading control.

responsible for binding a proximal region of the 3' UTR of Bcl2 mRNA. This interaction was shown to stabilise the message and thereby positively influence its translation (Hopkins et al. 2015). Therefore in our study, we were curious to see whether 72 hour LARP1 depletion impacted Bcl-2 protein levels. Following depletion of LARP1 the levels of BCL2 did indeed remain constant, compared to controls which show increase in protein levels. Our data does not however distinguish between direct effects and indirect effects; the higher levels of Bcl-2 protein in control transfected cells could possibly be as a result of stimulated survival signalling due to maintained growth in an increasingly nutrient depleted environment, as they reach confluence. Or indeed, with cell numbers remaining so low in the LARP1 depleted HeLa cells (indicated by detection of PARP cleavage product as likely due to apoptosis); there may not be upregulation of Bcl2 levels to promote cell survival. Therefore further investigation of the relationship between Bcl-2 mRNA expression and LARP1 protein levels is required.

#### **4.2.11. LARP1 depletion leads to dramatic morphological changes 72 hours post-transfection, possibly due to induction of apoptosis, as indicated by PARP cleavage**

Phase contrast microscopy conducted 72 hours post-transfection showed obvious cell stress, with the majority of cells rounded and clustered, and few still adhering to the plate (Figure 4.14A). As live cell microscopy using this method does not permit for capturing images over multiple planes with ease, it is important to note that there were also a considerable proportion of cells detached and floating in the media; these were however collected for western blotting and subsequent FACS analysis. Figure 4.14B is a representative western showing the knockdown of LARP1 using siRNA 72 hours post-transfection is efficient, and accompanied by obvious PARP cleavage, supporting morphological observations of Figure 4.14A and 4.13B, showing the occurrence of programmed cell death.

#### **4.2.12. Depletion of LARP1 by siRNA for 72 hours leads to apoptosis of HeLa cells, possibly due to a defect in mitosis as indicated by cell cycle distribution**

Indeed, when the induction of cell death was investigated using Annexin-FITC and DRAQ7 fluorophore FACS analysis, a considerable difference in the population scatter can be seen in representative dot plots (Figure 4.15A) as an increase in all apoptotic populations. The mean differences in the percentage of cells comprising each

measured quadrant changed significantly between LARP1 depleted and control transfected conditions (n=3). The percentage of viable cells in each condition dropped from 95.6% of the population in the control transfected condition to only 36.4% in the LARP1 siRNA transfected HeLa cells (Figure 4.15B). The greatest increase was in cells positive for staining with both Annexin-FITC and DRAQ7, indicating a late apoptotic stage of cell death. The population of this quadrant grew by 43.7% following 72 hours of LARP1 depletion by siRNA; this increase represents almost the entire difference between conditions. By comparison, in control siRNA transfected conditions this increase was minimal, at less than 3% of the total cell population. It is fairly certain therefore, that LARP1 depletion in HeLa cells beyond 48 hours leads to activation of apoptosis, and thus results in death of almost 60% of these cells by 72 hours post-depletion with siRNA. This provides an explanation for the exaggerated difference in viable cell number 96 hours post-transfection as seen in Figure 4.13A.

Additionally, propidium iodide staining of DNA content in HeLa cells 72 hours post-transfection with siRNA against LARP1 supported the evidence to show the difference in cell number at 96 hours to be largely due to apoptotic catastrophe. Apoptotic cells and debris can be seen in the representative dot plot (Figure 4.16A, right panel) within the drawn gate toward the bottom of the scatter. When considered in later quantification of cells within each cell cycle phase as a Sub-G1 population (n=3), it was observed that there was an increase in the mean percentage of cells in this category from 1.1% to 17.9% (Figure 4.16B). Sub-G1 cells represent apoptotic cells; the DNA content in these cells is identified in FACS as being fractional in comparison to G1 phase, due to DNA fragmentation which occurs as the nucleus breaks down during apoptosis (Kajstura et al. 2007). Cell cycle distribution of LARP1 depleted HeLa cells also differs from control siRNA transfected in other key ways; firstly, there is a large and highly significant (as determined by two tailed t-test) decrease in the percentage of cells comprising G1, from just fewer than 60% in control transfected to 29% in LARP1 depleted population. Furthermore, an increase in the >4n population from 2.3% to 11.7% is also seen at this time point following LARP1 depletion. Taken together

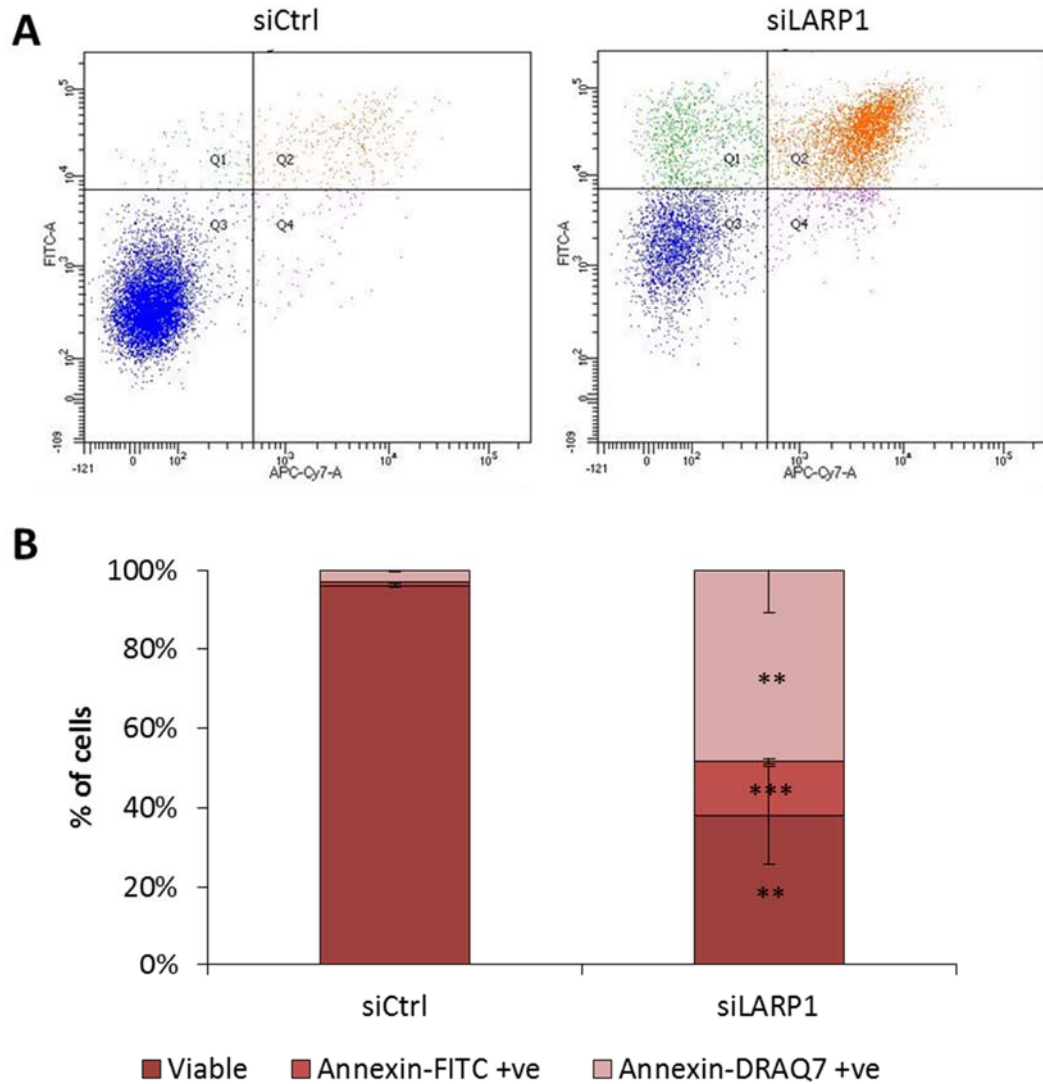


**Figure 4.15 FACS analysis following 72 hours knockdown of LARP1 shows depletion leads to a dramatically increased rate of apoptosis in HeLa cells.** (Efficiency of knockdown can be seen in representative western Fig 4.14) Following 72 hours of LARP1 depletion using siRNA, cells were harvested and stained for FACS analysis using Annexin-FITC and DRAQ7 fluorophores. (A) Representative dot plot showing distribution of HeLa cells in quadrants Q1, Q2, Q3 and Q4, representing Annexin-FITC positive, both Annexin-FITC and DRAQ7 positive, unstained viable and DRAQ7 only stained populations respectively. (B) Bar chart showing the distribution between populations across repeats (n=3). A paired t-test was performed between conditions and significance was assigned as follows: \* = p value < 0.05, \*\* = p value < 0.01, \*\*\* = p value < 0.005.

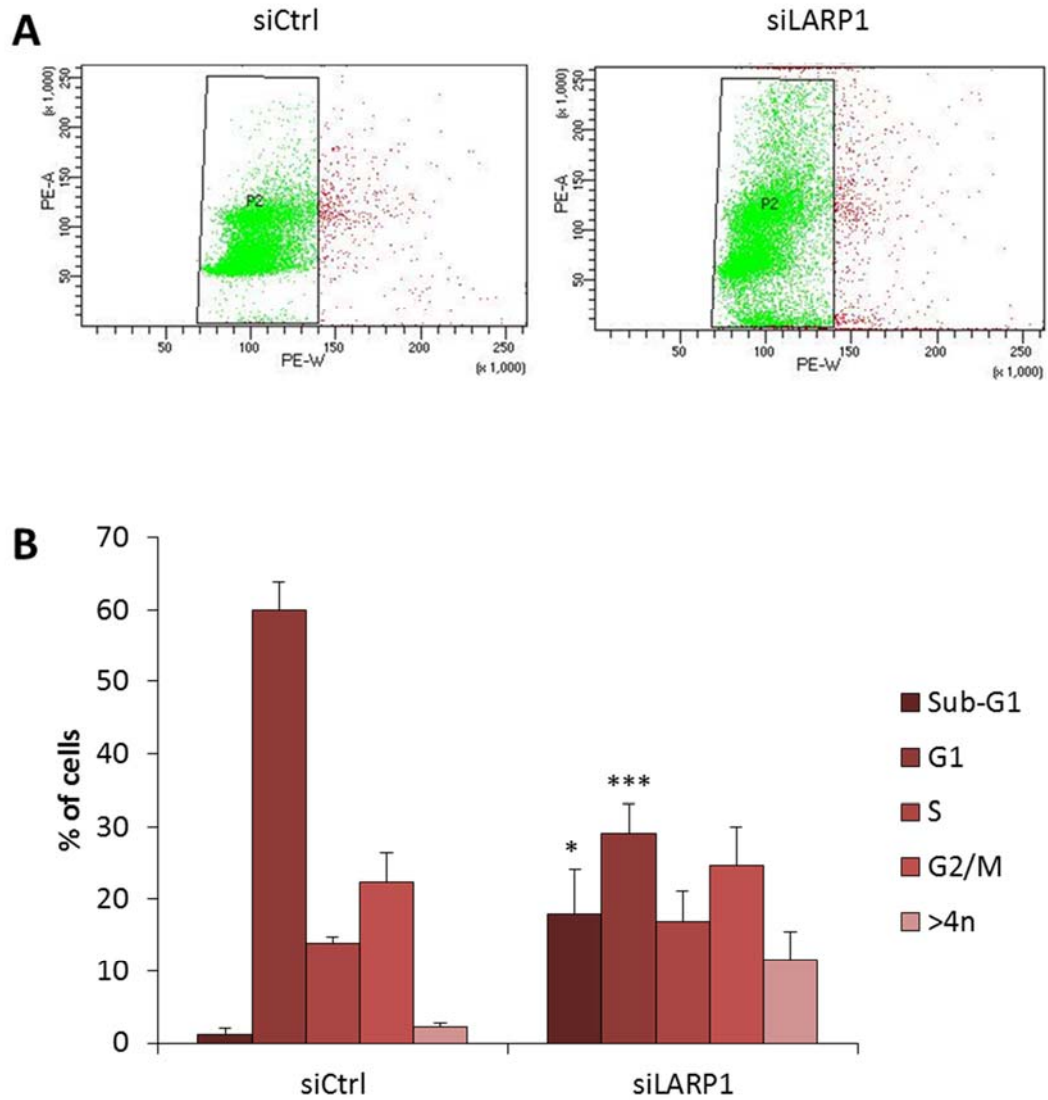


**Figure 4.16 Cell cycle distribution following 72 hours LARP1 knockdown shows depletion leads to a depletion of cells in G1 phase in HeLa cells.** (Efficiency of knockdown can be seen in representative western Fig 4.14) Following 72 hours of LARP1 depletion using siRNA technologies, cells were harvested and stained using Propidium Iodide for cell cycle FACS analysis. (A) Representative dot plot showing distribution of HeLa cells by cellular area versus DNA content shows the difference in distribution of cells between conditions. (B) Bar chart showing the cell cycle distribution between scrambled control siRNA transfected cells and LARP1 siRNA transfected across repeats (n=3). A paired t-test was performed between conditions and significance indicated was assigned as follows: : \* = p value < 0.05, \*\* = p value < 0.01, \*\*\* = p value < 0.005.

these two population increases explain the drop in the percentage of cells within G1 phase. This suggests a possible defect in mitosis which could prompt initiation of apoptosis pathway signalling (seen in Figure 4.15), thereby reducing the number of cells progressing to G1. There are no significant differences between the number of cells in S phase between conditions, nor in G2/M phase, suggesting viable LARP1 depleted HeLa cells are able to progress through these phases of the cell cycle with no major concern.

#### **4.2.13. Investigation of effects of LARP1 depletion in a variety of cell lines indicates p53 status may determine outcome of cell fate**

The apoptotic effect of LARP1 depletion by siRNA in HeLa cells has been noted by several other groups previously (Burrows et al. 2010; Mura et al. 2015). A recent review (Stavraka & Blagden 2015) hypothesised a connection between LARP1 depletion having an exclusively apoptotic response, as opposed to cell cycle arrest, dependent on p53 status of the cell type in which LARP1 was depleted. Establishing whether this was indeed the case would potentially provide us with a cell line in which LARP1 could be manipulated with greater ease, and without inducing apoptosis of the cells. Initially, we used the H1299 cell line, stably transfected with a doxycycline-inducible p53 expression vector was trialled in an effort to delineate the association between cell survival following LARP1 depletion and p53 expression status (Supplemental Figure S2). Three different stably transfected inducible expression vector H1299 cells were used; one possessing an empty vector, one expressing wild type p53 and finally one expressing a mutant p53 possessing the R175H mutation. However, following initial investigations there did not seem to be differences between the three inducible cell lines apoptotic responses nor their cell cycle profiles, indicating that these cell lines had potentially adapted to the lack of p53 expression under non-induced conditions of culture (Supplemental Figure S2).

Therefore to investigate this further I proceeded to knockdown LARP1 in a range of cell types with wild-type endogenous p53 status, including A549, HEK293, MCF10A and U2OS cells (Figure 4.17). In all cases, reverse transfection with siRNA against LARP1 mRNA resulted in a robust knockdown of LARP1 protein level 48 hours

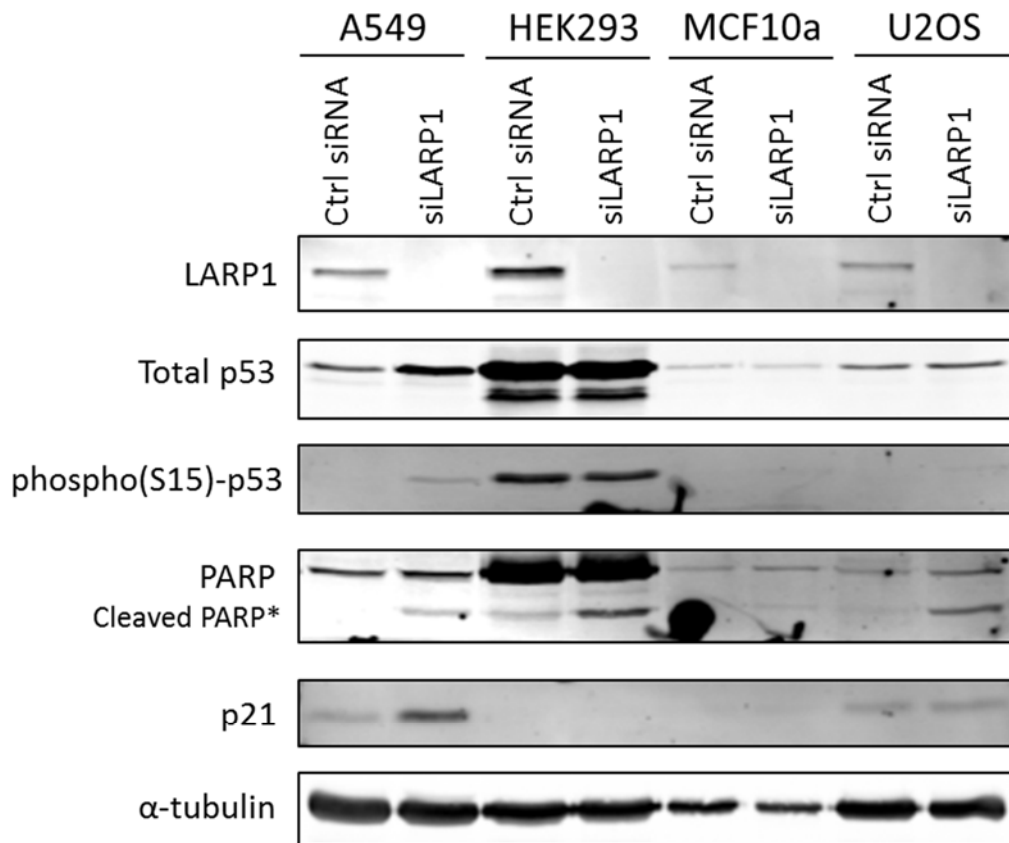


**Figure 4.17 PARP cleavage and p53 signalling in 4 different cell lines following 72 hours LARP1 depletion by siRNA.** A549, HEK293, MCF10a and U2OS cells were seeded per well of a 6 well plate and reverse transfected using siRNA targeting LARP1, or a scrambled siRNA control (siCtrl). Cells were left to grow in humidified incubators at 37°C for 72 hours, before being harvested and lysed at indicated time points (as described in materials and methods). (A) Cells were spun to a pellet, lysed, normalised by Bradford between conditions for each line and subjected to western blotting using the indicated antibodies. Westerns showed efficient LARP1 knockdown in all cases. Here,  $\alpha$ -tubulin was used as a loading control.

post-transfection. Total p53 levels were detectable in all cell lines, confirming all to be p53 positive; in all except A549 the total levels remained constant regardless of LARP1 absence. However, in A549 cells, the absence of LARP1 was accompanied by an increase in total p53 levels. This is of interest, as it has been noted previously that though the exact mechanisms through which p53 signalling decides apoptosis versus cell cycle arrest are still unknown, levels of p53 may play a role in part of this decision (Vousden & Lu 2002)

The primary role of p53 is to promote cell cycle arrest in order to facilitate DNA repair, thereby minimising mutation propagation, or in cases where the damage is irreparable or too extensive, to initiate apoptosis (Chehab et al. 1999). Activation of p53 through phosphorylation allows for its signalling in response to ribosomal stress, DNA damage and other stresses. However, constitutive phosphorylation of p53 at Serine 15 has been reported in tumours (Melnikova et al. 2003), and is usually attributed to cellular stress signalling. HEK293 cells appear to have constitutively phosphorylated p53 at this Serine residue, both in the presence and absence of LARP1, where other cell lines examined did not (Figure 4.17). Constitutive phosphorylation at Ser-15 prevents binding by its main regulatory protein Mdm2, thereby resulting in constitutively active p53 signalling. The ultimate aim for use of p53 positive cell lines in investigation of LARP1 depletion was to identify a cell system in possession of functional wild-type p53 signalling, as this could allow for manipulation of said system to better define the potential relationship between p53 and LARP1 depletion-induced apoptosis or cell cycle arrest. Aside from the fact HEK293 cells underwent apoptosis following LARP1 depletion (as indicated by PARP cleavage), the visibly constitutive activation of p53 indicated a loss of wild-type inducible p53 signalling which might otherwise be responsible for the decision between apoptosis or cell cycle arrest; therefore these cells were not optimal for the progression of this study. A549 cells appeared to possess relatively functional p53 signalling, with a small increase in serine 15 phosphorylated levels.

Investigation of apoptotic response following LARP1 depletion in these cell lines was of great importance for the development of this study; to determine whether the decision of apoptosis versus cell cycle arrest is due to p53 signalling, it was vital to

determine whether any of the p53 wild-type cell lines chosen here underwent apoptosis as HeLa cells before. Should any undergo large scale apoptosis in a similar time frame, they would not provide a different perspective, nor allow for further manipulation of LARP1 expression levels than the HeLa cells previously. This could be determined through detection of an 89 kDa PARP cleavage fragment by western blotting. The extent of PARP cleavage (when considered as cleavage product relative to full length PARP) was greatest in U2OS cells, and least in A549 cells. The A549 cells following depletion of LARP1 appeared least distressed, though all cell lines displayed an obvious difference in overall cell number between conditions (as determined by and n=1 cell counts at 72 hours and visual observations, data not shown).

As well as regulating the transcription of several genes involved in apoptosis, and thereby controlling the apoptotic response, p53 is able to exert control over cell cycle progression, allowing for arrest at key checkpoints in order to repair detected DNA damage or ribosomal stress. Decisions governed by p53 over induction of cell cycle arrest or progression are determined by several factors downstream of its activation, including p21, the transcription of which is carried out by active p53 directly. Through binding of two cyclin D/cyclin dependent kinase complexes, p21 is able to prevent phosphorylation of retinoblastoma protein and thereby cause cell cycle arrest in a p53 dependent manner.

Despite all four cell lines tested here expressing p53, downstream p21 appeared only detectable in two of the four chosen cell lines (U2OS and A549); absence indicating possible disconnect in signalling between these two proteins. In U2OS, levels of p21 remained constant between LARP1 depleted and control conditions, whereas A549 cells exhibited an elevated level of p53 in LARP1 depleted conditions relative to control. This difference in A549 cells mirrored the upstream change in total p53 levels, indicating integrity of signal transduction in the same signalling pathway. Taken together, this indicates A549 cells as a promising cell system for the investigation of p53-dependence of survival in LARP1 depleted cells; induction of p53 and downstream mediator of cell cycle arrest p21 were both intact, and signalling was inducible as opposed to constitutively active. Furthermore, there did not appear to be drastic evidence of PARP cleavage following depletion, indicating apoptotic pathway

activation has not occurred to the same extent as HeLa cells used previously and that A549 cells are more tolerant of LARP1 depletion than other cell types investigated.

#### **4.2.14. Depletion of LARP1 in A549 cell line leads to a reduced growth rate, as well as an increase of total p53 levels**

A549 cells were able to tolerate LARP1 depletion over 72 hours and survive where HeLa cells could not, though the cells appeared to be less confluent than expected for a 72 hour period of culture. Therefore a comparative growth curve experiment was conducted in the A549 cells with LARP1 siRNA transfection, harvesting over the same time points as for the HeLa growth curves previously shown. From this (Figure 4.18A) it is clear that knockdown of LARP1 in A549 cells results in a steady slowed proliferation, beginning at 24 hours post-transfection. Growth begins to plateau after 72 hours post-transfection and by 96 hours, the number of viable cells in the LARP1 depleted condition is 78% less than for the control siRNA transfected. This proportional difference is comparable to the difference in cell number seen in HeLa cells (Figure 4.13A). Knockdown of LARP1 is robust in A549, shown in western blot in Figure 4.18B, with levels of LARP1 barely detectable by 48 hours onwards. PARP cleavage products appear 72 hours after LARP1 siRNA transfection, which is far later than in HeLa cells, where PARP cleavage products were detected from 48 hours after transfection.

Total p53 levels and subsequently p21 levels increased from 72 hours post-transfection with LARP1 siRNA, around the same time period as PARP cleavage appeared to begin. It is therefore conceivable that cells' ability to regulate total levels of p53, and therefore p53 signalling, contributes directly to their ability to survive stress induced by LARP1 depletion. Representative microscopy images of A549 cells 72 hours post-transfection either with control siRNA or a siRNA against LARP1 are shown in Figure 4.19A. From these images it can be seen how, in contrast to HeLa cells, A549 cells display no major stress or apoptotic catastrophe, with very few cells appearing rounded or detached from the plate. Western blots accompanying these images (Figure 4.19B) show efficient LARP1 knockdown, but very faintly detected PARP cleavage product relative to full length PARP. Furthermore, a definite increase in total p53 levels can be seen again, as previously in growth curve experiments.

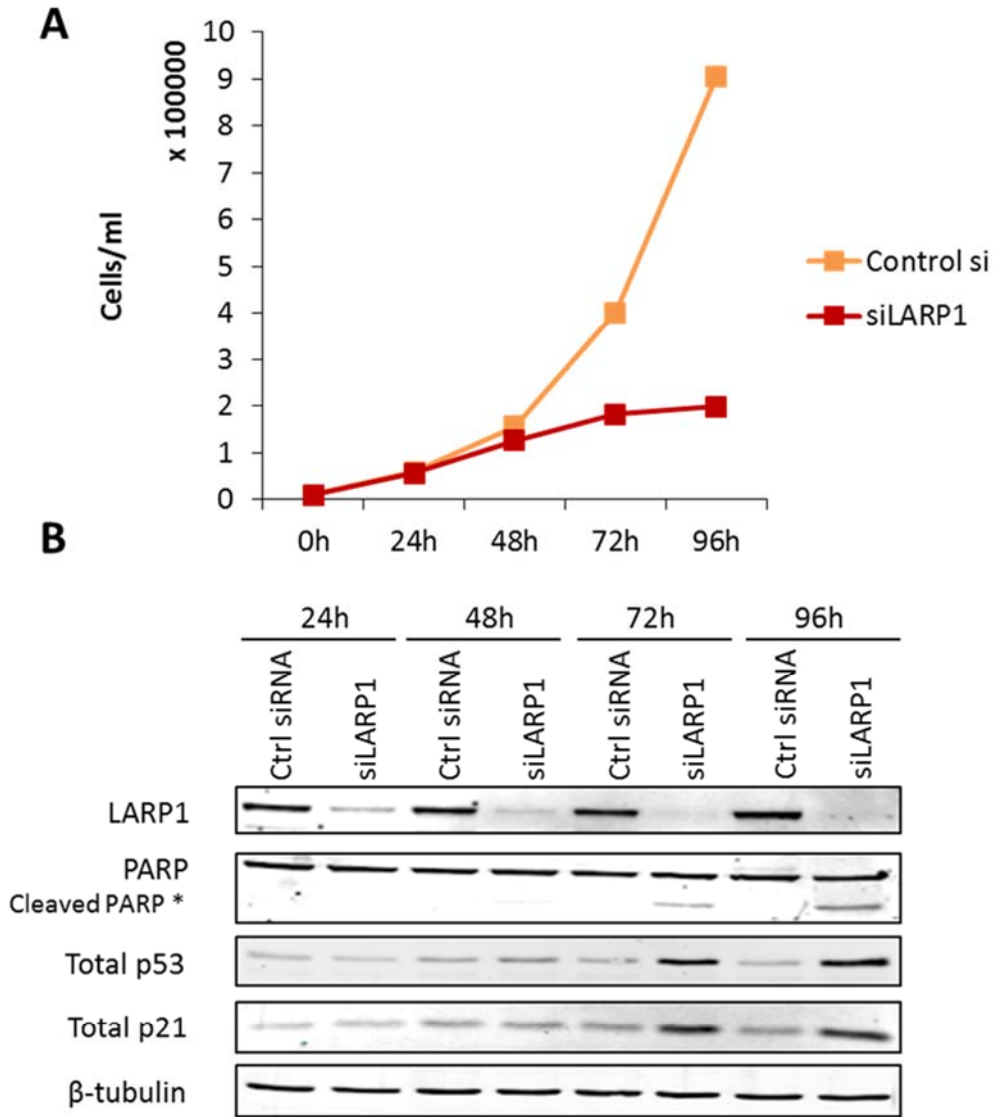


**Figure 4.18** Growth curves in A549 cell line following LARP1 knockdown showed slow in cellular growth rate relative to scrambled siRNA control. A549 cells were seeded at 50,000 cells per well of a 6 well plate and reverse transfected using siRNA targeting LARP1, or a scrambled siRNA control (siCtrl). (A) Cells were left to grow for the indicated durations post-transfection and harvested at indicated time points (as described in materials and methods). Viable cell number counted using a Model TT CASY Counter (n=1). (B) Remaining cells were spun to a pellet, lysed, normalised by Bradford assay and subjected to western blotting (representative shown) using the indicated antibodies. Investigation of activation of apoptosis was determined by probing for PARP cleavage. Here  $\beta$ -tubulin was used as a loading control.

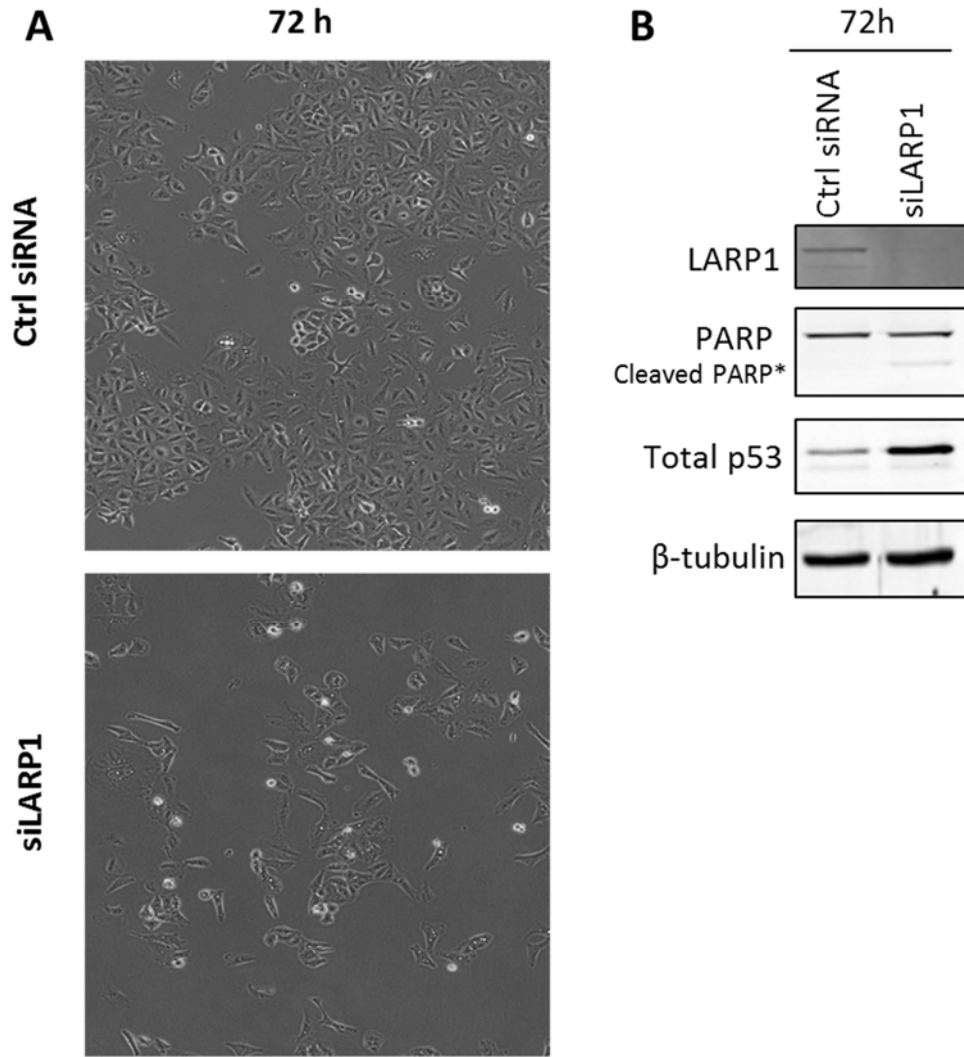


**Figure 4.19 Cell morphology and PARP cleavage following 72 hour LARP1 knockdown in A549 cells provokes notable visual changes in cell morphology.** A549 cells were seeded at 50,000 cells per well of a 6 well plate and reverse transfected with siRNA against LARP1, or a scrambled siRNA control (siCtrl). Cells were then incubated in a humidified incubator at 37°C for 72 hours. (A) Representative images taken using 10x magnification of a phase contrast microscope showing cell morphology and density 72 hours post-transfection illustrates the apparent difference in cell number between conditions, as well as a notable change in phenotype. (B) Once harvested (as described in materials and methods) a proportion of cells were lysed and subjected to western blotting using indicated antibodies. Probing for PARP and its cleavage products showed very little activation of apoptosis at this time point in A549 cells. Here β-tubulin was used as a loading control.

#### **4.2.15. A549 cells showed a small increase in apoptotic populations 72 hours following transfection with siRNA against LARP1, as well as a small increase in the proportion of cells in G1 and S phase**

The extent of apoptotic induction was investigated further through the use of Annexin-FITC and DRAQ7 staining and FACS analysis (Figure 4.20 A and B), showing a small change in viable and apoptotic populations. The greatest increase is in the Annexin-FITC positive only population, representing early stages of apoptosis, which displayed an increase by 7.3%, followed by late apoptotic population Annexin-FITC and DRAQ7 positive, which saw an increase of 1.1%. The overall decrease in the percentage of viable cells as determined by FACS was hugely different from that seen in HeLa cells at the same time point; A549 cells saw a drop in viability of 9.1% between control and LARP1 siRNA transfected conditions, whereas HeLa cells displayed a decrease of 59.2% between the two conditions.

With the prominent increase in both total p53 and p21 levels, and the conclusive decrease in apoptotic induction between A549 and HeLa cells following depletion of LARP1 using siRNA, it follows that there may be a potential effect on cell cycle distribution accounting for the reduced rate of proliferation. Thus, FACS following propidium iodide staining of fixed cells was conducted; using cells harvested 72 hours following transfection with either the scrambled control siRNA or LARP1 targeting siRNA (Figure 4.21 A and B). This showed a small decrease in the percentages of cells in both G1 and S phase, of 4.7 and 3.7% respectively. Conversely, this was mirrored by a small increase of 6.3% more cells in G2/M phase. The difference between control and LARP1 siRNA transfected conditions' population of sub-G1 cells is only 1.1% in A549 cells, notably smaller than the difference seen in HeLa cells depleted of LARP1 at the same time point. Altogether this indicates LARP1 depletion in A549 cells causes a slow or arrest in proliferation, whilst not dramatically inducing the apoptotic signalling, nor causing a large shift in the cell cycle distribution across the population.

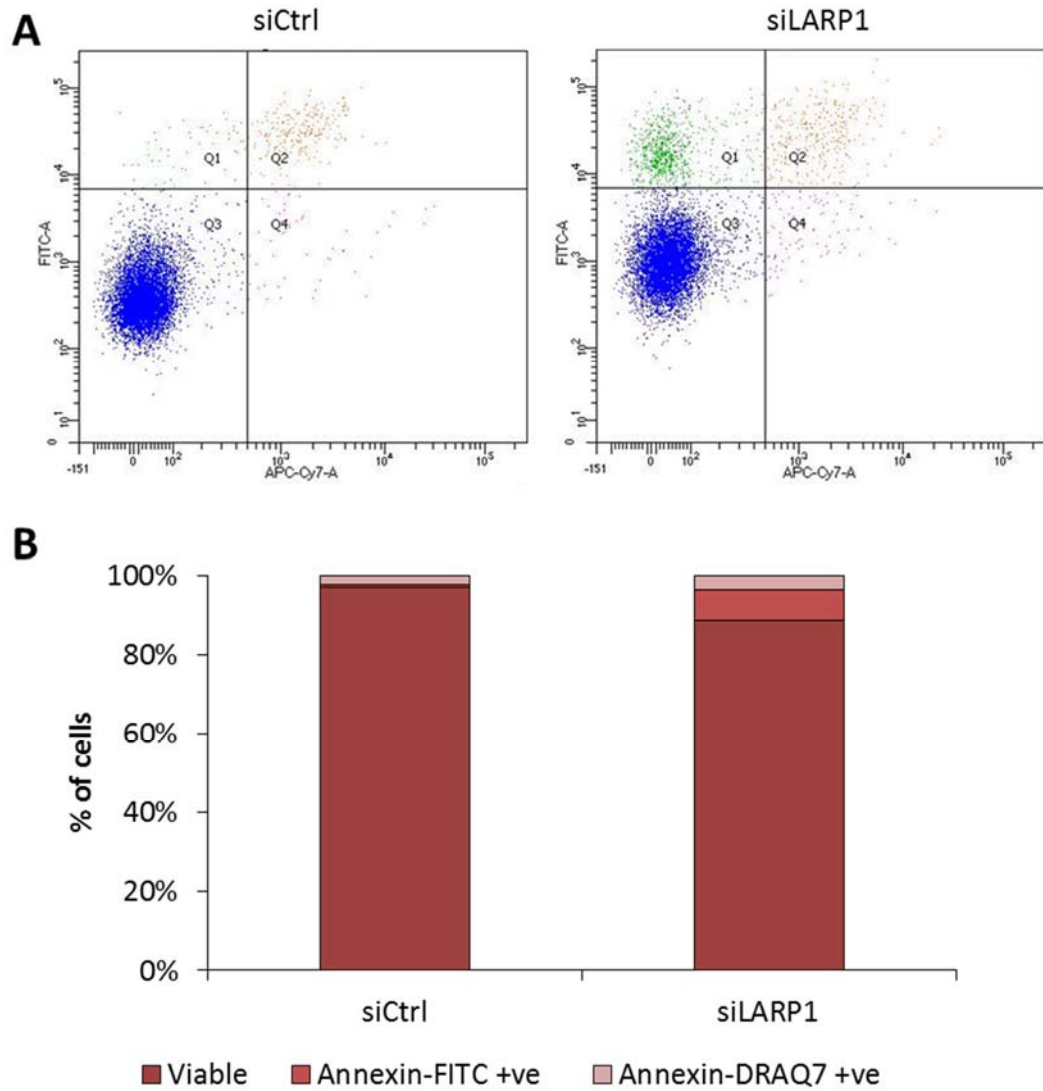


**Figure 4.20 FACS analysis following 72 hours knockdown of LARP1 shows depletion leads to a modestly increased rate of apoptosis in A549 cells.** (Efficiency of knockdown can be seen in representative western Fig 4.19) Following 72 hours of LARP1 depletion using siRNA, cells were harvested and stained for FACS analysis using Annexin-FITC and DRAQ7 fluorophores. (A) Dot plot showing distribution of HeLa cells in quadrants Q1, Q2, Q3 and Q4, representing Annexin-FITC positive, both Annexin-FITC and DRAQ7 positive, unstained viable and DRAQ7 only stained populations respectively. (B) Bar chart showing the distribution between populations (n=1)

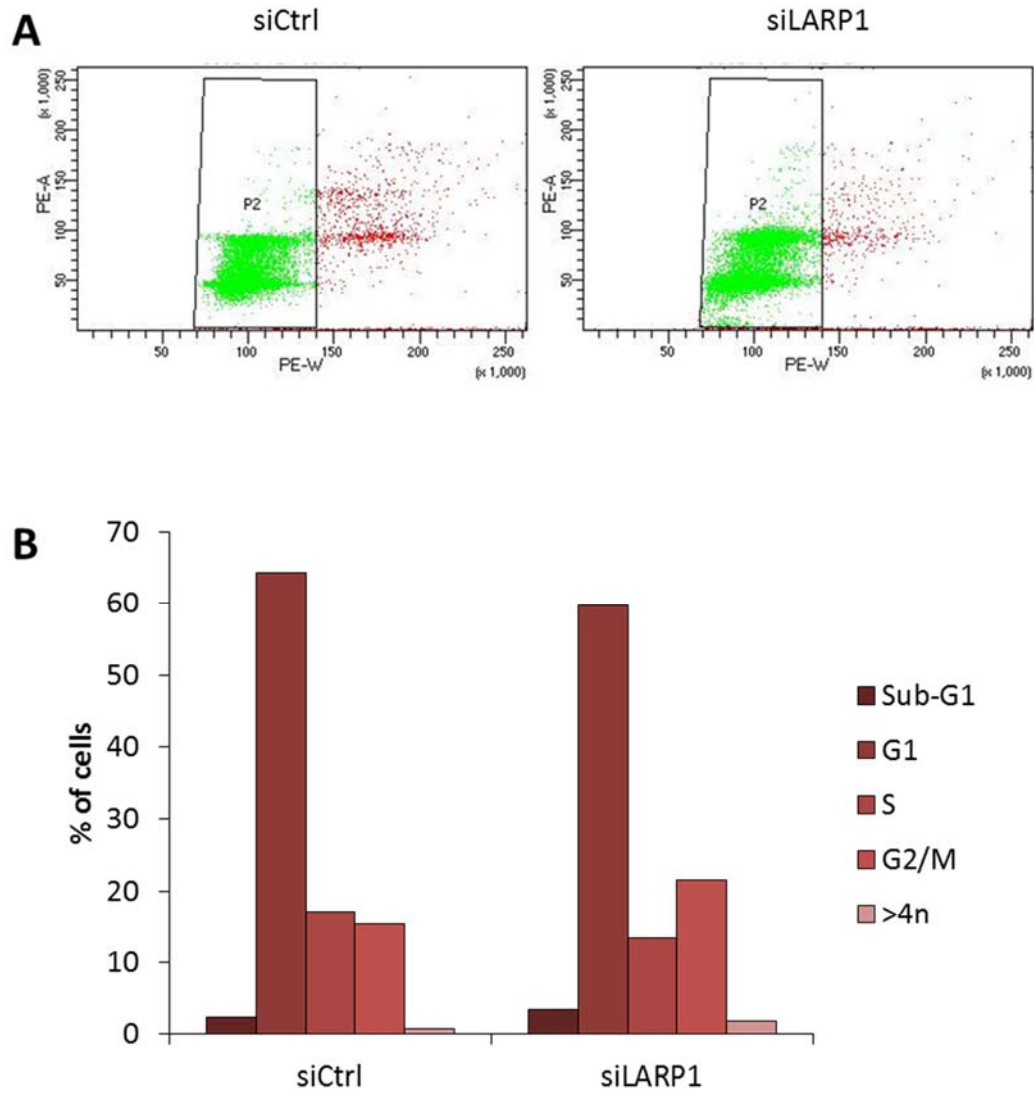


**Figure 4.21** Cell cycle distribution following 72 hours LARP1 knockdown shows a depletion of cells in G1 phase in A549 cells. (Efficiency of knockdown can be seen in representative western Fig 4.19) Following 72 hours of LARP1 depletion using siRNA technologies, cells were harvested and stained using Propidium Iodide for cell cycle FACS analysis. (A) Representative dot plot showing distribution of A549 cells by cellular area versus stained DNA content shows the difference in distribution of cells following LARP1 depletion. (B) Bar chart showing cell cycle stage distribution showed a noticeably smaller difference in the percentage of cells in G1 phase between conditions following LARP1 depletion by siRNA (n=1) than was previously seen in HeLa cells.

#### **4.2.16. Simultaneous knockdown of p53 and LARP1 in A549 cells does not appear to initiate greater levels of apoptosis, as determined by PARP cleavage**

As outlined in section 4.2.13, a connection between survival following LARP1 depletion and p53 signalling was proposed in a review by Stavrika & Blagden (2015); investigation of this hypothesis led us to investigate the effects of LARP1 depletion in a variety of cell lines expressing p53, including A549 cells. Here we have shown how A549 cells are able to survive 72 hour LARP1 knockdown in a way HeLa cells cannot; though both cell lines show a marked decrease in cellular proliferation following LARP1 depletion the drop in the proportion of viable cells is much greater in HeLa cells (59.2% as opposed to 9.1% in A549). To address the outstanding question of A549 cells survival being p53 dependent, a double knockdown of p53 and LARP1 using siRNA was performed, alongside individual knockdowns of each protein for 72 hours (n=1). Changes in cell morphology were investigated through capture of 10x magnification phase contrast images 72 hours post-transfection (Supplemental Figure S2) prior to harvesting cells as described in materials and methods. Following harvest, cells were lysed, normalised by Bradford and subjected to western blotting; PARP and its cleavage products identified and compared across conditions (Figure 4.22A).

From these westerns it can be determined that LARP1 knockdown after 72 hours is robust, and in the LARP1 depleted only condition an increase in total p53 is again observed. Total p53 levels are reduced by more than half in p53 siRNA transfection conditions; this is accompanied by a corresponding decrease in p21 levels. PARP cleavage product was not detected in the control siRNA transfected, p53 siRNA transfected alone or the LARP1 siRNA transfected alone. A very low level of 89 kDa PARP cleavage product was detected in the double transfected cells; however the cells in this condition were not exhibiting any major morphological changes (Supplemental Figure S2) nor apoptotic phenotype as seen in the LARP1 depleted HeLa cells. Further work using FACS analysis following the double knockdown of p53 and LARP1 in order to quantify any increase in apoptotic populations of A549 cells is required, before any strong conclusions can be drawn regarding the p53 dependence of survival in this cell line.

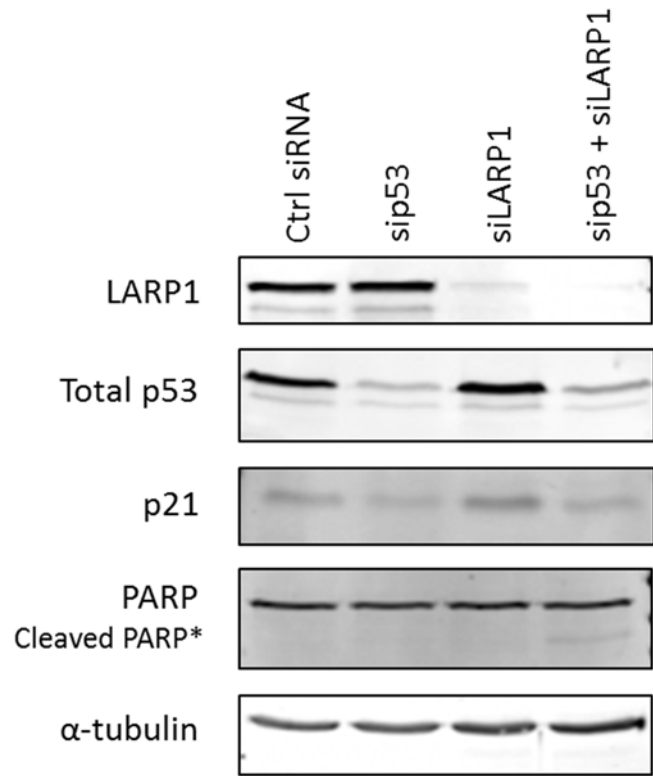


**Figure 4.22 PARP cleavage following 72 hour depletion of LARP1 and p53 in A549 cell line.** A549 were seeded at 50,000 cells per well of a 6 well plate and reverse transfected with siRNA against p53 or LARP1 as described in materials and methods. 72 hours post-transfection cells were harvested, lysed and subjected to western blotting using the indicated antibodies. Here,  $\alpha$ -tubulin was used as a loading control.

### 4.3. Discussion

The aim of this chapter was to better characterise the role of four proteins validated as RNA binding proteins changing their binding activity following mTOR inactivation, within the context of cellular growth and proliferation. Specifically, through the use of siRNA, the proteins were depleted one at a time in HeLa cells and screened for effects on cellular proliferation, cell viability and cell cycle as a means to highlight any interesting candidates for future study.

HeLa cells were utilised to examine knockdown phenotypes in the first instance, as they were used in the whole cell interactome capture and identification of the RBPs. Depletion of SERBP1, PWP2 and TRIM25 produced relatively modest phenotypic responses in HeLa cells (Figures 4.1 to 4.12), whereas LARP1 depletion initiated a dramatic effect on cell growth, and also stimulated apoptosis. As LARP1 has been identified in this study as a candidate intermediary RBP acting downstream of mTOR signalling, and may be responsible for the unexplained mechanism of mTOR-TOP mRNA gene expression, this is quite an intriguing effect. It has also been shown here that in another immortalised cell line (A549) the effects of LARP1 knockdown by siRNA are significantly different; the absence of extensive cell death and possible effects on metabolism indicate a possible connection between the absence of LARP1 and p53 compensation in these wild-type p53 cells. This also provides a cell system in which levels of LARP1 may be manipulated further and for greater durations before induction of apoptosis, allowing for investigation of gene expression changes in response to LARP1 abundance, as well as to mTOR signalling. As such, LARP1 was chosen for further characterisation within the next chapter.

SERBP1 has been shown to interact with the 40S ribosomal subunit proteins and eIF3 complex components (Anger et al. 2013); therefore it may be that its depletion leads to disruption of translation in some way, or removes some specificity of the ribosome, should its interaction be directly with the actively translating ribosome. A reduced translation rate would be expected to result in a slow in proliferation of cells, as it would take an increased time to grow and reach the size required to progress into S phase. Alternatively, it may be that depletion of SERBP1 stimulates senescence or the

prevention of further proliferation; though this is considered to be primarily a p53 dependent response and therefore may not be as prominent in HeLa.

A screen of nucleolar pre-rRNA processing factors (Tafforeau et al. 2013) showed that both SERBP1 depletion and PWP2 depletion cause different shifts in the overall pre-rRNA profile of HeLa cells. SERBP1 depletion for 72 hours, with two different siRNAs, led to a decrease of 47S, 45S and 41S pre-rRNA, required for synthesis of ribosomal RNA downstream, association with ribosomal proteins and thus for assembly of the ribosome. It may be therefore that a decrease in overall levels of these pre-rRNA leads to a deficiency in key ribosomal RNA components of translational machinery. The same study showed depletion of PWP2 for 72 hours using three different siRNAs caused an increase in 47S, 34S and 30S pre-rRNA, possibly due to a defect in processing leading to an accumulation of longer pre-rRNA species as has been seen in yeast. Furthermore, for PWP2 siRNA transfected cells it was shown that this change in pre-rRNA processing was conserved across various cell types, including two different HCT116 cell lines that were both p53 wild-type and p53 null, suggesting that the response generated by PWP2 depletion is p53 independent. This is of particular interest here as it has been shown previously that disruption of ribosome biogenesis often leads to stabilisation of p53, cell cycle arrest and apoptosis (Golomb et al. 2014; Chakraborty et al.) yet in HeLa cells here, neither SERBP1 nor PWP2 depletion caused either response. This suggests that the slow in proliferation of HeLa cells seen in our study following SERBP1 or PWP2 depletion by siRNA is a result of disruption of pre-rRNA processing, likely affecting the ribosome biogenesis pathway and ultimately affecting global translation and growth. Investigation of whether the reduced proliferation seen in both in SERBP1 and PWP2 depleted cells was due to reduced rate of de novo protein synthesis following disruption of ribosome biogenesis could be achieved through measuring <sup>35</sup>S-Methionine incorporation.

As mentioned in the previous chapter, TRIM25 has been identified as an E3 ubiquitin ligase, among its determined targets were Mdm2, the negative regulator of p53, and p53 itself. TRIM25 was shown to stabilise p53 through reducing its ubiquitination as well as that of and Mdm2. In addition, p53 has crucial roles in transcription and initiation of pro-apoptotic mRNA, as well as influence on cell cycle progression.

Perhaps unsurprisingly therefore, Zhang et al. (2015) noted that when TRIM25 was depleted by siRNA in HCT116 cells possessing wild-type p53, the activity of p53 increased resulting in caspase activation, PARP cleavage and ultimately, apoptosis. However, in HCT116 cells of negative p53 status, there was no cell death but instead they described a reduced proliferation rate, much as was seen in the HeLa cells used in this study. It is still unclear why TRIM25 should be recruited to mRNA and which proteins it affects. The mechanism through which TRIM25 depletion affects cellular growth still remains unresolved; should it be the result of a reduced translation rate again this can be investigated through the use of <sup>35</sup>S-Methionine incorporation methodologies.

Since p53 is so extensively involved in such a variety of cell signalling networks, in both healthy and pathogenic contexts, attempting to delineate its role in relation to depletion of these proteins, as well as with specific relation to LARP1 across immortalised cell types is likely to remain elusive. Early attempts to address the p53 dependence of LARP1 depletion-induced apoptosis included the use of a doxycycline-inducible p53 expression vector system in H1299 cells (discussed briefly earlier, in section 4.2.13). It is unclear however, how these cells have adapted to existing in their p53 null state ahead of induction of expression vectors, and therefore whether the signalling networks usually activated through p53 have been adapted to compensate for its absence in culture. Use of p53 wild-type cell lines however, assumes p53 has remained integral to all the usual signalling pathways, though there is the possibility other pathways upstream or downstream may be harbouring mutations instead that enable the cell lines' immortalised nature.

Simultaneous knockdown over 72 hours of both p53 and LARP1 in A549 cells did not result in an exaggerated apoptotic phenotype as seen in HeLa cells, following LARP1 depletion of the same duration. However through western blotting a very slight elevation in the 89 kDa fragment of cleaved PARP, considered an indicator of apoptosis, was detected. There were no obvious morphological changes in these cells, nor any phenotypic evidence of apoptosis resembling that seen in HeLa cells following LARP1 depletion, as determined by microscopy. Quantification of any change in the

percentage of cells comprising an apoptotic population would be achievable in the manner used for other knockdown phenotypes, with FACS analysis.

LARP1 depletion by siRNA in both HeLa cells and A549 cells results in comparable decrease in viable cell number following 96 hours of growth post-transfection; however the difference in cell number appeared to be brought about by different mechanisms. In the HeLa cells, following 48 hours of LARP1 depletion PARP cleavage product became detectable by western blotting, and Annexin-FITC/DRAQ7 FACS analysis 72 hours following transfection with siRNA showed that the difference in cell number relative to control transfected cells was indeed due to apoptosis. Cell cycle FACS of fixed cells stained with PI appeared to show that apoptosis occurred as a result of failure to progress through M phase to G1 of the cell cycle, though this could be investigated further through synchronisation and release of cell populations at various stages of the cell cycle. Interestingly, investigation of hypotheses put forward by other groups (Stavraka & Blagden 2015) showed that in A549 cells, a cell line expressing wild-type p53, the difference in cell number following 72 hours LARP1 depletion was not as a result of apoptosis as seen for HeLa cells. However the small increase in Annexin-FITC positive, sub-G1 population of cells indicated that there were a few cells dying at the same point in cell cycle progression; it is possible therefore that the presence of p53 allows for the slowing of growth and proliferation in A549 with circumvention of apoptotic initiation.

LARP1 has an established binding partner in cytoplasmic Poly-A Binding Protein (PABPC1, or PABP), a highly conserved RBP with an affinity for poly(A)<sup>+</sup> stretches on mature mRNA. PABP has well characterised roles in the control of mRNA stability (Coller et al. 1998; Parker & Song 2004), as well as a role in translation initiation (Galili et al. 1988). Through simultaneous interaction with the scaffold protein eIF4G at the 5' cap of mRNA as well as the poly(A) tract of the 3' tail, PABP is able to bring the ends into close proximity and create a closed loop structure (Gebauer & Hentze 2004). This circularisation of the mRNA was shown to promote the recruitment of 40S ribosomal subunits and thereby stimulate translation initiation (Tarun & Sachs 1996; Tarun et al. 1997; Wells et al. 1998), and has also been postulated to provide increased

opportunity for ribosomal recycling and re-initiation (discussed in supplemental material in Jackson et al. 2010).

Depletion of PABP in HeLa cells has been shown to result in apoptosis and global inhibition of both cap-dependent and IRES dependent mRNA translation (Thangima Zannat et al. 2011). PABP is also able to selectively modulate translation of specific mRNAs; one example of this is its autoregulation of its own mRNA levels through binding of an oligoadenylate tract in the 5' UTR (Hornstein et al. 1999). In addition to this oligoadenylate sequence PABP possesses a 5' TOP sequence at its 5' UTR, though it has a higher cytosine: uracil content than usual and its translation appears sensitive to mTOR inhibitors rapamycin and Torin1 in a LARP1 dependent manner (Meyuhas 2000; Fonseca et al. 2015).

The interaction between LARP1 and PABP has been shown to be both RNA-independent, binding via a PAM2-like motif within the LAM of LARP1, and RNA dependent (Fonseca et al. 2015). Both RBPs have been shown to bind RNA and influence their translation through their binding; however there are remain outstanding questions regarding their effects on mRNA stability, and the exact subset of messages affected through each protein's specific translational regulation. The association between LARP1, PABP and the 5' cap complex of mRNA strongly indicates a role for LARP1 in the control of 5' TOP mRNA specific translational control; this is supported even further by recent work showing LARP1 binding of Raptor, a component of the mTORC1 complex critical for its function (Tcherkezian et al. 2014; Fonseca et al. 2015). The control of mTOR over 5' TOP mRNA translation was first identified over two decades ago by two separate groups (Jefferies et al. 1994; Terada et al. 1994), though the exact signal transduction and mechanism has remained elusive for several years. Many studies have since expanded the understanding of the role of mTOR signalling in the translation regulation of these subsets of messages (Thoreen et al. 2012; Patursky-Polischuk et al. 2014). In addition, large scale proteomic screens have identified LARP1 phosphorylation sites targeted by mTORC1 signalling (Y. Yu et al. 2011; Hsu et al. 2011); providing deeper characterisation of this pathway's regulation over translation and cell growth. However to date, the question of whether LARP1 functions as an activator or a repressor of 5' TOP mRNA translation downstream of mTOR remains

unanswered and heavily debated with several groups providing arguments for either side.

The next step to this study is to further investigate the role of LARP1 in post-transcriptional control of gene expression, through identification of the mRNAs to which it binds and investigate the effect of this binding on the translation and stability of these mRNAs. Furthermore, it will be interesting to add a dimension to this through comparing the subset of mRNA bound by LARP1 to those bound by PABP, to identify whether differences exist between the repertoires of mRNAs controlled by each protein. As PABP is ubiquitous and binds all transcripts with a poly(A) tail or oligoadenylate sequence, we would not expect to see differential binding of mRNAs between LARP1 and PABP, though differential binding may occur following Torin1 treatment.

## **Chapter 5**

## **5. Identification of mRNAs bound by LARP1 and its binding partner PABP, and investigation of their relationship in post-transcriptional regulation**

### **5.1. Introduction**

Recent work by several groups (Tcherkezian et al. 2014; Fonseca et al. 2015) has identified LARP1 and PABP as interacting partners, and begun to outline the importance of their interaction in the context of mTOR signalling, and with respect to 5' TOP regulation. As mentioned in the previous chapter, work published by Damgaard & Lykke-Andersen (2011) has inferred the existence of additional, as yet unidentified components of the 5' TOP translation regulation pathway, having identified stress induced RBPs TIA1 and TIAR as inhibitors of ribosomal proteins. Furthermore, knockdown of these two proteins in another study failed to rescue effects of mTOR inhibition on TOP translation, confirming the involvement of other players in TOP translation (Thoreen et al. 2012).

LARP1 has emerged as a potential candidate in the regulation of gene expression downstream of mTOR inhibition. Aside from this study which has shown that LARP1 acts as an RBP which increases binding to mRNA downstream of mTOR inhibition with Torin1, several studies have shown potential roles for LARP1 in the mediation of 5' TOP mRNA expression. This included Tcherkezian et al. (2014) who showed depletion of LARP1 in HEK293 cells resulted in decreased polysomally associated 5' TOP messages, suggesting LARP1 acts as a translational activator; which correlated with, but did not explain, findings by Aoki et al. (2013) that LARP1 expression affects basal levels of 5' TOP mRNAs. Conversely, (Fonseca et al. 2015) showed LARP1 interacted with TOP mRNAs but acted to negatively impact their translation. These opposing findings mean that the role of LARP1 in gene expression regulation remains unresolved, particularly with respect to the control of specific subsets of messages.

PABP is a well characterised RBP with a high preferential affinity for poly(A) stretches such as those located at the 3' poly(A) tail of processed, mature mRNA and certain poly(A) ncRNAs. It has been shown to interact simultaneously with eIF4G of the eIF4F complex located at the 5' cap of the mRNA, thereby bringing the mRNA into a circularised form, and enhancing stability of these mRNA by enabling re-initiation and

ribosome recycling. It is possible that LARP1 and PABP interaction plays some part in the control of gene expression mediated by LARP1; the observation that the interaction of each protein with RNA is independent of the other, as well as their interaction with one another being possible both in the presence and absence of RNA, opens a new consideration for the model of LARP1-mediated gene expression control.

In this chapter, I aim to describe work undertaken to identify and characterise mRNA bound by LARP1 and PABP, as well as each differentially, following inhibition of mTOR signalling. Using overexpression constructs encoding FLAG-tagged LARP1 and PABP proteins; RNA bound by each was isolated and validated by qPCR. Furthermore, upon the identification of certain mRNAs as key components of metabolic energy pathways, preliminary investigations into the effect of LARP1 depletion on mitochondrial and glycolytic metabolism was conducted.

## **5.2. Results**

### **5.2.1. LARP1 and PABP interact in HeLa cells, as shown through FLAG co-immunoprecipitation experiments**

In order to begin addressing the question of which mRNAs are bound and therefore likely regulated by LARP1, I first conducted a co-immunoprecipitation experiment to verify the interaction of LARP1 and PABP in HeLa cells. pCMV-FLAG tagged LARP1 and PABP constructs together with a pCMV-FLAG tagged GFP control, were forward transfected into HeLa cells as described in materials and methods section 2.4.7. They were then harvested 24 hours later, lysed and subjected to co-immunoprecipitation purification using M2 FLAG magnetic beads to isolate FLAG-tagged proteins, any proteins and mRNAs in complex with them. In the first instance, Co-IPs were conducted in the presence of an RNase cocktail in order to digest away any bound mRNA, thereby showing whether the LARP1-PABP interaction was RNA independent, and to confirm the interaction between LARP1 and PABP.

Western blotting to detect LARP1, PABP and the FLAG-tag of overexpressed protein constructs following the co-immunoprecipitation in the presence of an RNase cocktail showed successful overexpression of each protein (all of which are visible in FLAG blot in pulldown lanes, Figure 5.1A). Blots probed with LARP1 antibody show the difference

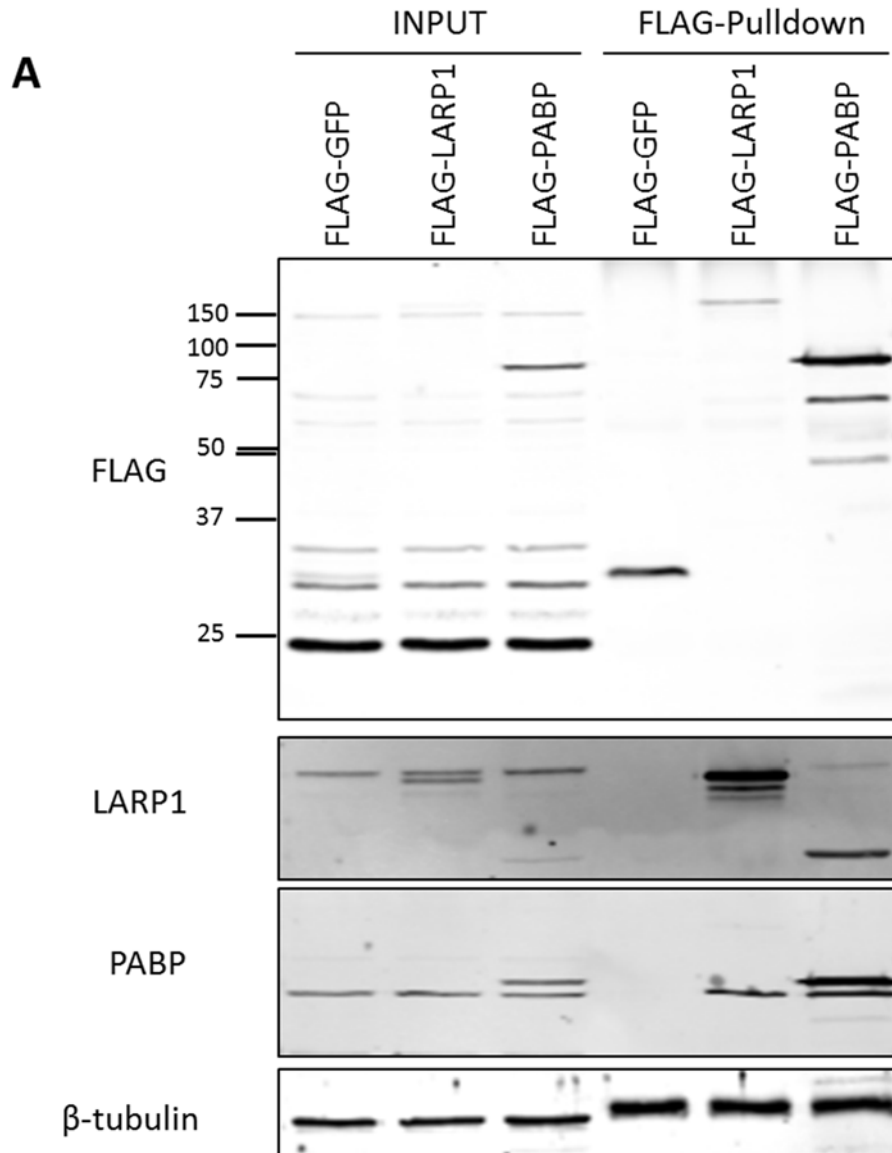


**Figure 5.1** Co-immunoprecipitation experiment in HeLa cells over expressing Flag-tagged GFP, LARP and PABP shows interaction in an RNA-independent manner HeLa cells were seeded at  $1.5 \times 10^6$  cells per 15 cm plate, and incubated under normal cell culture conditions for 24 hours prior to forward transfection with 16.8  $\mu\text{g}$  overexpression pCMV-FLAG tagged protein vectors as described in materials and methods. (A) Cells were harvested 24 hours post-transfection for co-immunoprecipitation experiments (as described in materials and methods). Input and pulldown samples were subjected to western blotting using indicated antibodies. Here  $\beta$ -tubulin was used as a loading control.

in size between endogenous LARP1, visible in all three lanes of input samples, and the over-expressed vector LARP1, visible immediately below the endogenous band in the FLAG-LARP1 input lane and in the FLAG-LARP1 lane alone of pulldown conditions. Furthermore, from this blot we can see endogenous LARP1 was detected in the FLAG-PABP pulldown band, indicating that it has been captured through RNA-independent association with FLAG-PABP.

Probing for PABP also indicates a size discrepancy between the FLAG-PABP over expression vector product and endogenous PABP; again here this can be easily determined as endogenous PABP can be seen across all input conditions, whereas the FLAG-tagged version appears immediately above this band in the FLAG-PABP input lane, as well as in the FLAG-PABP pulldown condition. Also here, endogenous PABP is detected in the FLAG-LARP1 pulldown, to a similar level as in the FLAG-PABP condition. This further confirms that LARP1 and PABP interaction is RNA-independent. Endogenous PABP presence alongside FLAG-PABP supports previous reports in the literature of a multimerisation of PABP or several PABP proteins binding to poly(A) tail stretches and being brought into proximity for interaction (Kühn & Pieler 1996; Melo et al. 2003). Finally, probing for  $\beta$ -tubulin as a loading control showed equal loading, indicating differences in expression was not due to different levels of total protein. This confirmed that LARP1 and PABP interact in an RNA independent manner in HeLa cells, as seen by previous groups (Fonseca et al. 2015; Tcherkezian et al. 2014).

### **5.2.2. Depletion of PABP using siRNA in HeLa cells leads to apoptosis and slowed proliferation**

PABP and LARP1 have previously been identified as interacting partners in the context of translation, and work in the previous chapter in this study has shown the negative impact LARP1 depletion has on cellular proliferation over time in both HeLa cells and A549 cells. PABP depletion in HeLa cells has been shown recently to affect cell survival, leading to apoptosis and reduced protein translation (Thangima Zannat et al. 2011). As a first step in this part of the study, we first set out to investigate the effect of PABP depletion on HeLa cell proliferation; both to attempt to reproduce previous groups' findings, as well as to compare back to LARP1 depletion and to determine whether a difference existed between cell lines.

HeLa cells were reverse transfected with siRNA against PABP (also known as PABPC1) and grown as described in materials and methods. The number of cells in each well at various time points was compared back to a scrambled siRNA control reverse transfected at the same time zero and seeded at the same seeding density. In this way, as for the knockdown studies described in the previous chapter, it was possible to investigate effects of depletion of PABP on growth rate, cell survival, and morphology. Figure 5.2A shows the effect of PABP depletion by siRNA at various time points post-transfection relative to scrambled control siRNA transfected HeLa cells. A robust reduction in proliferation with respect to control can be seen for the PABP depleted HeLa cells, with significant differences in cell number between conditions as early as 24 hours post-transfection. After 96 hours post-siRNA transfection the mean total cell number was 39% of that for the control transfected cells; loss of PABP had reduced cellular proliferation by over half as determined by viable cell number.

Figure 5.2B shows a representative set of western blots for one of n=3 growth curve experiments conducted following PABP knockdown. These westerns show the robust knockdown of PABP from 48 hours post-transfection, with efficiency of transfection increasing over time. Here  $\alpha$ -tubulin was used as a loading control. To identify any drastic morphological changes in the HeLa cells following PABP depletion, phase contrast microscopy was used to capture images of wells representing each condition 72 hours post transfection (Figure 5.3A). These images showed no severe difference in cell morphology between control and PABP siRNA transfected cells, though it did appear to show several cells rounded, potentially undergoing apoptosis, as well as clearly demonstrating the difference in cell number between conditions. It is likely, from these images and data shown previously in the literature that depletion of PABP leads to apoptosis and slowed cell proliferation in the HeLa cell line.

### **5.2.3. Depletion of PABP using siRNA in A549 cells also leads to apoptosis and slowed proliferation**

Having observed PABP depletion effects on cell growth in HeLa cells, we moved to investigate whether this effect was consistent in the A549 cell line also, or whether there was a differential as seen following LARP1 depletion. Hence, A549 cells were

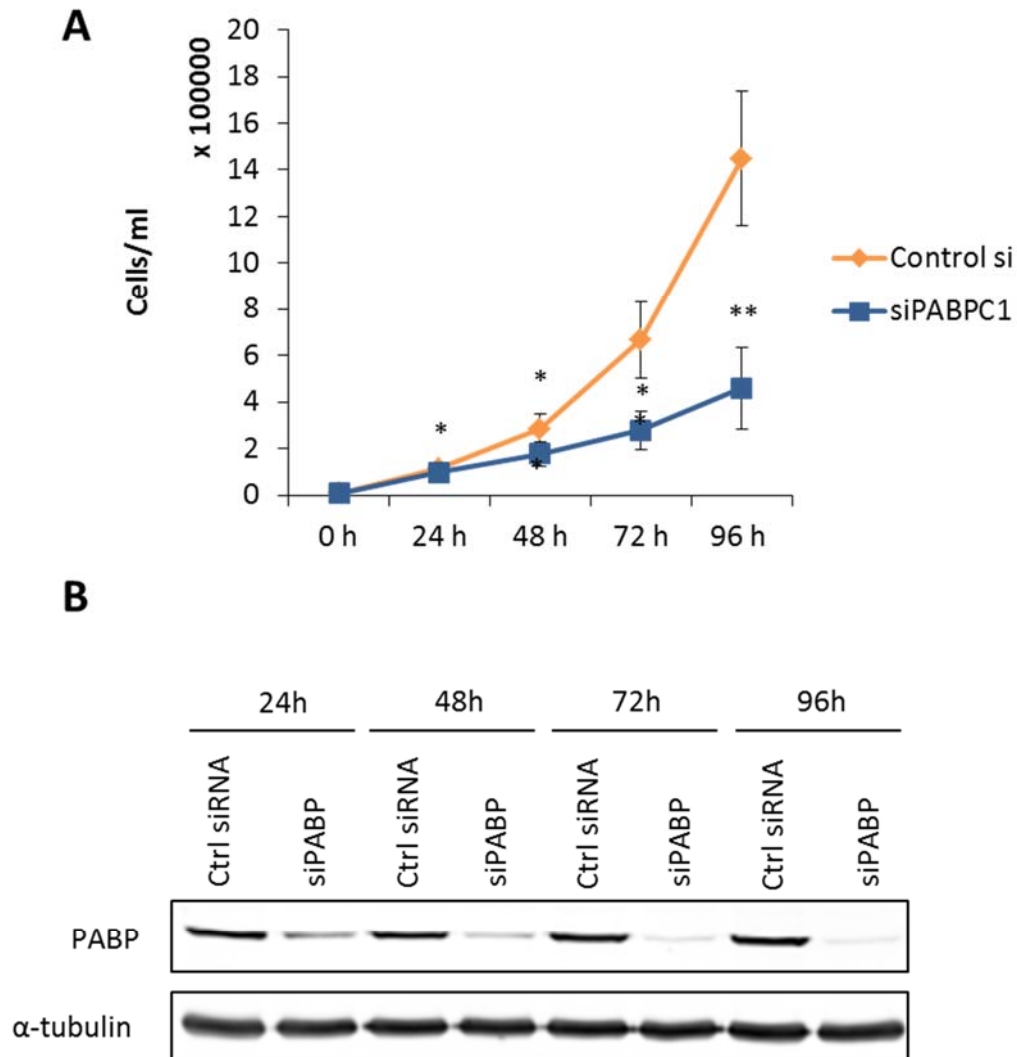


**Figure 5.2 Growth curves following PABP knockdown in HeLa cells showed slow in cellular proliferation rate relative to scrambled siRNA control.** HeLa cells were seeded at 40,000 cells per well of a 6 well plate and reverse transfected using siRNA targeting PABPC1, or a scrambled siRNA control (siCtrl). (A) Cells were left to grow for indicated durations post-transfection and harvested at indicated time points (as described in materials and methods). Viable cell number counted using a Model TT CASY Counter (in triplicate, n=3). Cell count was compared between conditions by paired t-test: \* = p value < 0.05, \*\* = p value < 0.01, \*\*\* = p value < 0.005. (B) Cells were spun to a pellet, lysed, normalised by Bradford assay and subjected to western blotting (representative shown) with indicated antibodies. Here  $\alpha$ -tubulin was used as a loading control.

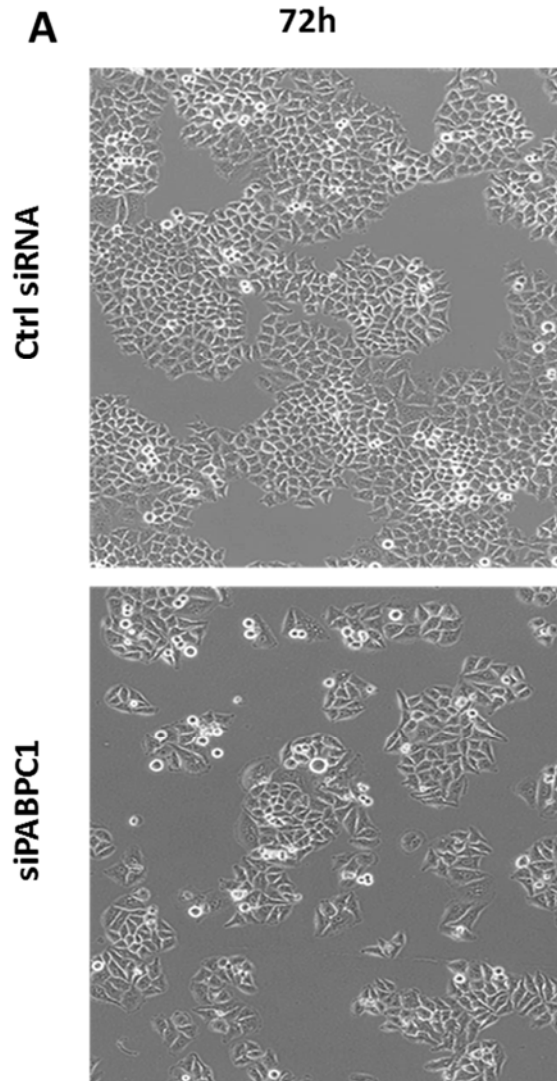


**Figure 5.3 Cell morphology following 72 hours siRNA knockdown of PABPC1** knockdown instigates notable visual changes in HeLa cell morphology. HeLa cells were seeded at 40,000 cells per well of a 6 well plate and reverse transfected with siRNA against PABPC1, or a scrambled siRNA control (siCtrl). Cells were then incubated in a humidified incubator at 37°C for 72 hours. (A) Representative images taken using 10x magnification of a phase contrast microscope showing cell morphology and density 72 hours post-transfection illustrates the slower growth rate following PABPC1 knockdown, with notable increase in cells exhibiting a potentially apoptotic phenotype.

seeded at equal densities in a 6 well plate of 50,000 cells per well and reverse transfected, using either scrambled control siRNA or one targeting PABP, as described previously for the HeLa cells. Cells were then harvested and counted using a CASY cell counter Model TT in the same manner as described for other growth curve experiments; this data can be seen in the growth curve in Figure 5.4A (n=1). From this, it is fair to conclude that depletion of PABP in A549 also leads to a reduction in cell number beginning after 24 hours and progressing over a period of 96 hours following siRNA transfection. By 96 hours post-transfection, viable cell number in the PABP depleted condition was 81% lower than in the control transfected condition. The difference in effect between cell lines could be dependent on transfection efficiency, though it was noted following western blotting for PABP and a loading control ( $\alpha$ -tubulin) that the extent of PABP depletion appeared comparable in this cell line to that seen in HeLa cells (Figure 5.4B). PABP depletion therefore leads to comparable effects on cell proliferation in both HeLa and A549, despite depletion of its binding partner LARP1 having contrasting effects in each cell line.

#### **5.2.4. Endogenous co-immunoprecipitation of LARP1 and PABP in the presence and absence of Torin1, and subsequent arrays allowed identification of mRNA bound to each**

Work conducted by Dr Ewan Smith in the Bushell lab, toward a collaborative aspect of this project, involved performing endogenous LARP1 and PABP co-IPs in the presence and absence of Torin1 treatment. These co-IP experiments were performed using RNase inhibitors in order to protect mRNA bound to either protein from degradation; the mRNA from each sample was then used to perform an mRNA micro-array (Figure 5.5). This “reverse experiment” allowed identification of messages bound to each protein, and their abundance within each condition. Gene set enrichment analysis was then performed by Dr Ania Wilczynska, a list of enriched mRNA for each protein IP (relative to an IgG control) was generated for each condition. This allowed for identification of any enriched mRNA, as determined by binding to LARP1 or PABP, following Torin1 treatment (as well as those in the totals). Figure 5.6 shows Venn diagrams representing the differences between the number of constitutively bound mRNAs and those mRNA enriched following LARP1 IPs (A) and PABP IPs (B) in HeLa

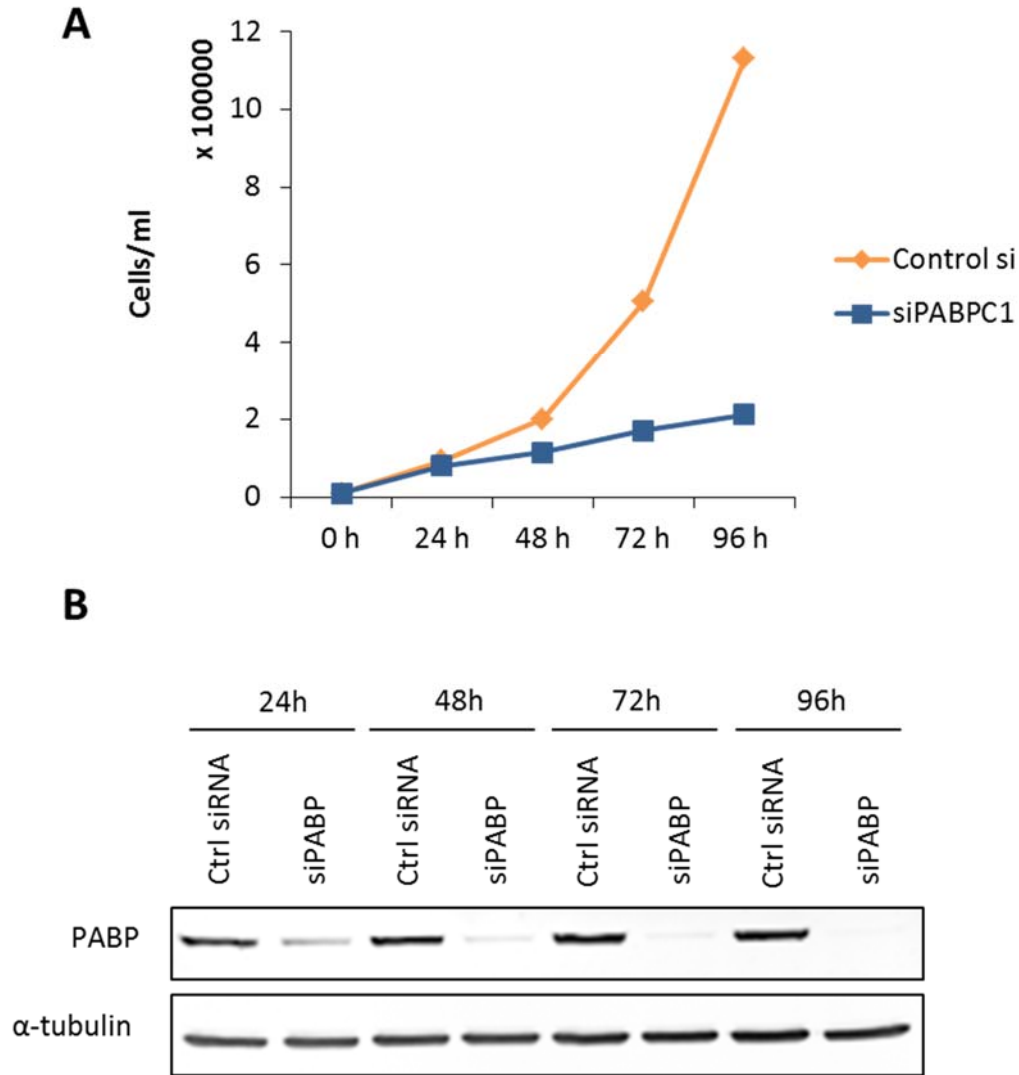


**Figure 5.4 Growth curves following PABP knockdown in A549 cells showed slow in cellular proliferation rate relative to scrambled siRNA control.** A549 cells were seeded at 50,000 cells per well of a 6 well plate and reverse transfected using siRNA targeting PABPC1, or a scrambled siRNA control. (A) Cells were left to grow for indicated durations post-transfection and harvested at indicated time points (as described in materials and methods). Viable cell number counted using a Model TT CASY Counter (in triplicate, n=1). (B) Cells were spun to a pellet, lysed, normalised by Bradford assay and subjected to western blotting (representative shown) with indicated antibodies. Here  $\alpha$ -tubulin was used as a loading control.

cells. GO term analysis of the mRNAs significantly enriched over input ( $\log$  fold change ( $\log$ FC)  $> 0.5$ ) in LARP1 IPs showed there was enrichment of mRNAs associated with specific terms, including structural components of the ribosome, mTOR signalling components and regulation of apoptosis. Furthermore, following Torin1 treatment in LARP1 IPs it was seen that LARP1 bound and enriched a wealth of RNAs compared to the IgG control; including both 5' TOP mRNAs and non-TOP mRNAs, but interestingly there was no enrichment of histone genes. Enriched mRNAs following Torin1 treatment identified with a variety of GO terms including: ribosomal proteins, translation or release factors, protein targeting to endoplasmic reticulum (ER), 'de novo' posttranslational protein folding, translational termination, monosaccharide biosynthetic process, and respiratory electron transport chain. Interestingly, in PABP IPs there was also significant enrichment ( $\log$ FC  $> 0.5$  relative to input) of mRNAs corresponding to the 'respiratory electron transport chain' GO term following Torin1 treatment, indicating a further avenue for metabolic regulation.

Overlap of enriched mRNAs from LARP1 IPs versus those in PABP IPs showed a strong positive correlation between the changes in enrichment of mRNAs between Torin1 treated lysates and DMSO control lysates, in RNAs bound to both proteins (Figure 5.7). Cohorts of mRNAs identified as bound to only LARP1 or PABP were also identified through analysis of these datasets. Examination of these separate groups of mRNA allowed for selection of a subset meeting different enrichment criteria across IPs and treatments for validation and further investigation (i.e. enriched overall, enriched binding to LARP1 only or PABP only, enrichment following Torin1 treatment in both IPs and so on), these are outlined in Figure 5.8.

Included in these categories are genes whose binding to both LARP1 and PABP increased following Torin1 treatment; such as FOS, MYC and GDF15, and those whose abundance appeared to decrease in the LARP1 and PABP totals following Torin1 treatment; RHOV, HSP6 and AMD1. In the IP samples, a selection of genes were identified as being more bound by both LARP1 and PABP (LDHA, SAMM50, MDH2), by LARP1 only (EEF2, ACHY, EIF4A) or by PABP only (HMOX1, CYBA). Also included were two categories of genes whose abundance in LARP1 or PABP IP samples remained

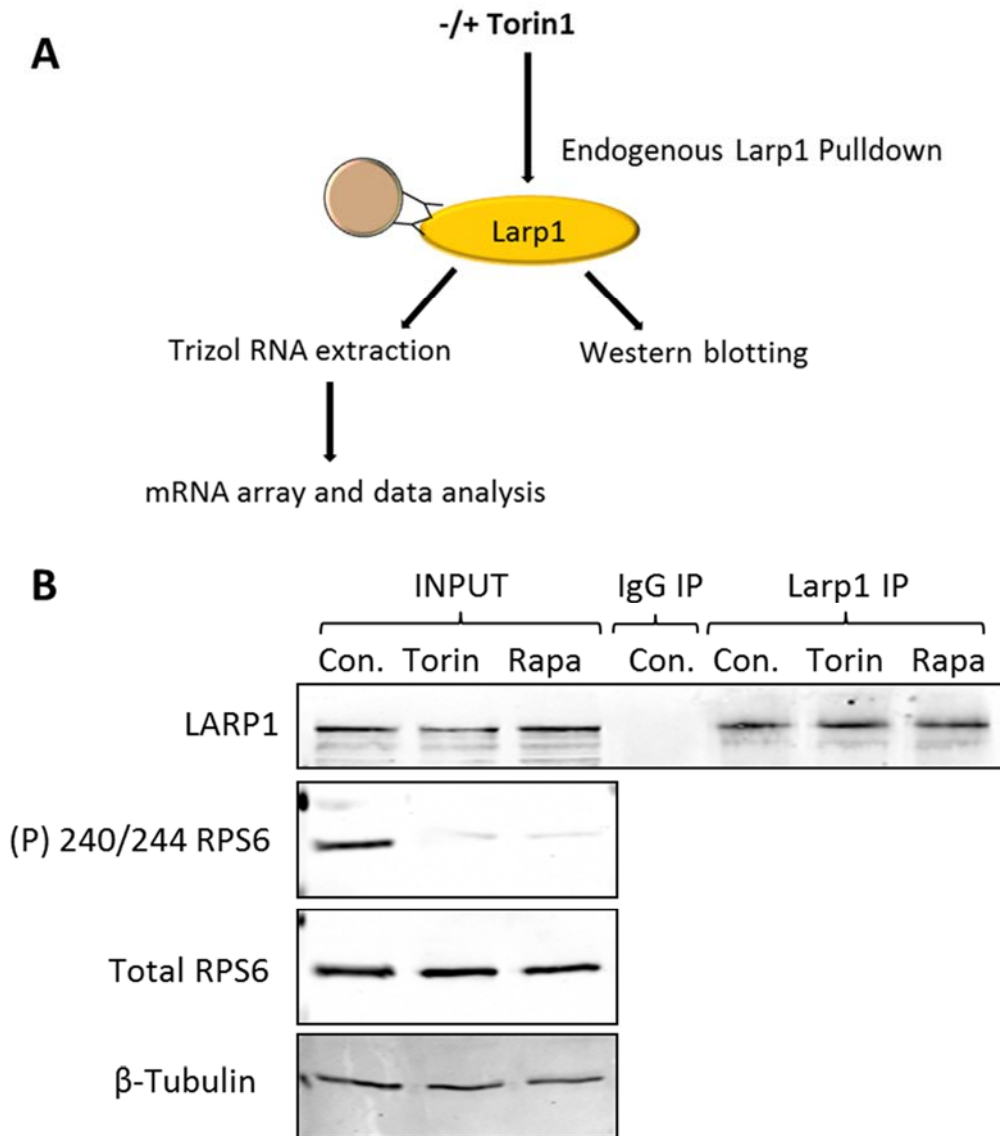


**Figure 5.5 Endogenous LARP1 immunoprecipitation experiments with gene expression arrays to identify mRNAs showing enriched binding.** HeLa cells were seeded at 600,000 cells per 15 cm plate and incubated for 24 hours. 30 minutes prior to treatment with 200 nM Torin1 or DMSO control, media was supplemented with an additional 2% FCS and 1% L-glutamine. 1 hour later cells were harvested and lysed; lysates were subjected to endogenous IP. (A) Schematic briefly outlining process for endogenous IP of LARP1 (also applied to PABP IPs). (B) Samples were subjected to western blotting to check efficiency of Torin1 inhibition of mTOR signalling in samples used for array analysis. Data presented are all from E. Smith.

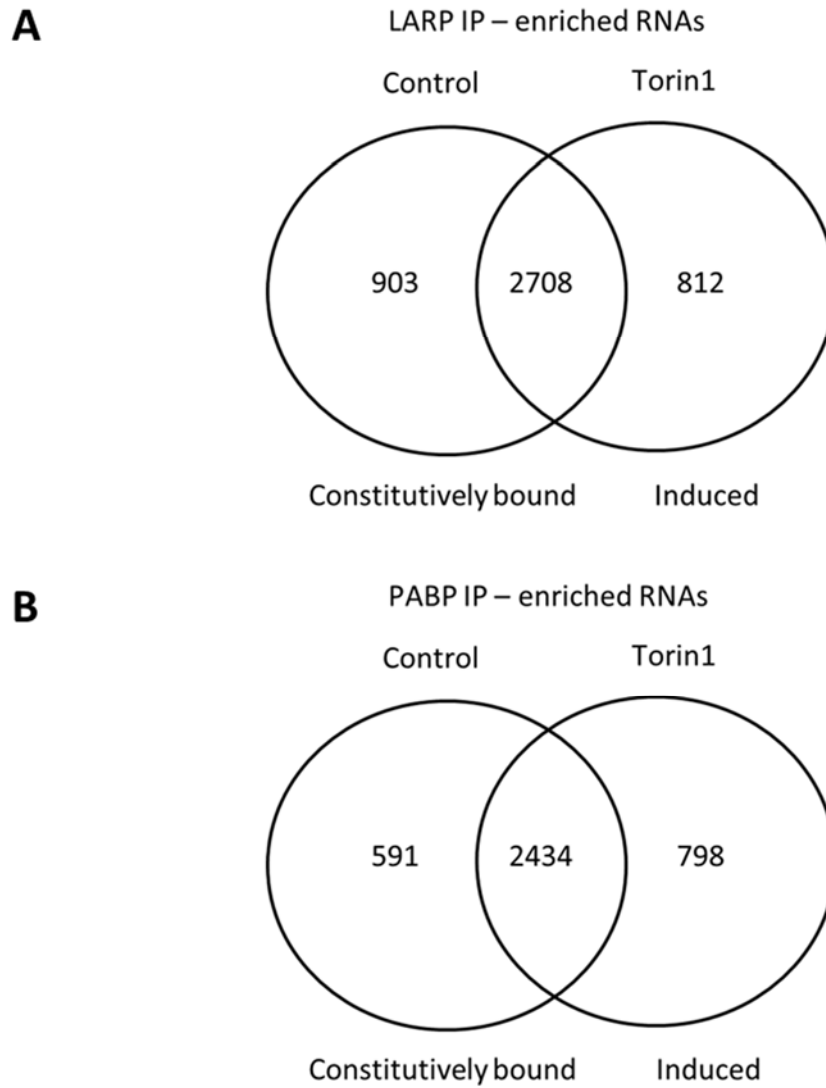


**Figure 5.6 Differences between messages constitutively versus induced enrichment following Torin1 treatment in endogenous IPs of LARP1 and PABP.** Following endogenous IP of LARP1 and PABP in the presence and absence of Torin1 treatment, gene enrichment analysis was performed by A. Wilczynska. Venn diagrams show messages identified as significantly enriched over input. ( $\log_{FC} > 0.5$ ) in both (A) LARP1 IPs and (B) PABP IPs. Data presented are all from experiment conducted by E. Smith

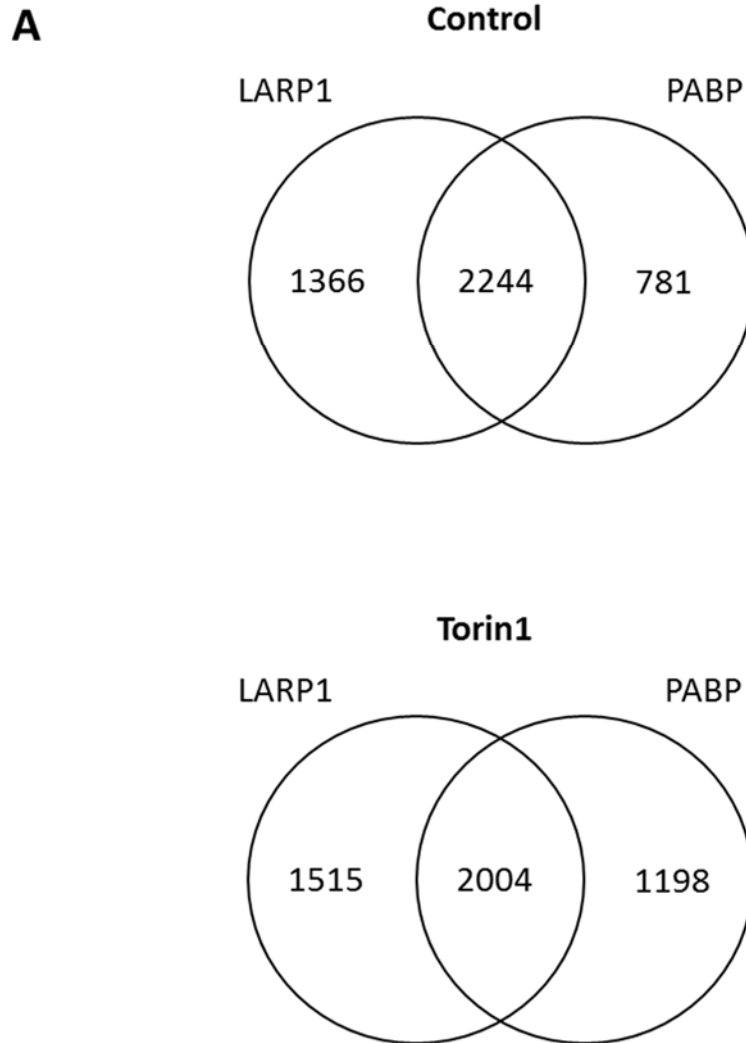


**Figure 5.7** **Overlap and differentials between LARP1 and PABP bound mRNA from endogenous IP and gene expression arrays, in the presence and absence of Torin1 treatment.** Following endogenous IP of LARP1 and PABP in the presence and absence of Torin1 treatment, gene enrichment analysis was performed by A. Wilczynska. (A) Venn diagrams show messages with enriched binding to LARP1, PABP or both, identified as significantly enriched over input ( $\log_{FC} > 0.5$ ) in each condition. Data presented are all from experiment conducted by E. Smith

**A**

| Torin1 treatment affect on mRNA abundance |                  | Gene name                   |
|---|------------------|-----------------------------|
| <b>Totals<br/>(relative to IgG)</b>       |                  |                             |
| Up  | -                | FOS, MYC, GDF15             |
| Down                                      | -                | RHOV, HPS6, AMD1            |
| <b>IP</b>                                 |                  |                             |
| Up  | Both             | LDHA, SAMM50, MDH2          |
| Up  | LARP1 only       | EEF2, ACHY, EIF4A           |
| Up  | PABP only        | HMOX1, CYBA                 |
| Unchanged                                 | Bound to both    | BCL7C, GUK1, IDS            |
| Unchanged                                 | Bound to neither | HIST2H2AC, HIST1H4H, MALAT1 |

**Figure 5.8 Categories of a selection of mRNA identified from endogenous IP experiments as binding LARP1 and/or PABP, and any differences following Torin1 treatment of HeLa cells.** A selection of mRNAs detected through endogenous IP and subsequent gene expression arrays conducted by Ewan Smith, selected for further validation as part of this study. mRNA are categorised according to their change in abundance as detected in totals, LARP1 bound or PABP bound endogenous IP samples, as well as any differences detected in Torin1 treated relative to control (DMSO) treated conditions.

unchanged following Torin1 treatment, but that were in fact bound by both proteins (BCL7C, GUK1, IDS), and those that were not remarkably bound by either protein in either treatment (HIST2H2AC, HIST1H4H, MALAT1).

Interestingly, the sub-selection of genes identified as being increasingly bound by LARP1 following Torin1 treatment include EEF2 and EIF4A1, which are both TOP mRNAs encoding proteins involved in translation: eEF2 in translation elongation, and eIF4A1, one of two isoforms of eIF4A helicase that forms part of the eIF4F cap complex crucial for translation initiation. To the best of knowledge, none of the other selected genes are TOP mRNAs; the inclusion of a variety of genes including 5' TOP and non-TOP mRNAs could provide greater insight into any particular characteristics or types of mRNA targeted or regulated by LARP1 and PABP. Genes listed as not showing enriched binding to LARP1 or PABP, according to the endogenous IP and gene expression arrays, include two mRNA encoding histone proteins (HIST2H2AC and HIST1H4H), which do not possess poly(A) tails, and also one long non-coding mRNA (lncRNA); MALAT1.

#### **5.2.5. Total mRNA levels of several targets determined by qPCR following depletion of LARP1 or PABP in the presence and absence of Torin1 treatment**

Identified mRNAs bound by LARP1 or PABP, in the presence and absence of Torin1, in HeLa cells confirmed their association with these RBPs. However this did not indicate whether there were any effects on the total levels of these mRNA under these conditions, and provided no information as to the basal expression of these in A549 cells. As such, an experiment in A549 was conducted where either LARP1 or PABP1 was depleted by siRNA, in the presence or absence of Torin1 treatment. Samples from lysed cells of each condition were divided between protein investigations and RNA extraction for RT-qPCR investigations of mRNA expression.

Western blotting following harvests and normalisation of samples from this experiment showed robust knockdown of LARP1 and PABP where the corresponding siRNA had been used (Figure 5.9). Furthermore, probing for key mTOR signalling pathway components and phosphorylation showed effective inhibition of mTOR signalling; total levels of P70S6K and RPS6 remained steady though a band-shift was

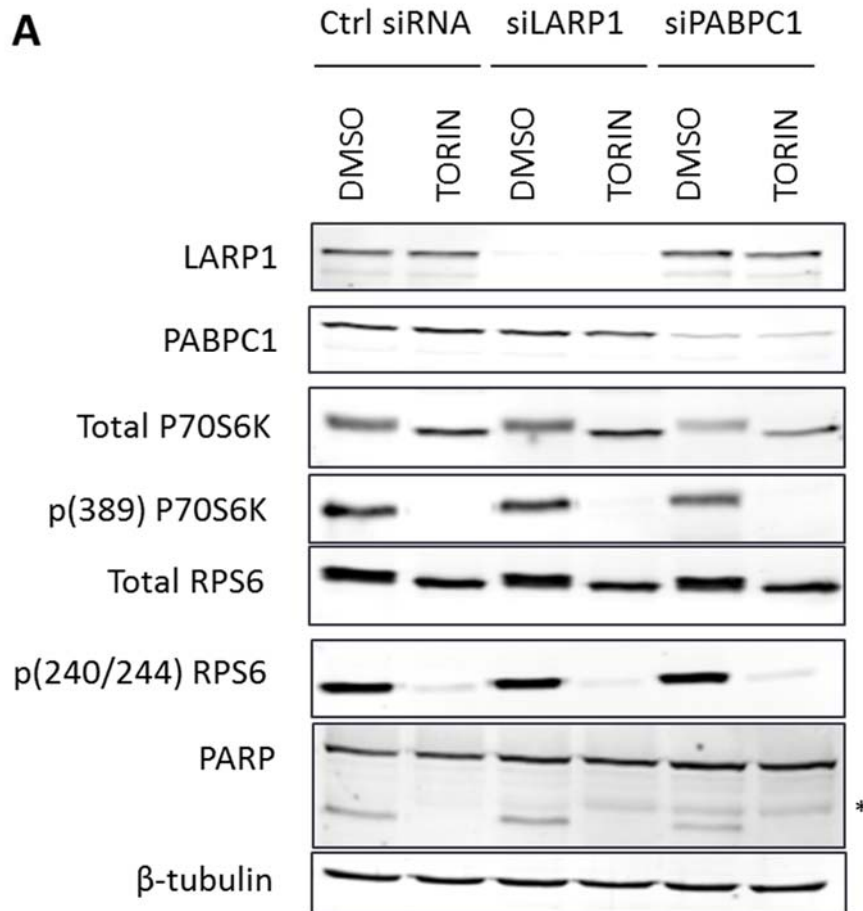
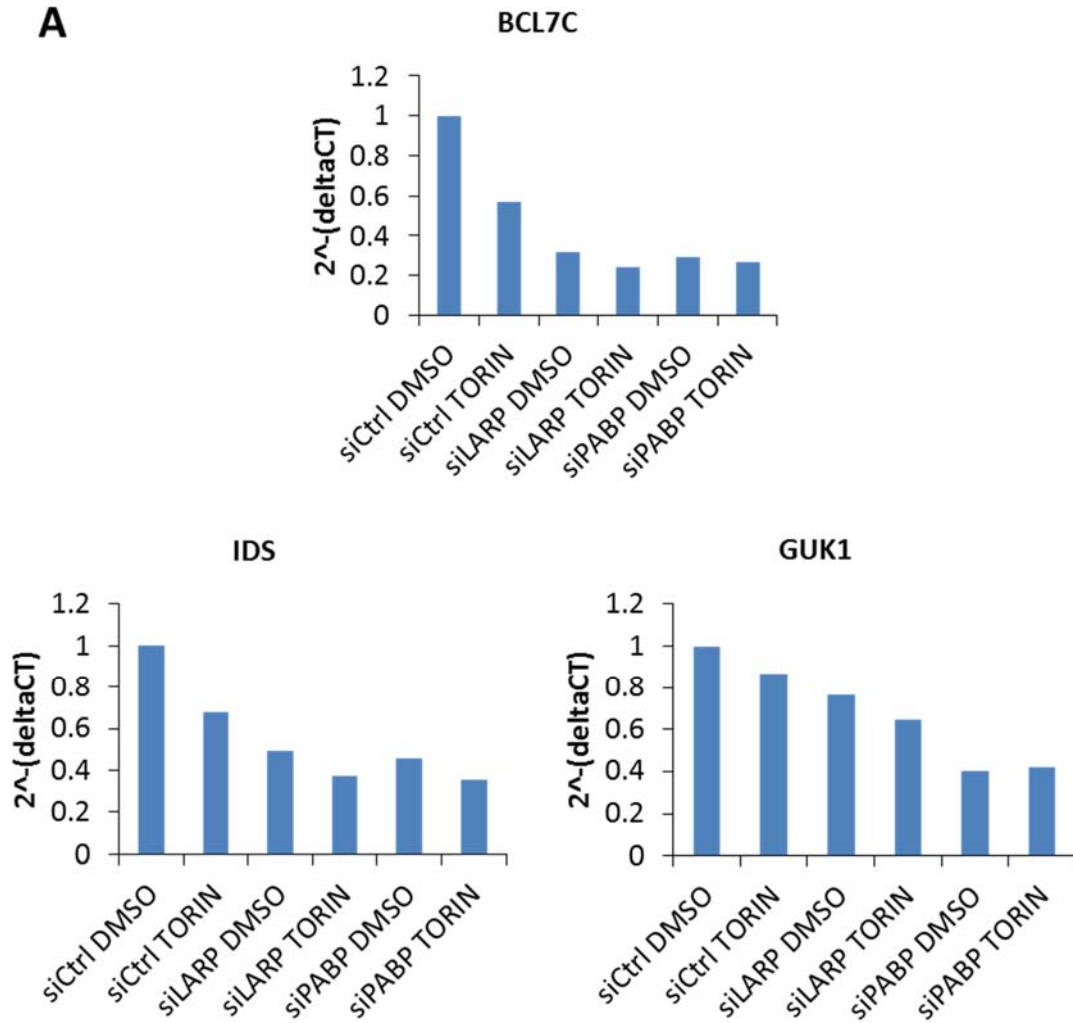


**Figure 5.9** Samples generated for qPCR analysis of total mRNA abundance in A549 cells, following depletion of LARP1 or PABPC1 in the presence and absence of Torin1 treatment. A549 cells were seeded in 10 cm plates and reverse transfected with indicated siRNA before incubation. Media was supplemented with an additional 2% FBS and 1% L-glutamine 30 mins prior to treatment with Torin1 or DMSO control for one hour before harvesting. Harvested cells were split for RNA and (A) protein analyses. Cells were lysed, normalised and subjected to western blotting with indicated antibodies. Here, β-tubulin was used as a loading control.

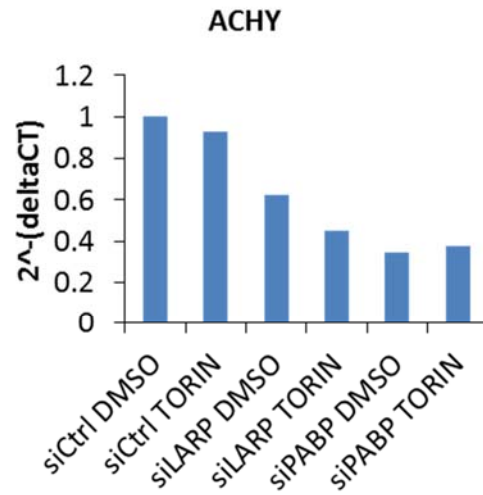
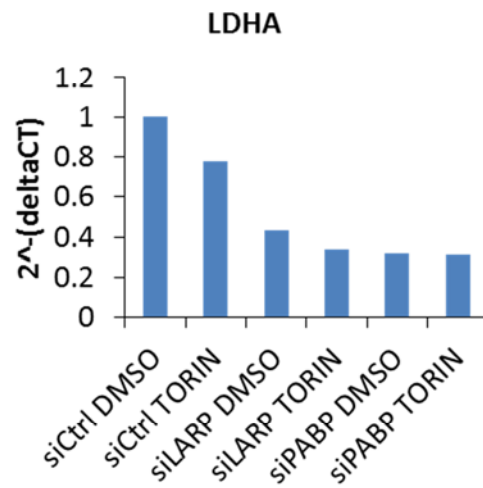
visible in both; alongside corresponding dephosphorylation of p(389)-P70S6K and p(240/244)-RPS6 this indicated inhibition of mTOR signalling. PARP cleavage product at 89 kDa was detected (denoted by an asterisk) in the Torin1 treated LARP and PABP depleted conditions as well as the control (DMSO) treated PABP siRNA transfected condition; in all three of these conditions the level of detected cleavage product was comparable.

RT-qPCR was conducted on RNA extracted from the remaining half of material harvested for these samples; equal concentrations were used per RT reaction from each condition and qPCR performed using the generated cDNA and primers designed against a selection of the genes listed in Figure 5.8; the results of these qPCR (n=1) are shown in Figure 5.10. In all cases a  $2^{-(\Delta CT)}$  was calculated; there was no normalisation to a control gene. This decision was for the most part due to the main question of this investigation: which genes were bound by LARP1 and PABP. As PABP is a ubiquitous protein bound to any mRNA or ncRNA possessing a poly(A) tail, this made selection of a control gene for totals difficult. All conditions were therefore normalised to the control transfected, control treated condition (siCtrl, DMSO).

In total abundance of genes from the first category, which was those bound by both LARP1 and PABP but unchanging following Torin1 treatment, we included BCL7C, IDS and GUK1 (Figure 5.10A). In all three genes, abundance appeared lower in LARP1 and PABP depleted samples than in control siRNA transfected conditions. Furthermore, considering each siRNA condition separately, Torin1 treatment did appear to reduce abundance of each gene relative to the control treated sample transfected with the same siRNA. However it is important to note that the cells in PABP depleted conditions may in fact have lower abundance due to apoptosis of these cells (mild levels of PARP cleavage products were detected in western blots Figure 5.9); this cannot be ruled out as equal concentrations of RNA were utilised to conduct the RT reaction. For ACHY (Figure 5.10B, representing gene bound by LARP1 only) however, there was less difference between control transfected Torin1 treated and the control treated, though LARP1 and PABP depleted conditions still exhibited lower delta(CT) values than control transfected overall. Finally for LDHA (Figure 5.0C, bound by both LARP1 and PABP,



**Figure 5.10 RT-qPCR analysis of total mRNA abundance of a selection of genes in A549 cells, following depletion of LARP1 or PABPC1 in the presence and absence of Torin1 treatment.** Following identification of a selection of genes whose mRNA are bound by LARP1 and/or PABP in endogenous IPs in HeLa cells, investigation of these mRNAs' total abundance in A549 was conducted. (A) BCL7C, GUK1 and IDS, three genes identified as being bound to both LARP1 and PABP but not exhibiting changes in abundance following mTOR inhibition.

**B****C**

**Figure 5.10 RT-qPCR analysis of total mRNA abundance of a selection of genes in A549 cells, following depletion of LARP1 or PABPC1 in the presence and absence of Torin1 treatment.** Following identification of a selection of genes whose mRNA are bound by LARP1 and/or PABP in endogenous IPs in HeLa cells, investigation of these mRNAs' total abundance in A549 was conducted.

increasingly bound following Torin1 treatment) much the same pattern is seen, with lower relative abundance in LARP1 and PABP depleted conditions, as well as a marginally decreased abundance in Torin1 treated samples relative to their control treated counterparts of the same siRNA transfection condition. In hindsight, inclusion of qPCR primers for 18S and 28S rRNA as an indication of global changes in RNA transcription would provide benefit, in order to better gauge how depletion of either LARP1 or PABP affects the global pool of RNA in a cell. As displayed here, it is unclear whether the decrease in abundance, which is in many cases by as much as two fold for LARP1 and PABP depleted conditions relative to control, is in fact true or whether it reflects a greater effect of the transfection on transcription or global mRNA levels in the cells.

#### **5.2.6. Western blots of Co-IP experiments following overexpression of LARP1 and PABP in both HeLa and A549 cells shows comparable interaction between cell lines**

Having examined the effect on total levels of these mRNA in the context of LARP1 and PABP depleted A549 cells, next FLAG-tagged versions of each protein (alongside a FLAG-GFP control) were over-expressed for co-immunoprecipitation, to identify differences in which mRNAs are bound by each protein. Through use of over-expression vectors, the expected mRNA yield following FLAG-pulldown can be much higher than for endogenous purification, assuming the same amount of starting material. These co-IP experiments were conducted in much the same way as discussed in section 5.2.1 with one key exception; in place of an RNase cocktail to encourage digestion of RNA this IP was conducted in the presence of RNase inhibitor RIBOLock to prevent RNA degradation during the purification, and tRNA was used in order to prevent non-specific binding (see materials and methods section 2.4.7.). A proportion of inputs and elution was then subjected to SDS-PAGE and western blotting (Figure 5.11).

Figure 5.11A shows the resulting FLAG-probed blot following the overexpression of FLAG-tagged GFP, LARP1 and PABP in HeLa cells. As seen in Figure 5.1, FLAG-PABP appears the most expressed of the three vectors, followed second by FLAG-GFP and finally FLAG-LARP1. The centre three lanes loaded were of eluted protein bound to

mRNA, whilst the final three lanes represent the beads, to show how efficient the elution was in each case. From this it is clear that just under half of FLAG-GFP and FLAG-PABP eluted successfully from the beads, whilst FLAG-LARP1 eluted far more successfully, leaving very little detectable LARP1 on the FLAG-beads. Also visible in the FLAG-LARP1 lane of the pulldown conditions is a band corresponding to endogenous PABP; this supports evidence provided by other groups that LARP1 and PABP are interacting factors also in the presence of RNA (Fonseca et al. 2015; Tcherkezian et al. 2014).

Figure 5.11B shows the same as outlined for the panel above it in Figure 5.11B; except in this case the overexpression and co-IP was conducted in A549 cells. A comparison of the two FLAG-probed blots demonstrates the exact same key points outlined as those identified in the HeLa FLAG-probed blots, including the observation of FLAG-LARP1 co-precipitating with endogenous PABP. Also of note here, is the efficiency of elution seen for FLAG-LARP1; with barely any detectable in the fraction still bound to beads. This confirms the reproducibility of this experiment across two cell lines, allowing for investigation and comparison of mRNA abundance in FLAG-LARP1 and FLAG-PABP bound fractions from each.

#### **5.2.7. Comparative qPCR of mRNA bound by LARP1 or PABP in both HeLa and A549 shows differential binding between proteins, as well as effects of Torin1 on binding of certain messages**

Having generated samples of FLAG-LARP1 and FLAG-PABP bound mRNAs following overexpression co-IP experiments; we could move to validate the commonalities and differences in mRNA repertoires between these two proteins. RNA was extracted from these samples and cDNA generated by reverse transcription reactions; using equal concentrations for input fractions and equal volumes for IP fractions. Following the generation of cDNA, primers were designed and used in qPCR to investigate the abundance and differential binding of mRNA identified and shown in Figure 5.8, with the assistance of Gaia Di Timoteo. It is however important to note at this stage as no Torin1 treatment was implemented in the co-IP experiments conducted to generate these samples, the validation in question attempted only to address the mRNAs'

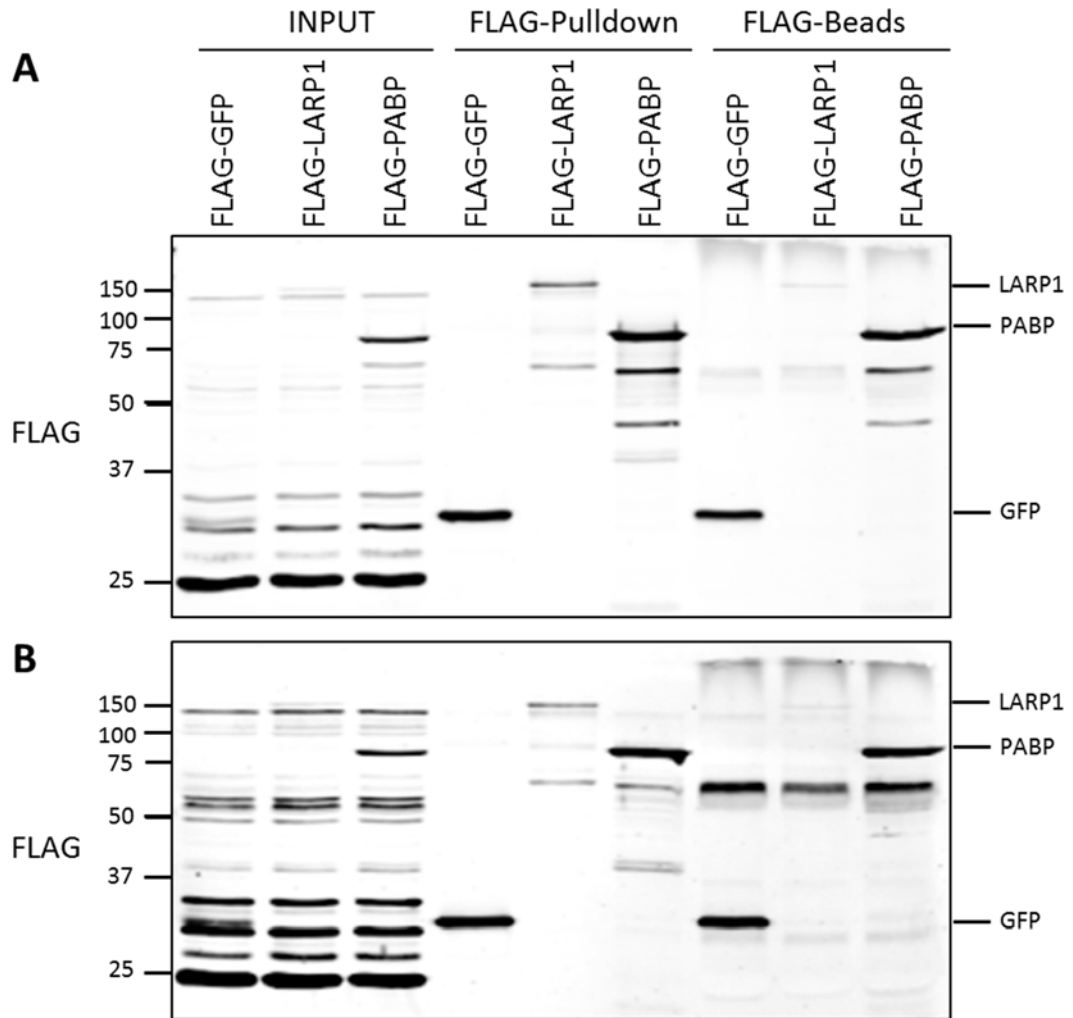
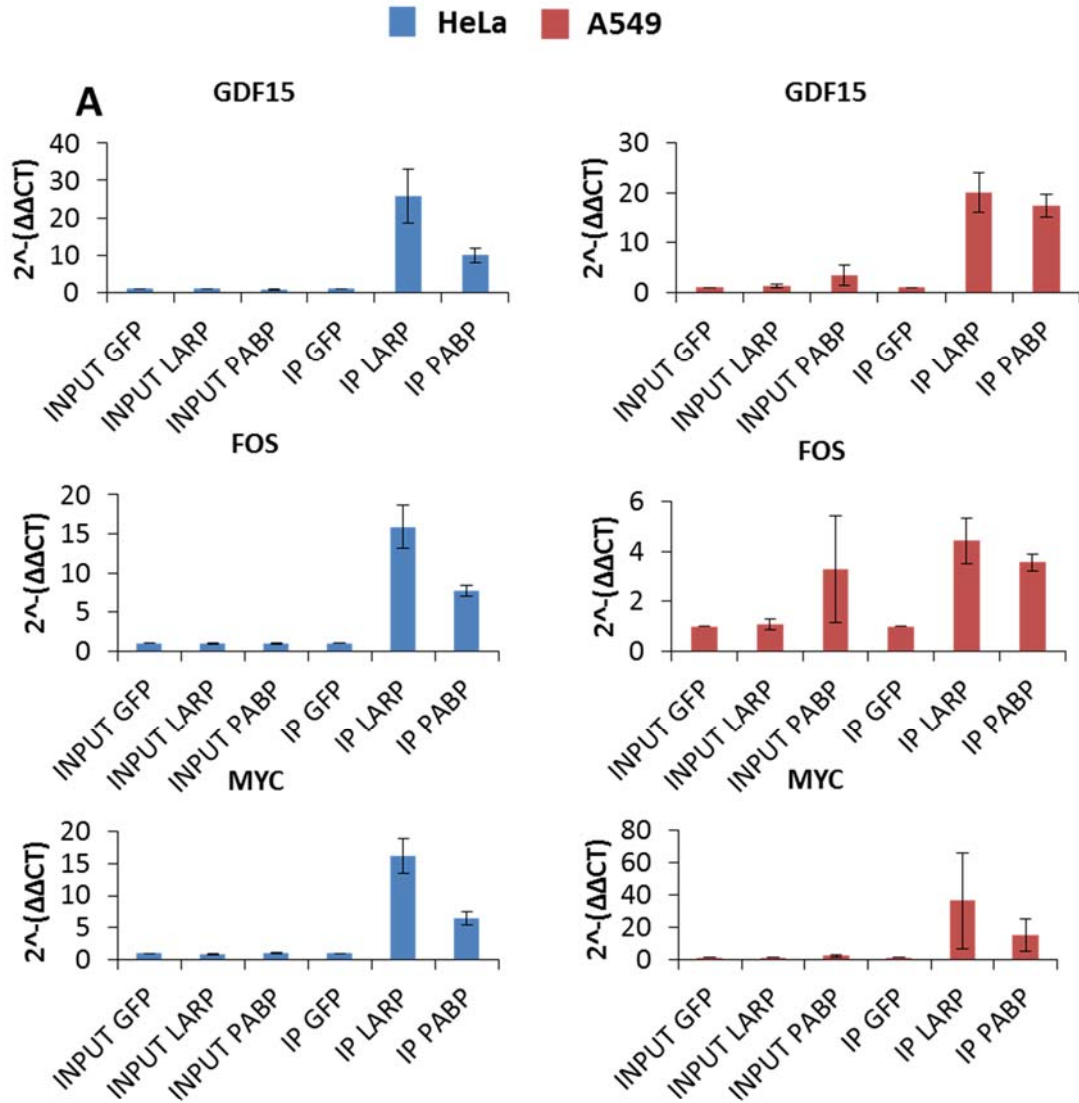


**Figure 5.11** Co-immunoprecipitation experiment in the presence of an RNase inhibitor in cells over expressing Flag-tagged GFP, LARP and PABP shows RNA-dependent interaction. Cells were seeded in 15 cm plates for a final density of 70 to 80% after 48 hours, and incubated under normal cell culture conditions for 24 hours prior to forward transfection with 16.8  $\mu$ g overexpression pCMV-FLAG tagged protein vectors as described in materials and methods. (A) HeLa and (B) A549 cells were harvested 24 hours post-transfection for co-immunoprecipitation experiments in the presence of yeast tRNA and RNase inhibitor (as described in materials and methods). Input, pulldown eluates and residual bead samples were subjected to western blotting using anti-FLAG antibody.

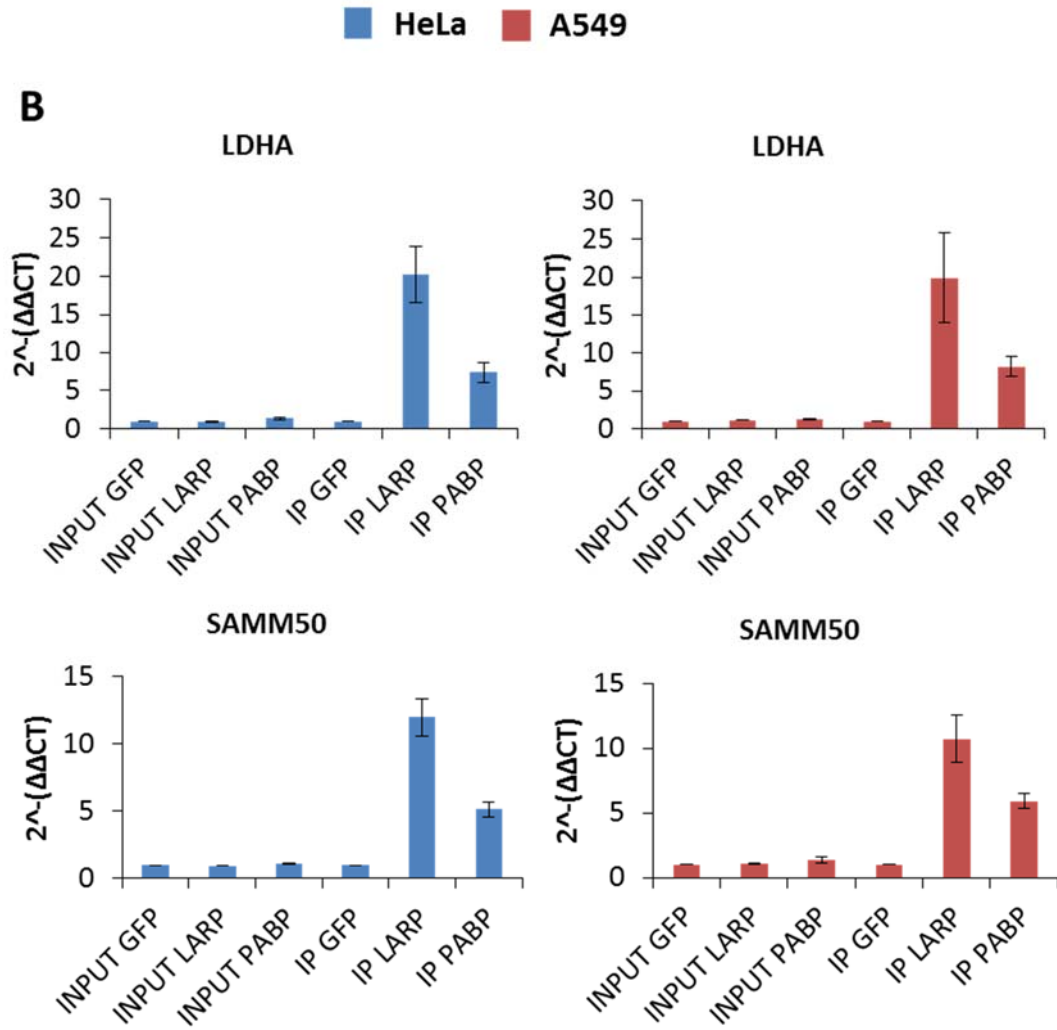
specific binding by LARP1 and/or PABP. In all cases, a  $2^{-(\Delta\Delta CT)}$  was calculated through normalisation back to a selected reference gene: HIST1H4H. This histone RNA was classified according the endogenous IP/gene expression array experiments to be not notably bound by either LARP1 or PABP.

Figure 5.12A shows qPCR validation for those mRNAs identified as increasingly bound in totals following Torin1 treatment, namely GDF15, FOS and MYC. All three genes exhibited increased binding by PABP in the IP fractions of greater than 4 fold relative to that in IP of FLAG-GFP control, in both HeLa (blue, left) and A549 cells (red, right). This was accompanied by an even greater increase in binding in all cases by FLAG-LARP1 in the IP conditions, up to almost 40 fold in the case of MYC in A549 cells. FOS was the only of the three genes to exhibit comparably increased binding in the input fractions however, with FLAG-PABP input showing an increased binding (relative to GFP input control) of approximately 3 fold.

Second category of mRNA investigated were those genes identified as being increasingly bound by both LARP1 and PABP following Torin1 treatment (Figure 5.12B). This category included genes of metabolic GO terms: LDHA, SAMM50 and MDH2. LDHA showed increased abundance in LARP1 and PABP IP fractions, indicating it is strongly bound by both proteins. In HeLa cells (blue, left), LDHA appeared increased by 20 fold in LARP1 IP and by a more modest 7 fold in PABP IP. In A549 cells (red, right) LDHA was bound by LARP1 20 fold more and PABP 8 fold more. Similarly, SAMM50 showed increased abundance in LARP1 bound fractions to a greater extent than in PABP bound IP; though the difference as fairly modest. In HeLa cells SAMM50 was almost 12 fold more abundant than control in LARP1 bound IP fractions and 5 times more in PABP bound, whilst in A549 these increase were almost 11 fold for LARP1 bound and almost 6 for PABP bound. Of the TOP mRNAs identified as increasing binding to LARP1 only following the endogenous IP, we investigated EEF2 and EIF4A1 (Figure 5.12C). Both of these genes showed dramatic increased abundance in LARP1 bound fractions and a more modest increase in PABP bound IP. In HeLa cells (left, blue), the increase of EEF2 abundance in LARP1 and PABP IP respectively was 20 fold and 5.5 fold respectively; in



**Figure 5.12** RT-qPCR validations of LARP1 and PABP bound mRNA targets following purification using FLAG-tagged overexpressed proteins in HeLa and A549 cells. Following RNA extraction from FLAG-tagged protein IP experiments, reverse transcription reactions and qPCR using primers to targets selected from those listed in Figure 5.5 was conducted. (A) qPCR of targets identified as having increased abundance in totals from endogenous IP experiments conducted previously Conducted in both HeLa(blue) and A549 (red) cell lines. All normalised to HIST1H4H expression; (n=3).



**Figure 5.12 continued** – (B) Genes identified as being increasingly bound by both LARP1 and PABP following Torin1 treatment in endogenous IP experiments conducted previously were investigated through IPs in a FLAG-tagged over-expression system. Conducted in both HeLa(blue) and A549 (red) cell lines. All normalised to HIST1H4H expression; (n=3).

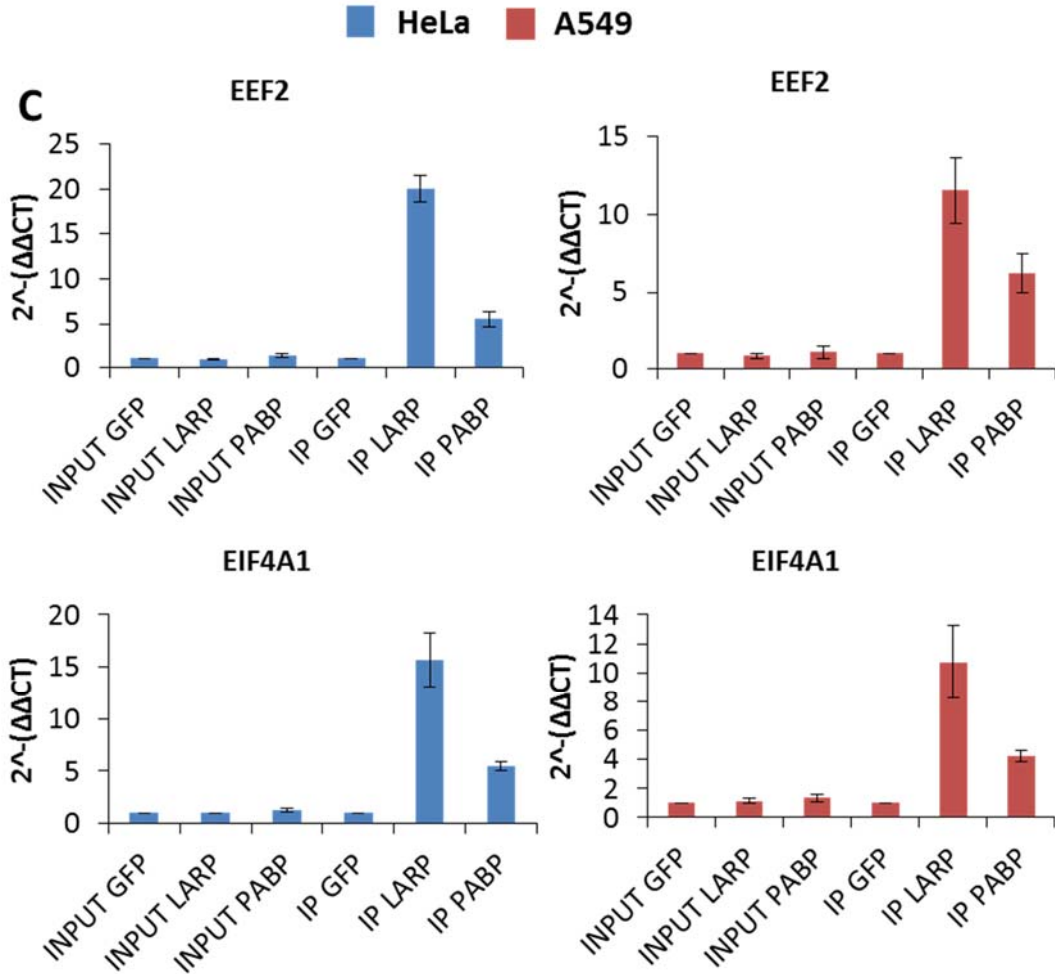


**Figure 5.12 continued** – (C) Genes identified as being increasingly bound by LARP1 following Torin1 treatment in endogenous IP experiments conducted previously were investigated through IPs in a FLAG-tagged over-expression system. Conducted in both HeLa (blue) and A549 (red) cell lines. All normalised to HIST1H4H expression; (n=3).

A549 cells (red, right) these numbers corresponded to over 11 fold and 6 fold respectively. For EIF4A1, the increases were also very similar between cell lines; HeLa cells showed an increase in abundance in LARP1 bound IP of over 15.6 fold and in PABP IP of 5.5 fold. In A549 cells these increases were almost 11 fold and over 4 fold respectively.

Two genes selected which were identified as being enriched in PABP IP were HMOX1 and CYBA, interestingly both involved in redox reactions (Figure 5.12D). However qPCR showed both genes were also enriched in the LARP1 IPs. HMOX1 showed comparable enrichment between LARP1 IP and PABP IP in both cell lines; 38 and 36 fold respectively for HeLa cells and 17 and 14 fold for A549 cells, the closest enrichment values between conditions of any genes in our panel bar “non-binders”. CYBA however did not exhibit this same similarity.

Another category of mRNA mentioned previously, was those bound by both LARP1 and PABP but unchanging following Torin1 treatment in IP conditions. These included BCL7C, IDS and GUK1 (Figure 5.12E). In all three of these genes, across both cell lines, the increase in abundance of the mRNA in LARP1 IP was over double that of the increase in abundance in the PABP IP relative to control. Also, as seen for the TOP mRNAs among our gene list here, the fold changes in abundance relative to control were notably highly similar across the two cell lines, suggesting perhaps a more conserved role in LARP1 binding of these messages.

Our final category of mRNA for which qPCR was conducted included those which were considered “non-binders” in either condition, remaining unchanged in abundance throughout the IP even following Torin1 treatment. Other than the HIST1H4H gene selected for use throughout these qPCR as a reference gene, HIST2H2AC (another histone RNA) and the lncRNA MALAT1 were investigated (Figure 5.12F). From the qPCR data for HIST2H2AC it can be seen that histone RNA do not appear to be bound more in the IP conditions than the INPUT for any condition, including LARP1 or PABP IP. This provides reassurance that histones may be a suitable reference gene as this study progresses to normalise differential binding of mRNA bound by LARP1 and PABP. Also included was MALAT1, which showed a similar profile to histone RNA in the A549 cells,

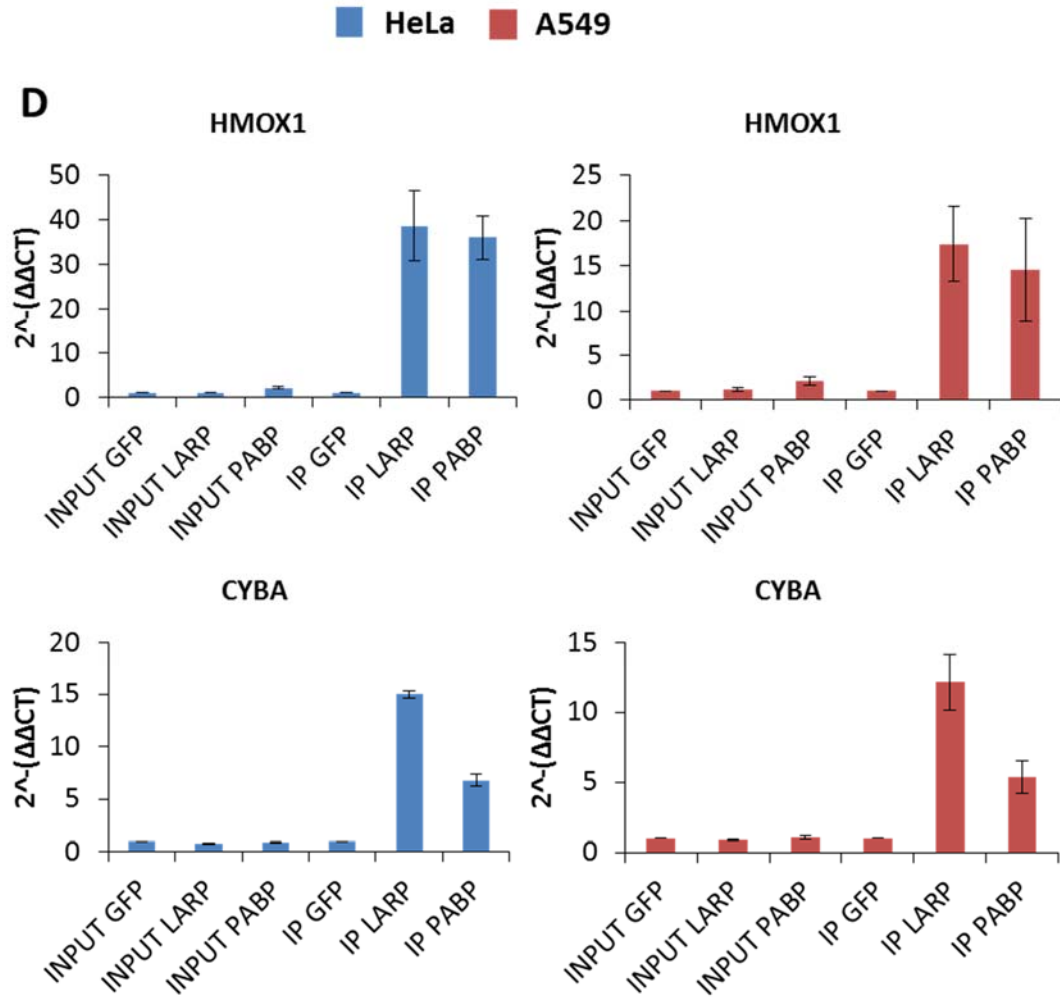


**Figure 5.12 continued** – (D) Genes identified as being increasingly bound by PABP following Torin1 treatment in endogenous IP experiments conducted previously were investigated through IPs in a FLAG-tagged over-expression system. Conducted in both HeLa(blue) and A549 (red) cell lines. All normalised to HIST1H4H expression; (n=3).

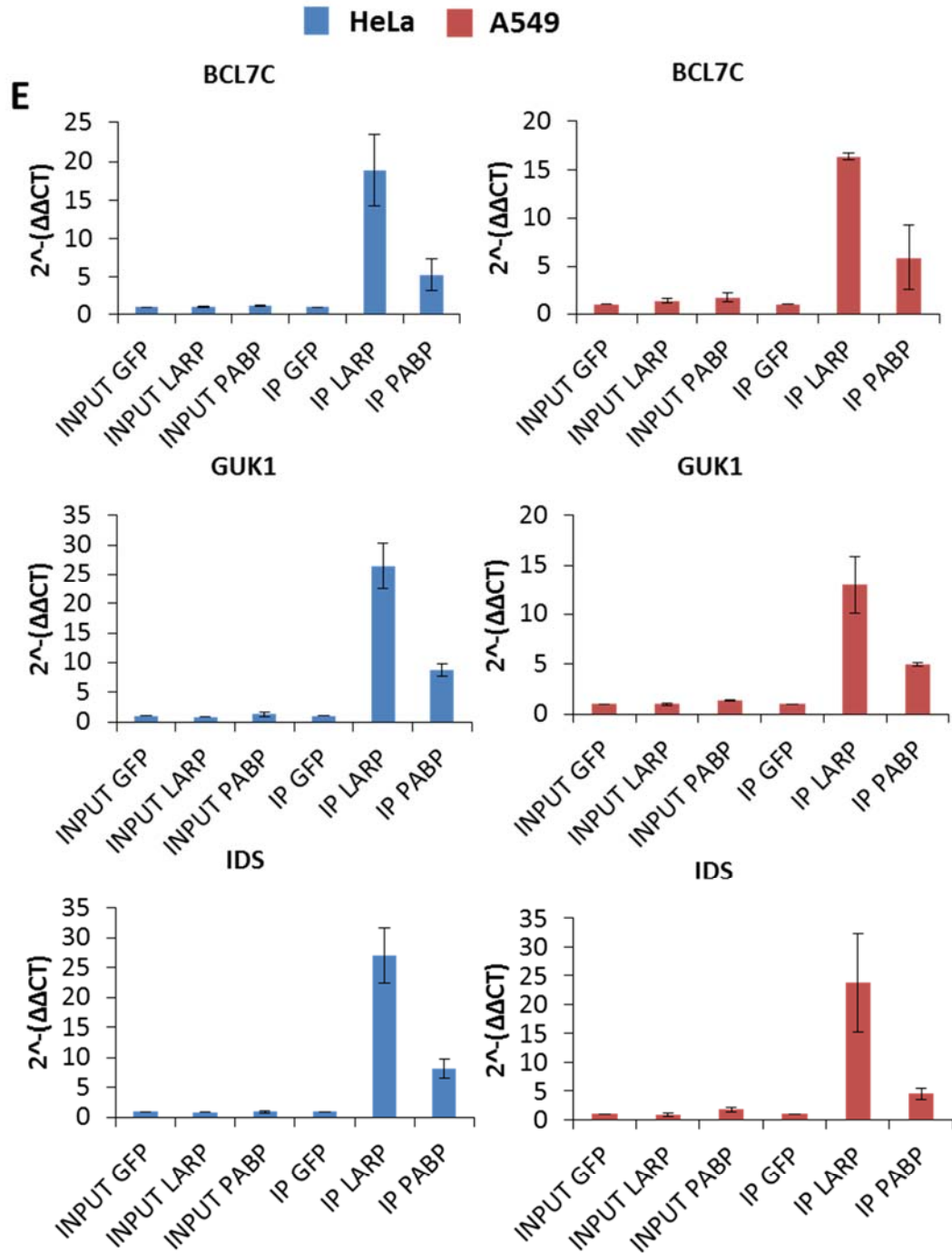


**Figure 5.12 continued – (E)** Genes identified as being bound by both LARP1 and PABP above control, but whose binding remained unchanged following Torin1 treatment in endogenous IP experiments conducted previously were investigated through IPs in a FLAG-tagged over-expression system. Conducted in both HeLa(blue) and A549 (red) cell lines. All normalised to HIST1H4H expression; (n=3).

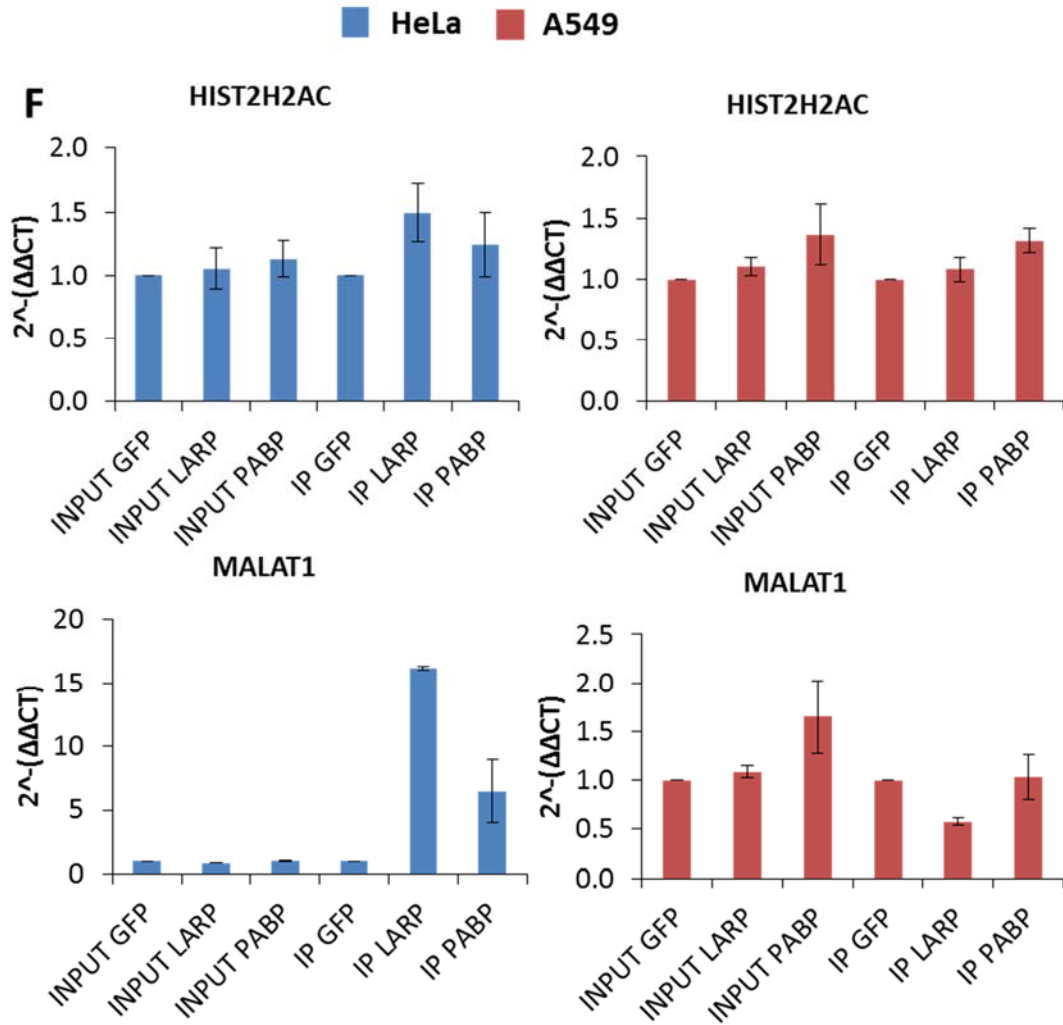


**Figure 5.12 continued** – (F) Genes identified whose binding by both LARP1 and PABP was sufficiently close to background as to be termed “non-bound messages”, both in the presence and absence of LARP1 treatment following endogenous IP experiments conducted previously; qPCR of these genes was investigated following IPs in a FLAG-tagged over-expression system. Conducted in both HeLa (blue) and A549 (red) cell lines. All normalised to HIST1H4H expression; (n=3).

yet appears to be bound and enriched in LARP1 and PABP IP conditions in HeLa cells to a similar extent to some of the other genes investigated, The role of lncRNA in regulation of other transcripts and transport of mRNA may be one hypothesised role for the HeLa-specific enrichment seen here; regardless it would not be a suitable reference gene and is the main differing gene in terms of LARP1 binding behaviour across the two cell types.

#### **5.2.8. Polysome profiling of Torin1 treated A549 cells shows shift off polysomes to sub-polysomal fractions**

As a final step to investigate the effect on messages bound by RBPs downstream of mTOR signalling, polysome profiling of A549 cells in the presence and absence of Torin1 treatment was conducted. The profiles generated, of which a representative example is provided in Figure 5.13, demonstrate that in A549 cells following Torin1 treatment there is a large shift from polysomal to sub-polysomal fractions. This is indicative of a large decrease in translation, as the peaks increase on the left hand side of the trace, it can be interpreted as ribosomes (or poly-ribosomes) become detached from the mRNA as they are no longer actively translated. This corresponds to similar traces generated for HeLa cells treated with Torin1 (data not shown) as well as in the case of LARP1 depletion.

As the gradients were run, 1 ml fractions were collected to represent each interval on the polysome trace. Moving forward, the aim would be to investigate where the mRNA identified from co-IP/gene expression array experiments conducted in our lab previously are distributed with respect to each fraction, and in relation, where LARP1 and PABP proteins were distributed across these fractions also.

#### **5.2.9. Seahorse investigation of LARP1 depleted A549 showed some differences in mitochondrial respiratory reserve capacity following LARP1 depletion**

Several of the mRNA which appeared in the dataset from analysis of gene expression arrays as bound to LARP1 fell under metabolic GO terms; these included some listed in Figure 5.8, such as lactate dehydrogenase A (LDHA) and malate dehydrogenase 2 (MDH2), which were categorised as increasing binding by both LARP1 and PABP following Torin1 treatment. Both of these genes play fairly central roles in metabolism,

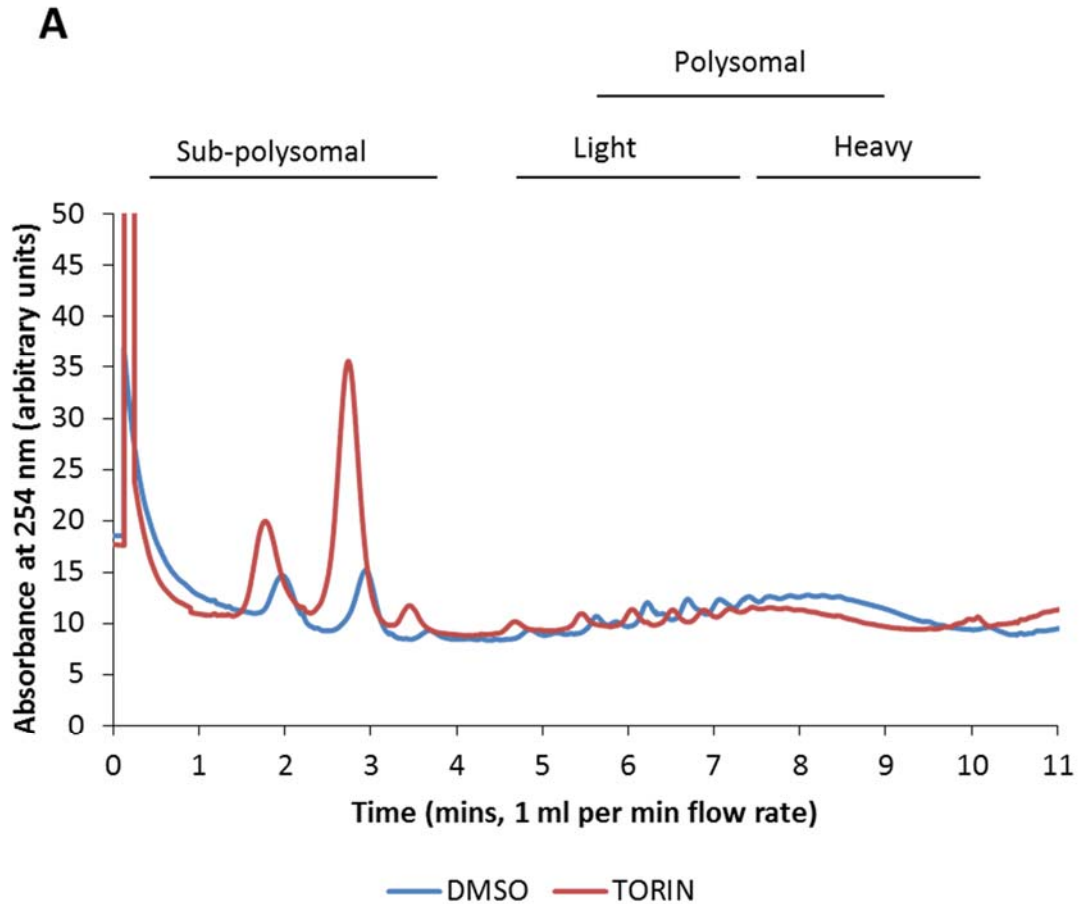


**Figure 5.13 Polysome profile for Torin1 treated A549 cells**

24 hours following plating in a 10cm plate, A549 cells were treated with 200 nM Torin1 as described in materials and methods. Media was supplemented with cycloheximide prior to harvest to “freeze” translating ribosomes on mRNA, before samples were spun on sucrose gradients and separated according to density. (A) Absorbance (correlating with number of bound ribosomes) was measured as fractions were displaced at a rate of 1 ml/min into collection tubes. A shift from polysomal to sub-polysomal fractions relative to control can be seen in Torin1 treated A549.

poised to generate substrates within oxidative phosphorylation or glycolysis pathway which are responsible for the production of ATP within a cell.

Also in the larger, more comprehensive list of mRNAs generated from experiments by Dr Smith (data unpublished) were several genes in the glycolytic and lipid metabolism pathways. It is well known that mTOR signalling plays a part in regulating several metabolic processes, in order to tightly control cell growth (Laplante & Sabatini 2012a; Lamming et al. 2013). It is not known whether part of this regulation may stem from gene expression control via LARP1 binding of metabolic mRNAs downstream of mTOR signalling. In order to determine whether the effect of LARP1 binding of metabolic mRNA has a direct effect on key energy pathways such as the mitochondrial oxidative phosphorylation pathway, or the glycolytic pathway, a series of Seahorse Flux experiments were conducted using LARP1 depleted cells.

Normalisation to total protein content, often reported by previous users of this technology as an optimal method for minimising variability in readings, was deemed inappropriate for this study. It is already established that LARP1 depletion has an effect on global translation, and it is therefore reasonable to predict that for the same seeded cell number, differences between absorbance readings for LARP1 depleted and control transfected cells would be present following this type of normalisation. Therefore in this study crystal violet staining of DNA content was conducted (details described in materials and methods section 2.5.3) and these absorbance readings, taken per well, used for normalisation. Blank readings were taken from crystal violet staining of cell-devoid control wells of the same Seahorse Flux plate.

Representative bioenergetics profiles generated through conducting a traditional mitochondrial stress test in A549 can be seen in Figure 5.14A and 5.14B; sequentially injecting inhibitors of various complexes and processes within the electronic transport chain (ETC) and measuring oxygen consumption rate (OCR) or extracellular acidification rate (ECAR) in real time. There are no significant differences in basal respiration rate between LARP1 depleted and control A549 cells. Initial attempts to conduct these experiments in HeLa cells proved unsuccessful; following LARP1 depletion (as seen in the previous chapter) for greater than 24 hours these cells

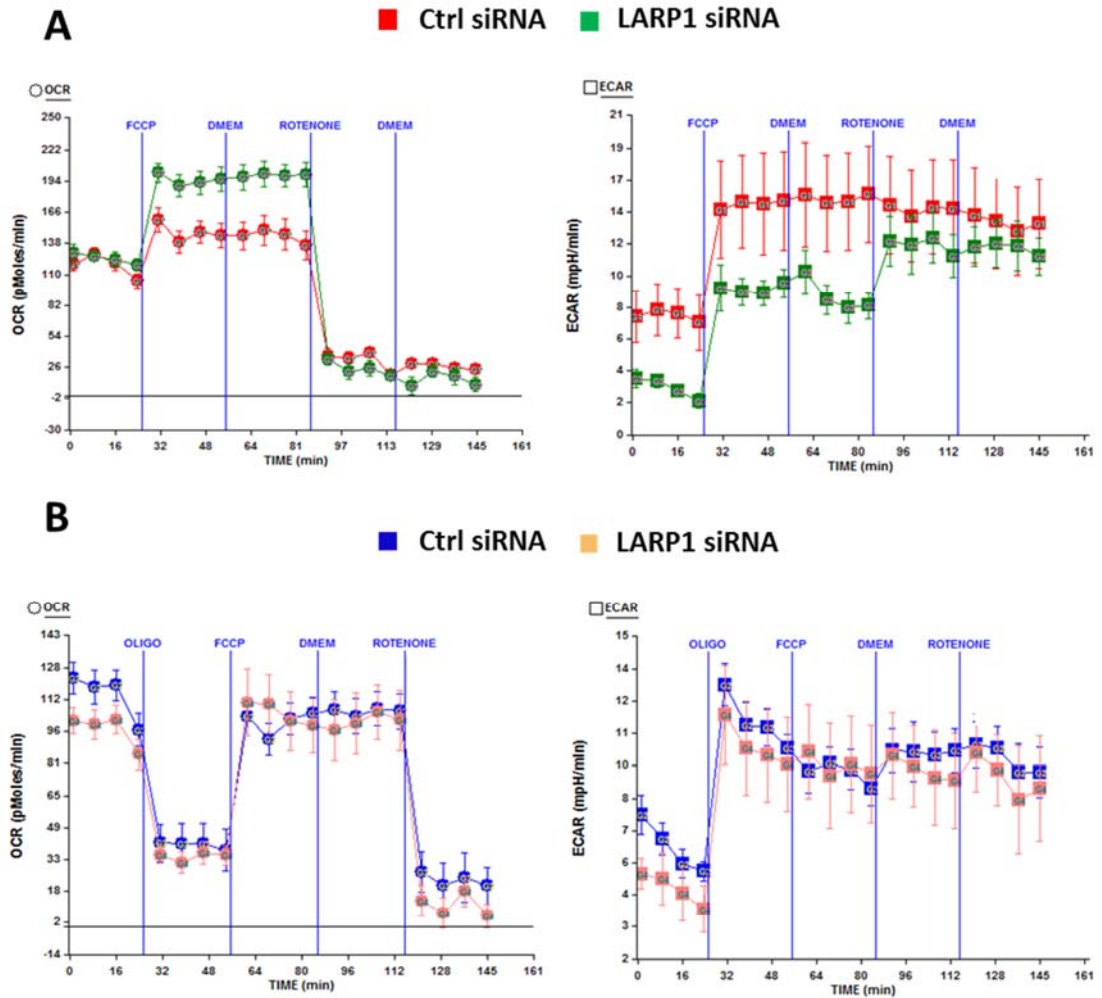


**Figure 5.14 OCR and ECAR in A549 cells during a mitochondrial stress test conducted 48 hours post transfection with LARP1 siRNA** A549 cells were seeded and reverse transfected in 6 well plates as described previously for growth curve experiments. 24 hours following transfection cells were trypsinised, counted and seeded in Seahorse 24 well plates to the same final density, allowing growth under normal culture conditions for a further 24 hours prior to Seahorse analysis as described in materials and methods (A) Representative trace showing OCR (left) and ECAR (right) of A549 following injections of FCCP and rotenone (B) Representative trace showing OCR (left) and ECAR (right) following a first injection of oligomycin, followed by FCCP and rotenone. Wells were normalised for cell number using crystal violet staining as outlined in materials and methods; plots shown here represent normalised experiments.

underwent apoptosis and were unsuitable for Seahorse investigations. However attempting to conduct mitochondrial stress or glycolytic function tests on HeLa cells 24 hours post-transfection yielded no conclusive results, as it was not possible to achieve a robust enough depletion of the LARP1 protein. A549 cells had been shown to survive LARP1 depletion in a way HeLa cells were not able to; therefore the time point of 48 hours was selected as an efficient depletion of LARP1 was seen at this duration post-transfection, but apoptotic initiation did not appear to have begun (see Chapter 4).

Figure 5.14A shows representative traces of A549 cells 48 hours post-transfection with either LARP1 siRNA (green) or a scrambled control siRNA (red). Measurements shown on the left are the OCR for these cells, and on the right ECAR measurements; in both cases these readings are shown normalised to crystal violet absorbance readings from each well. Of particular note, the difference in oxygen consumption between conditions following FCCP injection (injection times and compounds indicated in blue) shows following LARP1 depletion, A549 cells appear to possess an enhanced maximal respiratory capacity; though this respiration was not coupled to the same level of proton production, which was considerably higher (as indicated by ECAR readings) for the control A549 cells. Figure 5.14B shows OCR measurements (left) and ECAR measurements (right) for control (dark blue) and LARP1 depleted cells (orange), following a standard mitochondrial stress test involving a first injection of oligomycin prior to subsequent FCCP and rotenone treatments. Oligomycin is an ATP-synthase inhibitor; its use therefore allows for visualisation of ATP-linked respiration, placing a limit on the electron transport chain productivity by inhibiting its end-point. In the situation where ATP-synthase activity is disrupted before uncoupling of the proton gradient with FCCP, the maximal respiration rate (and also therefore the reserve capacity) of LARP1 depleted cells appears the same as for control cells; they appear to lose their adaptive advantage to mitochondrial stress. ECAR measurements for the same period reveal the proton spike seen following FCCP treatment alone is now not seen following FCCP treatment; it has occurred instead as a consequence of oligomycin treatment. The difference between OCR readings post-oligomycin and post-rotenone indicates a possible portion of energy production is not linked to oxidative

phosphorylation in control transfected cells as their OCR does not drop to the same extent as LARP1 depleted cells; this indicates increased proton leak.

Analysis of specific readings from the OCR profile of four repeats allowed for the calculation and plotting of various parameters (Figure 5.14C) including basal mitochondrial respiration, ATP- production linked respiration, proton leak, maximal respiratory capacity, respiratory reserve capacity and non-mitochondrial respiration. As seen in the representative traces provided, across the four repeats there was a significant difference in maximal respiratory capacity and also subsequently the respiratory reserve capacity of A549; but this effect was only significant in the absence of ATP-synthase inhibition. As mentioned earlier, when quantified there was evidence of significant difference in respiration as a result of proton leak between the two conditions, with LARP1 depleted cells appearing to show greater proton leak than control transfected.

Taken together with the ECAR traces seen in Figure 5.14A and B, this information suggests LARP1 depleted cells may have a higher propensity to “shift” between oxidative phosphorylation and glycolysis in times of stress, whereas control A549 cells may in fact be more heavily reliant on glycolysis and therefore be unable to embrace maximal capacities under mitochondrial stress. Oxidative phosphorylation is more efficient and generates a greater amount of ATP than glycolysis, however glycolysis can be initiated to compensate for sub-optimal conditions or mitochondrial dysfunction where necessary, to become the primary method for energy production. This is believed to be particularly common in cancer cell metabolism, and is referred to as the Warburg effect (Vander Heiden et al. 2009); emerging work suggests that environmental conditions, such as those in culture, may have a profound impact on influencing cells’ primary metabolic pathways. This is discussed in greater detail later in this chapter. It is plausible that the metabolic differences between HeLa cells, which are also well documented as being highly reliant on glycolysis (Xie et al. 2014) could account for the differing response compared to A549 following LARP1 depletion.

C

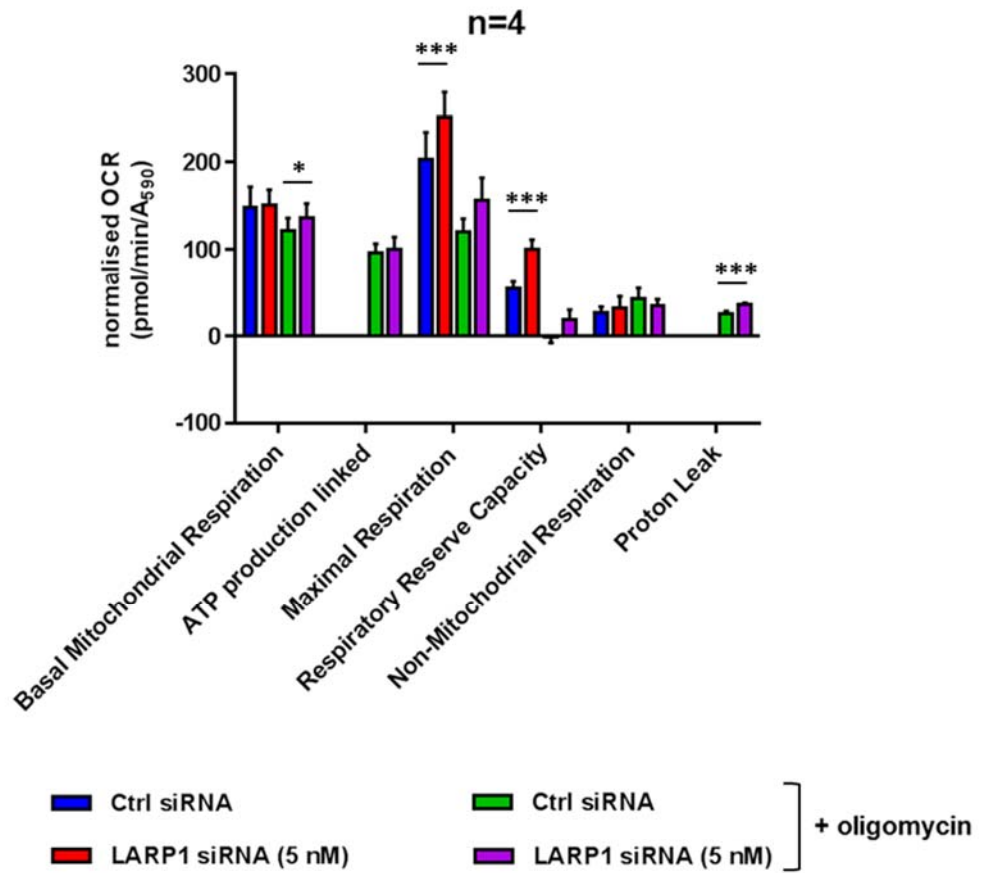


**Figure 5.14 continued** (C) n=4 mitochondrial stress tests allowed for calculation of various parameters for both non-oligomycin and oligomycin treated A549 cells depleted of LARP1. Paired two tailed t-tests were performed between non-oligomycin and oligomycin treated datasets, significance was assigned as follows: \* =  $p < 0.05$ ; \*\* =  $p < 0.01$ ; \*\*\* =  $p < 0.005$

### **5.2.10. Seahorse investigation of glycolytic capacity of LARP1 depleted A549 suggests differential reliance on glycolysis for ATP production**

A key component of extracellular acidification rate (ECAR), a parameter measured by the Seahorse XF24 Flux analyser, is the production of lactate during glycolysis. Lactate exists as a carboxylate anion at physiological pH, such as that of the media during these experiments, resulting in generation of protons and acidification of the media environment (Mookerjee et al. 2015; Xie et al. 2014). Certain cancer cell lines, including HeLa and A549, have been shown to transition from a glycolytic phenotype in high glucose conditions to oxidative phosphorylation under excessive acidification of culture media, such as that seen following production of high levels of lactate (Xie et al. 2014). In an attempt to gain a deeper insight into the relationship between A549 and glycolysis in the presence of LARP1, a test of glycolytic function was carried out. Here, cells began in glucose free DMEM media, before injections of glucose to stimulate glycolysis, oligomycin to uncouple ATP-synthase and disrupt oxidative phosphorylation revealing the full glycolytic capacity and finally 2-DG, a glucose analog to shut down glycolysis and ultimately reduce the cell to death.

Figure 5.15 shows a representative trace of such a glycolytic function test, including ECAR measurements (top panel) and OCR measurements (bottom panel). There is minimal difference in ECAR between the two conditions during glycolysis. From these traces, a few observations can be drawn; upon injection of glucose to the media it can be seen that the initial rate of glycolysis is slightly higher in control A549 cells than in LARP1 depleted cells. This difference is maintained following treatment with oligomycin, indicating that though the maximal glycolytic capacity is greater in control cells relative to LARP1 depleted cells, the glycolytic reserve (the difference between the two peaks) is actually very similar. This suggests the previously mentioned observation following the mitochondrial stress test that the LARP1 cells may be less reliant on glycolysis than control cells, may be correct. However, the exact metabolic profile of A549 with and without LARP1 would need to be investigated in much greater depth, possibly including periods of culture in different media to try to “condition” them to prioritise specific metabolic pathways. This is discussed in greater detail later in the discussion of this chapter.

**A**

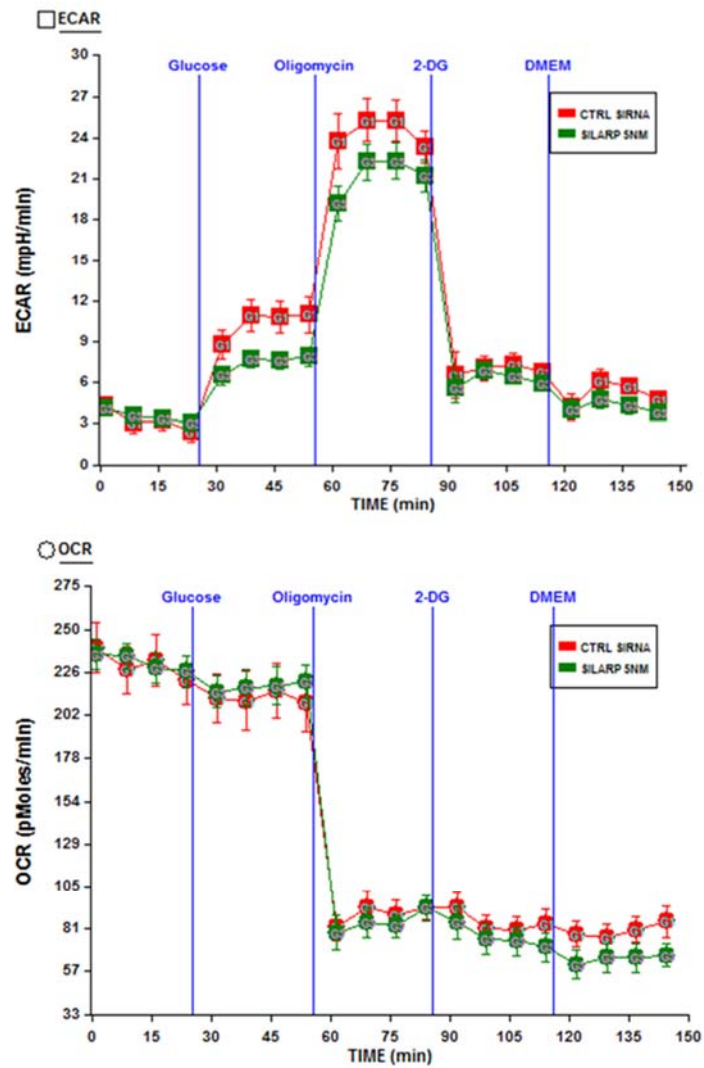


**Figure 5.15 Functionality of glycolytic pathway in A549 cells depleted of LARP1 investigated using Seahorse analyser.** A549 cells were seeded and reverse transfected in 6 well plates as described previously for growth curve experiments. 24 hours following transfection cells were trypsinised, counted and seeded in Seahorse 24 well plates for the same final density, allowing growth under normal culture conditions for a further 24 hours prior to Seahorse analysis as described in materials and methods. (A) Representative trace showing ECAR (top) and OCR (bottom) of A549 following glycolytic stress test using injections of glucose, analog 2-deoxyglucose and oligomycin (n=1). Normalisation for cell number was achieved through crystal violet staining, as described in materials and methods.

### **5.2.11. Lactate dehydrogenase A and Malate dehydrogenase 2 protein levels were unchanged following prolonged LARP1 depletion, despite appearing as potential targets of LARP1 binding in Co-IP/gene expression array experiments**

Another consideration for LARP1 binding of LDHA and MDH2 mRNA was the potential effect on protein level; it is still contested whether LARP1 association with mRNA has a positive or a negative effect on translation of bound transcripts. A key component of extracellular acidification rate (ECAR) is the production of lactate during glycolysis (Xie et al. 2014). Lactate exists as a carboxylate anion at physiological pH, such as that of the media during these experiments, resulting in generation of protons and acidification of the media environment (Mookerjee et al. 2015). Similarly, malate can be charged under physiological pH, which could contribute to the detected proton generation in the Seahorse metabolic flux experiments. LDHA and MDH2 are two genes responsible for the processing of these two metabolites; therefore it is not implausible to consider effects on the translation of these mRNA, possibly as a result of RBP activity, could alter cellular metabolism.

Utilising LARP1 depleted A549 cell samples from depletion growth curves and FACS experiments conducted previously, both LDHA and MDH2 proteins levels were investigated by western blotting (Figure 5.16). In both cases, these westerns showed that there was no discernible effect of LARP1 depletion on either of these two genes' protein levels, despite having been identified as targets of LARP1 RBP activity. This suggests that the proton production detected in Seahorse experiments following treatment with FCCP is likely not attributed to increased concentrations of either of these two metabolites as a consequence of increased (or decreased) enzyme translation, but may in fact be due to aforementioned increased proton leak in LARP1 depleted cells. This could be investigated further using various assays for lactate, malate and other charged metabolites' production.

### **5.3. Discussion**

In this chapter, through co-IP experiments we have confirmed that LARP1 and PABP interact both in the presence and absence of RNA, supporting data already available in the literature (Fonseca et al. 2015). Furthermore, using these techniques we have

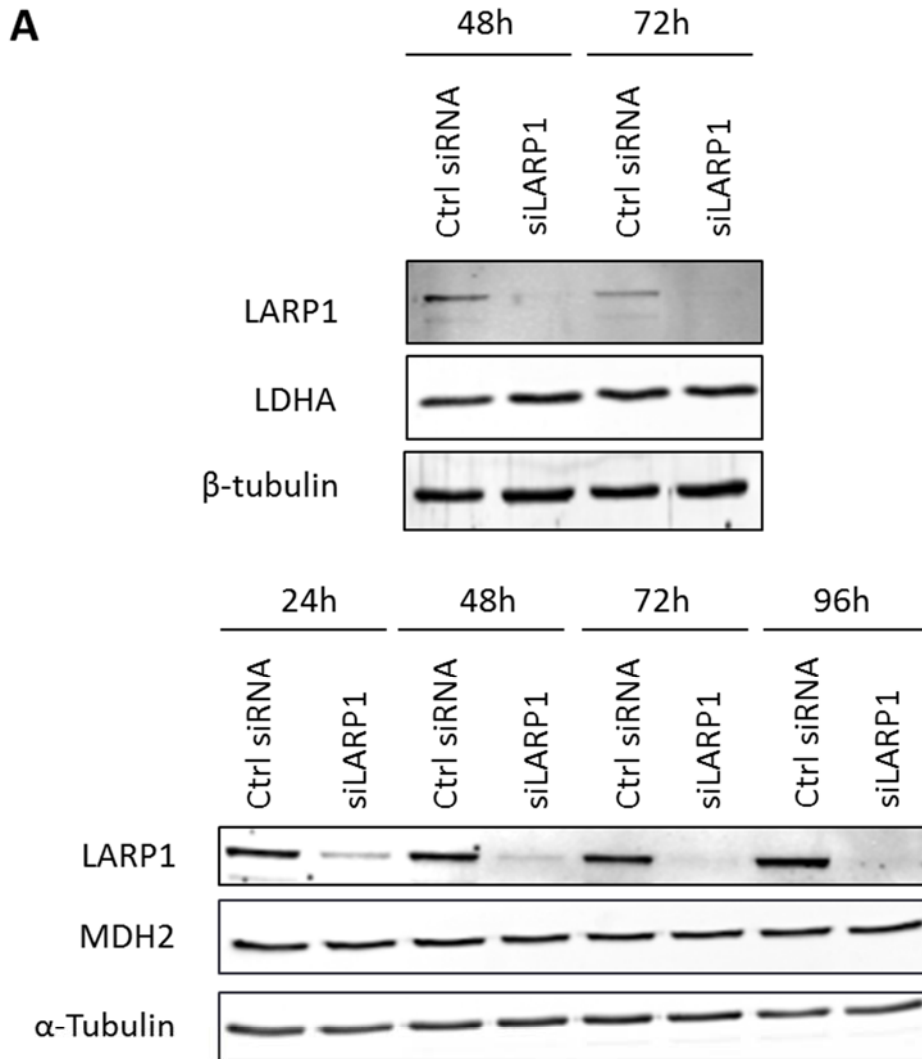


**Figure 5.16 Investigation of LDHA and MDH2 protein levels, two gene targets of LARP1 RBP activity.** Samples harvested from previously conducted growth curve experiments in LARP1 depleted A549 cells were normalised for protein using a Bradford assay and subjected to western blotting. Using appropriate antibodies against LARP1, LDHA and MDH2 protein levels were detected. In each case either  $\beta$ -tubulin or  $\alpha$ -tubulin were used as loading controls.

pulled down mRNA bound to each of these two overexpressed proteins, and used these samples to validate a list of genes identified as being subject to LARP1 and PABP RBP activity in HeLa cells within our lab (Smith, unpublished data, summary in Figure 5.8). A preliminary examination of total mRNA abundance of these messages relative to a control siRNA transfected, control treated sample in A549 cells showed a lower abundance in LARP1 and PABP depleted cells. As mentioned previously, investigations of the mRNA abundance in A549 (n=1) could be helped further through examination of the effects on the global RNA pool in these cells; such information could be gleaned from inclusion of 18S and 28S rRNA qPCR data in these samples. Another possible consideration could be the use of a non-coding RNA or histone RNA as a control gene; their relative stability in spite of global translational changes could provide a control gene for  $\Delta\Delta\text{CT}$  normalisations.

Polysomal profiling of A549 cells following Torin1 treatment clearly demonstrated the negative effect on translation, with a shift from polysomal messages to sub-polysomal fractions. Along with the strong correlation seen in data from an endogenous IP of LARP1 and PABP in the presence and absence of Torin1 treatment, this suggests a possible role for the joint modulation of message expression through binding by both proteins. However these analyses also revealed a differential in binding between LARP1 and PABP IPs in the presence of Torin1 treatment, indicating a possible role for LARP1 and PABP independently of each other in response to mTOR inhibition. This is particularly interesting given that connections have been realised to some extent between mTOR signalling, LARP1 and 5' TOP mRNA expression control. The next steps would be to approach the question of where LARP1 and PABP are distributed within these fractions, and secondly the relative localisation of the mRNAs they have both, or individually, been shown to bind.

Of the list generated following endogenous IP and gene expression array experiments (Smith, unpublished data) it was noticed that several genes whose binding by LARP1 and PABP increased following Torin1 treatment were related to GO terms for various aspects of metabolism. Among these were genes such as LDHA and MDH2, two key genes in the pathways involved in ATP synthesis via the tricarboxylic acid cycle and oxidative phosphorylation. This led to investigations of the effect of LARP1 depletion in

metabolic function; namely use of the Seahorse analyser to investigate effects on key energy production pathways; the oxidative phosphorylation pathway of mitochondria and the glycolytic pathway of the cytosol. From these experiments it was indicated that LARP1 depletion resulted in a differential reliance on glycolysis, and perhaps possessed a greater capability to “switch” from oxidative phosphorylation to glycolysis when required. In particular in these experiments it was noted that upon treatment with the protonophore FCCP a marked difference in the maximal respiration rate, or respiratory reserve, was recorded. In addition, where ATP-production linked oxygen consumption was inhibited using oligomycin, there was a significant difference in proton-leak between conditions; in addition ECAR measurements at this point indicated high proton production. This spike in extracellular acidification could potentially have been as a result of increased production of anions such as lactate; potentially correlating with the increased binding of these genes (should it result in a change in protein level of the relevant enzymes LDHA and MDH2). However no change in protein levels of either of the two genes selected for investigation was detected following LARP1 depletion in A549 cells.

Differences in glycolytic profiles following Seahorse glycolytic stress test were relatively inconclusive, though there was a mild difference in the extracellular acidification rate following glucose injection; possibly supporting the previous observation of an increased reliance of control transfected cells on glycolysis over oxidative phosphorylation for energy production; though this could be investigated in greater depth. Emerging work has suggested that much can be learnt about cell metabolism through investigation of metabolic function following culture in different media; often comparing a high glucose media with a contrasting galactose media (Dott et al. 2014). Cells cultured in high glucose media are able to adapt to mitochondrial dysfunction through use of glycolysis as the main source of ATP generation, rather than use of oxidative phosphorylation. However growth in galactose alone forces the use of the oxidative phosphorylation pathway to generate energy; this can make them significantly more sensitive to mitochondrial insults (Marroquin et al. 2007), and highlight any underlying mitochondrial impairment (Aguer et al. 2011). As such, conducting the functionality tests shown in our study using cells in different media

could provide some answers regarding the LARP1-depletion sensitivity of HeLa over A549; if A549 basal metabolism allows for this cell line to adapt to LARP1 depletion in a way that HeLa cannot for example, this may explain the difference seen previously between the two lines' apoptotic response.

Here, we have established a partial overlap between LARP1 and PABP bound RNAs and are further analysing how mTOR inhibition affects messages that are bound to LARP1 and PABP, LARP1 alone or PABP alone. Many questions remain outstanding in the field of LARP1-mediated gene expression regulation, and whether or how this regulation relates to 5' TOP mRNAs, which will be discussed in greater detail in the final summary of this work.

## **Chapter 6**

## 6. Final Discussion

This study had three key aims; firstly to identify and validate RNA binding proteins whose binding activity was changed following mTOR inhibition, secondly to characterise a selection of these proteins in depletion studies to screen for phenotypes caused by their absence, and finally to determine which mRNA these proteins bound and potentially regulated.

The first of these aims was approached using a novel technique for capture of whole cell RBP interactomes in vitro; the oligo(dT)<sub>25</sub> affinity isolation of poly(A) RNAs crosslinked to interacting RBPs (Castello, Horos, et al. 2013). This protocol was adapted to include treatment with Torin1, an mTOR inhibitor, so as to specifically identify differential RBP binding activity downstream of mTOR signalling. Torin1 is an ATP-competitive specific inhibitor of mTORC1 and mTORC2; its use was at concentrations far below the IC<sub>50</sub> for other kinases, thereby having no off target effects on their activities (Thoreen et al. 2009). mTOR signalling can become dysregulated in a variety of human diseases, including cancer, and so the clinical relevance of these inhibitors is evident. From a toxicological perspective, use of these types of kinase inhibitors in clinical trials produces a range of adverse side effects in the treatment of these conditions, as outlined in section 1.4.8. The control of mTOR substrates and downstream effectors, including RNA binding proteins, over post-transcriptional control of gene expression alludes to their potential to play a part in some of these side effects, and a better understanding of their role in the context of translational control has likely implications for clinical outcomes.

The technique of whole cell RBP capture was developed with the aim of expanding the knowledge of RBP repertoires in different cell types and following different stimuli; however this study commenced before any such works were published. During the progression of this work, several publications have been produced having implemented this technique in various cell types, including HeLa, HEK293 and Huh-7 human cell lines, as well as in *S. cerevisiae* (Castello et al. 2012; Baltz et al. 2012; Beckmann et al. 2015). These studies have revealed the previously unappreciated expanse of proteins possessing RBP activity, including proteins containing non-

canonical RNA binding domains and previously not known to possess any RNA metabolism functionalities. The mass spectrometry data from our current study requires a quantitative comparative analysis. The decision on how to approach the data analysis of such a novel dataset posed a significant challenge, due to the absence of a “gold-standard” accepted methodology as exists for other large data set types (e.g. next generation sequencing).

The execution of label-free mass spectrometry following an affinity isolation experiment in this way introduces significant variation, as shown in our data analysis for batch effects. Normalisation internally to a spike-in reference protein permits a semi-quantitative measurement of relative amounts of protein in each technical replicate, though it fails to remove batch effects; normalisation across biological repeats however did not seem achievable. Ultimately, the data was adjusted for batch effects to minimise inter-experiment variation and ensure that differences between treated and untreated conditions were not lost, before triplicates were subjected to paired t testing with multiple corrections using the Benjamini-Hochberg method; all of this was carried out in the R analysis environment using readily available packages. Other proteomics studies have utilised R packages originally designed for RNA sequencing and array analysis, such as “DESeq” (Anders & Huber 2010; Kuharev et al. 2015); furthermore, packages tailored specifically to large proteomic data sets also, including “R for Proteomics” (Gatto & Christoforou 2014) have become available in the time of this study. These provide two examples of alternative methods from those used here for data analysis following whole cell RBP capture following cell treatment. Whilst R is a remarkably useful environment for handling of large datasets, its unique language requires a strong knowledge and experience beyond the immediate scope of this user.

Despite the limitations and challenges of data analysis following the use of this method, the top hits of RBPs did correlate with what one may have expected following inhibition of mTOR signalling (and therefore inhibition of global translation); several proteins of the small ribosomal subunit and RNA helicases were identified as decreasing binding. Western blot validation of selected proteins identified from this list was successful; 4 proteins were validated clearly and carried forward for further

investigation. Some proteins were harder to validate in this way, including USP10, which was difficult to detect in various repeats using available antibodies. It is possible that the reduction in experimental scale in comparison to original papers using this technique, performed to allow for multiple samples to be processed simultaneously, may have resulted not only in increased difficulty of detection during mass spectrometry, but also of validation later by western blotting. Increasing depth could therefore reduce variation in mass spectrometry, potentially increase the number of proteins detected, and also yield more material for validation of less abundant proteins.

Following validation of SERBP1, PWP2, TRIM25 and LARP1 binding changes following mTOR inhibition, these proteins were depleted one at a time in HeLa cells to screen for notable phenotypic, growth and survival impact. A combination of growth curves, visual comparisons of morphology, FACS analysis of both live (apoptosis) and fixed (cell cycle) cells were implemented in each case, ultimately revealing SERBP1 and TRIM25 depletions to have very modest effects on cell proliferation compared to PWP2 or LARP1 depletion, with no significant increase of apoptosis or change in cell cycle distribution. Though depletion of PWP2 caused a notable depression in cellular proliferation, it did not appear to initiate any effects in terms of apoptotic initiation or autophagy (to which it had been connected in zebrafish, (Boglev et al. 2013)). Its highly conserved function in pre-rRNA processing however could explain this reduction in growth rate; disruption of rRNA synthesis would have impacted ribosome biogenesis and placed the cells under a high-stress, low translation rate status.

TRIM25 has been identified as an RBP shown to be preferentially expressed in mouse embryonic stem cells (Kwon et al. 2013); though no function with respect to RNA biology directly had been reported. As mentioned previously in this study, TRIM25 is a member of the TRIM family of E3 ubiquitin ligases, a family involved in several processes including differentiation and proliferation (Hatakeyama 2011). TRIM25 in particular has been shown to play a role in cancer progression and involvement in the modulation of p53 signalling (Urano et al. 2002). Though no distinct morphological changes were seen here following depletion studies, there was a noted slow in proliferation. This suggests that the increased RNA binding of TRIM25 downstream of

mTOR inhibition may play a role in the post-transcriptional regulation of messages governing cell growth and proliferation; one hypothesis could be that TRIM25 binds senescence associated or growth arrest mRNAs, and in binding them prevents their translation. Another, suggested by Kwon et al. (2013), could be that TRIM25 plays a role in localisation of specific mRNA subsets, for example allowing for their compartmentalisation in stress granules or P-bodies, thereby affecting their stability. The proximity of an E3 ubiquitin ligase with other RBPs when concurrently bound to specific mRNAs may in fact result in the “freeing” of messages otherwise targeted for degradation. Regardless, the role of TRIM25 and other E3 ligases with RBDs in RNA biology could be a very exciting avenue for research into gene expression regulation.

In hindsight, inclusion of <sup>35</sup>S-methionine incorporation measurements or sucrose gradient polysome profiling for each of these four depleted proteins could have provided interesting information regarding the effects of these four proteins on global translation; even more so as mTOR signalling is central to the control of translation and cellular growth. Additionally, investigations of slowed growth rate using FACS analysis of senescence associated β-gal activity to investigate activation of senescence may have gleaned more detail regarding the nature of the altered growth rate recorded. The knockdown of these proteins was performed here, conversely the overexpression of these four validated RBPs may also provide some insight into their functions; of the four proteins validated as changing binding here two increased binding and two decreased, implying equilibrium could be disturbed either through increased or decreased expression of these proteins. .

Of the four validated proteins chosen for characterisation, LARP1 depletion provided the most resounding response in HeLa cells, resulting in initiation of apoptosis from 48 hours post-transfection. From FACS analysis of cell cycle distribution it appeared apoptosis was occurring between the M phase/G1 phase transitions, as the only notable decrease in cell percentage was in G1 phase. Without synchronisation and release of cell cycle it would be difficult to tell whether this is definitely the case; however the effect of LARP1 depletion on cell viability as early as is seen in HeLa cells could make these types of studies difficult. A review by Stavraka & Blagden (2015) discussed how the ultimate outcome of LARP1 depletion appeared to have a

correlation with cell p53 status; certain cells, including A549 cells, have been documented to experience cell cycle arrest in lieu of apoptosis. LARP1 is an emerging protein of interest in the mTOR/5' TOP mRNA regulation axis; given the fact that LARP1 depletion induces apoptosis, it was appealing to look at LARP1 depletion in cells lines that are less susceptible to apoptosis to gain insight into its functions.

In the context of post-transcriptional gene regulation, LARP1 has a potentially crucial binding partner in PABP. These two proteins have been shown to interact both in the presence and absence of RNA (Fonseca et al. 2015; Tcherkezian et al. 2014), introducing an interesting caveat: is it possible that LARP1 interacts with different mRNAs in a PABP-dependent and PABP-independent manner? Future work therefore would include the depletion of LARP1 and the immunoprecipitation of PABP, and vice versa, in order to determine whether transcript specific regulation is mediated by LARP1 alone for certain messages and what these messages encode.

Endogenous IPs of LARP1 and PABP were conducted in the lab by Dr E. Smith as a collaborative aspect of this project; these experiments provided a large dataset of mRNA enriched in LARP1 or PABP bound conditions, some of whose extent of enrichment changed in the presence of Torin1 treatment. Overexpression IPs of FLAG-LARP1 and FLAG-PABP subsequently allowed validation of some of these enrichments, though no effect of Torin1 treatment was investigated in combination. Regardless, the majority of mRNAs identified as having enriched binding by LARP1 or PABP in the original endogenous IP experiment did validate, across both HeLa and A549 cell lines. This suggests the mRNAs bound to LARP1 are not cell-type specific, though this cannot necessarily be true of differentiating cells, which is beyond the scope of this study.

Several of the mRNAs identified as enriched LARP1 and PABP binding included those possessing GO terms related to metabolism, including (but by no means limited to ) lactate dehydrogenase, malate dehydrogenase, several cytochrome complex subunits of the electron transport chain and certain genes related to lipid metabolism. mTOR has well characterised roles in regulation of metabolism, and is a central to pathways responsible for sensing growth factor and nutrient availability; therefore these mRNAs are especially encouraging to see as part of this dataset. Preliminary investigations

regarding their effect on metabolism in LARP1 depleted A549 cells has not yielded conclusive results but has hinted at a potential difference in A549 reliability on glycolysis as its main source of energy synthesis. The importance of metabolic profiling of cell lines in various culture media compositions (e.g. high glucose versus galactose) and conditions (normoxia, hypoxia) has been stressed by several groups recently; though this would potentially have been another future area of investigation sadly due to time constraints it was not possible during this study. The elevated extracellular acidification rate seen in A549 following LARP1 depletion could be as a result of lactate production; this could be investigated using assays designed to detect this substrate in media of cultured cells. Previous work has also shown that lactate produced as a consequence of glucose starvation in A549 cells was able to increase survival of these cells in a concentration dependent manner (Huang et al. 2015); this response was shown to be mediated at least in part by activation of mTOR signalling. Therefore a connection has been drawn between this metabolic effect and mTOR, and also with LARP1 depletion in our study. However unanswered questions remain regarding the nature of the role of LARP1 in modulation of this metabolic response with respect to mTOR signalling specifically, or whether it is directly responsible for the improved survival of A549 cells in comparison to HeLa cells.

Taken together, our data suggests a role for LARP1 as an RBP responsible for gene expression regulation downstream of mTOR, potentially of both TOP mRNAs and non-TOP messages. The link between mTOR and TOP mRNA translation remains elusive; it is possible that LARP1 could be the missing intermediary factor, though much work remains to solve this mystery, including elucidation of RNA binding regions, and the exact mechanism and the nature of influence LARP1 exerts over gene expression control, which remains in contention (Blagden et al. 2009; Fonseca et al. 2015). A very recent work by (Castello, Fischer, et al. 2016; Castello, Horos, et al. 2016) has set about mapping peptides within RBDs of RNA binding proteins identified through interactome capture, through the use of mass spectrometry identification following cleavage using LysC or ArgC proteases. This study has shown amino acid enrichment in RBD surfaces, including glycine, arginine and tyrosine, often found in RGG boxes or disordered domains and substitution of which have been shown to affect RNA binding in some

cases (Phan et al. 2011). Furthermore, this study identified 7 peptide sequences in LARP1 which represent putative RNA binding domains; among these are one relating to a portion of the eIF4G-like domain at the N-terminal end of the protein (which correlates with findings LARP1 competes with eIF4G, (Thoreen et al. 2012)), and two which correspond to regions of the triple DM15 repeats (Castello, Fischer, et al. 2016; Fonseca et al. 2015). The DM15 region within LARP1 has as yet no confirmed function, though evidence has suggested it may be the site of RNA interaction in a concentration dependent manner (Lahr et al. 2015). In addition, (Tcherkezian et al. 2014) showed its mutation or deletion to decrease PABP, eIF4G and 5' cap association. The discovery through RBD mapping that two regions of DM15 repeats, within DM15B and DM15C, provides further support for the hypothesis that this region is responsible for RNA binding in LARP1 (Castello, Fischer, et al. 2016; Lahr et al. 2015).

Recent unpublished data presented by Lahr et al. (LARP society conference 2016) showed a resolved structure of LARP1 binding 5' UTRs of TOP mRNAs. This supports data shown by (Fonseca et al. 2015) which indicated LARP1 binds 5' UTRs of certain TOP mRNAs, repressing their translation yet also increasing stability of these messages. From these finding and those in this study, a model could be proposed through which mTOR activation leads to phosphorylation of LARP1 (Hsieh et al. 2012; Thoreen et al. 2012), either directly or through S6K, thereby interfering with its association with the 5' UTR of mRNAs and allowing for binding of initiation factors to allow for translation of these genes. Upon mTOR inactivation, such as that in our RBP capture experiments, an increase of LARP1 binding occurs; likely at 5' UTRs as indicated by unpublished data (Lahr et al., LARP society conference 2016), displacing eIF4G through competition and preventing translation (Thoreen et al. 2012; Fonseca et al. 2015). However, LARP1 interaction with PABP in conditions of mTOR inactivation may allow for circularisation of these transcripts, preventing de-adenylation and degradation, as when in interaction with eIF4G (Gebauer & Hentze 2004). Furthermore, if LARP1 were to show a preferential binding for the 5' UTR of TOP mRNAs, this may stabilise them and allow them to be "guarded" ready for activation of mTOR signalling, thereby freeing them for translation and increasing proteins required for translation and cellular growth.

The final figure of this thesis showed the polysome profiles of A549 cells in the presence and absence of Torin1 treatment, demonstrating its effect on translation. The next key step to this study would be to determine the abundance of each mRNA identified and validated as having enriched binding in IP experiments previously in each of these fractions of polysome gradients. Alongside this, to determine the distribution of LARP1 and PABP, and how it correlates to the abundances of the mRNAs to which they are bound, and finally to determine whether the LARP1 binding affects the stability of these mRNA, either positively or negatively, following Torin1 treatment. These steps could go some way toward answering outstanding questions regarding the purpose of LARP1 binding, including what effect it has on mRNA stability and translation, whether it specifically targets 5' TOP mRNAs in a different manner to other bound messages, and also whether it is the connection missing between mTOR signalling and 5' TOP mRNA translation regulation.

Upon future development of mTORC2 specific inhibitors, it would be intriguing to distinguish between RBPs changing binding downstream of mTORC1 signalling versus mTORC2 signalling. Growth curve experiments conducted as a parallel using rapamycin treatment and Torin1 treatment at time zero showed the remarkable difference between these two inhibitors (data not shown); rapamycin resulted in a prolonged slowed proliferation rate over 96 hours following treatment, whereas Torin1 treatment resulted in apoptosis of the majority of cells early on following treatment with surviving cells therefore being the only population left for proliferation and counting. However currently there are no specific mTORC2 inhibitors, only those which target mTORC1 (e.g. rapamycin), both mTORC1 and 2 (e.g. Torin1), or dual kinase inhibitors which target both mTOR complexes in conjunction with other kinases, such as PI3K.

In conclusion, the studies presented here have shown how inhibition of mTORC1 and 2 using the selective inhibitor Torin1 influences the binding activity of several RNA binding proteins, including LARP1. There is opportunity for follow-up studies to develop from the initial mass spectrometry dataset; though four RBPs were chosen for validation following statistical analysis, there were several other proteins present on this list which could be potential downstream substrates for mTOR, S6K or other

kinases' signalling. Furthermore, the scope of mTOR mediated RBP networks could be developed through the investigation of RBPs downstream of other stimuli, for example insulin signalling or amino acid deprivation.

The effect of LARP1 depletion varies in different cell lines; this may potentially be connected to p53 status of the cell type involved, though this requires further investigation. Alternatively, this may be connected to a metabolic advantage of some cells over others, dependent on their reliance on glycolysis; again this would require further study involving a variety of culture conditions and comparisons between cell lines. This highlights the importance of understanding the role of inhibitors such as Torin1 as treatments; should LARP1 prove to be a promising target for treatment in conditions including cancers (to which its expression has already shown correlations).

## **Supplemental** **Figures**

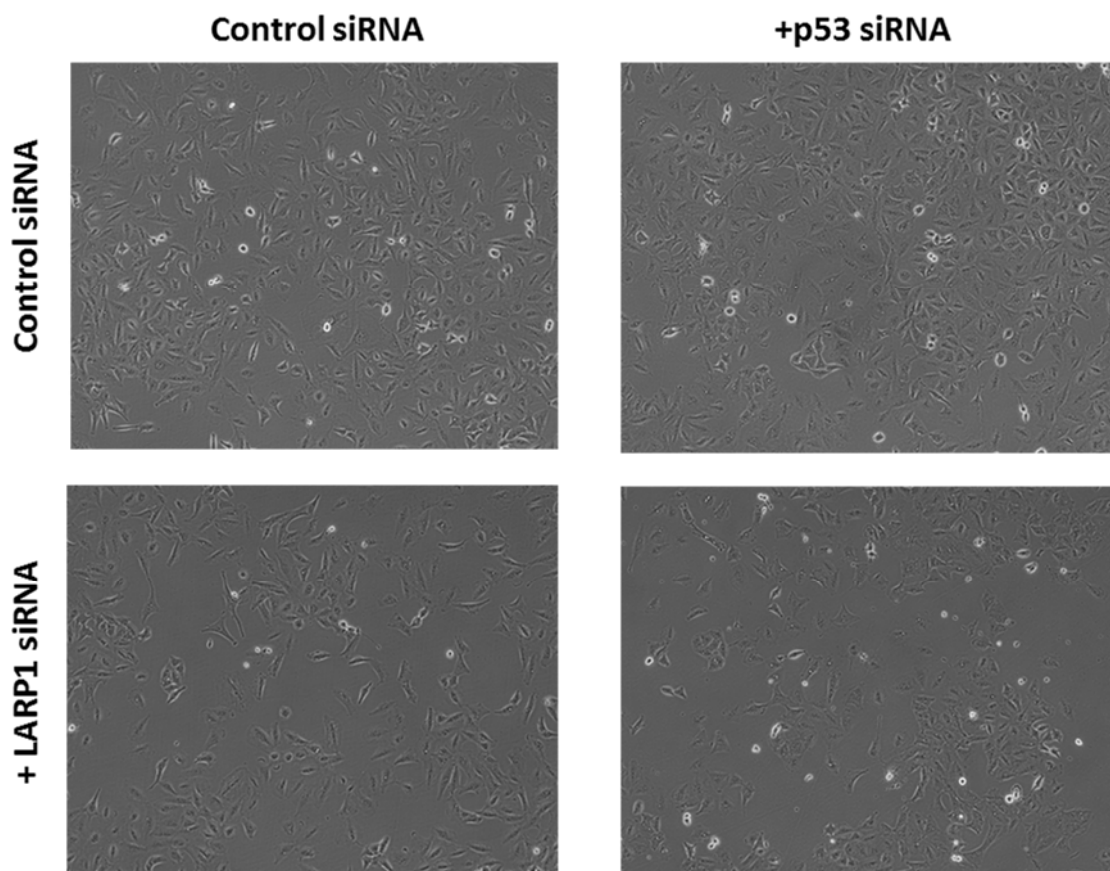
## Supplemental Figure S1. Code for R analysis

```
1. setwd("C:/Users/km219/Documents/R Packages and Projects/DvT
   Rworkup/")
2. library(sva)
3. library(pamr)
4. library(limma)
5. library(devtools)
6. library(ggbiplot)
7. DataTable<-read.table("PART1DvTbce.txt",header=TRUE,row.names=1)
8. DataTableNoNA<-na.omit(DataTable)
9. DataMatrix<-data.matrix(DataTable)
10. DataMatrixNoNA<-data.matrix(DataTableNoNA)
11. DataMatrixLogged<-log2(DataMatrix)
12. DataMatrixNoNALogged<-log2(DataMatrixNoNA)
13. DataTablePheno<-
read.table("PART1DvT_pheno_bce.txt",header=TRUE,row.names=1)
14. mod=model.matrix(~as.factor(Treatment),data=DataTablePheno
)
15. mod0=model.matrix(~1,data=DataTablePheno)
16. mod_1=model.matrix(~as.factor(Treatment)+as.factor(Expt),d
ata=DataTablePheno)
17. mod0_1=model.matrix(~as.factor(Expt),data=DataTablePheno)
18. svobj=sva(DataMatrixNoNALogged,mod,mod0)
19. svobj_1=sva(DataMatrixNoNALogged,mod_1,mod0_1)
20. tDMI<-t(DataMatrixNoNALogged)
21. results_pca_bde<-prcomp(tDMI,scale=TRUE)
22. names<-rownames(tDMI)
23. ggbiplot(results_pca_bde,groups=names,labels=names,var.axe
s=FALSE)
24. pValues=f.pvalue(DataMatrixNoNALogged)
25. pValues=f.pvalue(DataMatrixNoNALogged,mod,mod0)
26. qValues=p.adjust(pValues,method="BH")
27. modSv=cbind(mod,svobj$sv)
28. mod0Sv=cbind(mod0,svobj$sv)
29. pValuesSv=f.pvalue(DataMatrixNoNALogged,modSv,mod0Sv)
30. qValuesSv=p.adjust(pValuesSv,method="BH")
31. write.csv(as.data.frame(qValuesSv),file="Q_Values_sv.txt")
32. fit<-lmFit(DataMatrixNoNALogged,mod)
33. fit<-eBayes(fit)
34. allResultsSv<-
topTable(fit,coef="as.factor(Treatment)TORIN",number=60000)
35. write.csv(as.data.frame(allResultsSv),file="UnpairedResult
s_limma_modSv.txt")
36.
37.
38. ResultsmodSv<-
read.table("UnpairedResults_limma_modSv.txt")
39. ResultsmodSvMatrix<-data.matrix(ResultsmodSv)
40. head(ResultsmodSv)
41. str(ResultsmodSv)
42. write.table(allResultsSv)
43. allResultsSvMatrix<-data.matrix(allResultsSv)
44. colnames(allResultsSv,do.NULL=TRUE,prefix="col")
45. rownames(allResultsSv,do.NULL=TRUE,prefix="row")
46. barplot(allResultsSv$logFC[row=2:21])
47. pValues=f.pvalue(DataMatrixNoNALogged,mod_1,mod0_1)
48. pValues_1=f.pvalue(DataMatrixNoNALogged,mod_1,mod0_1)
49. qValues_1=p.adjust(pValues_1,method="BH")
50. modSv_1=cbind(mod_1,svobj_1$sv)
51. mod0Sv=cbind(mod0_1,svobj_1$sv)
```

```

52.     mod0Sv_1=cbind(mod0_1,svobj_1$sv)
53.     pValuesSv_1=f.pvalue(DataMatrixNoNALogged,modSv_1,mod0Sv_1
)
54.     allResults_2Sv<-
topTable(fit,coef="as.factor(Treatment)TORIN",number=60000)
55.     write.csv(as.data.frame(allResults_2Sv),file="Results_limma_
a_mod_1Sv.txt")
56.     write.table(allResults_2Sv)
57.
58.
59.     colnames(allResults_2Sv,do.NULL=TRUE,prefix="col")
60.     rownames(allResults_2Sv,do.NULL=TRUE,prefix="row")
61.     fit_1<-lmFit(DataMatrixNoNALogged,mod_1)
62.     fit<-eBayes(fit_1)
63.     allResults_2Sv_2<-
topTable(fit,coef="as.factor(Treatment)TORIN",number=60000)
64.     View(allResults_2Sv_2)
65.     write.table(allResults_2Sv_2)
66.     colnames(allResults_2Sv_2,do.NULL=TRUE,prefix="col")
67.     rownames(allResults_2Sv_2,do.NULL=TRUE,prefix="row")
68.     barplot(allResults_2Sv_2$logFC[row=1:22],ylab="logFC",col=
gray.colors(22))
69.     focusdata <- allResults_2Sv_2$rownames
70.
71.
72.     mydata <- read.delim("G:/Vplot att 1.txt", row.names = 1,
stringsAsFactors = FALSE)
73.
74.     smoothScatter(mydata, main = "Volcano plot", xlab =
"Log10(Fold change)", ylab = "-Log10(P-Value)")
75.     abline(v=log10(1.3))
76.     abline(v= -1 * log10(1.3))
77.     abline(h = -log10(0.05))
78.
79.     significant<-mydata[which(mydata$pvalue > -log10(0.05)),]
80.     foldChangeSign<-significant[(significant$logFC >
log10(1.3) | significant$logFC < -1*log10(1.3)),]
81.     folddown <- significant[significant$logFC < -
1*log10(1.3),]
82.     foldup <- significant[significant$logFC > log10(1.3),]
83.
84.     points(folddown, col = "red", pch = 20)
85.     points(foldup, col = "dark green", pch = 20)
86.     points(foldChangeSign, col = "red")
87.
88.write.csv(foldChangeSign, file = "folchange.csv")

```



**Supplemental Figure S2.** Phase contrast microscopy of A549 cells 72 hours post-transfection with indicated siRNA to investigate morphological differences following dual LARP1 and p53 depletion.

## **Bibliography**

## Bibliography

- Aguer, C. et al., 2011. Galactose enhances oxidative metabolism and reveals mitochondrial dysfunction in human primary muscle cells. *PLoS one*, 6(12), p.e28536. Available at: <http://www.pubmedcentral.nih.gov/articlerender.fcgi?artid=3240634&tool=pmc-entrez&rendertype=abstract> [Accessed September 28, 2016].
- Alers, S. et al., 2012. Role of AMPK-mTOR-Ulk1/2 in the regulation of autophagy: cross talk, shortcuts, and feedbacks. *Molecular and cellular biology*, 32(1), pp.2–11. Available at: <http://www.pubmedcentral.nih.gov/articlerender.fcgi?artid=3255710&tool=pmc-entrez&rendertype=abstract> [Accessed September 27, 2016].
- Anantharaman, V., Koonin, E. V & Aravind, L., 2002. Comparative genomics and evolution of proteins involved in RNA metabolism. *Nucleic acids research*, 30(7), pp.1427–64. Available at: <http://www.pubmedcentral.nih.gov/articlerender.fcgi?artid=101826&tool=pmc-entrez&rendertype=abstract> [Accessed September 27, 2016].
- Anders, S. & Huber, W., 2010. Differential expression analysis for sequence count data. *Genome biology*, 11(10), p.R106. Available at: <http://www.pubmedcentral.nih.gov/articlerender.fcgi?artid=3218662&tool=pmc-entrez&rendertype=abstract> [Accessed September 27, 2016].
- Andrei, M.A. et al., 2005. A role for eIF4E and eIF4E-transporter in targeting mRNPs to mammalian processing bodies. *RNA (New York, N.Y.)*, 11(5), pp.717–27. Available at: <http://www.pubmedcentral.nih.gov/articlerender.fcgi?artid=1370757&tool=pmc-entrez&rendertype=abstract> [Accessed September 27, 2016].
- Anger, A.M. et al., 2013. Structures of the human and Drosophila 80S ribosome. *Nature*, 497(7447), pp.80–5. Available at: <http://www.ncbi.nlm.nih.gov/pubmed/23636399> [Accessed September 28, 2016].
- Aoki, K. et al., 2013. LARP1 specifically recognizes the 3' terminus of poly(A) mRNA. *FEBS Letters*, 587(14), pp.2173–2178.
- Baltz, A.G. et al., 2012. The mRNA-Bound Proteome and Its Global Occupancy Profile on Protein-Coding Transcripts. *Molecular Cell*, 46, pp.674–690. Available at: <http://linkinghub.elsevier.com/retrieve/pii/S1097276512004376>.
- Beckmann, B.M. et al., 2015. The RNA-binding proteomes from yeast to man harbour conserved enigmRBPs. *Nature communications*, 6, p.10127. Available at: <http://www.pubmedcentral.nih.gov/articlerender.fcgi?artid=4686815&tool=pmc-entrez&rendertype=abstract> [Accessed September 27, 2016].
- Bernstein, K.A. et al., 2007. Ribosome biogenesis is sensed at the Start cell cycle checkpoint. *Molecular biology of the cell*, 18(3), pp.953–64. Available at: <http://www.pubmedcentral.nih.gov/articlerender.fcgi?artid=1805094&tool=pmc-entrez&rendertype=abstract> [Accessed September 28, 2016].

- Bernstein, K.A. & Baserga, S.J., 2004. The small subunit processome is required for cell cycle progression at G1. *Molecular biology of the cell*, 15(11), pp.5038–46. Available at: <http://www.pubmedcentral.nih.gov/articlerender.fcgi?artid=524768&tool=pmcentrez&rendertype=abstract> [Accessed September 28, 2016].
- Bi, X. & Goss, D.J., 2000. Wheat germ poly(A)-binding protein increases the ATPase and the RNA helicase activity of translation initiation factors eIF4A, eIF4B, and eIF-iso4F. *The Journal of biological chemistry*, 275(23), pp.17740–6. Available at: <http://www.ncbi.nlm.nih.gov/pubmed/10748132> [Accessed September 27, 2016].
- Biamonti, G. & Riva, S., 1994. New insights into the auxiliary domains of eukaryotic RNA binding proteins. *FEBS letters*, 340(1-2), pp.1–8. Available at: <http://www.ncbi.nlm.nih.gov/pubmed/7509757> [Accessed September 27, 2016].
- Blagden, S.P. et al., 2009. Drosophila Larp associates with poly(A)-binding protein and is required for male fertility and syncytial embryo development. *Developmental biology*, 334(1), pp.186–97. Available at: <http://www.ncbi.nlm.nih.gov/pubmed/19631203> [Accessed September 28, 2016].
- Blakeley, P. et al., 2010. Investigating protein isoforms via proteomics: a feasibility study. *Proteomics*, 10(6), pp.1127–40. Available at: <http://www.pubmedcentral.nih.gov/articlerender.fcgi?artid=3708446&tool=pmcentrez&rendertype=abstract> [Accessed September 27, 2016].
- Boglev, Y. et al., 2013. Autophagy Induction Is a Tor- and Tp53-Independent Cell Survival Response in a Zebrafish Model of Disrupted Ribosome Biogenesis. *PLoS Genetics*, 9(2).
- Buchan, J.R. & Parker, R., 2009. Eukaryotic stress granules: the ins and outs of translation. *Molecular cell*, 36(6), pp.932–41. Available at: <http://www.pubmedcentral.nih.gov/articlerender.fcgi?artid=2813218&tool=pmcentrez&rendertype=abstract> [Accessed September 27, 2016].
- Burrows, C. et al., 2010. The RNA binding protein Larp1 regulates cell division, apoptosis and cell migration. *Nucleic Acids Res*, 38(16), pp.5542–5553. Available at: [http://www.ncbi.nlm.nih.gov/entrez/query.fcgi?cmd=Retrieve&db=PubMed&dopt=Citation&list\\_uids=20430826](http://www.ncbi.nlm.nih.gov/entrez/query.fcgi?cmd=Retrieve&db=PubMed&dopt=Citation&list_uids=20430826).
- Butter, F. et al., 2009. Unbiased RNA-protein interaction screen by quantitative proteomics. *Proceedings of the National Academy of Sciences of the United States of America*, 106(26), pp.10626–31. Available at: <http://www.pubmedcentral.nih.gov/articlerender.fcgi?artid=2697111&tool=pmcentrez&rendertype=abstract> [Accessed September 27, 2016].
- Carracedo, A., Baselga, J. & Pandolfi, P.P., 2008. Deconstructing feedback-signaling networks to improve anticancer therapy with mTORC1 inhibitors. *Cell cycle (Georgetown, Tex.)*, 7(24), pp.3805–9. Available at: <http://www.pubmedcentral.nih.gov/articlerender.fcgi?artid=3130531&tool=pmcentrez&rendertype=abstract>

- entrez&rendertype=abstract [Accessed September 27, 2016].
- Castello, A., Fischer, B., et al., 2016. Comprehensive Identification of RNA-Binding Domains in Human Cells. *Molecular cell*, 63(4), pp.696–710. Available at: <http://www.pubmedcentral.nih.gov/articlerender.fcgi?artid=5003815&tool=pmcentrez&rendertype=abstract> [Accessed September 27, 2016].
- Castello, A., Horos, R., et al., 2016. Comprehensive Identification of RNA-Binding Proteins by RNA Interactome Capture. *Methods in molecular biology (Clifton, N.J.)*, 1358, pp.131–9. Available at: <http://www.ncbi.nlm.nih.gov/pubmed/26463381> [Accessed September 28, 2016].
- Castello, A. et al., 2012. Insights into RNA Biology from an Atlas of Mammalian mRNA-Binding Proteins. *Cell*, 149(6), pp.1393–1406. Available at: <http://dx.doi.org/10.1016/j.cell.2012.04.031>.
- Castello, A., Fischer, B., et al., 2013. RNA-binding proteins in Mendelian disease. *Trends in genetics : TIG*, 29(5), pp.318–27. Available at: <http://www.ncbi.nlm.nih.gov/pubmed/23415593>.
- Castello, A., Horos, R., et al., 2013. System-wide identification of RNA-binding proteins by interactome capture. *Nature protocols*, 8(3), pp.491–500. Available at: <http://www.ncbi.nlm.nih.gov/pubmed/23411631> [Accessed September 28, 2016].
- Chakraborty, A., Uechi, T. & Kenmochi, N., Guarding the “translation apparatus”: defective ribosome biogenesis and the p53 signaling pathway. *Wiley interdisciplinary reviews. RNA*, 2(4), pp.507–22. Available at: <http://www.ncbi.nlm.nih.gov/pubmed/21957040> [Accessed September 28, 2016].
- Chaudhuri, J., Chowdhury, D. & Maitra, U., 1999. Distinct functions of eukaryotic translation initiation factors eIF1A and eIF3 in the formation of the 40 S ribosomal preinitiation complex. *The Journal of biological chemistry*, 274(25), pp.17975–80. Available at: <http://www.ncbi.nlm.nih.gov/pubmed/10364246> [Accessed September 27, 2016].
- Chauvin, C. et al., 2014. Ribosomal protein S6 kinase activity controls the ribosome biogenesis transcriptional program. *Oncogene*, 33(4), pp.474–83. Available at: <http://www.ncbi.nlm.nih.gov/pubmed/23318442>.
- Chehab, N.H. et al., 1999. Phosphorylation of Ser-20 mediates stabilization of human p53 in response to DNA damage. *Proceedings of the National Academy of Sciences of the United States of America*, 96(24), pp.13777–82. Available at: <http://www.pubmedcentral.nih.gov/articlerender.fcgi?artid=24141&tool=pmcentrez&rendertype=abstract> [Accessed September 28, 2016].
- Chen, J. et al., 1995. Identification of an 11-kDa FKBP12-rapamycin-binding domain within the 289-kDa FKBP12-rapamycin-associated protein and characterization of a critical serine residue. *Proceedings of the National Academy of Sciences of the United States of America*, 92(11), pp.4947–51. Available at: <http://www.pubmedcentral.nih.gov/articlerender.fcgi?artid=41824&tool=pmcentrez&rendertype=abstract>

- rez&rendertype=abstract [Accessed September 27, 2016].
- Ciganda, M. & Williams, N., Eukaryotic 5S rRNA biogenesis. *Wiley interdisciplinary reviews. RNA*, 2(4), pp.523–33. Available at: <http://www.pubmedcentral.nih.gov/articlerender.fcgi?artid=3278907&tool=pmc-entrez&rendertype=abstract> [Accessed September 27, 2016].
- Coffer, P.J. & Woodgett, J.R., 1994. Differential subcellular localisation of two isoforms of p70 S6 protein kinase. *Biochemical and biophysical research communications*, 198(2), pp.780–6. Available at: <http://www.ncbi.nlm.nih.gov/pubmed/8297390> [Accessed September 27, 2016].
- Coller, J.M., Gray, N.K. & Wickens, M.P., 1998. mRNA stabilization by poly(A) binding protein is independent of poly(A) and requires translation. *Genes & development*, 12(20), pp.3226–35. Available at: <http://www.pubmedcentral.nih.gov/articlerender.fcgi?artid=317214&tool=pmc-entrez&rendertype=abstract> [Accessed September 28, 2016].
- Cosson, B. et al., 2002. Poly(A)-binding protein and eRF3 are associated in vivo in human and Xenopus cells. *Biology of the cell / under the auspices of the European Cell Biology Organization*, 94(4-5), pp.205–16. Available at: <http://www.ncbi.nlm.nih.gov/pubmed/12489690> [Accessed September 27, 2016].
- Costa, F.C. et al., 2014. Ki-1/57 and CGI-55 ectopic expression impact cellular pathways involved in proliferation and stress response regulation. *Biochimica et biophysica acta*, 1843(12), pp.2944–56. Available at: <http://www.ncbi.nlm.nih.gov/pubmed/25205453> [Accessed September 28, 2016].
- Damgaard, C.K. & Lykke-Andersen, J., 2011. Translational coregulation of 5'TOP mRNAs by TIA-1 and TIAR. *Genes & development*, 25(19), pp.2057–68. Available at: <http://www.pubmedcentral.nih.gov/articlerender.fcgi?artid=3197204&tool=pmc-entrez&rendertype=abstract> [Accessed September 27, 2016].
- Darnell, R.B., 2010. RNA regulation in neurologic disease and cancer. *Cancer research and treatment : official journal of Korean Cancer Association*, 42(3), pp.125–9. Available at: <http://www.pubmedcentral.nih.gov/articlerender.fcgi?artid=2953774&tool=pmc-entrez&rendertype=abstract> [Accessed September 27, 2016].
- Decker, C.J. & Parker, R., 2012. P-bodies and stress granules: possible roles in the control of translation and mRNA degradation. *Cold Spring Harbor perspectives in biology*, 4(9), p.a012286. Available at: <http://www.pubmedcentral.nih.gov/articlerender.fcgi?artid=3428773&tool=pmc-entrez&rendertype=abstract> [Accessed September 28, 2016].
- Dember, L.M. et al., 1996. Individual RNA recognition motifs of TIA-1 and TIAR have different RNA binding specificities. *The Journal of biological chemistry*, 271(5), pp.2783–8. Available at: <http://www.ncbi.nlm.nih.gov/pubmed/8576255> [Accessed September 27, 2016].

- Deo, R.C. et al., 1999. Recognition of polyadenylate RNA by the poly(A)-binding protein. *Cell*, 98(6), pp.835–45. Available at: <http://www.ncbi.nlm.nih.gov/pubmed/10499800> [Accessed September 27, 2016].
- Devlin, E.E. et al., 2010. A transgenic mouse model demonstrates a dominant negative effect of a point mutation in the RPS19 gene associated with Diamond-Blackfan anemia. *Blood*, 116(15), pp.2826–35. Available at: <http://www.pubmedcentral.nih.gov/articlerender.fcgi?artid=2974590&tool=pmc&rendertype=abstract> [Accessed September 27, 2016].
- Dorrello, N.V. et al., 2006. S6K1- and betaTRCP-mediated degradation of PDCD4 promotes protein translation and cell growth. *Science (New York, N.Y.)*, 314(5798), pp.467–71. Available at: <http://www.ncbi.nlm.nih.gov/pubmed/17053147> [Accessed September 27, 2016].
- Dosil, M. & Bustelo, X.M., 2004. Functional characterization of Pwp2, a WD family protein essential for the assembly of the 90 S pre-ribosomal particle. *Journal of Biological Chemistry*, 279(36), pp.37385–37397.
- Dott, W. et al., 2014. Modulation of mitochondrial bioenergetics in a skeletal muscle cell line model of mitochondrial toxicity. *Redox biology*, 2, pp.224–33. Available at: <http://www.pubmedcentral.nih.gov/articlerender.fcgi?artid=3909783&tool=pmc&rendertype=abstract> [Accessed September 28, 2016].
- Dowling, R.J.O. et al., 2010. mTORC1-mediated cell proliferation, but not cell growth, controlled by the 4E-BPs. *Science (New York, N.Y.)*, 328(5982), pp.1172–6. Available at: <http://www.pubmedcentral.nih.gov/articlerender.fcgi?artid=2893390&tool=pmc&rendertype=abstract> [Accessed September 27, 2016].
- Dragon, F. et al., 2002. A large nucleolar U3 ribonucleoprotein required for 18S ribosomal RNA biogenesis. *Nature*, 417(6892), pp.967–70. Available at: <http://www.ncbi.nlm.nih.gov/pubmed/12068309> [Accessed September 28, 2016].
- El'skaya, A. V et al., 1997. Three tRNA binding sites in rabbit liver ribosomes and role of the intrinsic ATPase in 80S ribosomes from higher eukaryotes. *Biochemistry*, 36(34), pp.10492–7. Available at: <http://www.ncbi.nlm.nih.gov/pubmed/9265629> [Accessed September 27, 2016].
- Fei, S.S. et al., 2011. Protein database and quantitative analysis considerations when integrating genetics and proteomics to compare mouse strains. *Journal of proteome research*, 10(7), pp.2905–12. Available at: <http://www.pubmedcentral.nih.gov/articlerender.fcgi?artid=3128464&tool=pmc&rendertype=abstract> [Accessed September 27, 2016].
- Feldman, M.E. et al., 2009. Active-site inhibitors of mTOR target rapamycin-resistant outputs of mTORC1 and mTORC2. *PLoS biology*, 7(2), p.e38. Available at: <http://www.pubmedcentral.nih.gov/articlerender.fcgi?artid=2637922&tool=pmc&rendertype=abstract> [Accessed September 27, 2016].

- Fonseca, B.D. et al., 2015. La-related protein 1 (LARP1) represses terminal oligopyrimidine (TOP) mRNA translation downstream of mTOR complex 1 (mTORC1). *Journal of Biological Chemistry*, 290(26), pp.15996–16020.
- Fonseca, B.D. et al., 2014. The ever-evolving role of mTOR in translation. *Seminars in cell & developmental biology*, 36, pp.102–12. Available at: <http://www.ncbi.nlm.nih.gov/pubmed/25263010> [Accessed September 27, 2016].
- Fumagalli, S. et al., 2009. Absence of nucleolar disruption after impairment of 40S ribosome biogenesis reveals an rpl11-translation-dependent mechanism of p53 induction. *Nature cell biology*, 11(4), pp.501–8. Available at: <http://www.pubmedcentral.nih.gov/articlerender.fcgi?artid=4810440&tool=pmc-entrez&rendertype=abstract> [Accessed September 27, 2016].
- Galili, G. et al., 1988. Role of the 3'-poly(A) sequence in translational regulation of mRNAs in *Xenopus laevis* oocytes. *The Journal of biological chemistry*, 263(12), pp.5764–70. Available at: <http://www.ncbi.nlm.nih.gov/pubmed/3356706> [Accessed September 28, 2016].
- Gatto, L. & Christoforou, A., 2014. Using R and Bioconductor for proteomics data analysis. *Biochimica et biophysica acta*, 1844(1 Pt A), pp.42–51. Available at: <http://www.ncbi.nlm.nih.gov/pubmed/23692960> [Accessed September 28, 2016].
- Gebauer, F. & Hentze, M.W., 2004. Molecular mechanisms of translational control. *Nature reviews. Molecular cell biology*, 5(10), pp.827–35. Available at: <http://www.ncbi.nlm.nih.gov/pubmed/15459663> [Accessed September 27, 2016].
- Geyer, P.K. et al., 1982. Regulation of ribosomal protein mRNA content and translation in growth-stimulated mouse fibroblasts. *Molecular and cellular biology*, 2(6), pp.685–93. Available at: <http://www.pubmedcentral.nih.gov/articlerender.fcgi?artid=369844&tool=pmc-entrez&rendertype=abstract> [Accessed September 27, 2016].
- Gingras, A.C. et al., 2001. Hierarchical phosphorylation of the translation inhibitor 4E-BP1. *Genes & development*, 15(21), pp.2852–64. Available at: <http://www.pubmedcentral.nih.gov/articlerender.fcgi?artid=312813&tool=pmc-entrez&rendertype=abstract> [Accessed September 27, 2016].
- Glisovic, T. et al., 2008. RNA-binding proteins and post-transcriptional gene regulation. *FEBS letters*, 582(14), pp.1977–86. Available at: <http://www.pubmedcentral.nih.gov/articlerender.fcgi?artid=2858862&tool=pmc-entrez&rendertype=abstract> [Accessed September 27, 2016].
- Golomb, L., Volarevic, S. & Oren, M., 2014. p53 and ribosome biogenesis stress: the essentials. *FEBS letters*, 588(16), pp.2571–9. Available at: <http://www.ncbi.nlm.nih.gov/pubmed/24747423> [Accessed September 27, 2016].
- Granneman, S. & Tollervey, D., 2007. Building ribosomes: even more expensive than expected? *Current biology : CB*, 17(11), pp.R415–7. Available at: <http://www.ncbi.nlm.nih.gov/pubmed/17550767> [Accessed September 27, 2016].

- Grummt, I., 2013. The nucleolus—guardian of cellular homeostasis and genome integrity. *Chromosoma*, 122(6), pp.487–97. Available at: <http://www.ncbi.nlm.nih.gov/pubmed/24022641> [Accessed September 27, 2016].
- Hafner, M. et al., 2010. PAR-CLIP—a method to identify transcriptome-wide the binding sites of RNA binding proteins. *Journal of visualized experiments : JoVE*, (41). Available at: <http://www.pubmedcentral.nih.gov/articlerender.fcgi?artid=3156069&tool=pmc-entrez&rendertype=abstract> [Accessed September 27, 2016].
- Haghighat, A. & Sonenberg, N., 1997. eIF4G dramatically enhances the binding of eIF4E to the mRNA 5'-cap structure. *The Journal of biological chemistry*, 272(35), pp.21677–80. Available at: <http://www.ncbi.nlm.nih.gov/pubmed/9268293> [Accessed September 27, 2016].
- Hara, K. et al., 1997. Regulation of eIF-4E BP1 phosphorylation by mTOR. *The Journal of biological chemistry*, 272(42), pp.26457–63. Available at: <http://www.ncbi.nlm.nih.gov/pubmed/9334222> [Accessed September 27, 2016].
- Hatakeyama, S., 2011. TRIM proteins and cancer. *Nature reviews. Cancer*, 11(11), pp.792–804. Available at: <http://www.ncbi.nlm.nih.gov/pubmed/21979307> [Accessed September 28, 2016].
- Heaton, J.H. et al., 2001. Identification and cDNA cloning of a novel RNA-binding protein that interacts with the cyclic nucleotide-responsive sequence in the Type-1 plasminogen activator inhibitor mRNA. *The Journal of biological chemistry*, 276(5), pp.3341–7. Available at: <http://www.ncbi.nlm.nih.gov/pubmed/11001948> [Accessed September 28, 2016].
- Vander Heiden, M.G., Cantley, L.C. & Thompson, C.B., 2009. Understanding the Warburg effect: the metabolic requirements of cell proliferation. *Science (New York, N.Y.)*, 324(5930), pp.1029–33. Available at: <http://www.pubmedcentral.nih.gov/articlerender.fcgi?artid=2849637&tool=pmc-entrez&rendertype=abstract> [Accessed September 6, 2016].
- Herbert, T.P., Tee, A.R. & Proud, C.G., 2002. The extracellular signal-regulated kinase pathway regulates the phosphorylation of 4E-BP1 at multiple sites. *The Journal of biological chemistry*, 277(13), pp.11591–6. Available at: <http://www.ncbi.nlm.nih.gov/pubmed/11799119> [Accessed September 27, 2016].
- Hinman, M.N. & Lou, H., 2008. Diverse molecular functions of Hu proteins. *Cellular and molecular life sciences : CMLS*, 65(20), pp.3168–81. Available at: <http://www.pubmedcentral.nih.gov/articlerender.fcgi?artid=2580827&tool=pmc-entrez&rendertype=abstract> [Accessed September 27, 2016].
- Hinnebusch, A.G., 2006. eIF3: a versatile scaffold for translation initiation complexes. *Trends in biochemical sciences*, 31(10), pp.553–62. Available at: <http://www.ncbi.nlm.nih.gov/pubmed/16920360> [Accessed September 27, 2016].
- Hochberg, Y. & Benjamini, Y., 1990. More powerful procedures for multiple

- significance testing. *Statistics in medicine*, 9(7), pp.811–8. Available at: <http://www.ncbi.nlm.nih.gov/pubmed/2218183> [Accessed September 27, 2016].
- Holz, M.K. et al., 2005. mTOR and S6K1 mediate assembly of the translation preinitiation complex through dynamic protein interchange and ordered phosphorylation events. *Cell*, 123(4), pp.569–80. Available at: <http://www.ncbi.nlm.nih.gov/pubmed/16286006> [Accessed September 27, 2016].
- Hopkins, T.G. et al., 2015. The RNA-binding protein LARP1 is a post-transcriptional regulator of survival and tumorigenesis in ovarian cancer. *Nucleic acids research*, 44(3), p.gkv1515–. Available at: <http://nar.oxfordjournals.org/content/early/2015/12/29/nar.gkv1515.long>.
- Hornstein, E. et al., 1999. Overexpression of poly(A)-binding protein down-regulates the translation or the abundance of its own mRNA. *FEBS letters*, 457(2), pp.209–13. Available at: <http://www.ncbi.nlm.nih.gov/pubmed/10471780> [Accessed September 28, 2016].
- Hornstein, E., Tang, H. & Meyuhas, O., 2001. Mitogenic and nutritional signals are transduced into translational efficiency of TOP mRNAs. *Cold Spring Harbor symposia on quantitative biology*, 66, pp.477–84. Available at: <http://www.ncbi.nlm.nih.gov/pubmed/12762050> [Accessed September 27, 2016].
- Hoshino, S. et al., 1999. Novel function of the eukaryotic polypeptide-chain releasing factor 3 (eRF3/GSPT) in the mRNA degradation pathway. *Biochemistry. Biokhimiia*, 64(12), pp.1367–72. Available at: <http://www.ncbi.nlm.nih.gov/pubmed/10648960> [Accessed September 27, 2016].
- Hsieh, A.C. et al., 2012. The translational landscape of mTOR signalling steers cancer initiation and metastasis. *Nature*, 485(7396), pp.55–61. Available at: <http://www.pubmedcentral.nih.gov/articlerender.fcgi?artid=3663483&tool=pmc-entrez&rendertype=abstract> [Accessed September 27, 2016].
- Hsu, P.P. et al., 2011. The mTOR-regulated phosphoproteome reveals a mechanism of mTORC1-mediated inhibition of growth factor signaling. *Science (New York, N.Y.)*, 332(6035), pp.1317–22. Available at: <http://www.pubmedcentral.nih.gov/articlerender.fcgi?artid=3177140&tool=pmc-entrez&rendertype=abstract> [Accessed September 28, 2016].
- Huang, C. et al., 2015. Lactate promotes resistance to glucose starvation via upregulation of Bcl-2 mediated by mTOR activation. *Oncology reports*, 33(2), pp.875–84. Available at: <http://www.ncbi.nlm.nih.gov/pubmed/25484022> [Accessed September 28, 2016].
- Huang, D.W., Sherman, B.T. & Lempicki, R.A., 2009a. Bioinformatics enrichment tools: paths toward the comprehensive functional analysis of large gene lists. *Nucleic acids research*, 37(1), pp.1–13. Available at: <http://www.pubmedcentral.nih.gov/articlerender.fcgi?artid=2615629&tool=pmc-entrez&rendertype=abstract> [Accessed August 22, 2016].

- Huang, D.W., Sherman, B.T. & Lempicki, R.A., 2009b. Systematic and integrative analysis of large gene lists using DAVID bioinformatics resources. *Nature protocols*, 4(1), pp.44–57. Available at: <http://www.ncbi.nlm.nih.gov/pubmed/19131956> [Accessed August 23, 2016].
- Imataka, H., Gradi, A. & Sonenberg, N., 1998. A newly identified N-terminal amino acid sequence of human eIF4G binds poly(A)-binding protein and functions in poly(A)-dependent translation. *The EMBO journal*, 17(24), pp.7480–9. Available at: <http://www.pubmedcentral.nih.gov/articlerender.fcgi?artid=1171091&tool=pmc-entrez&rendertype=abstract> [Accessed September 27, 2016].
- Jackson, R.J., Hellen, C.U.T. & Pestova, T. V, 2012. Termination and post-termination events in eukaryotic translation. *Advances in protein chemistry and structural biology*, 86, pp.45–93. Available at: <http://www.ncbi.nlm.nih.gov/pubmed/22243581> [Accessed September 27, 2016].
- Jackson, R.J., Hellen, C.U.T. & Pestova, T. V, 2010. The mechanism of eukaryotic translation initiation and principles of its regulation. *Nature reviews. Molecular cell biology*, 11(2), pp.113–27. Available at: <http://www.pubmedcentral.nih.gov/articlerender.fcgi?artid=4461372&tool=pmc-entrez&rendertype=abstract> [Accessed September 27, 2016].
- Jacob, F. & Monod, J., 1961. Genetic regulatory mechanisms in the synthesis of proteins. *Journal of Molecular Biology*, 3(3), pp.318–356. Available at: <http://www.ncbi.nlm.nih.gov/pubmed/13718526> [Accessed September 27, 2016].
- Jastrzebski, K. et al., 2007. Coordinate regulation of ribosome biogenesis and function by the ribosomal protein S6 kinase, a key mediator of mTOR function. *Growth factors (Chur, Switzerland)*, 25(4), pp.209–26. Available at: <http://www.ncbi.nlm.nih.gov/pubmed/18092230> [Accessed September 27, 2016].
- Jefferies, H.B. et al., 1994. Rapamycin selectively represses translation of the “polypyrimidine tract” mRNA family. *Proceedings of the National Academy of Sciences of the United States of America*, 91(10), pp.4441–5. Available at: <http://www.pubmedcentral.nih.gov/articlerender.fcgi?artid=43801&tool=pmc-entrez&rendertype=abstract> [Accessed September 27, 2016].
- Jefferies, H.B. et al., 1997. Rapamycin suppresses 5’TOP mRNA translation through inhibition of p70s6k. *The EMBO journal*, 16(12), pp.3693–704. Available at: <http://www.pubmedcentral.nih.gov/articlerender.fcgi?artid=1169993&tool=pmc-entrez&rendertype=abstract> [Accessed September 27, 2016].
- Jinek, M. et al., 2010. Structural insights into the human GW182-PABC interaction in microRNA-mediated deadenylation. *Nature structural & molecular biology*, 17(2), pp.238–40. Available at: <http://www.pubmedcentral.nih.gov/articlerender.fcgi?artid=2920127&tool=pmc-entrez&rendertype=abstract> [Accessed September 27, 2016].
- Kabeya, Y. et al., 2000. LC3, a mammalian homologue of yeast Apg8p, is localized in autophagosome membranes after processing. *The EMBO journal*, 19(21),

- pp.5720–8. Available at:  
<http://www.pubmedcentral.nih.gov/articlerender.fcgi?artid=305793&tool=pmcentrez&rendertype=abstract> [Accessed September 27, 2016].
- Kajstura, M. et al., 2007. Discontinuous fragmentation of nuclear DNA during apoptosis revealed by discrete “sub-G1” peaks on DNA content histograms. *Cytometry. Part A : the journal of the International Society for Analytical Cytology*, 71(3), pp.125–31. Available at: <http://www.ncbi.nlm.nih.gov/pubmed/17252584> [Accessed September 28, 2016].
- Kato, M. et al., 2015. MicroRNA-26a/b directly regulate La-related protein 1 and inhibit cancer cell invasion in prostate cancer. *International journal of oncology*, 47(2), pp.710–8. Available at: <http://www.ncbi.nlm.nih.gov/pubmed/26063484> [Accessed September 28, 2016].
- Kedersha, N.L. et al., 1999. RNA-binding proteins TIA-1 and TIAR link the phosphorylation of eIF-2 alpha to the assembly of mammalian stress granules. *The Journal of cell biology*, 147(7), pp.1431–42. Available at: <http://www.pubmedcentral.nih.gov/articlerender.fcgi?artid=2174242&tool=pmcentrez&rendertype=abstract> [Accessed September 27, 2016].
- Kessler, S.H. & Sachs, A.B., 1998. RNA recognition motif 2 of yeast Pab1p is required for its functional interaction with eukaryotic translation initiation factor 4G. *Molecular and cellular biology*, 18(1), pp.51–7. Available at: <http://www.pubmedcentral.nih.gov/articlerender.fcgi?artid=121449&tool=pmcentrez&rendertype=abstract> [Accessed September 27, 2016].
- Kiledjian, M. & Dreyfuss, G., 1992. Primary structure and binding activity of the hnRNP U protein: binding RNA through RGG box. *The EMBO journal*, 11(7), pp.2655–64. Available at: <http://www.pubmedcentral.nih.gov/articlerender.fcgi?artid=556741&tool=pmcentrez&rendertype=abstract> [Accessed September 28, 2016].
- Kim, D.-H. et al., 2002. mTOR interacts with raptor to form a nutrient-sensitive complex that signals to the cell growth machinery. *Cell*, 110(2), pp.163–75. Available at: <http://www.ncbi.nlm.nih.gov/pubmed/12150925> [Accessed September 27, 2016].
- Kimball, S.R. et al., 2003. Mammalian stress granules represent sites of accumulation of stalled translation initiation complexes. *American journal of physiology. Cell physiology*, 284(2), pp.C273–84. Available at: <http://www.ncbi.nlm.nih.gov/pubmed/12388085> [Accessed September 27, 2016].
- Koensgen, D. et al., 2007. Expression analysis and RNA localization of PAI-RBP1 (SERBP1) in epithelial ovarian cancer: association with tumor progression. *Gynecologic oncology*, 107(2), pp.266–73. Available at: <http://www.ncbi.nlm.nih.gov/pubmed/17698176> [Accessed September 28, 2016].
- König, J. et al., 2010. iCLIP reveals the function of hnRNP particles in splicing at individual nucleotide resolution. *Nature structural & molecular biology*, 17(7),

- pp.909–15. Available at:  
<http://www.pubmedcentral.nih.gov/articlerender.fcgi?artid=3000544&tool=pmc-entrez&rendertype=abstract> [Accessed September 27, 2016].
- Korneeva, N.L. et al., 2005. Interaction between the NH<sub>2</sub>-terminal domain of eIF4A and the central domain of eIF4G modulates RNA-stimulated ATPase activity. *The Journal of biological chemistry*, 280(3), pp.1872–81. Available at:  
<http://www.ncbi.nlm.nih.gov/pubmed/15528191> [Accessed September 27, 2016].
- Kozak, M., 1992. Regulation of translation in eukaryotic systems. *Annual review of cell biology*, 8, pp.197–225. Available at:  
<http://www.ncbi.nlm.nih.gov/pubmed/1335743> [Accessed September 27, 2016].
- Krieg, J., Hofsteenge, J. & Thomas, G., 1988. Identification of the 40 S ribosomal protein S6 phosphorylation sites induced by cycloheximide. *The Journal of biological chemistry*, 263(23), pp.11473–7. Available at:  
<http://www.ncbi.nlm.nih.gov/pubmed/3403539> [Accessed September 27, 2016].
- Kuharev, J. et al., 2015. In-depth evaluation of software tools for data-independent acquisition based label-free quantification. *Proteomics*, 15(18), pp.3140–51. Available at: <http://www.ncbi.nlm.nih.gov/pubmed/25545627> [Accessed September 27, 2016].
- Kühn, U. & Pieler, T., 1996. Xenopus poly(A) binding protein: functional domains in RNA binding and protein-protein interaction. *Journal of molecular biology*, 256(1), pp.20–30. Available at: <http://www.ncbi.nlm.nih.gov/pubmed/8609610> [Accessed September 28, 2016].
- Kwon, S.C. et al., 2013. The RNA-binding protein repertoire of embryonic stem cells. *Nature structural & molecular biology*, 20(9), pp.1122–30. Available at:  
<http://www.ncbi.nlm.nih.gov/pubmed/23912277>.
- Lahr, R.M. et al., 2015. The La-related protein 1-specific domain repurposes HEAT-like repeats to directly bind a 5' TOP sequence. *Nucleic acids research*, 43(16), pp.8077–88. Available at:  
<http://www.pubmedcentral.nih.gov/articlerender.fcgi?artid=4652764&tool=pmc-entrez&rendertype=abstract> [Accessed September 28, 2016].
- Lai, W.S. et al., 2000. Interactions of CCCH zinc finger proteins with mRNA. Binding of tristetraprolin-related zinc finger proteins to Au-rich elements and destabilization of mRNA. *The Journal of biological chemistry*, 275(23), pp.17827–37. Available at:  
<http://www.ncbi.nlm.nih.gov/pubmed/10751406> [Accessed September 27, 2016].
- Lamming, D.W. et al., 2013. Rapalogs and mTOR inhibitors as anti-aging therapeutics. *The Journal of clinical investigation*, 123(3), pp.980–9. Available at:  
<http://www.pubmedcentral.nih.gov/articlerender.fcgi?artid=3582126&tool=pmc-entrez&rendertype=abstract> [Accessed June 19, 2014].
- Laplante, M. & Sabatini, D.M., 2009. An emerging role of mTOR in lipid biosynthesis. *Current biology : CB*, 19(22), pp.R1046–52. Available at:

- <http://www.pubmedcentral.nih.gov/articlerender.fcgi?artid=3390254&tool=pmc&rendertype=abstract> [Accessed September 27, 2016].
- Laplanche, M. & Sabatini, D.M., 2012a. mTOR signaling in growth control and disease. *Cell*, 149(2), pp.274–93. Available at: <http://www.pubmedcentral.nih.gov/articlerender.fcgi?artid=3331679&tool=pmc&rendertype=abstract> [Accessed May 23, 2014].
- Laplanche, M. & Sabatini, D.M., 2012b. mTOR Signaling. *Cold Spring Harbor perspectives in biology*, 4(2). Available at: <http://www.pubmedcentral.nih.gov/articlerender.fcgi?artid=3281571&tool=pmc&rendertype=abstract> [Accessed May 27, 2014].
- Laplanche, M. & Sabatini, D.M., 2013. Regulation of mTORC1 and its impact on gene expression at a glance. *Journal of cell science*, 126, pp.1713–9. Available at: <http://www.pubmedcentral.nih.gov/articlerender.fcgi?artid=3678406&tool=pmc&rendertype=abstract>.
- Lau, C., Bachorik, J.L. & Dreyfuss, G., 2009. Gemin5-snRNA interaction reveals an RNA binding function for WD repeat domains. *Nature structural & molecular biology*, 16(5), pp.486–91. Available at: <http://www.ncbi.nlm.nih.gov/pubmed/19377484> [Accessed September 28, 2016].
- Lee, Y.-J. et al., 2014. Localization of SERBP1 in stress granules and nucleoli. *The FEBS journal*, 281(1), pp.352–64. Available at: <http://www.ncbi.nlm.nih.gov/pubmed/24205981> [Accessed September 28, 2016].
- Lee, Y.-J. et al., 2012. Protein arginine methylation of SERBP1 by protein arginine methyltransferase 1 affects cytoplasmic/nuclear distribution. *Journal of cellular biochemistry*, 113(8), pp.2721–8. Available at: <http://www.ncbi.nlm.nih.gov/pubmed/22442049> [Accessed September 28, 2016].
- Lee-Fruman, K.K. et al., 1999. Characterization of S6K2, a novel kinase homologous to S6K1. *Oncogene*, 18(36), pp.5108–14. Available at: <http://www.ncbi.nlm.nih.gov/pubmed/10490847> [Accessed September 27, 2016].
- Leek, J.T. et al., 2010. Tackling the widespread and critical impact of batch effects in high-throughput data. *Nature reviews. Genetics*, 11(10), pp.733–9. Available at: <http://www.pubmedcentral.nih.gov/articlerender.fcgi?artid=3880143&tool=pmc&rendertype=abstract> [Accessed August 30, 2016].
- Leek, J.T. et al., 2012. The sva package for removing batch effects and other unwanted variation in high-throughput experiments. *Bioinformatics (Oxford, England)*, 28(6), pp.882–3. Available at: <http://www.pubmedcentral.nih.gov/articlerender.fcgi?artid=3307112&tool=pmc&rendertype=abstract> [Accessed September 28, 2016].
- Lischwe, M.A. et al., 1985. Clustering of glycine and NG,NG-dimethylarginine in nucleolar protein C23. *Biochemistry*, 24(22), pp.6025–8. Available at: <http://www.ncbi.nlm.nih.gov/pubmed/4084504> [Accessed September 28, 2016].

- Lunde, B.M., Moore, C. & Varani, G., 2007. RNA-binding proteins: modular design for efficient function. *Nature reviews. Molecular cell biology*, 8(6), pp.479–90. Available at: <http://www.ncbi.nlm.nih.gov/pubmed/17473849> [Accessed September 27, 2016].
- Malina, A., Mills, J.R. & Pelletier, J., 2012. Emerging therapeutics targeting mRNA translation. *Cold Spring Harbor perspectives in biology*, 4(4), p.a012377. Available at: <http://www.pubmedcentral.nih.gov/articlerender.fcgi?artid=3312682&tool=pmc-entrez&rendertype=abstract> [Accessed September 27, 2016].
- Manning, G. et al., 2002. The protein kinase complement of the human genome. *Science (New York, N.Y.)*, 298(5600), pp.1912–34. Available at: <http://www.ncbi.nlm.nih.gov/pubmed/12471243> [Accessed August 19, 2016].
- Maris, C., Dominguez, C. & Allain, F.H.-T., 2005. The RNA recognition motif, a plastic RNA-binding platform to regulate post-transcriptional gene expression. *The FEBS journal*, 272(9), pp.2118–31. Available at: <http://www.ncbi.nlm.nih.gov/pubmed/15853797> [Accessed September 27, 2016].
- Marroquin, L.D. et al., 2007. Circumventing the Crabtree effect: replacing media glucose with galactose increases susceptibility of HepG2 cells to mitochondrial toxicants. *Toxicological sciences : an official journal of the Society of Toxicology*, 97(2), pp.539–47. Available at: <http://www.ncbi.nlm.nih.gov/pubmed/17361016> [Accessed September 28, 2016].
- Matia-González, A.M., Laing, E.E. & Gerber, A.P., 2015. Conserved mRNA-binding proteomes in eukaryotic organisms. *Nature structural & molecular biology*, 22(12), pp.1027–33. Available at: <http://www.ncbi.nlm.nih.gov/pubmed/26595419> [Accessed September 27, 2016].
- Mayer, C. & Grummt, I., 2006. Ribosome biogenesis and cell growth: mTOR coordinates transcription by all three classes of nuclear RNA polymerases. *Oncogene*, 25(48), pp.6384–91. Available at: <http://www.ncbi.nlm.nih.gov/pubmed/17041624> [Accessed September 27, 2016].
- Melnikova, V.O. et al., 2003. Mutant p53 is constitutively phosphorylated at Serine 15 in UV-induced mouse skin tumors: involvement of ERK1/2 MAP kinase. *Oncogene*, 22(38), pp.5958–66. Available at: <http://www.ncbi.nlm.nih.gov/pubmed/12955074> [Accessed September 28, 2016].
- Melo, E.O. et al., 2003. Identification of a C-terminal poly(A)-binding protein (PABP)-PABP interaction domain: role in cooperative binding to poly (A) and efficient cap distal translational repression. *The Journal of biological chemistry*, 278(47), pp.46357–68. Available at: <http://www.ncbi.nlm.nih.gov/pubmed/12952955> [Accessed September 28, 2016].
- Meng, Z. et al., 2005. The ELAV RNA-stability factor HuR binds the 5'-untranslated region of the human IGF-IR transcript and differentially represses cap-dependent and IRES-mediated translation. *Nucleic acids research*, 33(9), pp.2962–79.

- Available at:  
<http://www.pubmedcentral.nih.gov/articlerender.fcgi?artid=1140080&tool=pmc&rendertype=abstract> [Accessed September 27, 2016].
- Merret, R. et al., 2013. XRN4 and LARP1 are required for a heat-triggered mRNA decay pathway involved in plant acclimation and survival during thermal stress. *Cell reports*, 5(5), pp.1279–93. Available at:  
<http://www.ncbi.nlm.nih.gov/pubmed/24332370> [Accessed September 28, 2016].
- Meyuhas, O., 2000. Synthesis of the translational apparatus is regulated at the translational level. *European journal of biochemistry / FEBS*, 267(21), pp.6321–30. Available at: <http://www.ncbi.nlm.nih.gov/pubmed/11029573> [Accessed September 27, 2016].
- Miloslavski, R. et al., 2014. Oxygen sufficiency controls TOP mRNA translation via the TSC-Rheb-mTOR pathway in a 4E-BP-independent manner. *Journal of molecular cell biology*, 6(3), pp.255–66. Available at:  
<http://www.pubmedcentral.nih.gov/articlerender.fcgi?artid=4034726&tool=pmc&rendertype=abstract> [Accessed September 27, 2016].
- Mookerjee, S.A. et al., 2015. The contributions of respiration and glycolysis to extracellular acid production. *Biochimica et biophysica acta*, 1847(2), pp.171–81. Available at: <http://www.ncbi.nlm.nih.gov/pubmed/25449966> [Accessed September 28, 2016].
- Morley, S.J., McKendrick, L. & Bushell, M., 1998. Cleavage of translation initiation factor 4G (eIF4G) during anti-Fas IgM-induced apoptosis does not require signalling through the p38 mitogen-activated protein (MAP) kinase. *FEBS letters*, 438(1-2), pp.41–8. Available at: <http://www.ncbi.nlm.nih.gov/pubmed/9821956> [Accessed September 27, 2016].
- Morrissey, C. et al., 2008. Differential expression of angiogenesis associated genes in prostate cancer bone, liver and lymph node metastases. *Clinical & experimental metastasis*, 25(4), pp.377–88. Available at:  
<http://www.ncbi.nlm.nih.gov/pubmed/17972146> [Accessed September 28, 2016].
- Mowers, E.E., Sharifi, M.N. & Macleod, K.F., 2016. Autophagy in cancer metastasis. *Oncogene*. Available at: <http://www.ncbi.nlm.nih.gov/pubmed/27593926> [Accessed September 27, 2016].
- Mugnier, P. & Tuite, M.F., 1999. Translation termination and its regulation in eukaryotes: recent insights provided by studies in yeast. *Biochemistry. Biokhimiia*, 64(12), pp.1360–6. Available at: <http://www.ncbi.nlm.nih.gov/pubmed/10648959> [Accessed September 27, 2016].
- Mukhopadhyay, N.K. et al., 1992. An array of insulin-activated, proline-directed serine/threonine protein kinases phosphorylate the p70 S6 kinase. *The Journal of biological chemistry*, 267(5), pp.3325–35. Available at:  
<http://www.ncbi.nlm.nih.gov/pubmed/1737788> [Accessed September 27, 2016].

- Mura, M. et al., 2015. LARP1 post-transcriptionally regulates mTOR and contributes to cancer progression. *Oncogene*, 34(39), pp.5025–36. Available at: <http://www.pubmedcentral.nih.gov/articlerender.fcgi?artid=4430325&tool=pmc-entrez&rendertype=abstract> [Accessed September 28, 2016].
- Nakamura, J. et al., 2009. Overexpression of eukaryotic elongation factor eEF2 in gastrointestinal cancers and its involvement in G2/M progression in the cell cycle. *International journal of oncology*, 34(5), pp.1181–9. Available at: <http://www.ncbi.nlm.nih.gov/pubmed/19360331> [Accessed September 27, 2016].
- Nandagopal, N. & Roux, P.P., 2015. Regulation of global and specific mRNA translation by the mTOR signaling pathway. *Translation (Austin, Tex.)*, 3(1), p.e983402. Available at: <http://www.pubmedcentral.nih.gov/articlerender.fcgi?artid=4682803&tool=pmc-entrez&rendertype=abstract> [Accessed September 27, 2016].
- Norris, A.D. & Calarco, J.A., 2012. Emerging Roles of Alternative Pre-mRNA Splicing Regulation in Neuronal Development and Function. *Frontiers in neuroscience*, 6, p.122. Available at: <http://www.pubmedcentral.nih.gov/articlerender.fcgi?artid=3424503&tool=pmc-entrez&rendertype=abstract> [Accessed September 27, 2016].
- Nover, L., Scharf, K.D. & Neumann, D., 1989. Cytoplasmic heat shock granules are formed from precursor particles and are associated with a specific set of mRNAs. *Molecular and cellular biology*, 9(3), pp.1298–308. Available at: <http://www.pubmedcentral.nih.gov/articlerender.fcgi?artid=362722&tool=pmc-entrez&rendertype=abstract> [Accessed September 27, 2016].
- Nygård, O. & Nika, H., 1982. Identification by RNA-protein cross-linking of ribosomal proteins located at the interface between the small and the large subunits of mammalian ribosomes. *The EMBO journal*, 1(3), pp.357–62. Available at: <http://www.pubmedcentral.nih.gov/articlerender.fcgi?artid=553049&tool=pmc-entrez&rendertype=abstract> [Accessed September 27, 2016].
- Nykamp, K., Lee, M.-H. & Kimble, J., 2008. C. elegans La-related protein, LARP-1, localizes to germline P bodies and attenuates Ras-MAPK signaling during oogenesis. *RNA (New York, N.Y.)*, 14(7), pp.1378–89. Available at: <http://www.pubmedcentral.nih.gov/articlerender.fcgi?artid=2441978&tool=pmc-entrez&rendertype=abstract> [Accessed September 28, 2016].
- O'Reilly, K.E. et al., 2006. mTOR inhibition induces upstream receptor tyrosine kinase signaling and activates Akt. *Cancer research*, 66(3), pp.1500–8. Available at: <http://www.pubmedcentral.nih.gov/articlerender.fcgi?artid=3193604&tool=pmc-entrez&rendertype=abstract> [Accessed September 27, 2016].
- Parker, R. & Song, H., 2004. The enzymes and control of eukaryotic mRNA turnover. *Nature structural & molecular biology*, 11(2), pp.121–7. Available at: <http://www.ncbi.nlm.nih.gov/pubmed/14749774> [Accessed September 28, 2016].
- Passmore, L.A. et al., 2007. The eukaryotic translation initiation factors eIF1 and eIF1A

- induce an open conformation of the 40S ribosome. *Molecular cell*, 26(1), pp.41–50. Available at: <http://www.ncbi.nlm.nih.gov/pubmed/17434125> [Accessed September 27, 2016].
- Patton, J.G. et al., 1991. Characterization and molecular cloning of polypyrimidine tract-binding protein: a component of a complex necessary for pre-mRNA splicing. *Genes & development*, 5(7), pp.1237–51. Available at: <http://www.ncbi.nlm.nih.gov/pubmed/1906036> [Accessed September 27, 2016].
- Patton, J.G. et al., 1993. Cloning and characterization of PSF, a novel pre-mRNA splicing factor. *Genes & development*, 7(3), pp.393–406. Available at: <http://www.ncbi.nlm.nih.gov/pubmed/8449401> [Accessed September 27, 2016].
- Patursky-Polischuk, I. et al., 2014. Reassessment of the role of TSC, mTORC1 and microRNAs in amino acids-mediated translational control of TOP mRNAs. *PLoS one*, 9(10), p.e109410. Available at: <http://www.pubmedcentral.nih.gov/articlerender.fcgi?artid=4206288&tool=pmc&rendertype=abstract> [Accessed September 28, 2016].
- Pestova, T. V et al., 2000. The joining of ribosomal subunits in eukaryotes requires eIF5B. *Nature*, 403(6767), pp.332–5. Available at: <http://www.ncbi.nlm.nih.gov/pubmed/10659855> [Accessed September 27, 2016].
- Pestova, T. V & Hellen, C.U., 2001. Functions of eukaryotic factors in initiation of translation. *Cold Spring Harbor symposia on quantitative biology*, 66, pp.389–96. Available at: <http://www.ncbi.nlm.nih.gov/pubmed/12762041> [Accessed September 27, 2016].
- Phan, A.T. et al., 2011. Structure-function studies of FMRP RGG peptide recognition of an RNA duplex-quadruplex junction. *Nature structural & molecular biology*, 18(7), pp.796–804. Available at: <http://www.pubmedcentral.nih.gov/articlerender.fcgi?artid=3130835&tool=pmc&rendertype=abstract> [Accessed September 28, 2016].
- Qin, Y., Cui, H. & Zhang, H., 2015. Overexpression of TRIM25 in Lung Cancer Regulates Tumor Cell Progression. *Technology in Cancer Research & Treatment*, pp.1–9. Available at: <http://tct.sagepub.com/lookup/doi/10.1177/1533034615595903>.
- Raught, B. et al., 2000. Serum-stimulated, rapamycin-sensitive phosphorylation sites in the eukaryotic translation initiation factor 4G1. *The EMBO journal*, 19(3), pp.434–44. Available at: <http://www.pubmedcentral.nih.gov/articlerender.fcgi?artid=305580&tool=pmc&rendertype=abstract> [Accessed September 27, 2016].
- Redpath, N.T., Foulstone, E.J. & Proud, C.G., 1996. Regulation of translation elongation factor-2 by insulin via a rapamycin-sensitive signalling pathway. *The EMBO journal*, 15(9), pp.2291–7. Available at: <http://www.pubmedcentral.nih.gov/articlerender.fcgi?artid=450154&tool=pmc&rendertype=abstract> [Accessed September 27, 2016].

- Redpath, N.T. & Proud, C.G., 1993. Cyclic AMP-dependent protein kinase phosphorylates rabbit reticulocyte elongation factor-2 kinase and induces calcium-independent activity. *The Biochemical journal*, 293 ( Pt 1, pp.31–4. Available at:  
<http://www.pubmedcentral.nih.gov/articlerender.fcgi?artid=1134316&tool=pmc&rendertype=abstract> [Accessed September 27, 2016].
- Ritchie, M.E. et al., 2015. limma powers differential expression analyses for RNA-sequencing and microarray studies. *Nucleic acids research*, 43(7), p.e47. Available at:  
<http://www.pubmedcentral.nih.gov/articlerender.fcgi?artid=4402510&tool=pmc&rendertype=abstract> [Accessed September 27, 2016].
- Ruvinsky, I. et al., 2005. Ribosomal protein S6 phosphorylation is a determinant of cell size and glucose homeostasis. *Genes & development*, 19(18), pp.2199–211. Available at:  
<http://www.pubmedcentral.nih.gov/articlerender.fcgi?artid=1221890&tool=pmc&rendertype=abstract> [Accessed September 27, 2016].
- Sancak, Y. et al., 2010. Ragulator-Rag complex targets mTORC1 to the lysosomal surface and is necessary for its activation by amino acids. *Cell*, 141(2), pp.290–303. Available at:  
<http://www.pubmedcentral.nih.gov/articlerender.fcgi?artid=3024592&tool=pmc&rendertype=abstract> [Accessed September 27, 2016].
- Sanduja, S., Blanco, F.F. & Dixon, D.A., 2011. The roles of TTP and BRF proteins in regulated mRNA decay. *Wiley Interdisciplinary Reviews: RNA*, 2(1), pp.42–57. Available at:  
<http://www.pubmedcentral.nih.gov/articlerender.fcgi?artid=3030256&tool=pmc&rendertype=abstract> [Accessed September 27, 2016].
- Sarbassov, D.D. et al., 2005. Phosphorylation and regulation of Akt/PKB by the rictor-mTOR complex. *Science (New York, N.Y.)*, 307(5712), pp.1098–101. Available at:  
<http://www.ncbi.nlm.nih.gov/pubmed/15718470> [Accessed September 27, 2016].
- Sarbassov, D.D. et al., 2006. Prolonged rapamycin treatment inhibits mTORC2 assembly and Akt/PKB. *Molecular cell*, 22(2), pp.159–68. Available at:  
<http://www.ncbi.nlm.nih.gov/pubmed/16603397> [Accessed September 27, 2016].
- Sarbassov, D.D. et al., 2004. Rictor, a novel binding partner of mTOR, defines a rapamycin-insensitive and raptor-independent pathway that regulates the cytoskeleton. *Current biology : CB*, 14(14), pp.1296–302. Available at:  
<http://www.ncbi.nlm.nih.gov/pubmed/15268862> [Accessed September 27, 2016].
- Scherrer, T. et al., 2010. A screen for RNA-binding proteins in yeast indicates dual functions for many enzymes. *PLoS one*, 5(11), p.e15499. Available at:  
<http://www.pubmedcentral.nih.gov/articlerender.fcgi?artid=2988813&tool=pmc&rendertype=abstract> [Accessed September 27, 2016].
- Serce, N.B. et al., 2012. Overexpression of SERBP1 (Plasminogen activator inhibitor 1

- RNA binding protein) in human breast cancer is correlated with favourable prognosis. *BMC cancer*, 12, p.597. Available at: <http://www.pubmedcentral.nih.gov/articlerender.fcgi?artid=3538721&tool=pmc&rendertype=abstract> [Accessed September 28, 2016].
- Smith, E.M. et al., 2005. The tuberous sclerosis protein TSC2 is not required for the regulation of the mammalian target of rapamycin by amino acids and certain cellular stresses. *The Journal of biological chemistry*, 280(19), pp.18717–27. Available at: <http://www.ncbi.nlm.nih.gov/pubmed/15772076> [Accessed September 27, 2016].
- Sonenberg, N., 1993. Translation factors as effectors of cell growth and tumorigenesis. *Current opinion in cell biology*, 5(6), pp.955–60. Available at: <http://www.ncbi.nlm.nih.gov/pubmed/7907492> [Accessed September 27, 2016].
- Sonenberg, N. & Hinnebusch, A.G., 2009. Regulation of translation initiation in eukaryotes: mechanisms and biological targets. *Cell*, 136(4), pp.731–45. Available at: <http://www.pubmedcentral.nih.gov/articlerender.fcgi?artid=3610329&tool=pmc&rendertype=abstract> [Accessed September 27, 2016].
- Srikantan, S. & Gorospe, M., 2012. HuR function in disease. *Frontiers in bioscience (Landmark edition)*, 17, pp.189–205. Available at: <http://www.pubmedcentral.nih.gov/articlerender.fcgi?artid=4540328&tool=pmc&rendertype=abstract> [Accessed September 27, 2016].
- Stavraka, C. & Blagden, S., 2015. The La-Related Proteins, a Family with Connections to Cancer. *Biomolecules*, 5(4), pp.2701–22. Available at: <http://www.pubmedcentral.nih.gov/articlerender.fcgi?artid=4693254&tool=pmc&rendertype=abstract> [Accessed September 28, 2016].
- Steitz, T.A., 2008. A structural understanding of the dynamic ribosome machine. *Nature reviews. Molecular cell biology*, 9(3), pp.242–53. Available at: <http://www.ncbi.nlm.nih.gov/pubmed/18292779> [Accessed September 27, 2016].
- Suzuki, C. et al., 2008. PDCD4 inhibits translation initiation by binding to eIF4A using both its MA3 domains. *Proceedings of the National Academy of Sciences of the United States of America*, 105(9), pp.3274–9. Available at: <http://www.pubmedcentral.nih.gov/articlerender.fcgi?artid=2265113&tool=pmc&rendertype=abstract> [Accessed September 27, 2016].
- Sysoev, V.O. et al., 2016. Global changes of the RNA-bound proteome during the maternal-to-zygotic transition in *Drosophila*. *Nature communications*, 7, p.12128. Available at: <http://www.pubmedcentral.nih.gov/articlerender.fcgi?artid=4935972&tool=pmc&rendertype=abstract> [Accessed September 27, 2016].
- Tafforeau, L. et al., 2013. The complexity of human ribosome biogenesis revealed by systematic nucleolar screening of Pre-rRNA processing factors. *Molecular cell*, 51(4), pp.539–51. Available at: <http://www.ncbi.nlm.nih.gov/pubmed/23973377>

[Accessed September 27, 2016].

- Tamura, K., 2011. Ribosome evolution: emergence of peptide synthesis machinery. *Journal of biosciences*, 36(5), pp.921–8. Available at: <http://www.ncbi.nlm.nih.gov/pubmed/22116290> [Accessed September 27, 2016].
- Tarun, S.Z. et al., 1997. Translation initiation factor eIF4G mediates in vitro poly(A) tail-dependent translation. *Proceedings of the National Academy of Sciences of the United States of America*, 94(17), pp.9046–51. Available at: <http://www.pubmedcentral.nih.gov/articlerender.fcgi?artid=23022&tool=pmcentrez&rendertype=abstract> [Accessed September 27, 2016].
- Tarun, S.Z. & Sachs, A.B., 1996. Association of the yeast poly(A) tail binding protein with translation initiation factor eIF-4G. *The EMBO journal*, 15(24), pp.7168–77. Available at: <http://www.pubmedcentral.nih.gov/articlerender.fcgi?artid=452544&tool=pmcentrez&rendertype=abstract> [Accessed September 27, 2016].
- Tcherkezian, J. et al., 2014. Proteomic analysis of cap-dependent translation identifies LARP1 as a key regulator of 5'??TOP mRNA translation. *Genes and Development*, 28(4), pp.357–371.
- Tee, A.R. & Proud, C.G., 2002. Caspase cleavage of initiation factor 4E-binding protein 1 yields a dominant inhibitor of cap-dependent translation and reveals a novel regulatory motif. *Molecular and cellular biology*, 22(6), pp.1674–83. Available at: <http://www.pubmedcentral.nih.gov/articlerender.fcgi?artid=135612&tool=pmcentrez&rendertype=abstract> [Accessed September 27, 2016].
- Teixeira, D. et al., 2005. Processing bodies require RNA for assembly and contain nontranslating mRNAs. *RNA (New York, N.Y.)*, 11(4), pp.371–82. Available at: <http://www.pubmedcentral.nih.gov/articlerender.fcgi?artid=1370727&tool=pmcentrez&rendertype=abstract> [Accessed September 27, 2016].
- Terada, N. et al., 1994. Rapamycin selectively inhibits translation of mRNAs encoding elongation factors and ribosomal proteins. *Proceedings of the National Academy of Sciences of the United States of America*, 91(24), pp.11477–81. Available at: <http://www.pubmedcentral.nih.gov/articlerender.fcgi?artid=45254&tool=pmcentrez&rendertype=abstract> [Accessed September 27, 2016].
- Thandapani, P. et al., 2013. Defining the RGG/RG motif. *Molecular cell*, 50(5), pp.613–23. Available at: <http://www.ncbi.nlm.nih.gov/pubmed/23746349> [Accessed September 28, 2016].
- Thangima Zannat, M., Bhattacharjee, R.B. & Bag, J., 2011. Depletion of cellular poly (A) binding protein prevents protein synthesis and leads to apoptosis in HeLa cells. *Biochemical and biophysical research communications*, 408(3), pp.375–81. Available at: <http://www.ncbi.nlm.nih.gov/pubmed/21521633> [Accessed September 28, 2016].
- Thoreen, C.C. et al., 2012. A unifying model for mTORC1-mediated regulation of mRNA

- translation. *Nature*, 485(7396), pp.109–13. Available at:  
<http://www.pubmedcentral.nih.gov/articlerender.fcgi?artid=3347774&tool=pmc&rendertype=abstract> [Accessed September 27, 2016].
- Thoreen, C.C. et al., 2009. An ATP-competitive mammalian target of rapamycin inhibitor reveals rapamycin-resistant functions of mTORC1. *Journal of Biological Chemistry*, 284(12), pp.8023–8032.
- Tschochner, H. & Hurt, E., 2003. Pre-ribosomes on the road from the nucleolus to the cytoplasm. *Trends in cell biology*, 13(5), pp.255–63. Available at:  
<http://www.ncbi.nlm.nih.gov/pubmed/12742169> [Accessed September 27, 2016].
- Tsvetanova, N.G. et al., 2010. Proteome-wide search reveals unexpected RNA-binding proteins in *Saccharomyces cerevisiae*. *PLoS one*, 5(9). Available at:  
<http://www.pubmedcentral.nih.gov/articlerender.fcgi?artid=2937035&tool=pmc&rendertype=abstract> [Accessed September 27, 2016].
- Ueyama, K. et al., 2010. Knockdown of Efp by DNA-modified small interfering RNA inhibits breast cancer cell proliferation and in vivo tumor growth. *Cancer Gene Therapy*, 17(9), pp.624–632. Available at:  
<http://www.ncbi.nlm.nih.gov/pubmed/20467453> [Accessed September 28, 2016].
- Urano, T. et al., 2002. Efp targets 14-3-3 sigma for proteolysis and promotes breast tumour growth. *Nature*, 417(6891), pp.871–875.
- Vousden, K.H. & Lu, X., 2002. Live or let die: the cell's response to p53. *Nature reviews. Cancer*, 2(8), pp.594–604. Available at:  
<http://www.ncbi.nlm.nih.gov/pubmed/12154352> [Accessed September 28, 2016].
- Wang, X. et al., 2001. Regulation of elongation factor 2 kinase by p90(RSK1) and p70 S6 kinase. *The EMBO journal*, 20(16), pp.4370–9. Available at:  
<http://www.pubmedcentral.nih.gov/articlerender.fcgi?artid=125559&tool=pmc&rendertype=abstract> [Accessed September 27, 2016].
- Wells, S.E. et al., 1998. Circularization of mRNA by eukaryotic translation initiation factors. *Molecular cell*, 2(1), pp.135–40. Available at:  
<http://www.ncbi.nlm.nih.gov/pubmed/9702200> [Accessed September 27, 2016].
- Wilson, D.N. & Doudna Cate, J.H., 2012. The structure and function of the eukaryotic ribosome. *Cold Spring Harbor perspectives in biology*, 4(5). Available at:  
<http://www.pubmedcentral.nih.gov/articlerender.fcgi?artid=3331703&tool=pmc&rendertype=abstract> [Accessed September 28, 2016].
- Wu, J. et al., 2006. Molecular cloning and characterization of rat LC3A and LC3B--two novel markers of autophagosome. *Biochemical and biophysical research communications*, 339(1), pp.437–42. Available at:  
<http://www.ncbi.nlm.nih.gov/pubmed/16300744> [Accessed September 27, 2016].
- Xie, C. et al., 2013. LARP1 predict the prognosis for early-stage and AFP-normal hepatocellular carcinoma. *Journal of translational medicine*, 11, p.272. Available

- at:  
<http://www.pubmedcentral.nih.gov/articlerender.fcgi?artid=3814951&tool=pmc&rendertype=abstract> [Accessed September 28, 2016].
- Xie, J. et al., 2014. Beyond Warburg effect--dual metabolic nature of cancer cells. *Scientific reports*, 4, p.4927. Available at:  
<http://www.pubmedcentral.nih.gov/articlerender.fcgi?artid=4018627&tool=pmc&rendertype=abstract> [Accessed September 28, 2016].
- Xue, S. & Barna, M., 2012. Specialized ribosomes: a new frontier in gene regulation and organismal biology. *Nature reviews. Molecular cell biology*, 13(6), pp.355–69. Available at:  
<http://www.pubmedcentral.nih.gov/articlerender.fcgi?artid=4039366&tool=pmc&rendertype=abstract> [Accessed September 27, 2016].
- Yamashita, R. et al., 2008. Comprehensive detection of human terminal oligopyrimidine (TOP) genes and analysis of their characteristics. *Nucleic acids research*, 36(11), pp.3707–15. Available at:  
<http://www.pubmedcentral.nih.gov/articlerender.fcgi?artid=2441802&tool=pmc&rendertype=abstract> [Accessed September 27, 2016].
- Yang, H.-S. et al., 2003. The transformation suppressor Pcd4 is a novel eukaryotic translation initiation factor 4A binding protein that inhibits translation. *Molecular and cellular biology*, 23(1), pp.26–37. Available at:  
<http://www.pubmedcentral.nih.gov/articlerender.fcgi?artid=140682&tool=pmc&rendertype=abstract> [Accessed September 27, 2016].
- Yarosh, C.A. et al., 2015. PSF: nuclear busy-body or nuclear facilitator? *Wiley Interdisciplinary Reviews: RNA*, 6(4), pp.351–367. Available at:  
<http://doi.wiley.com/10.1002/wrna.1280> [Accessed September 27, 2016].
- Yu, M. et al., 2011. Nuclear factor p65 interacts with Keap1 to repress the Nrf2-ARE pathway. *Cellular signalling*, 23(5), pp.883–892.
- Yu, Y. et al., 2011. Phosphoproteomic analysis identifies Grb10 as an mTORC1 substrate that negatively regulates insulin signaling. *Science (New York, N.Y.)*, 332(6035), pp.1322–6. Available at:  
<http://www.pubmedcentral.nih.gov/articlerender.fcgi?artid=3195509&tool=pmc&rendertype=abstract> [Accessed September 28, 2016].
- Zhang, P. et al., 2015. TRIM25 has a dual function in the p53/Mdm2 circuit. *Oncogene*, 34(May 2014), pp.1–10. Available at:  
<http://www.ncbi.nlm.nih.gov/pubmed/25728675>.
- Zhu, Z. et al., 2016. TRIM25 blockade by RNA interference inhibited migration and invasion of gastric cancer cells through TGF- $\beta$  signaling. *Scientific reports*, 6, p.19070. Available at:  
<http://www.pubmedcentral.nih.gov/articlerender.fcgi?artid=4709557&tool=pmc&rendertype=abstract> [Accessed September 28, 2016].

